

THESIS FOR THE DEGREE OF DOCTOR OF PHILOSOPHY

Planning and Operation of Large
Amounts of Wind Power in a Distribution System

SHEMSEDIN NURSEBO SALIH



Department of Energy and Environment
Division of Electric Power Engineering
CHALMERS UNIVERSITY OF TECHNOLOGY
Gothenburg, Sweden, 2015

Planning and Operation of Large Amounts of
Wind Power in a Distribution System

Shemsedin Nursebo Salih
ISBN 978-91-7597-292-3

©Shemsedin Nursebo Salih, 2015
except where otherwise stated.
All rights reserved.

Doktorsavhandlingar vid Chalmers Tekniska Högskola
Ny serie nr 3973
ISSN 0346-718X

Department of Energy and Environment
Division of Electric Power Engineering
Chalmers University of Technology
SE-412 96 Gothenburg
Sweden
Telephone +46(0)31-772 1000

Printed by Chalmers Reproservice
Gothenburg, Sweden 2015

To the One who gave me life!

Abstract

The global installed capacity of wind power has shown a significant growth, from 24 GW in 2001 to 370 GW in 2014. The trend shows that an increasing capacity of wind power is being connected to the electric power system. Due to lower costs associated with the connection of wind power to distribution systems, their wind power hosting capacity needs to be fully exploited. The hosting capacity of distribution systems is limited due to a number of issues such as voltage flicker and harmonics, overvoltage and thermal overloading, and increased fault level. A further issue that deserves attention is that the effect of wind power on the frequency of tap changes (FTC) of the substation transformer due to highly fluctuating nature of wind power. Thus, the thesis investigates these integration issues of wind power and identifies the limiting factors. Then, the thesis proposes mitigation solutions so as to maximize the hosting capacity of a distribution system. Moreover, the thesis investigates the control and coordination of different mitigation solutions.

The investigation of the effect of wind power on the FTC shows that the change on the FTC in a distribution system connected to an external grid with $X/R \geq 5$ is negligible up to a significant level of wind power penetration. However, in a distribution system connected to an external grid with lower X/R ratio, a significant increase in the FTC has been observed as wind power penetration increases. This issue has been effectively mitigated by using reactive power from the wind turbines.

Furthermore, the thesis identifies voltage rise and thermal overloading as the two main limiting factors of wind power integration into distribution systems. Thus, active management strategies (AMSs)—such as wind energy curtailment (WEC), reactive power compensation (RPC), and coordinated on load tap changer (OLTC) voltage control—have been investigated in the thesis to increase the wind power hosting capacity of distribution systems. To facilitate the investigation, an optimization model whose objective function is to maximize the profit gained by the distribution system operator (DSO) and the wind farm owner (WFO) is developed. The results of the analysis show that by using AMSs the wind power hosting capacity of a distribution system can be increased up to twice the capacity that would have been installed without AMSs. Further wind power installation calls for grid reinforcement as a preferred strategy.

In order to implement these AMSs, the system states, i.e. bus voltages, need to be known. Thus, state estimation is proposed as a cost efficient way of obtaining information about the system states. The investigation of the state estimation (SE) algorithms for distribution system applications has identified that the node-voltage-based weighted least square SE algorithm is more appropriate in a system where only few real time measurements are available. Moreover, the analysis of measurement types and locations has shown that power injection and voltage measurements from wind turbine sites provide cost-effective solution with superior SE accuracy.

Consequently, the control of the OLTC is carried out by relaxing the deadband of the automatic voltage control (AVC) relay so that the AVC relay acts on the network's maximum or minimum voltage obtained through the SE. This is found to be simpler to realize than adjusting the set point of the AVC relay. Voltage control through RPC and WEC as well as overload mitigation through WEC is actualized by using integral controllers implemented locally at the wind turbine site. Furthermore, RPC from the local wind turbine is also used to mitigate an overvoltage at a remote bus on the same feeder when the remote wind turbine reaches its regulation limit.

The coordination of voltage regulation between RPC and WEC is achieved by using slightly varying reference voltages for each controller and they are in turn coordinated to the SE-assisted OLTC voltage control by using time delays. The different control and coordination strategies proposed in the thesis are successfully demonstrated using an actual distribution network, measured load, and wind power data.

Index Terms: distribution system, integration issues of wind power, frequency of tap change, active management strategies, cost benefit analysis, control, coordination.

Acknowledgements

I would like to take this opportunity to thank my supervisor Dr. Peiyuan Chen for his consistent assistance and help during the course of the project, for his detailed revision of the present work, and for his friendly approach. I would like also to thank my supervisor and examiner Prof. Ola Carlson for allowing me to participate in this project, for his valuable inputs during the course of the project, and for facilitating the course of the project. My gratitude goes to Prof. Torbjörn Thiringer for his willingness to help and for provision of useful data on flicker and harmonics.

This project has been funded by Chalmers Energy Initiative (CEI) and Chalmers Energy Area of Advance and the financial support is highly appreciated.

Network data and measurement data from Falbygden Energi are extensively used in this thesis. In this regard, I would like to thank Lars Olsson for making these data available, for his valuable inputs from the utility perspectives, and for his quick response to my e-mails.

During the course of the project my wife has given me the strength I need with endless love. Thank you for your patience and support. Thank you my parents for the sacrifice you pay to make me who I am today. Praise be to the Almighty for His countless blessings He bestowed on me.

Last, but not least, I would like to thank my colleagues at the division of Electric Power Engineering for making my stay at Chalmers fun and enjoyable. Special thanks to Khalid, Tarik, Mebtu, and my roommate Georgios for their friendly help whenever needed.

*Shemsedin Nursebo Salih,
Gothenburg, December 2015*

Contents

Abstract	v
Acknowledgements	vii
Contents	ix
Nomenclature	xiii
1 Introduction	1
1.1 Objective of the thesis and the main contributions	2
1.2 Overview of previous works	2
1.3 Thesis structure	3
1.4 List of publications	4
2 Wind power and its impact on a distribution system	5
2.1 Wind power	5
2.1.1 The wind	5
2.1.2 The wind turbine	8
2.2 Impact of wind power on a distribution system	12
2.2.1 Flicker emission	12
2.2.2 Harmonics	13
2.2.3 Increase in fault level	13
2.2.4 Overvoltage	14
2.2.5 Overloading	18
2.3 Summary	19
3 Effect of wind power on frequency of tap changes	21
3.1 Introduction	21
3.2 Model set up for analyzing the effect of wind power on frequency of tap changes .	22
3.2.1 The inequality constraints	23
3.2.2 Equality constraints	24
3.2.3 Modified load flow equations	24
3.3 Modeling the use of reactive power compensation to decrease the frequency of tap changes	26
3.3.1 The objective function	26
3.3.2 The constraints	27

CONTENTS

3.4	The flow chart of the proposed sequential load flow simulation	27
3.5	Case Study	29
3.5.1	Network and data description	29
3.5.2	Effect of wind power on frequency of tap changes	30
3.5.3	Analyzing the frequency of tap changes with a different set of wind power data	33
3.5.4	The frequency of tap changes with different reference voltage at the secondary side of the substation transformer	33
3.5.5	The frequency of tap changes for varying levels of grid strength	34
3.5.6	The effect on FTC when wind turbines consume reactive power	36
3.5.7	Using reactive power compensation to reduce the number of tap changes	37
3.6	Summary	43
4	Siting wind turbines in a distribution system	45
4.1	Background	45
4.2	Siting wind power	46
4.2.1	Overvoltage	46
4.2.2	Overloading	48
4.2.3	Loss consideration	49
4.2.4	Flicker emission	50
4.2.5	Harmonic emission	50
4.2.6	Increase in short circuit level	51
4.3	Summary	51
5	Wind power hosting capacity of a distribution system	53
5.1	Assessing the hosting capacity of a distribution system	53
5.1.1	Worst case analysis	53
5.1.2	Active management strategies	54
5.1.3	Comparison of the different active management schemes for voltage regulation	55
5.2	Costs and benefits of wind power	59
5.2.1	Costs & benefits of a distribution system operator	60
5.2.2	Costs & benefits of a wind farm owner	61
5.2.3	Tools for cost benefit analysis	62
5.3	Modeling the hosting capacity problem	63
5.3.1	The Objective function	63
5.3.2	The constraints	64
5.3.3	Model implementation	67
5.4	Stochastic wind power and load data modeling	67
5.4.1	Using copula to model the stochastic nature of load and wind power	67
5.4.2	Estimating parameters of the Gaussian copula from empirical data	69
5.4.3	Sample generation using the Gaussian copula	69
5.5	Case study	70
5.5.1	Cost-benefit data	70
5.5.2	Case study I: 69 bus system	73

5.5.3	Case study II: Falbygdens Energi's network	79
5.6	Summary	84
6	State Estimation Algorithms for Distribution System Application	87
6.1	Introduction	87
6.2	Voltage profile in distribution system with DG: The need for state estimation	88
6.3	State Estimation Algorithms	90
6.3.1	Node-voltage-based state estimation algorithm	91
6.3.2	Branch-current-based state estimation algorithm	92
6.4	Case study system	95
6.4.1	Network and data description	95
6.4.2	The simulation set up	95
6.4.3	Analysis of the accuracy of the state estimation algorithms for different measurement types and their placement	98
6.4.4	Two measurement points with two wind turbine sites and the accuracy of the state estimation algorithms	102
6.4.5	Variance calculation of the voltage estimates	104
6.5	Summary	104
7	Control algorithms for the different active management strategies	105
7.1	Introduction	105
7.2	Voltage regulation using coordinated OLTC control	107
7.3	Voltage regulation with reactive power compensation	109
7.3.1	The control algorithm	109
7.3.2	Design of the PI controller	113
7.4	Curtailement of wind power	114
7.4.1	Controlling curtailement for overvoltage mitigation	116
7.4.2	Curtailement for overload mitigation	117
7.5	Coordination of the different active management strategies	117
7.5.1	Coordinating the active management strategies for overvoltage mitigation .	119
7.5.2	Coordinating curtailement for overvoltage and overload mitigation	121
7.6	Case study system	121
7.6.1	Network and data description	121
7.6.2	Simulation set up	121
7.6.3	Simulation results from the proposed active voltage regulation schemes . .	122
7.6.4	Simulation results from overload mitigation using curtailement	131
7.7	Summary	133
8	Conclusions and future work	135
8.1	Main conclusions	135
8.2	Future work	138
	References	140
	Appendices	155

CONTENTS

A	Simulink Implementation	157
A.1	Reactive power compensation control blocks	157
A.2	Curtailement control blocks	159

Nomenclature

Acronyms

ABC	Artificial bee colony
AMS	Active management strategy
AVC	Automatic voltage control
C-OLTC	Coordinated OLTC voltage control
CF	Capacity factor
CML	Canonical maximum likelihood
DFIG	Doubly-fed induction generator
DG	Distributed generation
DR	Discount rate
DSO	Distribution system operator
DSSE	Distribution system state estimation
ECM	Equivalent current measurement
FTC	Frequency of tap changes
IFM	Inference functions for margins
MPP	Maximum power point
OLTC	On load tap changer
OO	Ordinal optimization
OPF	Optimal power flow
PCC	Point of common coupling
PF	Power factor

NOMENCLATURE

PSO	Particle swarm optimization
RPC	Reactive power compensation
SCIG	Squirrel-cage induction generator
SE	State estimation
STATCOM	Static synchronous compensator
SVC	Static VAR compensator
THD	Total harmonic distortion
WEC	Wind energy curtailment
WFO	Wind farm owner
WRIG	Wound rotor induction generator

Roman Symbols

A	The present worth of a cash flow at future time t [€]
B_t	A net cash flow at future time t [€]
$b_{k,j}$	Series susceptance between bus k and bus j [p.u.]
$b_{k,j}^c$	Shunt susceptance between bus k and bus j [p.u.]
C^{am}	The present value of the implementation cost of AMSs [€]
C^c	Capital cost of wind power [€/MW]
C^e	Cost of electricity based on spot market [€/MWh]
C^{gc}	Cost of green certificate [€/MWh]
C^v	Variable costs of wind power [€/MWh]
C_x	Covariance matrix of the state vectors \mathbf{x}
E_{TWT}	Total energy yield of the wind turbine [MWh]
$E_{th,r}$	The real part of the Thevenin voltage seen from the wind turbine terminal [p.u.]
E_{th}	The Thevenin voltage seen from the wind turbine terminal [p.u.]
F	The scaling factor in Weibull distribution
$f(w)$	The probability distribution of the wind speed at a given site
f^{mp}	The average monthly peak power from the wind turbines [p.u.]

f^{npw}	Net present worth factor, see equation (5.5)
f_i^{cf}	Capacity factor in numbers of hours of full power production in a year
$f_l(\mathbf{x})$	The measurement function that relate the state vector with measurement at point l
$g_{k,j}$	Series conductance between bus k and bus j [p.u.]
H	The Jacobian of $f_l(\mathbf{x})$
h^{yr}	Number of hours per year [€/MWh]
I	Current [p.u.]
i	$\in \Xi$
I_{max}	Maximum loading current [p.u.]
I_{min}	Minimum loading current [p.u.]
I_d	The d-axis component of the current vector [p.u.]
I_d^{ref}	The reference for the d-axis component of the current vector [p.u.]
$I_{i,j}$	Branch currents between bus i and bus j [p.u.]
$I_{k,j}^{\text{rat}}$	Current rating of a link between bus k and j
I_q	The q-axis component of the current vector [p.u.]
j	$\in J$
J	The set of all buses excluding the buses connected to the tap side of a transformer
k	$\in K$
K	The set of all buses excluding the buses connected to the non tap side of a transformer
l	Measurement points in the network
h	Iteration number
m	The shape factor in Weibull distribution
n^{mon}	Number of months per year
n_i	The capacity of wind power installed at bus i in MW
$n_{k,j,t}$	Tap ratio of the transformer between bus k and bus j at time t [p.u.]
$n_{k,j}^{\text{max}}$	The maximum tap ratio of the tap changer [p.u.]

NOMENCLATURE

$n_{k,j}^{\min}$	The minimum tap ratio of the tap changer [p.u.]
$P_{2,t}$	Active power consumed at node '2' [p.u.]
P_{Wrat}	The rated power output of the wind turbine [MW]
$P_{WT}(w)$	The power curve of the wind turbine versus the wind speed [MW]
P_{cur}^{ref}	The curtailment power reference to the wind turbine controller [p.u.]
$P_{i,t}$	Active power produced at bus i and time t [p.u.]
$P_{i,t}^{\max}$	Maximum value of active power production at bus i at time t [p.u.]
$P_{i,t}^{\min}$	Minimum value of active power production at bus i at time t [p.u.]
$P_{i,t}^D$	Active power consumed at bus i and time t [p.u.]
$P_{i,t}^W$	Available wind power at time t and at bus i [p.u.]
$P_{i,t}^{cur}$	Curtailed wind energy at bus i and time t [MWh]
P_i	The net active power injected at bus i [p.u.]
$P_{k,j,t}^F$	Active power flow from bus k to bus j at time t [p.u.]
P_w	The active power output of the wind turbine [p.u.]
P_w^{ref}	The active power reference to the wind turbine controller [p.u.]
$Q_{2,t}$	Reactive power consumed at node '2' [p.u.]
$Q_{measured}$	Measured reactive power output of the wind turbine [p.u.]
$Q_{i,t}$	Reactive power produced at bus i and time t [p.u.]
$Q_{i,t}^{\max}$	Maximum available values of reactive power at bus i and time t [p.u.]
$Q_{i,t}^{\min}$	Minimum available values of reactive power at bus i and time t [p.u.]
$Q_{i,t}^D$	Reactive power consumed at bus i and time t [p.u.]
Q_i	The net reactive power injected at bus i [p.u.]
$Q_{k,j,t}^F$	Reactive power flow from bus k to bus j at time t [p.u.]
Q_w	The reactive power output of the wind turbine [p.u.]
Q_w^{ref}	The reactive power reference to the wind turbine controller [p.u.]
R	Resistance between two nodes [p.u.]
r	Discount rate of the investment

R_{set}	The resistance setting of the AVC relay [p.u.]
R_{th}	The Thevenin resistance seen from the wind turbine terminal [p.u.]
R_{th}^0	The assumed value of the Thevenin resistance seen from the wind turbine terminal [p.u.]
S_i^{\max}	The maximum MVA output capability of the wind turbine at bus i [MVA]
$S_{j,k}^{\text{rat}}$	The MVA rating of the transformer [MVA]
T	The length of time period of interest, e.g. a year [hours]
t	Time index
u	$\in \Xi$
v^l	The levelized value of cash flows occurring at different future time [€]
v^{np}	The net present value of cash flows occurring at different future time [€]
V_i^{\max}	The maximum voltage limit at Bus i [p.u.]
V_i^{\min}	The minimum voltage limit at Bus i [p.u.]
V_i^{cal}	Calculated voltage at bus i [p.u.]
V_i^{meas}	Measured voltage at bus i [p.u.]
V_w^0	Assumed voltage magnitude at the wind turbine terminal [p.u.]
V_w^{ac}	Actual voltage magnitude at the wind turbine terminal [p.u.]
V_{local}	Voltage level at the terminal of the local wind turbine [p.u.]
V_{measured}	Measured voltage at the terminal of the wind turbine [p.u.]
V_{ref}	The voltage reference to the reactive power PI controller [p.u.]
V_{remote}	Voltage level at the terminal of the remote wind turbine [p.u.]
V_{set}	The voltage set point of the AVC relay [p.u.]
v_d	The d-axis component of the voltage vector [p.u.]
$V_{i,t}$	Voltage magnitude at node i and time t [p.u.]
V_i	Voltage magnitude at node i [p.u.]
V_{lb}	The magnitude of the lower bound voltage $1 - \Lambda_v$, e.g. 0.95, [p.u.]
V_{ub}	The magnitude of the upper bound voltage $1 + \Lambda_v$, e.g. 1.05, [p.u.]

NOMENCLATURE

V_w	Voltage magnitude at the wind turbine terminal [p.u.]
\hat{V}_i	Voltage magnitude estimate at Bus i [p.u.]
$\hat{V}_{\min/\max}^t$	The voltage signal estimate sent to the AVC relay by the voltage level analyzer at time t [p.u.]
$\hat{\mathbf{V}}^t$	The voltage magnitude estimate vector of the network at time t [p.u.]
$W_{k,j,t}$	The change in the tap position from $t - 1$ to t between bus k and bus j
$W'_{k,j,t}$	The continuous substitute of the integer variable $W_{k,j,t}$
\bar{w}	The long term mean wind speed of the area [m/s]
w	wind speed of the area [m/s]
\mathbf{W}_z	The diagonal matrix of measurement covariance
\mathbf{x}	The state vector
X	Reactance between two nodes [p.u.]
X_{set}	The reactance setting of the AVC relay [p.u.]
X_{th}	The Thevenin reactance seen from the wind turbine terminal [p.u.]
X_{th}^0	The assumed value of the Thevenin reactance seen from the wind turbine terminal [p.u.]
X_{th}^{ac}	The actual value of the Thevenin reactance seen from the wind turbine terminal [p.u.]
$Y_{i,j}$	Magnitude of the $(i, j)^{th}$ element of the bus admittance matrix [p.u.]
$y_{k,j}$	Series admittance between bus k and bus j [p.u.]
\mathbf{z}	The measurement data vector
Z	Impedance of a component [p.u.]
z_l	Measurement at point l

Greek Symbols

α_r	The bandwidth of the voltage control loop through reactive power compensation [rad/s]
α_{cur}	The bandwidth of the voltage control loop through curtailment [rad/s]
ΔFTC	The change in the frequency of tap changes

ΔP^{loss}	Change in the network losses P^{loss} [p.u.]
$\Delta P_{2,t}$	The change in active power consumption at node '2' due to wind power [p.u.]
ΔU	Voltage change in per unit value for one tap step [p.u.]
ΔV_t	Voltage difference between reference node '1' $V_{1,t}$ and node '2' $V_{2,t}$ at time t [p.u.]
ΔV_t	Voltage difference between reference node '1', $U_{1,t}$ and node '2', $U_{2,t}$ [p.u.]
$\Delta V_{2,t}$	The change in voltage at node '2' from time $t - 1$ to time t [p.u.]
$\delta_{i,t}$	Voltage angle at node i and time t [rad]
δ_i	Voltage angle at node i [rad]
ε	A very low value chosen based on the sensitivity of the tap operating system [p.u.]
ε_Q	A small positive value, e.g. 0.025, [p.u.]
$\varepsilon_{v,c}$	The additional change in voltage above the upper bound that triggers the curtailment system, e.g. 0.002, [p.u.]
$\varepsilon_{v,r}$	The additional change in voltage above the upper bound that triggers the RPC of other wind turbine, e.g. 0.001, [p.u.]
γ	The net present worth of a MWh of electricity from wind power [€/MWh]
λ_i	The maximum allowed percentage of curtailed energy with respect to the total available wind energy
Λ_v	The allowed voltage variation in the network around the nominal voltage level, e.g. 0.05, [p.u.]
ω	The rotational speed of the wind turbine [p.u.]
ϕ	The power factor angle
Φ^{min}	Allowed minimum power factor
$\varphi_{k,j}$	Angle of the series admittance between bus k and bus j [rad]
Ψ_ρ	The standardized multivariate normal distribution with correlation matrix ρ
$\Psi^{-1}(u_1)$	The inverse of the standard normal distribution at u_1
ρ	A linear correlation matrix
ρ^{df}	Distribution fee [€/MWh]
ρ^{pf}	Peak power fee [€/MW]
ρ^{sf}	Subscription fee [€]

NOMENCLATURE

ρ^{tb}	Transmission benefit [€/MWh]
σ_v^t	Vector of the standard deviation of voltage estimates at time t [p.u.]
σ_l	Standard deviation of the l^{th} measurement [p.u.]
$\theta_{i,j}$	Angle of the $(i,j)^{\text{th}}$ element of the admittance matrix [rad]
χ	The net present value of the cost of the alternative investment [€]
Ξ	A set containing all buses in the network

1

Introduction

The global installed wind power capacity has shown a significant growth from 24 GW in 2001 to 370 GW in 2014 [1]. This growth is expected to continue for some years to come [2]. The growth is mainly attributed to government policies to increase the share of electric energy production from renewable resources. By doing so governments are trying to decrease the emission of greenhouse gases to the atmosphere and the dependence on using coal and imported petroleum.

This substantial amount of wind power needs to be connected to the power system for supplying its electricity to potential consumers. But wind power plants have various characteristics which make their integration different from conventional power plants. On one hand, in contrast to conventional power plants, the size of wind power plants varies from single wind turbine at kW range to wind farms of hundreds of MW. Hence wind power plants are connected to the grid at different voltage levels. On the other hand, during the normal operation of conventional power plants the required power can be generated at any time, given that the power demand is within the technical constraints of the plant. Hence the power output is controllable and predictable. However, the power output from wind power plants depends on the wind condition of the area, and in addition, it fluctuates. Moreover, conventional sources use mainly synchronous generators to produce electrical energy. However wind power plants use different types of generator systems such as induction generators, double fed induction generators, and induction or synchronous generator with full power converters. Each of these generator systems poses different opportunities and challenges to the grid.

While most large wind farms are connected to high voltage transmission systems, medium sized farms are preferably connected to lower voltage distribution systems. This preference stems from comparatively lower connection costs associated with installing wind farms/turbines in lower voltage systems [3]. Thus, there is a need to effectively exploit the available headroom in distribution systems for installing wind power. This available headroom is also known as the wind power hosting capacity of distribution systems [4].

However medium voltage distribution systems have lower grid strength than their high voltage counter parts. Hence they are more vulnerable to the power quality and reliability issues introduced by wind power. Depending on the wind turbine technology, these issues of wind power include voltage flicker, harmonics, overvoltage, overloading, increased short circuit power level, and protection malfunctioning. Some distribution system operators (DSOs) are also concerned about the effect of wind power on increasing the frequency of tap changes (FTC) of a substation

1. INTRODUCTION

transformer.

Therefore the thesis tries to find solutions for the following problems that a distribution system operator may face: what are the limiting factors of wind power integration in a distribution system? what is the optimal level of wind power capacity in a given distribution system? how to control and operate distribution system with a large amount wind power of wind power in an efficient and effective way?

1.1 Objective of the thesis and the main contributions

The overall aim of this thesis is to evaluate strategies that can maximize the wind power hosting capacity of distribution systems in a cost-effective manner i.e. without using costly grid reinforcement solutions. To this end, different integration issues of wind power are examined as limiting factors for wind power integration. Furthermore, different AMSs—which include reactive power compensation, coordinated OLTC voltage control, and energy curtailment—are investigated to tackle these limiting factors in the grid. The costs associated with different usage levels of AMSs are also evaluated against the cost of grid reinforcement. In the end, the control and coordination algorithms are proposed and simulated to demonstrate the implementation of these active management strategies in a distribution system.

To the best knowledge of the author the following points are the contributions of the thesis.

- **The determination of the effect of wind power on the frequency of tap changes** with respect to varying grid conditions and the use of RPC from wind turbines to reduce the FTC (Chapter 3).
- **The proposed simple method of siting wind power** to maximize the hosting capacity of a given distribution system (Chapter 4).
- **The development of a new optimization model based on cost benefit analysis** for determining the optimal usage level of AMSs and optimal hosting capacity of a given distribution system (Chapter 5).
- **The comparison of two state estimation algorithms** for distribution system application with respect to measurement data type and measurement points (Chapter 6).
- **The proposed control and coordination algorithms** that enable the realization of AMSs with minimum power loss as well as investment cost (Chapter 7).

1.2 Overview of previous works

Presently, it is widely accepted that the most common limiting factors of wind power integration to distribution system are the voltage rise problem and overloading of the system components [3]. Both of them are more likely to occur under low system loading condition and high wind power generation. Hence DSOs use this worst system condition to evaluate the possibility of connecting a given capacity of wind power. This works fine under passively operated distribution systems. But it severely limits the hosting capacity of distribution systems, which will in turn hinder the

penetration of wind power to the power system. Thus, various AMSs have been proposed to increase the hosting capacity of distribution systems. These AMSs include wind energy curtailment (WEC), reactive power compensation (RPC), coordinated on load tap changer (OLTC) voltage control (C-OLTC) [3, 5–9].

However, there is still a limit to the amount of wind power that can be installed using AMSs. For example, the hosting capacity of the distribution system can be increased by curtailing part of the wind power during system overload or overvoltage. But WEC causes loss in revenue for the wind farm owner (WFO) and cannot be used excessively. Similarly, RPC can be used to increase the hosting capacity of a distribution system by avoiding overvoltage which would otherwise happen due to wind power. However, if used excessively, RPC may lead to unacceptable power losses in the system. Thus, there is a limit on the amount of wind power that can be installed using AMSs. In the literature reviewed, for example, in the case of WEC, this is done either by limiting the amount of curtailed energy [7, 10] or by constraining the capacity of wind power [3, 5, 6, 9]. This approach, however, does not ensure the optimal use of the AMSs as the limit of energy curtailed set at each case is chosen arbitrarily and not based on the cost benefit analysis. Therefore, the increase in hosting capacity using these active management strategies requires further investigation.

On the other hand, once the optimal capacity of wind power for a given distribution system is determined, one needs to know how the different AMSs are controlled and coordinated to realize the specified amount of wind power. In this respect, different control algorithms are proposed for voltage regulation in literature using each of the AMS– i.e. OLTC voltage control [11–16], RPC [17–20], curtailment [21, 22] or using two of these AMSs– i.e. RPC and curtailment [23, 24]– or coordinating all of them [25–29]. Similar control strategies of curtailment for overload mitigation are provided in [24, 30]. In this thesis, the focus is to provide an overall control and coordination algorithm which actualizes voltage regulation by using all the AMSs and realizes overload mitigation using curtailment.

Moreover, in addition to the main limiting factors, other effects of wind power (such as flicker, harmonics) are examined to determine if and when they can be a limiting factor for the wind power integration in distribution systems. Special attention is given to the effect of wind power on the FTC of transformers since such analysis is rarely found in literature.

1.3 Thesis structure

With the introduction of the thesis already given in this chapter i.e. Chapter 1, the rest of the thesis is structured as follows:

- **Chapter 2** provides the basics of wind power integration in a distribution system which includes the discussion of the nature of the wind power and its effect on power quality and reliability of the distribution system.
- In **Chapter 3** the effect of wind power on the FTC of a substation transformer is investigated. The chapter also analyses the use of RPC from the wind turbines to decrease the FTC of substation transformer.
- **Chapter 4** proposes a simple approach of sitting wind power in order to maximize the hosting capacity of distribution systems.

1. INTRODUCTION

- **Chapter 5** discusses the different active management strategies and develops a mathematical model based on cost benefit analysis to optimize the hosting capacity of distribution systems.
 - **Chapter 6** provides the comparison of the two state estimation algorithms for electrical distribution system application.
 - **Chapter 7** provides the control and coordination algorithms of the different AMSs.
- Finally the conclusions of the thesis and future works are presented in **Chapter 8**.

Chapter 3 through Chapter 5 generally deals with the planning of wind power integration while Chapter 6 and Chapter 7 deal with the operation of large amount of wind power in an electrical distribution system.

1.4 List of publications

The following papers are published during the course of this thesis:

- I. S. N. Salih, P. Chen, and O. Carlson, "Maximizing Wind Power Integration in Distribution System," in 10th International Workshop on Large-Scale Integration of Wind Power into Power Systems as well as on Transmission Networks for Offshore Wind Power Plants, Aarhus, Oct. 2011.
- II. S. N. Salih, P. Chen, and O. Carlson, "The effect of wind power integration on the frequency of tap changes of a substation transformer," *Power Systems, IEEE Transactions on*, vol.28, no.4, pp.4320,4327, Nov. 2013.
- III. S.N. Salih, P. Chen, and O. Carlson, L.B. Tjernberg, "Optimizing Wind Power Hosting Capacity of Distribution Systems Using Cost Benefit Analysis," *Power Delivery, IEEE Transactions on*, vol.29, no.3, pp.1436,1445, June 2014.
- IV. S.N. Salih, P. Chen, and O. Carlson, "Using reactive power from wind turbines for loss reduction in distribution system," *CIGRE Workshop 2014, Rome*, June 2014.
- V. S.N. Salih and P. Chen, "On coordinated control of OLTC and reactive power compensation for voltage regulation in distribution systems with wind power," *Power Systems, IEEE Transactions on*, 2015, under third review.
- VI. S.N. Salih, P. Chen, and O. Carlson, "Analysis of state estimation algorithms for distribution system application with respect to measurement types and locations," *Power Systems, IEEE Transactions on*, 2015, submitted for publication.
- VII. S.N. Salih, P. Chen, and O. Carlson, "On control of wind turbines for voltage regulation and overload mitigation in radial distribution systems," *Power Delivery, IEEE Transactions on*, 2015, submitted for publication.

2

Wind power and its impact on a distribution system

The introduction of wind power to an electrical distribution system poses different types of power quality and reliability issues. Depending on the location and technology of the wind turbine and the characteristics of the distribution system, these integration issues of wind power include overloading of system components, over voltage, malfunction of protection system, voltage flickers and harmonics, etc. Thus this chapter is devoted to the discussion of these integration issues of wind power. However, the discussion of the characteristic of the wind power itself is vital to the understanding of the power quality and reliability issues that arise due to the introduction of wind power as well as mitigating solutions. Hence the chapter starts with the discussion of the characteristics of wind power in terms of the nature of the source of energy, i.e. the wind, and the generator system that converts the kinetic energy extracted from the wind into electrical energy. Then the different integration issues of wind power are discussed.

2.1 Wind power

Wind power is stochastic in nature which mainly stems from the stochasticity of the wind. This is the primary difference between conventional energy sources and wind energy. Thus, it demands particular attention when it comes to integrating wind power into the power system. Moreover, understanding the characteristic of the wind turbines is also vital to understand the effect of wind power on the grid. Hence, this section provides the discussion of the wind and the wind turbine.

2.1.1 The wind

2.1.1.1 Temporal and spatial variation of wind power

Wind fluctuates both temporally and spatially. The temporal fluctuation ranges from a time scale of less than one second to several days. In this respect three peaks are identified: turbulent peak, diurnal peak, and synoptic peak [31]. The turbulent peak is caused mainly by wind gusts in the sub-seconds to minute range. The knowledge of this variation is vital for analyzing mechanical loads on

2. WIND POWER AND ITS IMPACT ON A DISTRIBUTION SYSTEM

the wind turbine [32] and, in turn, for assessing the effect of wind power on the power quality of the grid, though its effect depends on the technology of the wind turbine connected to the system. To this end, this short term variation is represented through the average value of the wind speed in the considered time (mostly 10 min) and the turbulence intensity [32]. Turbulence intensity is the ratio of the standard deviation of the wind speed to the average wind speed. Roughly considered, the turbulent fluctuations have a Gaussian distribution around the mean wind speed with its standard deviation. The turbulence intensity varies in a wide range, from 0.05 to 0.40 [32].

The diurnal peak is the result of daily wind speed variation caused by such factors as land breeze and sea breeze, which happen due to temperature differences between land and sea. The synoptic peak is the result of changing weather patterns, which typically vary daily to weekly but includes also seasonal cycles [31]. From a wind turbine's point of view, the diurnal and synoptic fluctuations of the wind are used together with the mean wind speed to predict the energy yield for a site. From the power system's point of view, the diurnal and the synoptic peaks mainly affect the operational aspect of the power system. On most of the globe the diurnal peak occurs in the early afternoon [33]. When it comes to the synoptic peak, particularly in Europe, the wind speed tends to be higher in winter than in summer [34]. This is ideal because the electricity consumption has also a similar seasonal pattern in this region.

On the other hand, the spatial variations range from some millimeters to several kilometers [32]. The knowledge of these variations and the correlation between different sites is vital in the planning and operation of the power system. In this regard, a study carried out using two-year wind data with a three-hour resolution obtained from 142 synoptic stations in Sweden shows that the distance at which the correlation between wind speeds from two location drops to approximately 0.37 ranges from 38 to 530 km [35]. Since the area covered by a typical radial distribution system is not that large, the study implies that wind power in distribution systems can have a high level of correlation. In fact, a correlation that ranges from 0.82 to 0.95 is observed among an hourly time series wind power data of one year. The data are obtained from 10 sites in a distribution system where there is a maximum distance of around 10 km among the sites. Hence in a distribution system of such size, full correlation can be assumed between wind turbine sites for planning studies.

2.1.1.2 Energy yield of wind

In wind power planning studies it is vital to know the energy available from a wind turbine to assess the expected yield and the profitability of the project. To this end, the expected power output of a wind turbine at a given site depends on the power curve of the wind turbine and long term wind speed distribution of the area. The long term wind speed distribution of an area is represented in a concise mathematical description, i.e. the Weibull distribution function (2.1). Weibull distribution uses two parameters: the shape factor m and the scaling factor F . Thus, the representation of wind data using the Weibull distribution is quite handy and facilitates data sharing.

$$f(w) = \frac{m}{F} \left(\frac{w}{F}\right)^{m-1} \exp\left(-\left(\frac{w}{F}\right)^m\right) \quad (2.1)$$

The scaling factor F is a measure for the characteristic wind speed of the considered time series [32] and is given by

$$F = \frac{\bar{w}}{\Gamma\left(1 + \frac{1}{m}\right)} \quad (2.2)$$

where \bar{w} is the long term, such as annual, mean speed of the area, and Γ is the gamma function. The shape factor m describes the curve shape. It is in the range between 1 and 4 [32]. If there are small fluctuations around the mean wind speed, the value of m is high; whereas large fluctuations give a smaller shape factor m (see Fig. 2.1). In general, the reference energy yield given by wind turbine manufacturers in the data sheets is calculated based on a Weibull distribution with $m = 2$, i.e. a Rayleigh distribution function [32].

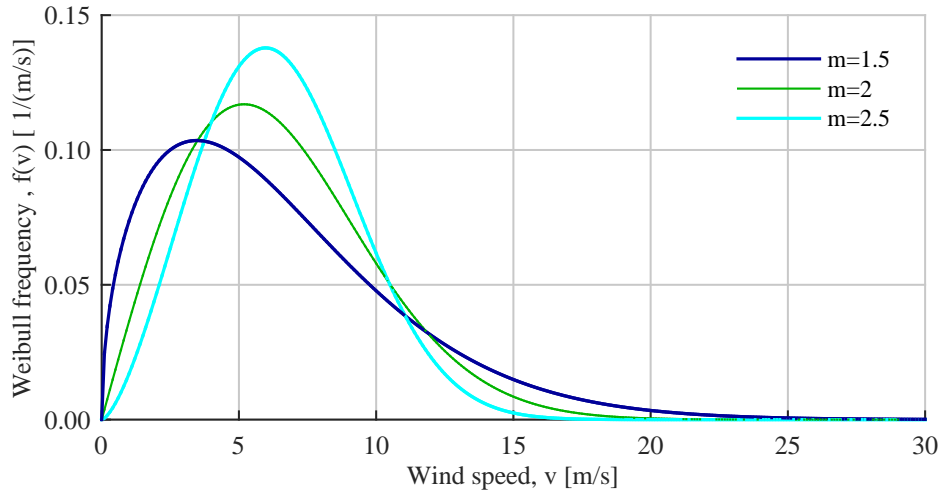


Figure 2.1: The Weibull distribution representation of wind with average speed of 6.5 m/s and a varying shape factor.

On the other hand the wind turbine can only harvest the wind energy when the wind speed is within some fixed interval. For example, Fig. 2.2 shows the power curve of a typical fixed speed and variable speed wind turbine. Below the cut in speed, since the wind is too low for useful energy production, the wind turbine is shut down. Then, once operating, the power output increases following a broadly cubic relationship with wind speed (although modified by the variations in power coefficient C_P) until maximum rotor speed is reached. Above the rated wind speed, the rotor is arranged to limit the mechanical power extracted from the wind [36]. Above the cut-out wind speed, the turbine is shut down to avoid mechanical damage on the wind turbine.

Based on the power curve P_{WT} of the wind turbine and the probability distribution the wind speed at a given site $f(w)$, the total energy yield of the wind turbine, E_{TWT} , can be calculated using

$$E_{TWT} = T \int_0^{\infty} f(w) P_{WT}(w) dw \quad (2.3)$$

where T is the time period of interest, e.g. a year. The energy yield is usually expressed in terms of the the capacity factor (C_F) of the wind turbine at that particular site, which is calculated using

$$C_F = \frac{E_{TWT}}{8760 P_{Wrat}} \quad (2.4)$$

where P_{Wrat} is the rated power of the wind turbine and 8760 is the number of hours per year. In practice this capacity factor lies in the range about 0.20 to 0.40 [31] while some offshore wind

2. WIND POWER AND ITS IMPACT ON A DISTRIBUTION SYSTEM

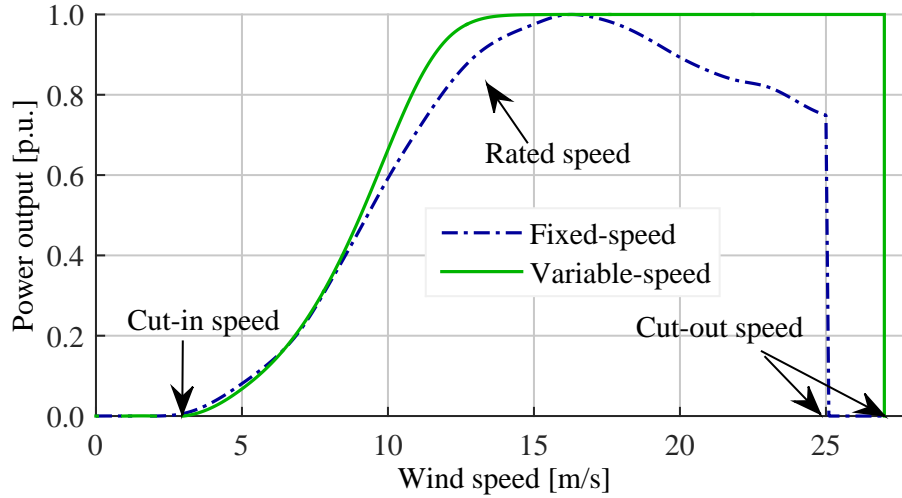


Figure 2.2: Power curves of a typical fixed and variable speed wind turbines.

farms, such as Horns Rev 2, can reach a capacity factor of 0.50 [37]. It is sometimes convenient to represent the capacity factor as the utilization time t_{util} in hours per year, calculated as

$$t_{util} = 8760C_F \quad (2.5)$$

2.1.2 The wind turbine

A wind turbine is composed of various components: the turbine blades, the tower, the generator system, etc. However, the aim in this thesis is to investigate the impact of wind power on power quality and reliability of an electrical distribution system. Thus, it is of interest to study the characteristic of the power output from the wind turbine which is governed by the characteristic of the generator system. In this respect, today's commercial wind turbines can be classified into four major groups depending on their ability to control the rotational speed, hence the power output, of the wind turbine [31].

2.1.2.1 Type A: Fixed speed wind turbines

Wind turbines equipped with squirrel-cage induction generators (SCIGs) are generally known as fixed speed wind turbines since these wind turbines work at almost constant speed, with slip of the order 2% at rated power [31]. A typical fixed wind speed turbine has the configuration given in Fig. 2.3. Since there is a large inrush current during the starting of the induction generator, which can be as high as 6 to 8 times the current at the rated operation [32], these wind turbines are equipped with soft-starters to limit the inrush current and bring the drive train slowly to the operational speed [36]. These wind turbines also consume a substantial amount of reactive power during idling as well as operation, as long as they are connected to the grid; the higher the power output is, the higher is the reactive power consumption as shown in Fig. 2.4. Consequently, these wind turbines are equipped with capacitor banks to provide a reactive support. However, these capacitor banks only shift the reactive power consumption curve downward.

Fixed speed wind turbines constitute most of the early generation utility scale wind turbines. In the year 2000, these wind turbines still represented 39 % of the total installed wind turbines in

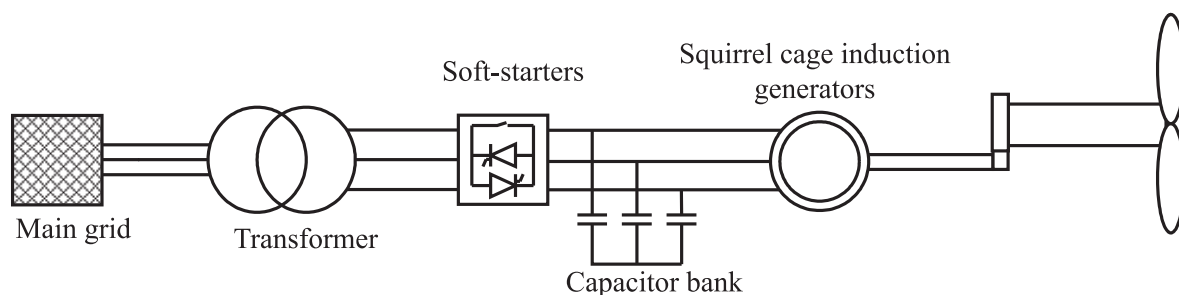


Figure 2.3: Schematic of fixed speed wind turbine.

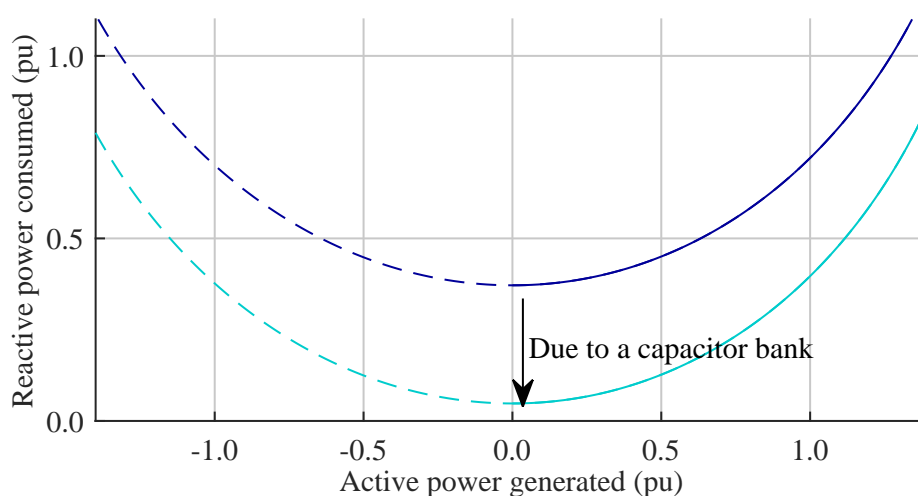


Figure 2.4: PQ curve of a typical fixed speed wind turbine.

the world [38]. The main reason for the use of SCIGs is the damping they provide for the drive train. The damping is provided by the difference in speed between the rotor and the stator magneto motive force, i.e. the slip speed. Additional benefits include the simplicity and robustness of their construction and no need for synchronizing [39]. However, regardless of the power control principle (pitch or stall), the wind fluctuation is converted to mechanical fluctuations and consequently into electrical power fluctuation. The electrical power fluctuation can yield voltage fluctuation and flicker emission in weak grids while the mechanical fluctuation increases the stress on the drive train.

2.1.2.2 Type B: Limited variable speed wind turbines

One of the disadvantages of fixed wind speed turbines is that during wind gusts and high wind speeds, the drive train is exposed to high mechanical stresses. If a larger slip is allowed temporarily, the drive train will be relieved. Moreover during high wind speeds, a smoother increase in power output is possible. This is done by varying the resistance of the rotor circuit. Such control of the rotor circuit resistance is possible if the rotor winding of the generator is connected in series with an optically controlled resistance. This optical coupling eliminates the need for slip-rings. Using this approach a brief increase in rotational speed up to 20% has been achieved [32]. At normal wind speeds, the additional variable resistor is shorted out for maximum efficiency. During strong wind the variable resistors are manipulated to get the required torque. Hence during wind gusts the

2. WIND POWER AND ITS IMPACT ON A DISTRIBUTION SYSTEM

additional wind power is dissipated in the resistors, which needs additional cooling consideration. Whenever necessary, pitching can be combined with varying the rotor circuit resistance to get an optimum performance. In this regard, varying the rotor circuit resistance is convenient whenever fast response is required while pitching can be used to reduce the power extracted from the wind rather than dissipating it in the resistors. Apart from this improved power controllability described, the characteristic of Type B wind turbine can be considered similar to Type A wind turbines.

2.1.2.3 Type C: Double fed induction generators

Though Type B wind turbines have improved some of the drawbacks of their Type A counterparts, they have their own shortcomings. One of this is the fact that the speed variability achieved is at the expense of increased power loss in the rotor circuit. Besides, the achieved variability in speed is not sufficient to ensure maximum energy extraction under varying wind speed condition. The next generation of wind turbines with improved performance is Type C, i.e. double fed induction generator (DFIG) wind turbines.

Fig. 2.5 presents the schematic diagram of this type of wind turbine. The rotor windings, that are accessible through slip rings, are connected back to the grid through a back to back AC/DC/AC power converter. This converter circuit, through injecting a controllable voltage at the rotor frequency, realizes a variable speed operation of the wind turbine [40]. Moreover, the energy that

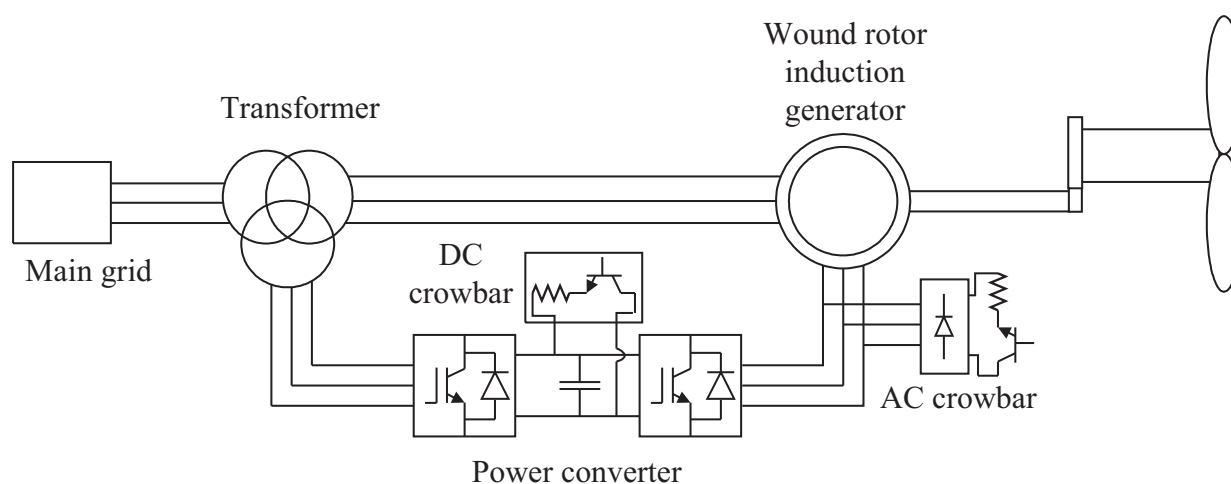


Figure 2.5: Schematic diagram of DFIG wind turbines [41].

used to be dissipated in the external resistors in Type B wind turbines is now fed back to the grid through the machine-side converter. The power converters can also be used for smooth connection of the wind turbines to the grid as well as to provide the required reactive power compensation. During faults, the crowbar switches the rotor circuit to an external resistor to protect the machine-side converter from excessive current [42]. Similarly, the DC-link crowbar activates to protect the DC-link capacitor from overvoltage [41, 43].

The extent of speed variability achieved and the amount of wind power absorbed or delivered by the rotor depend on the size of the power converter used. Considering also the economic aspect of the converter, it is usually sized to be around 30% of the rated power of the wind turbine.

And the usual speed range of operation of these wind turbines is between -40% to $+30\%$ of the synchronous speed [31].

The reactive power capability of a DFIG wind turbine depends on the stator current limit, the rotor current limit, and the rotor voltage. In general, the rotor current limits the reactive power production capacity of the machine while the stator current limits reactive power absorption capacity. The rotor voltage becomes a limiting factor only at high slips [44]. The grid side converter can provide additional reactive power support when it is not fully used for active power transfer. A typical reactive power curve of a DFIG wind turbine is shown in Fig. 2.6 (adapted from [44, 45]). This is assuming that the wind turbine is always connected to the grid. However, at zero power output, the wind turbine is switched off. Hence reactive power support would only be available from the grid side converter. The magnitude of this reactive support will then depend on the ratings of the converter [45].

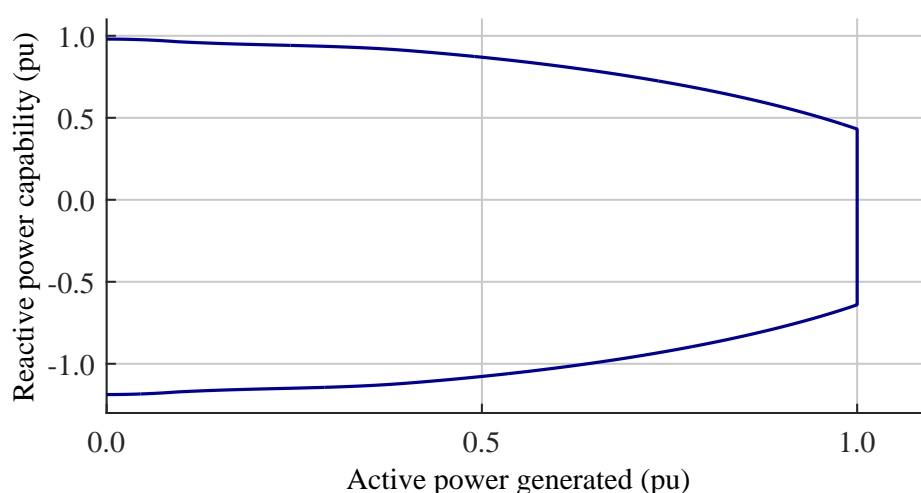


Figure 2.6: A reactive power capability diagram of a typical DFIG wind turbine.

2.1.2.4 Type D: Full power converter wind turbines

In this wind turbine type the converter is rated to handle the full capacity of the wind turbine. That is, it completely decouples the wind turbine generator from the grid, giving the opportunity to vary the frequency of the generator as required. This also makes it possible to employ different types of generators such as induction, wound rotor synchronous, and permanent magnet synchronous generators [46]. The schematic diagram of a full power converter wind turbine is shown in Fig. 2.7.

These wind turbines can provide a wider range of speed variability than the DFIG wind turbines. The converter is used for smooth connection of the wind turbine as well as for providing the required reactive power support [31].

The reactive power capability of these wind turbines depends on the current rating as well as the voltage of the grid side converter. These ratings are chosen to meet grid code requirements in terms of providing specific level of reactive power support at varying conditions of system voltage and frequency [47]. For example, Fig. 2.8 shows the reactive power capability curve of a full power converter wind turbine with design power factors (pf_d) of 1 and 0.95 at grid voltages (V_g) of 1.0 and 1.05 pu. Similar to the case of DFIG wind turbines, they can provide larger reactive support

2. WIND POWER AND ITS IMPACT ON A DISTRIBUTION SYSTEM

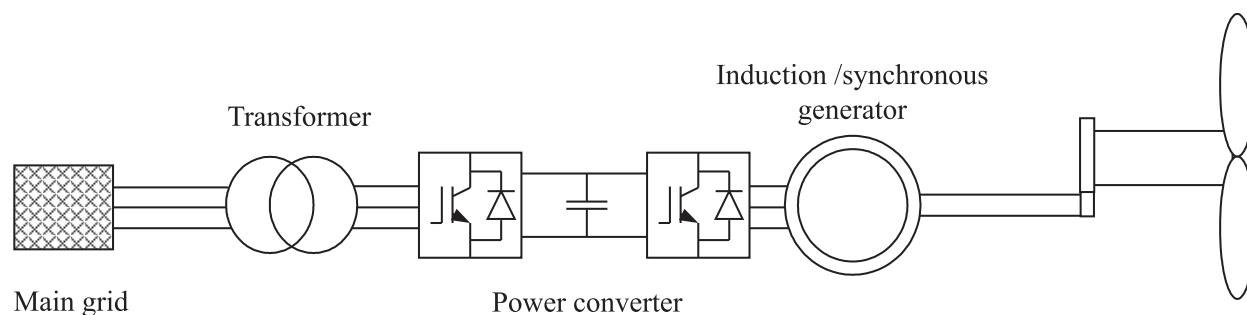


Figure 2.7: Schematic diagram of full power converters [46].

at absorption compared to production. However, if the converter voltage is selected such that the converter voltage limitation is avoided, then Type D wind turbines can provide similar level of reactive support at both absorption and production [47].

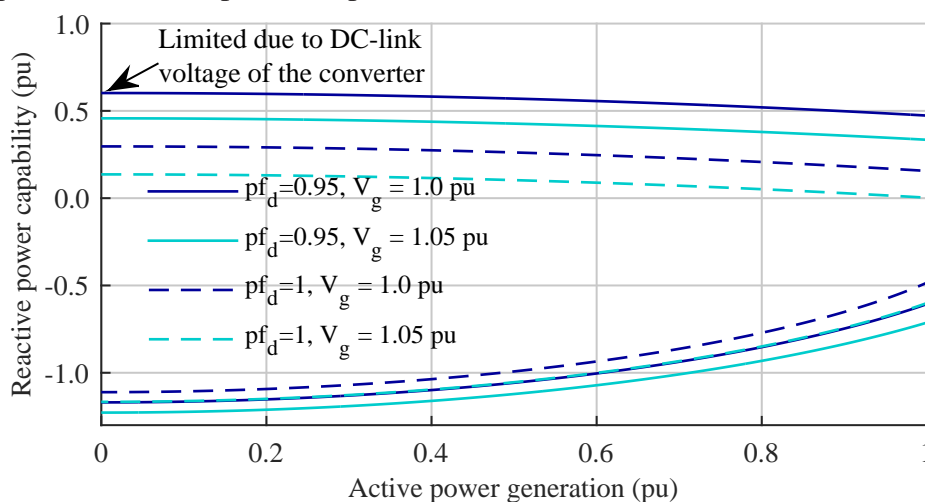


Figure 2.8: Reactive power capability a typical full power converter wind turbine.

2.2 Impact of wind power on a distribution system

The introduction of wind power to an electrical distribution system poses different types of power quality and reliability issues. Depending on the location and technology of the wind turbine and the characteristics of the distribution system, these integration issues of wind power include voltage flickers, harmonics, increase in fault level, overloading of system components, over voltage, and malfunction of protection system, etc.

2.2.1 Flicker emission

In general, the flicker emission from variable speed wind turbines can be considered fairly low during both continuous and switching operation, whereas the flicker emission from fixed speed wind turbines depends on the control mechanism: stall or pitch [31]. The flicker emission from stall controlled wind turbines is average during continuous operation. However, due to limited

controllability of the torque input of the turbine, the flicker emission is high during switching operation. With better controllable turbine torque input, the flicker emission from pitch controlled wind turbines during switching operation can be considered average. However, due to limited bandwidth of the pitching system, their flicker emission during continuous operation is high [48]. Moreover, flicker emission from wind turbines depends on the short circuit capacity of the network relative to the capacity of the wind turbines, measured by the short circuit ratio (SCR), the angle of the Thevenin impedance of the grid seen from the point of connection of the wind turbine, and the average wind speed. In general, with the advent of variable speed wind turbines, flicker emission is not seen as a concern as it once was.

2.2.2 Harmonics

Harmonics of different levels are emitted by wind turbines depending on the technology of the generator system. In general fixed wind speed turbines do not cause significant harmonic¹ or interharmonic² disturbances. Hence the specification of harmonics and interharmonics are not required by IEC 614000-21 for fixed speed wind turbines [31]. However, variable speed wind turbines, equipped with power electronic converters, emit harmonics and interharmonics components. A simple analysis done in [49] based on the voltage harmonic emission limits given in the IEC standard [50] and the current harmonic emission level of wind turbines shows that harmonic emissions due to a wind farm can be beyond the absorption capacity of the system at low order even harmonics (such as the 4th, 6th and 8th). That is, based on the current harmonic emission data available from a couple of variable speed wind turbines, the voltage emission limits at these harmonics are more stringent to fulfill by the wind turbines in a given distribution system. It seems that the limits on this harmonic level are kept unnecessarily low and needs a revision on the standard. Otherwise harmonic emission can be a limiting factor for wind power integration.

2.2.3 Increase in fault level

Fault levels of various magnitude are contributed from different wind turbine technologies in a given distribution system. In the worst case, the short circuit current contribution from SCIGs can be as high as 8 pu [51], but generally higher than 3 pu [52]. Though WRIGs can contribute less fault current, treatment of these generators like SCIGs will result in a more conservative fault current contribution. With respect to fault current contribution, DFIGs can also roughly be treated as SCIGs with higher rotor resistance [53–55]. Simulation results have shown the short circuit current to vary between 3 pu to 10 pu [52, 54–56] depending on the machine parameters, which is similar to the case of SCIGs. However, fault current contribution from Type D wind turbines is limited by the overcurrent capability of the converter system. The converter is usually designed to have an overload capability of a little above, around 10% [56], of the rating of the wind turbine.

In distribution networks where short circuit level is already around the design limit of the switchgear, the additional short circuit current, in the worst case, can affect the fault current handling capacity of the switchgear. This may lead to malfunctioning or even destruction of the switchgear. In addition to increasing fault current, the introduction of wind power may also contribute to the reduction

¹Harmonics are components with frequencies that are multiple of the supply frequency

² Interharmonic disturbances have frequencies that are located between harmonics of the supply frequency

2. WIND POWER AND ITS IMPACT ON A DISTRIBUTION SYSTEM

in fault current with overall impact of jeopardizing the protection coordination of the system. But such situation does not limit the integration of wind power as it only needs a change in the settings of the affected relays.

2.2.4 Overvoltage

Network components and consumer loads are designed to operate within a given voltage range beyond which the equipment involved can be severely damaged. Depending on the magnitude, the effect can be immediate or long-term, such as slow degradation caused by long-term heating [57]. To avoid this, national and international standards specify the voltage range that needs to be maintained at a given voltage level. For example, the European standard requires the 10-minute average value of the voltage rms supplied at consumer premises should be within $\pm 10\%$ for 95% of the week. This requirement holds irrespective of where the consumer is connected to the MV or LV level. Based on this limit, the Swedish AMP standard specifies that the network owner should plan the network so that the voltage at LV be within $+6/-10\%$ of the nominal voltage to accommodate unforeseen voltage increase due to the introduction of distributed generations.

2.2.4.1 Voltage regulation in a distribution system

In an electrical distribution system there are one or more transformers through which electricity is supplied to the consumers in the network. The purpose of these transformers is to step down the voltage from transmission or sub-transmission systems. These transformers are also equipped with on-load tap changers (OLTC) that regulate the voltage at the secondary side of the transformer so as to keep the voltage in the distribution system within the ranges specified by the standards. The OLTC regulates of the turns ratio of the transformer by adding or subtracting turns on one side (usually primary side in case of distribution system transformers) of the transformer. This results in turns ratio variation of, for example, $\pm 10\%$ of the nominal value. These range is not continuous, but divided into steps of, for example, 1.67% so that each change represents a specific voltage increment. Moreover, tap changers have adjustable deadbands and time delays. The deadband is the voltage range around the reference value within which the tap changer does not take action. The time delay is the duration during which the voltage should be outside this deadband before the tap changer takes action. This time delay can be fixed or can be made inversely proportional to the magnitude of the deviation from the voltage set point [58].

The tap changers can accomplish the voltage regulation in two ways [59]. One way is through maintaining the voltage at the secondary side of the transformer at a given deadband around a constant voltage set point. In Fig. 2.9, this would avoid the line voltage drop compensation (LDC) provided by the dashed signal. The second alternative includes the voltage drop compensation where the the AVC relay controls the voltage V_L at some chosen load point rather than the voltage at the secondary side of the transformer. That is, depending on the loading condition I and the measured voltage V at the substation, voltage V_L at the assumed load center is calculated according to (2.6) and is compared with the reference voltage V_{ref} . This load point is chosen to give the required voltage boost for the system from low to high loading condition. The rest of the AVC relay, i.e. the time delay and the voltage deadband, functions the same in both alternatives.

$$V_L = V - I \times (R_{set} \cos(\phi) + X_{set} \sin(\phi)) \quad (2.6)$$

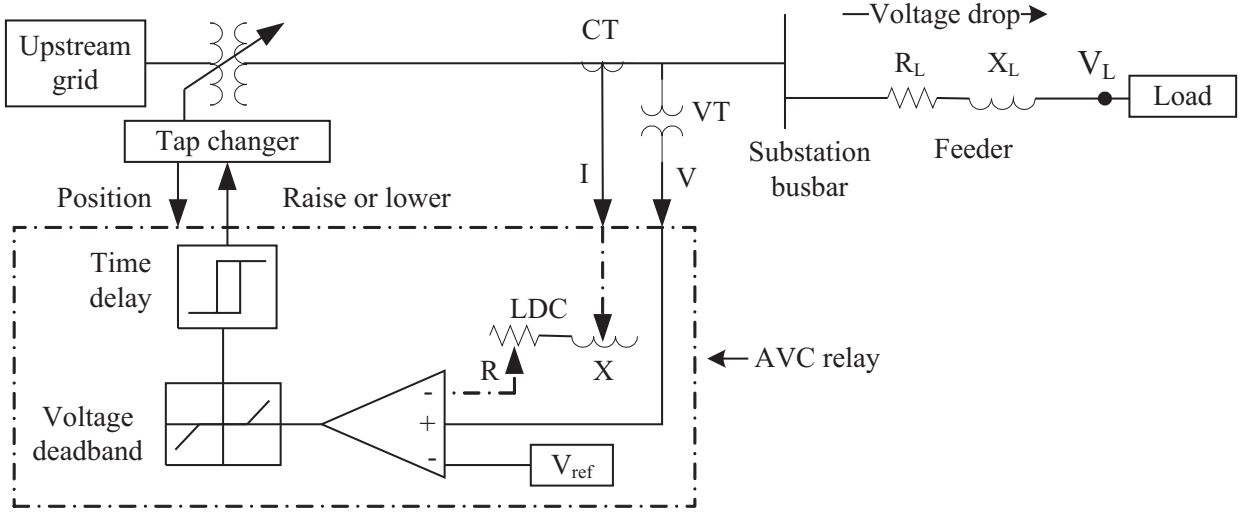


Figure 2.9: Traditional automatic voltage control in transformers.

where $\cos(\phi)$ is the expected power factor of the load and p.u. calculation is assumed.

There are two main approaches when choosing the load point, i.e. the value of R_{set} and X_{set} , to achieve efficient voltage regulation [59]:

Load center : In this case, the settings are chosen to regulate the voltage at a given point downstream of the regulator. If the load point impedance as seen from the substation is R_L and X_L , then one can set $R_{set} = R_L$ and $X_{set} = X_L$, where per unit calculation is assumed.

Voltage spread : In this approach, the R and X settings are chosen to keep the load side voltage within a chosen band when operating from light load to full load. For example, if the voltage V at the regulated point is to be V_{max} at maximum loading of I_{max} and V_{min} at minimum load of I_{min} , then the setting of R and X can be chosen according to (2.7) [59].

$$R_{set} = \frac{V_{max} - V_{min}}{\left(\cos \phi + \frac{X}{R} \sin \phi \right) (I_{max} - I_{min})} \quad (2.7)$$

$$X_{set} = \frac{X}{R} R_{set}$$

And the regulator set voltage can be calculated from one of the extreme operating points:

$$V_{set} = V_{min} - (R_{set} \cos \phi + X_{set} \sin \phi) I_{min} \quad (2.8)$$

The $\frac{X}{R}$ ratio can be chosen arbitrarily. For example, when it is chosen the same as the line X/R ratio, these equations move the effective load center based on the choice of voltage and current minimums and maximums [59]. Other X/R ratios can be chosen to reduce the sensitivity of the regulator to changes in power factor of the load. But still the change in power factor of the load complicates the application of the line drop compensation method. Many regulators are, thus, set

2. WIND POWER AND ITS IMPACT ON A DISTRIBUTION SYSTEM

up without line drop compensation. It is obviously easier and less prone to mistakes, but at the expense of losing some significant capability [59].

2.2.4.2 Wind turbines contribution to overvoltage

Whichever is used, the above voltage regulation approaches have been utilized and found to be effective in passively operated distribution systems for many years. But due to the introduction of wind power, or any distributed generation for that matter, voltage regulation has become a challenge. This is because on one hand, distributed generation affects only the voltage level of the feeder they are installed in. On the other hand, especially in the case of wind power, its output is not easily predictable. Hence traditional voltage regulation mechanisms can not be used to effectively regulate the voltage level on the system.

Wind power introduces a reverse power to the external grid. If the transformer regulates the voltage at its secondary side, with the voltage being held almost constant, this results in a higher voltage at the point of common connection (PCC) compared to that at the substation. Depending on the amount of reverse power flow, the voltage at the PCC could be above the allowed voltage level in the distribution system.

Consider a simple network with wind power shown in Fig. 2.10. The cable between the reference

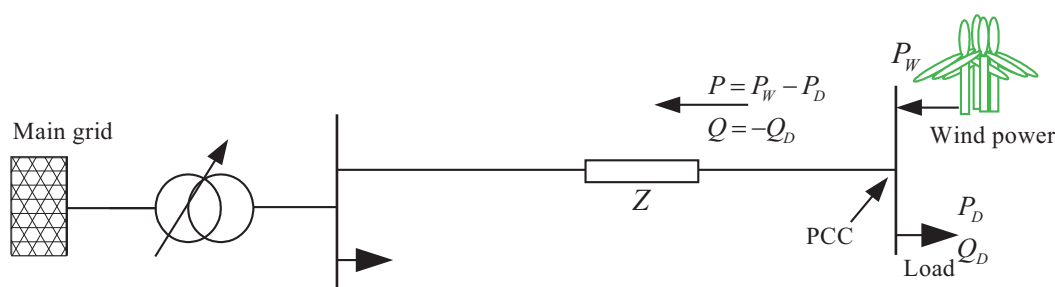


Figure 2.10: A simple distribution system with wind power.

node 1 and the PCC can be represented by the π -model of a transmission line (see Fig 2.11). Given

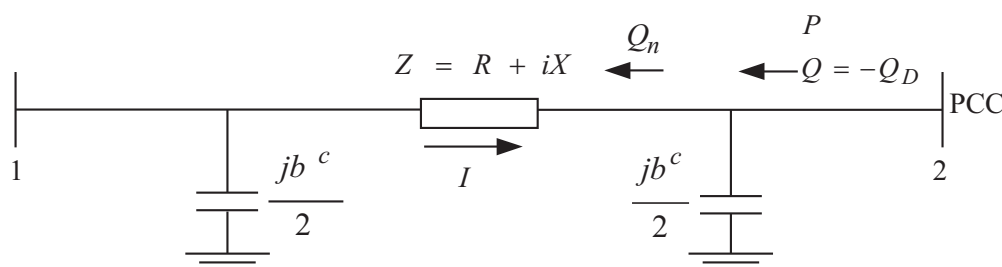


Figure 2.11: A π -model of power line between two buses.

a constant voltage V_1 at node 1, the voltage V_2 at node 2 in p.u. is given by

$$V_2 = V_1 - I \times Z \quad (2.9)$$

2.2 Impact of wind power on a distribution system

where

$$I = \frac{-P + iQ_n}{V_2^*} \quad (2.10)$$

and

$$Q_n = Q + \frac{b^c}{2}|V_2|^2 \quad (2.11)$$

Hence

$$V_2 = V_1 + \frac{P - iQ_n}{V_2^*} \times (R + iX) \quad (2.12)$$

As long as the wind power capacity is within the limit imposed by the overvoltage limit, the angle between V_1 and V_2 is usually small and the magnitude of V_2 is usually close to 1 pu. Hence it follows that:

$$|V_2| - |V_1| \approx PR + Q_n X \quad (2.13)$$

Since the length of the cable between any two buses in distribution networks can be considered electrically short, the capacitance part can also be neglected. Hence for most practical cases of a short line

$$\Delta|V| \approx PR + QX \quad (2.14)$$

where $\Delta|V| = |V_2| - |V_1|$. From (2.14), one can see that the higher the value of P , the larger the increase in voltage level at bus 2 (PCC) will be. Thus, depending on the power output from the wind farm and the network impedance between the wind farm and the substation, this can cause an overvoltage in the network.

Fig. 2.12a shows the voltage at the PCC for different cable types (given in Table 2.1) and for varying level of wind power. The error introduced in calculating the voltage by using (2.14) is shown in Fig. 2.12b. The calculation is done assuming the distance between the PCC and the substation is 5km and the wind farm operates at unity power factor. However, similar results are obtained for wind power operating at power factors different from unity.

It can be clearly seen from Fig. 2.12a that the voltage level increases with the increase in the wind power injection. Moreover, the amount of wind power that can be installed without violating the $\pm 5\%$, also known as the wind power hosting capacity of the network, decreases with the increase in per km resistance of the cable. This is evident from (2.14), since the power output from the wind turbine is mainly composed of active power, the voltage rise is approximately proportional to the resistance of the cable. Moreover, given that the capacity of the wind power is within the hosting capacity of the network, Fig. 2.12b shows that the error introduced by using the approximate formula is less than 0.4%.

Though $\pm 5\%$ voltage limit has been used in Fig. 2.12a, the Swedish AMP standard specifies the limit at the PCC with the first customer to be within $\pm 2.5\%$ while $\pm 5\%$ requirement is fulfilled at the terminal of the wind power installation [62]. Thus, with the AMP standard voltage limits in place, the hosting capacity of the network in Fig. 2.10 will be lower than those implied by Fig. 2.12a. However a better understanding of the system condition may allow a voltage rise higher than those specified by the AMP manual.

2. WIND POWER AND ITS IMPACT ON A DISTRIBUTION SYSTEM

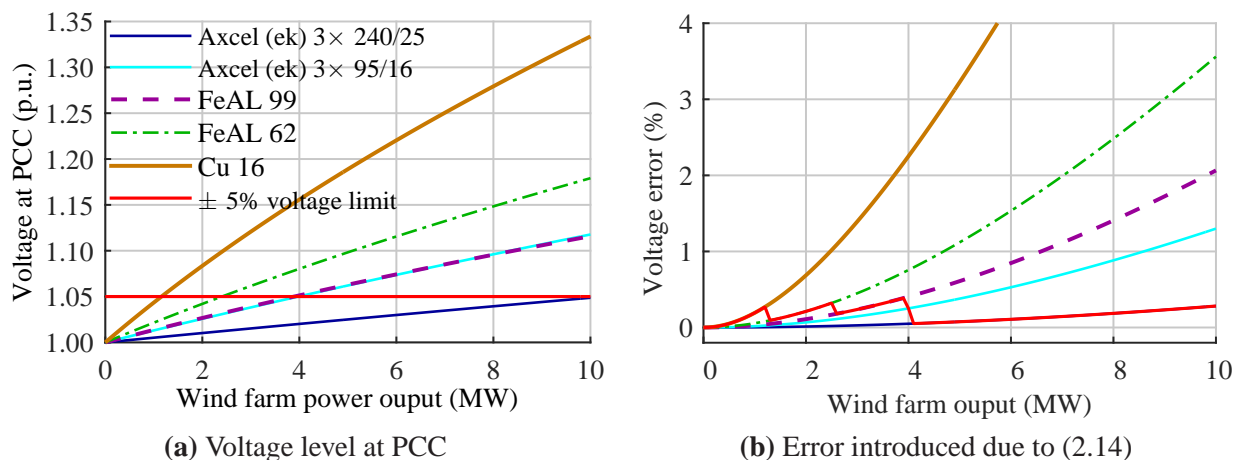


Figure 2.12: Voltage rise effect of wind power.

Table 2.1: Cable types and their characteristic [60, 61]

Type	Conductor	Resistance r (Ω/km)	Reactance x (Ω/km)	Shunt reactance $b_c/2$ (S/km)	X/R	Current rating (A)
Underground cable	AXCEL(EK) 3X240/25	0.125	0.085	6.28E-05	0.679	360
	AXCEL(EK) 3X95/16	0.320	0.094	4.40E-05	0.295	215
Overhead line	FEAL 99	0.336	0.354	1.88E-06	1.053	435
	FEAL 62	0.535	0.369	1.88E-06	0.689	305
	Cu 16	1.100	0.385	1.88E-06	0.350	120

2.2.5 Overloading

The components of a distribution system, such as cables and transformers, can continuously carry only up to a given current level. This limit is based on their thermal rating and varies depending on surrounding weather condition and altitude [63].

The introduction of wind power can have both positive and negative effect on the loading level of distribution system components. If the capacity of the wind power is relatively low compared to the load in the system, it can reduce the power flow through network thereby relieving the thermal stress on the system components. It may also decrease the system loss. On the other hand, if the installed wind power in the distribution system is relatively high there will be a substantial reverse power flow. This reverse power flow can also be higher than the forward power flow that used to flow through the system before the introduction of wind power. This of course will increase both the thermal stress in the network components and the system loss. Under special cases, this reverse power flow can even exceed the thermal rating of the network components, resulting in an overloading situation.

For example, Table. 2.2 provides the maximum current flows through the cables for the case considered in Fig. 2.12. It can be seen that for the case of AXCEL(EK) 3X240/25 cable, the thermal

limit is violated. Hence, even though the voltage limit allows the installation of almost 11 MW wind power capacity, the thermal limit imposes a considerable reduction on the allowed level of wind power capacity.

Fig.2.13 shows the hosting capacity of different cable types at different distances from the substation. In the figure the horizontal part of the different lines shows the hosting capacity as limited by the thermal capacity of the different cables whereas the exponentially decaying part shows the hosting capacity as limited by the overvoltage limit. It can be seen that for highly resistive cables overvoltage starts to limit the hosting capacity after a short distance.

Table 2.2: The maximum current flows through the conductors for the case considered in Fig. 2.12

Conductor	Current rating (A)	Maximum wind power capacity based on voltage limit (MW)	Maximum current flow through the cable (A)
AXCEL(EK) 3X240/25	360	10.6	556
AXCEL(EK) 3X95/16	215	4.0	210
FE-AL 99	435	4.0	210
FE-AL 62	305	2.4	126
Cu 16	120	1.0	52

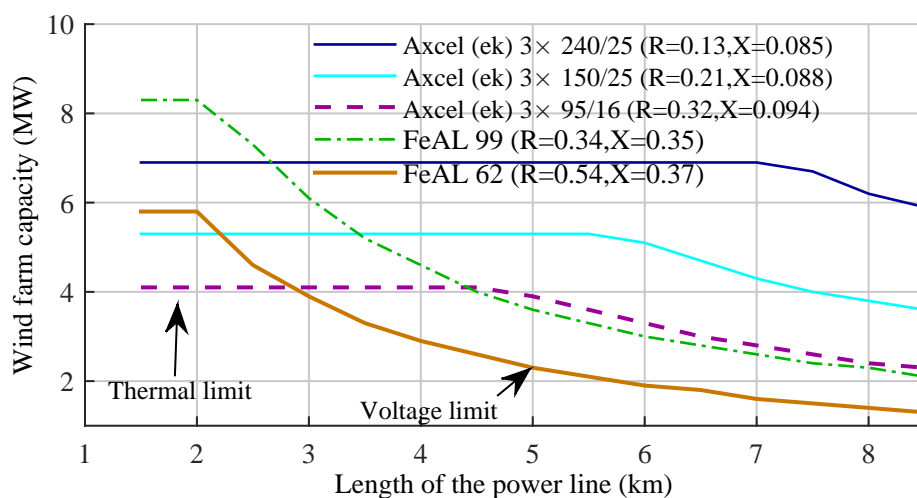


Figure 2.13: Maximum wind power hosting capacity of a cable considering both loading capacity of the cable and overvoltage in the network.

2.3 Summary

This chapter discusses the stochastic nature of wind power and the impact of wind power integration in medium voltage distribution systems. Wind power has a stochastic nature with a high level of correlation between wind parks at distribution system level. The long term wind speed distribution at a particular location can be roughly represented using a simple and concise mathematical expression, i.e. the Weibull distribution. For wind power planning studies this data can be used

2. WIND POWER AND ITS IMPACT ON A DISTRIBUTION SYSTEM

along with the power curve of a wind turbine to assess the expected energy yield of a given wind power installation.

The introduction of wind power in a given distribution system poses a number of known power quality and reliability concerns. Overvoltage and overloading can occur more or less independent of the generator technology. However, other impacts of wind power—such as flicker and harmonic emission, increased fault level—depend on the technology of the generator system of the wind turbine. Flicker emission, for example, is higher in fixed speed wind turbines while voltage harmonics are introduced mainly due to variable speed wind turbines. The fault current contribution is highest with Type A wind turbines while significant fault currents are also injected by Type B and C wind turbines. Type D wind turbines, on the other hand, have a low level of fault current contribution as determined by the overcurrent capability of the converter system.

Flicker emission is directly related to the stochastic nature of wind power and harmonics is indirectly related to it since power electronic converters are used to avoid the negative impact of the stochastic nature. The other integration issues can arise due to any type of DG and are not specific to DGs with intermittent output.

3

Effect of wind power on frequency of tap changes

This chapter is devoted to the investigation of the issue of wind power related to the increase in the frequency of tap changes (FTC). The chapter starts by providing a background to the issue. This is followed by a formulation of a mathematical model that can be used in assessing the effect of wind power on the FTC. In the end, the results of a case study based on measured load, wind, and network data is provided.

3.1 Introduction

Substation transformers are the most critical components of a distribution system. Since they are capital intensive, only a small number of transformers supply power to a large number of customers in a distribution system. Hence high availability of these components is given the utmost importance by any DSO.

The failure of a transformer, besides jeopardizing the reliability of the distribution system, will expose the DSO to a huge amount of cost. The causes of transformer failure are numerous [64–69]. However the majority of transformer failures can be traced back to a faulty tap changer [67–70]. Hence, in terms of the reliability of the transformer, tap changers can be considered as the critical part of the transformer. This is evident from the extensive literature that is devoted for condition monitoring and maintenance of tap changers [69–75].

The main reasons for the failure of tap changers are the erosion of the diverters contact due to switching arcs, the wear and tear of the mechanical components such as the energy accumulator springs, carbon formation in the diverter oil caused by arcing, and breakdown of the insulating materials due to accumulation of sludge. Among these, the first three are directly related to the number of tap operations that occur in tap changers. Especially the wear in the diverter contacts depends not only on the number of tap changes but also on the transformer loading during the tap change [75].

With the increased introduction of wind power in distribution systems, some DSOs are concerned about its possible effect on the wear and tear of the tap changers. This concern mainly arises from

3. EFFECT OF WIND POWER ON FREQUENCY OF TAP CHANGES

a fluctuating nature of wind power as well as the possible increase in the power flow through the transformer. The fluctuating power output from the wind turbines can introduce high power flow fluctuation through the transformer. This may ultimately lead to an increase in frequency of tap changes (FTC). If this is the case, considering the power system is already vulnerable to wear and tear due to aging, the DSO may limit the integration of wind power to its network to avoid potential increase in maintenance costs or unexpected tap changer failures. Hence, such concerns may hinder the integration of renewable energy sources at a time governments are working to increase the share of these energy sources.

However the investigation of the effect of wind power integration on the FTC is given only a minor attention. To the author's knowledge, published works that even mention the issue of FTC in relation to wind power integration are limited to [18, 76–78]. In this chapter, a detailed analysis of the effect of wind power integration on the FTC is carried out. Moreover, most variable speed wind turbines have the capability to provide a considerable amount of controllable reactive power support. Thus, a further investigation is carried out to use this readily available reactive power from the wind turbines to decrease the FTC. Such investigation is valuable because, as mentioned above, tap changers are exposed to wear depending on the number of operation they have undergone. Moreover reactive power can provide a better voltage regulation at secondary side of the transformer since, unlike tap changer, it almost have no a time delay in operation.

Thus, the following section formulates the mathematical model that can be used to determine the number of tap changes in a given distribution. Later on, the model is further developed to incorporate reactive power compensation (RPC) as a means to reduce the FTC.

3.2 Model set up for analyzing the effect of wind power on frequency of tap changes

To analyze the effect of wind power on the FTC, one has to determine the FTC with and without wind power. Thus, a mathematical model is needed to determine the FTC in each case. Such a model can be used to carry out a series of load flow calculations using the network, load and wind power data as inputs. The main aim of these load flow calculations is to determine the tap position at each time step satisfying the different equality and inequality constraints.

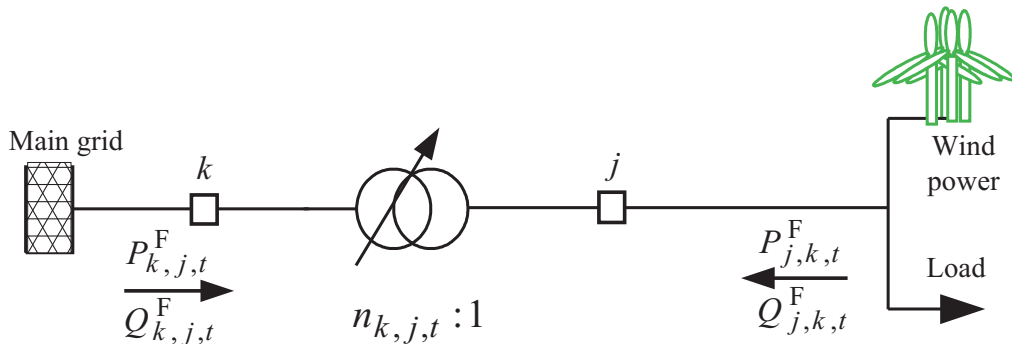


Figure 3.1: A simple distribution network with wind power and load connected.

3.2 Model set up for analyzing the effect of wind power on frequency of tap changes

During a load flow calculation at time step t , the difference between the tap ratio at time t , $n_{k,j,t}$, and $t - 1$, $n_{k,j,t-1}$ needs to be as small as possible while keeping the voltage within a given range (see Fig. 3.1). Let this difference be the tap step taken at time t i.e. $W_{k,j,t}$, which can assume positive or negative value. Thus the load flow calculation at each time step, t , can be formulated as an optimization problem with the objective function O_t to minimize the number of tap changes at each time step t :

$$\min_W O_t := \sum_k \sum_j W_{k,j,t}^2 \quad (3.1)$$

where

$$k \in K$$

K set of all buses excluding the buses connected to the non tap side of the transformer

$$j \in J$$

J set of all buses excluding the buses connected to the tap side of a transformer.

Subject to equality and inequality constraints described as follows.

3.2.1 The inequality constraints

The inequality constraints include:

- The limit on secondary side voltage of the transformer,

$$V_k^{\min} \leq V_{k,t} \leq V_k^{\max} \quad (3.2)$$

where

$V_{k,t}$ voltage magnitude at node k and time t

V_k^{\min} the maximum voltage limit at the secondary side of the transformer

V_k^{\max} the minimum voltage limit at the secondary side of the transformer

- The limit on the available range of tap ratio,

$$n_{k,j}^{\min} \leq n_{k,j,t} \leq n_{k,j}^{\max} \quad (3.3)$$

where $n_{k,j}^{\min}$ and $n_{k,j}^{\max}$ are the maximum and minimum tap ratios that the tap changer can attain.

- The limit on the available active and reactive power of generators at each node in the network,

$$\begin{aligned} P_{i,t}^{\min} &\leq P_{i,t} \leq P_{i,t}^{\max} \\ Q_{i,t}^{\min} &\leq Q_{i,t} \leq Q_{i,t}^{\max} \end{aligned} \quad (3.4)$$

where

3. EFFECT OF WIND POWER ON FREQUENCY OF TAP CHANGES

$P_{i,t}$	active power produced at bus i and time t
$P_{i,t}^{\max}$	maximum value of active power production at bus i and time t
$P_{i,t}^{\min}$	minimum value of active power production at bus i and time t
$Q_{i,t}$	reactive power produced at bus i and time t
$Q_{i,t}^{\max}$	maximum available values of reactive power at bus i and time t
$Q_{i,t}^{\min}$	minimum available values of reactive power at bus i and time t
i	$\in \Xi$
Ξ	a set containing all buses in the network

In the case study, it is only at the slack bus (infinite grid) that the active and reactive power is produced. Hence $P_{j,t}$ and $Q_{j,t}$ is limited to zero at all buses except the slack bus. Wind power generation is included into the load flow equations as a negative load with unity power factor.

3.2.2 Equality constraints

The equality constraints consist of:

- The load flow equations,

$$\begin{aligned} P_{i,t} - P_{i,t}^D &= \sum_u Y_{i,u} V_{i,t} V_{u,t} \cos(\theta_{i,u} + \delta_{u,t} - \delta_{i,t}) \\ Q_{i,t} - Q_{i,t}^D &= -\sum_u Y_{i,u} V_{i,t} V_{u,t} \sin(\theta_{i,u} + \delta_{u,t} - \delta_{i,t}) \end{aligned} \quad (3.5)$$

where

$P_{i,t}^D$	active power consumed at bus i and time t
$Q_{i,t}^D$	reactive power consumed at bus i and time t
$Y_{i,u}$	magnitude of the $(i,u)^{th}$ element of the bus admittance matrix
$\theta_{i,u}$	angle of the $(i,u)^{th}$ element of the bus admittance matrix
$\delta_{i,t}$	voltage angle at node i and time t
u	$\in \Xi$

- The relation between consecutive tap ratios,

$$n_{k,j,t} = n_{k,j,t-1} + W_{k,j,t} \Delta U \quad (3.6)$$

where ΔU is voltage change in per unit value for one tap step.

In the load flow equations the tap ratio of the transformer may change from one time step to another. This tap change affects three elements of the admittance matrix, which increases the number of variables in the model. Clearly, this imposes an extra computational burden on the simulation. Hence the load flow equations in (3.5) are modified so that they do not use the bus admittance matrix directly. The discussion of these modified load flow equations is provided as follows.

3.2.3 Modified load flow equations

The link between two buses is usually either a power line or a transformer. The power line can be represented by an equivalent π -model as shown in Fig. 3.2.

3.2 Model set up for analyzing the effect of wind power on frequency of tap changes

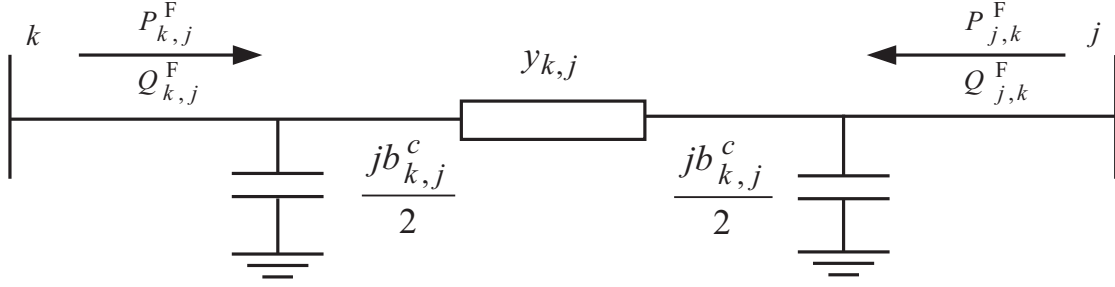


Figure 3.2: π -model of a power line.

A transformer between two buses is represented by the equivalent π -model shown in Fig. 3.3

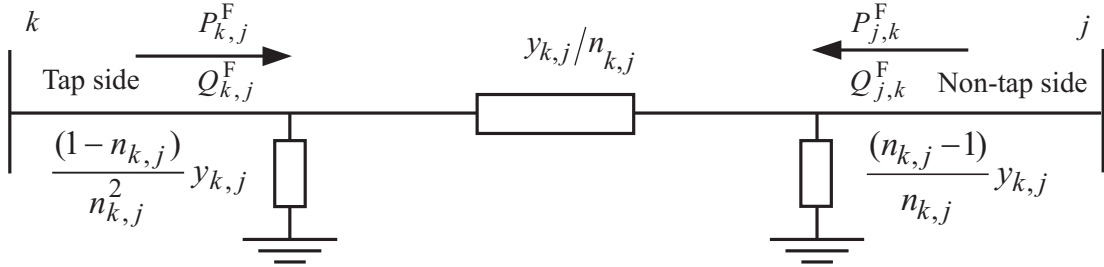


Figure 3.3: Equivalent circuit of a tap changing transformer [79].

Hence, for the network which contains both of these elements, i.e. power lines and transformers, the link between any two buses can be represented as in Fig. 3.4.

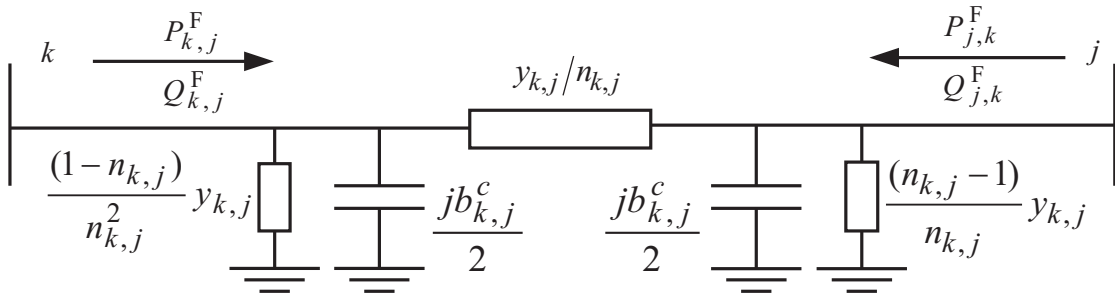


Figure 3.4: An equivalent model for a link between any two nodes.

The active $P_{k,j,t}^F$ and reactive $Q_{k,j,t}^F$ power flow from bus k to any other bus j at time t is given by

$$\begin{aligned} P_{k,j,t}^F &= \left(\frac{V_{k,t}}{n_{k,j,t}} \right)^2 g_{k,j} - \frac{V_{k,t}V_{j,t}}{n_{k,j,t}} y_{k,j} \cos(\delta_{j,t} - \delta_{k,t} + \varphi_{k,j}) \\ Q_{k,j,t}^F &= -V_{k,t}^2 \left(\frac{b_{k,j}}{n_{k,j,t}^2} + \frac{b_{k,j}^c}{2} \right) + \frac{V_{k,t}V_{j,t}}{n_{k,j,t}} y_{k,j} \sin(\delta_{j,t} - \delta_{k,t} + \varphi_{k,j}) \end{aligned} \quad (3.7)$$

where

3. EFFECT OF WIND POWER ON FREQUENCY OF TAP CHANGES

- $b_{k,j}$ series susceptance between bus k and bus j
- $b_{k,j}^c$ shunt susceptance between bus k and bus j
- $g_{k,j}$ series conductance between bus k and bus j
- $y_{i,u}$ series admittance between bus i and bus u
- $\varphi_{k,j}$ angle of the series admittance between bus k and bus j

and the reverse flow from bus j to bus k is given by

$$\begin{aligned} P_{j,k,t}^F &= V_{j,t}^2 g_{j,k} - \frac{V_{j,t} V_{k,t}}{n_{k,j,t}} y_{j,k} \cos(\delta_{k,t} - \delta_{j,t} + \varphi_{k,j}) \\ Q_{j,k,t}^F &= -V_{j,t}^2 \left(b_{j,k} + \frac{b_{j,k}^c}{2} \right) + \frac{V_{j,t} V_{k,t}}{n_{k,j,t}} y_{j,k} \sin(\delta_{k,t} - \delta_{j,t} + \varphi_{k,j}) \end{aligned} \quad (3.8)$$

In (3.7) and (3.8), if the link between two buses is a cable or overhead line, the tap ratio is one and the equations will represent the power flow in the circuit shown in Fig. 3.2. On the other hand, if the link between two buses is a transformer, the shunt capacitance is equal to zero. Then (3.7) and (3.8) represent the power flow in the circuit shown in Fig. 3.3.

Now the load flow equations in (3.5) are replaced by (3.9) and (3.10) below as equality constraints. For bus in $k \in K$:

$$\begin{aligned} P_{k,t} - P_{k,t}^D &= \sum_j P_{k,j,t}^F \\ Q_{k,t} - Q_{k,t}^D &= \sum_j Q_{k,j,t}^F \end{aligned} \quad (3.9)$$

For bus $j \in J$:

$$\begin{aligned} P_{j,t} - P_{j,t}^D &= \sum_k P_{j,k,t}^F \\ Q_{j,t} - Q_{j,t}^D &= \sum_k Q_{j,k,t}^F \end{aligned} \quad (3.10)$$

Equations (3.7) - (3.10) do not contain the variable bus admittance matrix. In other words, there will be only one variable for a single tap change as opposed to four that would be in (3.5). With the reduction in the number of variables, there will be a reduced computational effort.

3.3 Modeling the use of reactive power compensation to decrease the frequency of tap changes

This section develops the model used for analyzing the use of reactive power from the wind turbines to decrease the FTC.

3.3.1 The objective function

When there is a continuously controllable reactive power from wind turbines, it can be used to decrease the FTC. In principle, for a transformer where the tap is located on the primary side,

3.4 The flow chart of the proposed sequential load flow simulation

reactive power is consumed to avoid a tap increase during low load condition and produced to avoid a tap decrease during high load condition. However reactive power is not consumed or produced when there is no potential tap change or the available reactive power is not sufficient to prevent a tap change. In the latter case, it is better to use tap regulation directly as unnecessary reactive power flow increases system power losses. In order to model this, the objective function is modified to

$$\min_{W,Q} O_t := \sum_k \sum_j a W_{k,j,t}^2 + \sum_i Q_{i,t}^2 \quad (3.11)$$

The term on the far right side is added to produce or consume as minimum amount of reactive power as possible from the wind turbines. On the other hand a is a constant of sufficiently large value added to prioritize using RPC, whenever possible, instead of tap changing.

3.3.2 The constraints

The equality constraints discussed in (3.6), (3.9), (3.10) and the inequality constraints discussed in (3.2), (3.3) holds true here as well.

The reactive power limits, $Q_{i,t}^{\min}$ and $Q_{i,t}^{\max}$ in (3.4), can be defined in terms of a given minimum operating power factor limit, Φ^{\min} . These limits can also be constrained by the thermal capability of the wind turbine, S_i^{\max} . This happens when the wind turbines are operating around the rated power output. Hence for a given wind turbine at bus i , the reactive power limits are given by

$$-Q_{i,t}^{\text{cap}} \leq Q_{i,t} \leq Q_{i,t}^{\text{cap}} \quad (3.12)$$

where

$$Q_{i,t}^{\text{cap}} = \min \left(\sqrt{(S_i^{\max})^2 - P_{i,t}^2}, \frac{P_{i,t} \sqrt{(1 - (\Phi^{\min})^2)}}{\Phi^{\min}} \right) \quad (3.13)$$

In case Φ^{\min} is extended to zero, i.e. when the wind turbines are providing reactive power support even when they are not producing active power, (3.12) and (3.13) can be reduced to

$$-\sqrt{(S_i^{\max})^2 - P_{i,t}^2} \leq Q_{i,t} \leq \sqrt{(S_i^{\max})^2 - P_{i,t}^2} \quad (3.14)$$

3.4 The flow chart of the proposed sequential load flow simulation

The model formulated in this chapter is to be used in a radial distribution system where there are usually one or two transformers in parallel. Under such condition the binary variable, $W_{k,j,t}$, can be replaced by a continuous variable, $W'_{k,j,t}$, and (3.15) can be used to calculate $W_{k,j,t}$. This results in a model which can be solved more efficiently using solvers developed for standard nonlinear programs, e.g. [80]. However whenever this model is used in networks where there are a couple of tap changing transformers at different locations there could be an optimality problem. Hence

3. EFFECT OF WIND POWER ON FREQUENCY OF TAP CHANGES

under such situation the problem should be solved as mixed integer nonlinear programming model (MINLP).

$$W_{k,j,t} = \begin{cases} \text{round}(W'_{k,j,t}), & \text{if } |W'_{k,j,t}| \leq \varepsilon \\ \text{ceil}(W'_{k,j,t}), & \text{if } W'_{k,j,t} > \varepsilon \\ \text{floor}(W'_{k,j,t}), & \text{if } W'_{k,j,t} < -\varepsilon \end{cases} \quad (3.15)$$

where ε is a very low value chosen based on the sensitivity of the tap operating system i.e. how sensitive it is when the voltage is above the upper or lower bound.

The flow chart of the overall simulation is presented in Fig. 3.5.

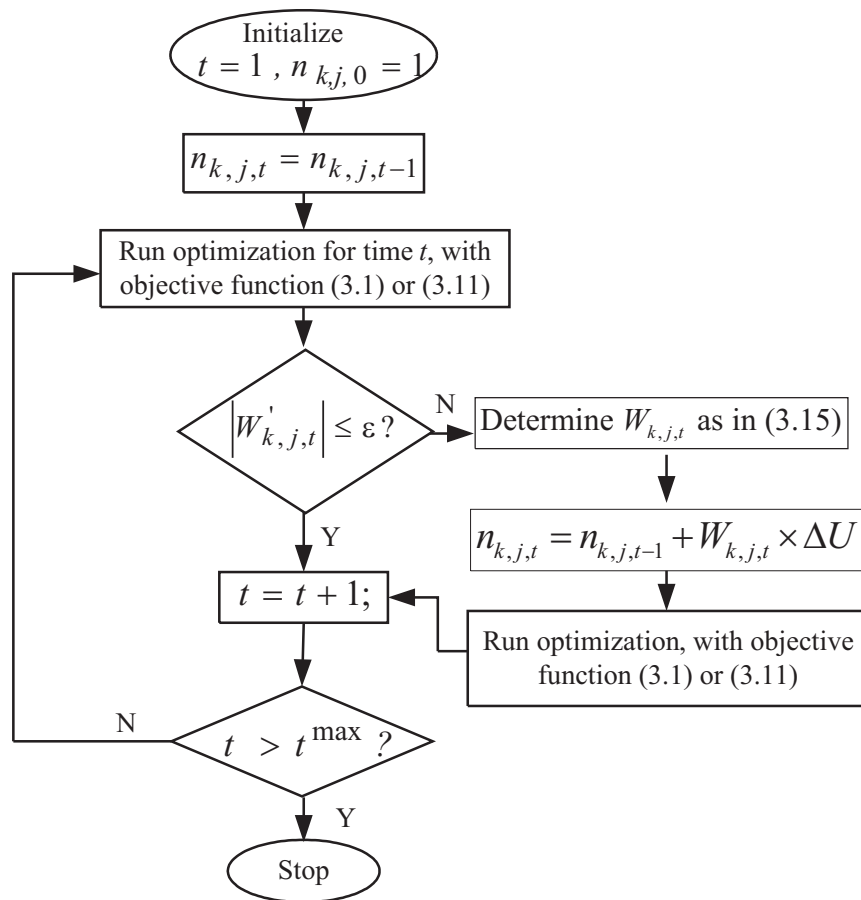
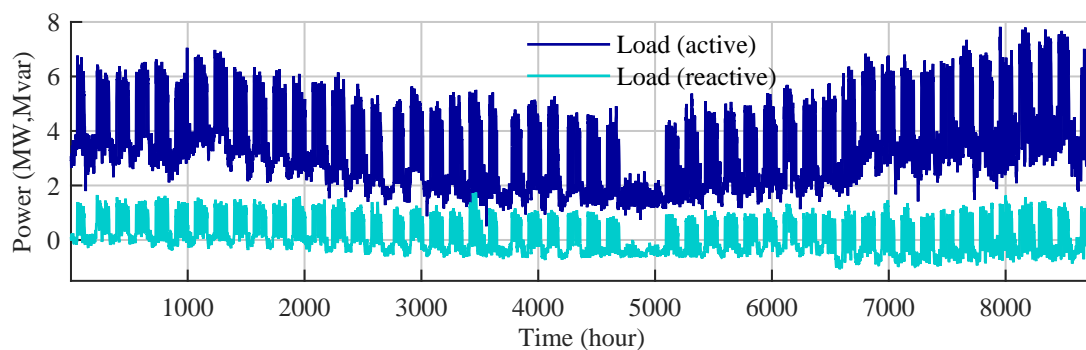


Figure 3.5: The flow chart of the proposed sequential load flow simulation.

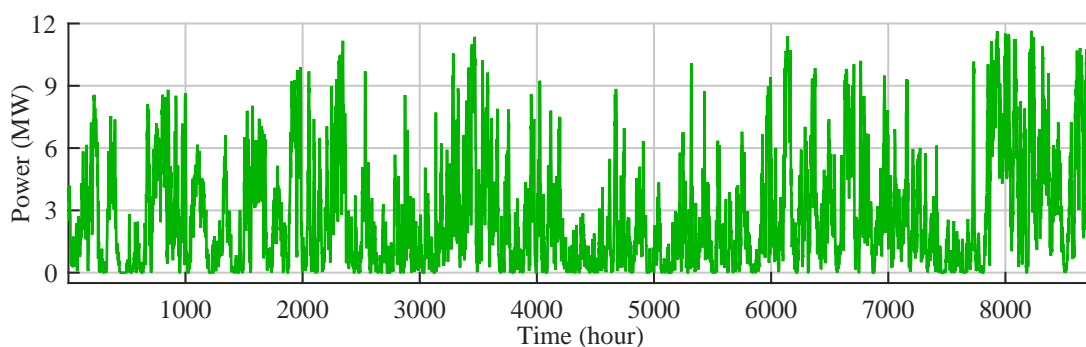
3.5 Case Study

3.5.1 Network and data description

The case study is based on a rural 11 kV network operated by Falbygdens Energi located in Falköping area in Sweden. The network is fed by a 40 kV grid through a 10 MVA $45 \pm 8 \times 1.67\% / 11.5$ kV transformer with a percentage impedance of 8%. The tap changer regulates the voltage at the secondary side of the transformer with the set point voltage of 10.7 kV and a $\pm 1.2\%$ deadband. In this distribution system, there are 13 wind turbines (composed of Type A, B, and D) installed, with an overall installed capacity of 12.225 MW. From these wind turbines there are hourly measured time series power data available for one year, i.e. 2011. Hourly measured active and reactive power data at the substation are also available for the same year. Active power consumption in the network is then calculated by adding the measured wind power data and active power measurement at the substation. The resulting load and wind power data pattern for the year are presented in Fig. 3.6. Currently the wind turbines operate at unity power factor (PF) setting, thus the reactive power is assumed to come from consumer loads only. Moreover, the simplified form of Falbygdens Energi's network as shown in Fig. 3.7 is used in the forthcoming analysis. That is, both load and wind power are assumed to be directly connected to the substation busbar without any connecting cable in-between. This is valid because as the net active and reactive power measurements are done at the substation.



(a) Load data



(b) Wind power data

Figure 3.6: Load and wind power data pattern for year 2011 in the network.

3. EFFECT OF WIND POWER ON FREQUENCY OF TAP CHANGES

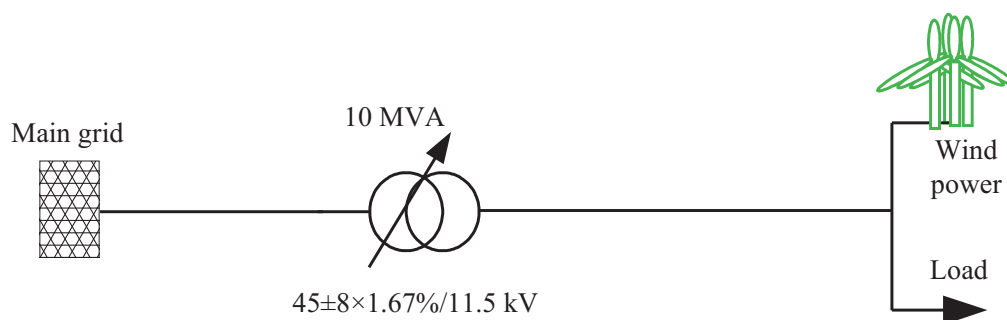


Figure 3.7: Simplified form of Falbygdens Energi's network used in the analysis.

3.5.2 Effect of wind power on frequency of tap changes

The aim here is to find out if wind power may lead to an increase in the FTC. Thus, no RPC from the wind turbines is considered.

With the data described in the above subsection, the mathematical model developed in Section 3.2 is implemented in GAMS. Two cases are investigated:

- Case 1: only consumer load is assumed to be connected to the network without wind power in the system.
- Case 2: both load and wind power are connected to the system. This is the existing system condition.

Fig. 3.8 shows the number of tap changes at each hour of a day summed over one year. It can

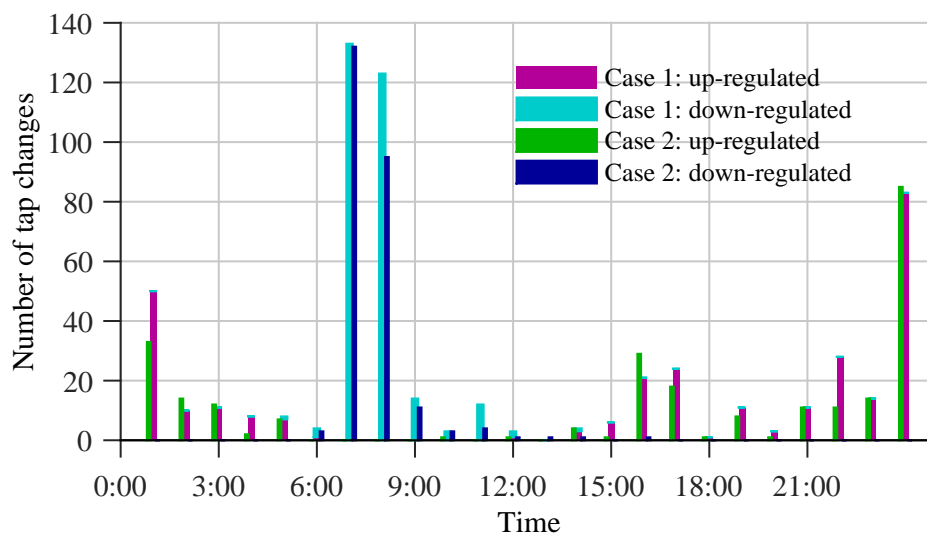


Figure 3.8: Number of tap changes on each hour of a day summed over a year.

be seen that for both cases, the diurnal variation of tap changes follows a similar trend: with a large number of tap changes at 6:00 and 7:00 in the morning and at 23:00 and 0:00 during the night. There are also considerable tap changes at 15:00 and 16:00. Usually the tap changes in the morning (specifically between 5:00 and 10:00) are down regulations to boost the voltage on the

secondary side. During this period, the load increases due to the start up of a factory, connected to this distribution system, and residential loads. During the rest of the day, the tap is usually up-regulated due to the dominance of lighter load conditions than in the morning. The total number of tap changes for Case 1 is 585 and for Case 2 is 505 for one year of operation. Thus, in contrary to our expectation, the FTC has decreased when there is wind power in the distribution system. The reason for the decrease in number of tap changes is explained using Fig. 3.9 and Fig. 3.10.

Fig. 3.9 shows the load and wind power profile for a specific day and Fig. 3.10 shows the tap positions of the tap changer in the same day. It can be seen in Fig. 3.10 that between the period 5:00 and 16:00, there are three tap changes in Case 1 compared to a single tap change in Case 2 (see Fig. 3.10). From Fig. 3.9, one can make two observations. On one hand, the variability of load follows the variability of wind power. These results in a less variable net active power. On the other hand, during part of this period (for example between 14:00 and 20:00) when the net active power increases, the reactive power decreases and vice versa. This, according to (3.16) [81], results in a lower voltage change on the secondary side of the transformer compared to Case 1.

$$\Delta V_t \approx RP_{2,t} + XQ_{2,t} \tag{3.16}$$

where

- ΔV_t voltage difference between reference node ‘1’ (infinite bus) $V_{1,t}$ and node ‘2’ (secondary side of the transformer) $V_{2,t}$
- $P_{2,t}$ active power consumed at node ‘2’
- $Q_{2,t}$ reactive power consumed at node ‘2’
- R resistance between node ‘1’ and ‘2’
- X reactance between node ‘1’ and ‘2’

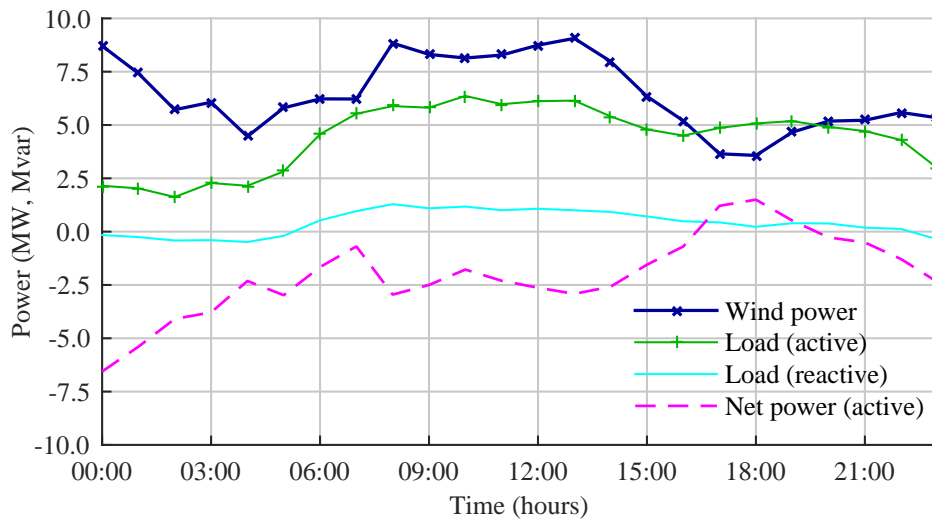


Figure 3.9: Load and wind power profile at specific day of the year.

Moreover wind power causes fluctuation mostly in active power. Fluctuations in active power, according to (3.16), will not lead to significant voltage fluctuations when the X/R ratio of the external grid is high.

3. EFFECT OF WIND POWER ON FREQUENCY OF TAP CHANGES

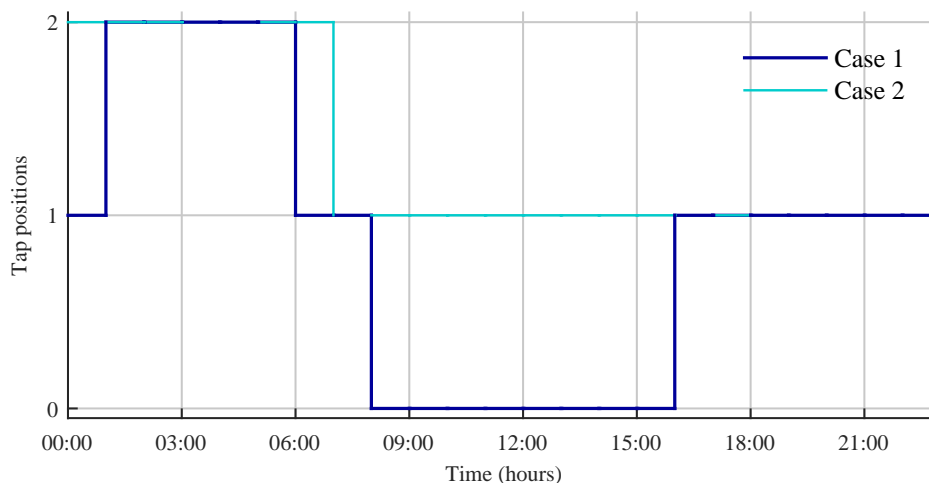


Figure 3.10: Tap position of the tap changer at specific day of the year.

In Fig. 3.9 and Fig. 3.10, the aim is to show how wind power can contribute to a decrease in the number of tap changes in some days. But wind power do also contribute to an increase in the number of tap changes on some other days. However, in this case, wind power has led to a reduction in the total number of tap changes.

Seasonal variations in the number of tap changes is compared in Fig. 3.11. The figure shows that the effect of wind power on FTC changes from one month to another. Though the FTC has decreased in most of the months, there are also months where the FTC has increased because of the wind power. Thus, an analysis based on only one month data, as it has been done in [78], cannot give the true picture of the effect of wind power on the FTC.

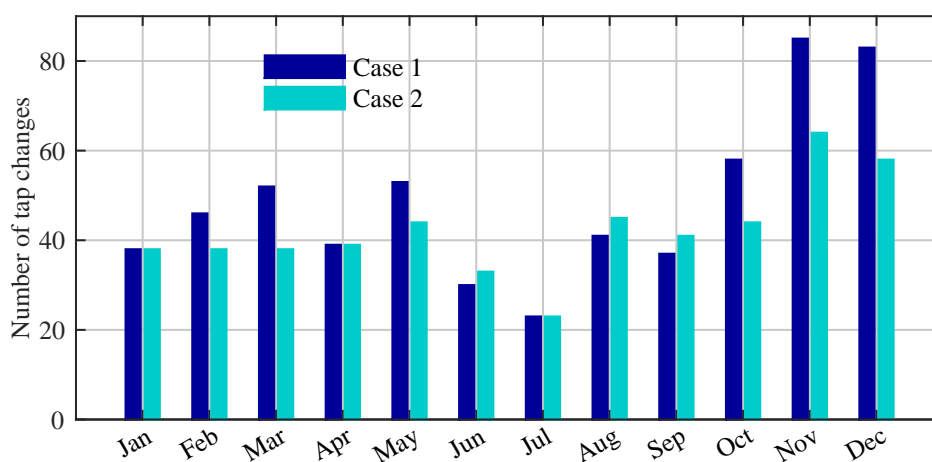


Figure 3.11: Number of tap changes distributed on monthly basis.

3.5.3 Analyzing the frequency of tap changes with a different set of wind power data

In the Section 3.5.2, the analysis of the effect of wind power on the FTC is done based on a particular set of data. To test the validity of the observation made in the previous section, an analysis based on different sets of data may be required. To this end, an analysis is done using a number of synthetic data (WPs1-WPs5 in Fig. 3.12) and one more measurement data (WPM), both having a capacity of around 8 MW. The synthetic data is generated using the stochastic model of wind power proposed in [82]. The load data, on the other hand, is kept the same as the one used in Section 3.5.2. This is valid since, though the details of the data could be different from year to year, the general profile of a load data will remain almost the same from one year to another.

As shown in Fig. 3.12, the FTC with the new wind data lies between 549 and 573 which is still below the number tap changes that occur when there is no wind power. But one can observe that compared to the FTC with the original wind power of the same size (WPO) (i.e. 509), there is an increase by around 10%. These increase is not significant, and it can partly be attributed to the reduction in correlation between the load data and the new wind power data compared to the original one.

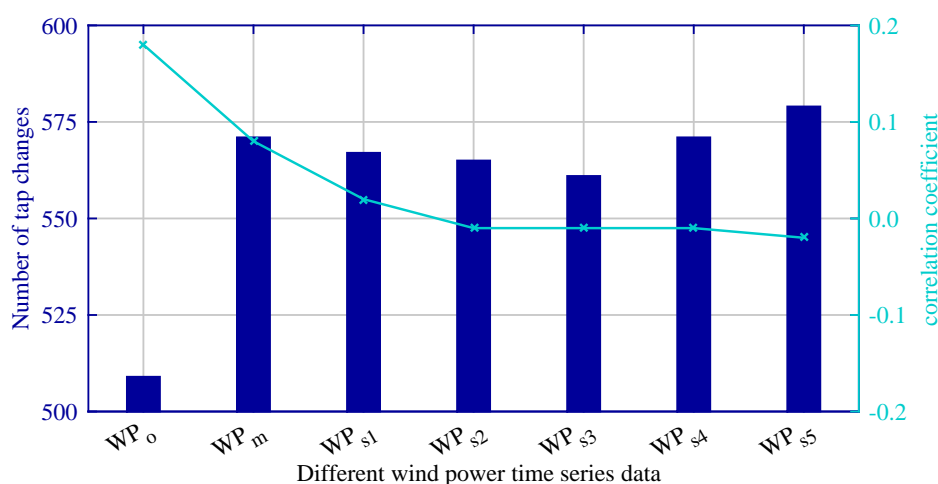


Figure 3.12: Number of tap changes with different wind power time series data.

3.5.4 The frequency of tap changes with different reference voltage at the secondary side of the substation transformer

The discussion up to this point shows wind power contributing to the reduction in FTC. To test if this also holds for some other case, the FTC problem is simulated with different reference voltages at the secondary side of the transformer for varying levels of wind power. The argument is that if the introduction of wind power should decrease the FTC, it would do so irrespective of the voltage set point. The result of the analysis (presented in Fig. 3.13) shows that wind power does not necessarily lead to a decrease in the FTC. However in general the increase in FTC due to wind power is insignificant for the distribution system studied so far. Thus, wind power in such distribution systems does not pose a reliability concern to the transformer tap changers.

3. EFFECT OF WIND POWER ON FREQUENCY OF TAP CHANGES

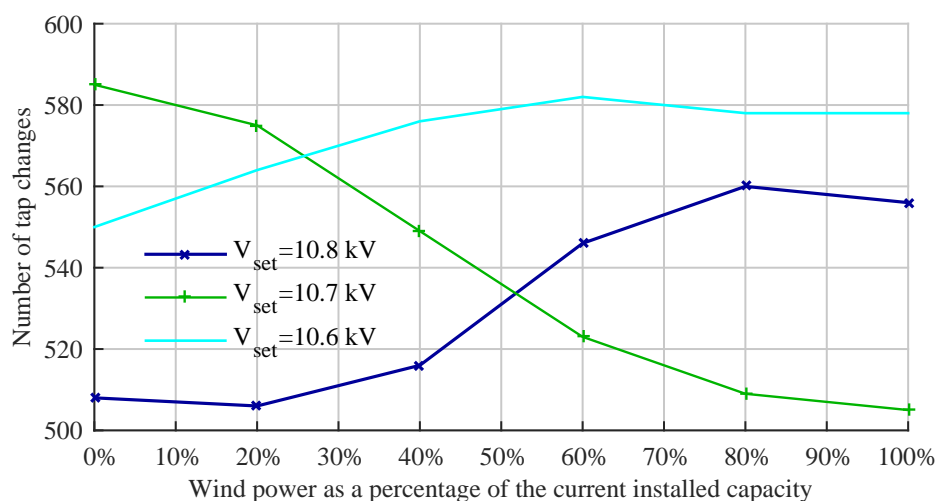


Figure 3.13: The frequency of tap changes for varying level of wind power and different voltage set point.

3.5.5 The frequency of tap changes for varying levels of grid strength

The analysis in the previous sections is done assuming the short circuit capacity (SCC) and the X/R ratio of the external grid to be 171 MVA and 10 respectively. For this distribution system, it is seen that wind power does not pose a significant threat to the FTC. In fact, it may reduce the FTC. In this subsection the same investigation is done for grids with different SCCs and with varying X/R ratios.

Fig. 3.14 shows the trend in FTC as the power penetration level increases for grids with different SCC. The figure shows that, overall, the FTC increases with decrease in SCC. This is understand-

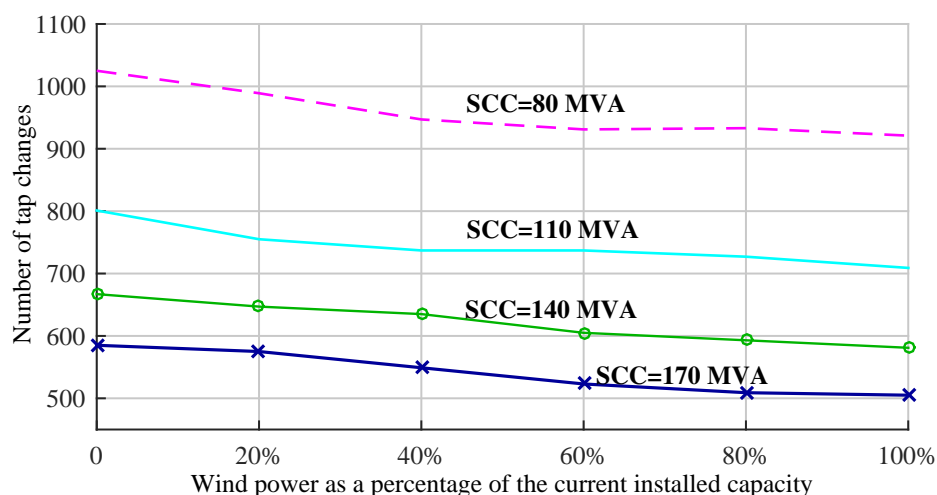


Figure 3.14: Number of tap changes per year for different SCC of external grid with X/R=10.

able as a higher impedance leads to a higher voltage drop for a given loading condition. In other words, for the same variation of transformer loading, the voltage variation will become larger in a weaker grid.

Though the curves in Fig. 3.14 show a general decrease in FTC with an increase in the capacity of wind power, it has already been noted in Fig. 3.13 that wind power does not always lead to a decrease in FTC. However, the similarity in the profile of the curves in Fig. 3.14 can be explained as follows.

A tap change occurs when there is a voltage change at the secondary side of a transformer due to a change in power flow. Hence one can roughly approximate the FTC to be proportional to the voltage change that occurs at each time step t due to power flow changes. In the absence of wind power in the system, the change in voltage at the secondary side of the transformer due to load flow changes is given by (3.16). In the presence of wind power in the system, there are additional fluctuations in active power; this fluctuation causes an additional voltage fluctuation at the secondary side of the transformer which can be given by (3.17). The percentage change in voltage change at the secondary side of the transformer can, thus, be given by (3.18). Since the FTC is proportional to the voltage change at the transformer secondary, (3.19) follows from (3.18).

$$\Delta V_{2,t} \approx \Delta P_{2,t} \times R \quad (3.17)$$

where

$\Delta V_{2,t}$ the change in voltage at node '2' relative to the previous value

$\Delta P_{2,t}$ the change in active power consumption at node '2' due to the wind power

$$\frac{\Delta V_{2,t}}{\Delta V_t} = \frac{\Delta P_{2,t}}{P_{2,t} + Q_{2,t} \times (X/R)} \times 100\% \quad (3.18)$$

and

$$\% \Delta FTC \propto \frac{\Delta P_{2,t}}{P_{2,t} + Q_{2,t} \times (X/R)} \times 100\% \quad (3.19)$$

Equation (3.19) implies that the percentage change in FTC, $\% \Delta FTC$, is proportional to the X/R ratio and is constant for a given X/R ratio irrespective of the SCC of the grid. However the tap change does not only depend on the voltage change at the secondary side of the transformer but also whether the resulting voltage will be outside of the deadband. Hence based on (3.19) one can only roughly expect the implications to hold. Fig. 3.14 proves the same.

The above analysis shows that for an X/R ratio of 10 no significant increase in the FTC is expected due to introduction of wind power operating at unity power factor. Fig. 3.15 provides the results of the analysis with different X/R ratios. The results show that when the X/R ratio gets lower the effect of wind power on the FTC changes becomes considerable. This is clear from (3.19) that for a given active power change, the lower the X/R ratio the bigger is the change in FTC.

As mentioned above, the results presented in Figs. 3.14- 3.15 are based on assuming a wind farm directly connected to the substation, i.e. without any connecting cable in-between. However, almost similar results are observed even when there is a cable or an overhead line connecting the wind power plant to the substation, as shown in Fig. 3.16. The results in the figure compares the FTC with a wind farm located at different distances from substation and connected to the station through different cable types; the external grid here is assumed to have a SCC of 80 MVA with X/R ratio of 5.

3. EFFECT OF WIND POWER ON FREQUENCY OF TAP CHANGES

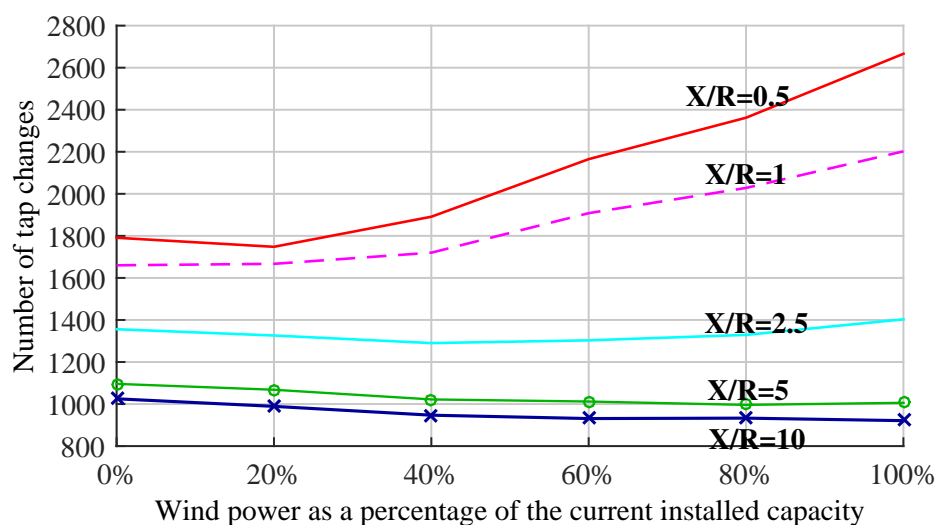


Figure 3.15: Number of tap changes per year in a distribution system connected to 80 MVA external grid having different X/R ratio.

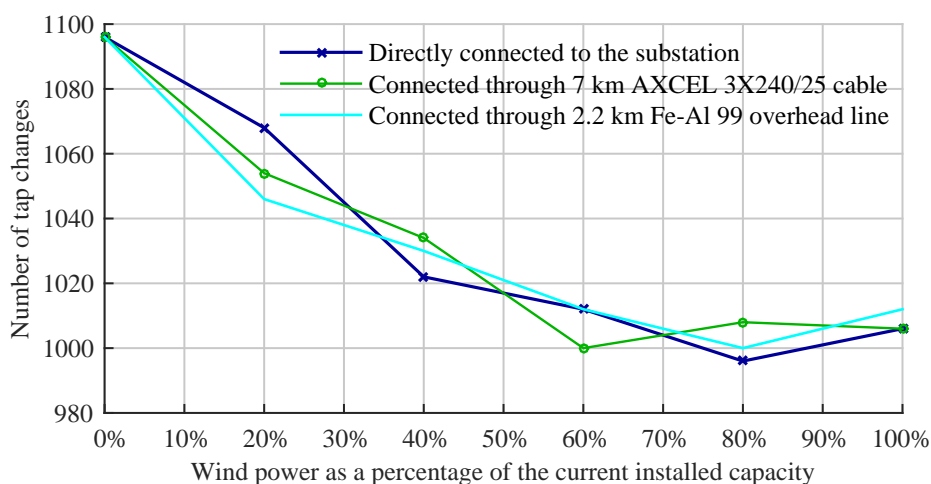


Figure 3.16: Comparing the FTC when the wind power is at varying distance from the substation.

Based on the analysis so far, it can be concluded that for distribution networks with an X/R ratio greater than 5, wind power operating at unity power factor does not cause a reliability concern for the tap changers. But for distribution networks with an X/R ratio less than 5, there could be some problems of increase in FTC due to wind power introduction. This is especially true for those grids with an X/R ratio less than 2.5.

3.5.6 The effect on FTC when wind turbines consume reactive power

This section investigates the effect on FTC of wind power operating at a power factor other than unity. This situation may arise when the wind turbines connected to the distribution system are of Type A or B, which cannot provide a controllable reactive power support. As shown in Fig. 3.17, when the wind turbines operate at a PF other than unity there is a considerable increase in the FTC.

Of course, the closer the PF to unity is, the lower is the increase in FTC due to wind power. Some DFIG wind turbines work at around 0.99 PF lagging and such operation is not seen to increase the FTC considerably. Hence in a distribution system where there is a concern on the number of tap changes, it is necessary to make sure that only wind turbines that are able to operate at or close to unity power factor are being installed.

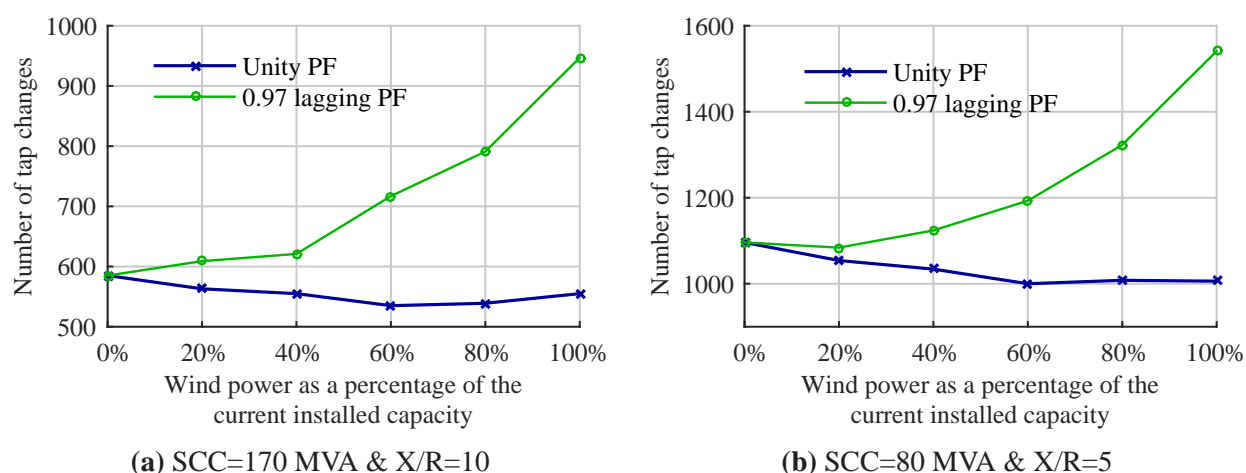


Figure 3.17: The effect on FTC of wind turbines working at power factor other than unity.

3.5.7 Using reactive power compensation to reduce the number of tap changes

This section investigates the use of reactive power from wind turbines to decrease the FTC. The need for reducing the FTC may arise due to the existence of a high level of FTC induced by load changes. It can also be induced by a high level of wind power for the reasons mentioned in Subsections 3.5.5 and 3.5.6. The current practice for decreasing the FTC in such conditions is to increase the deadband of the tap changer, say from 1.2% to 1.6% or more. However this solution may pose voltage quality problems.

Among the available wind turbines in the network (described in Section 3.5.1), a wind farm composed of four 0.8 MW wind turbines is chosen to provide reactive power support to the grid. These wind turbines are of the variable speed design (full converter based) from Enercon and are recently installed at a site close to the substation. Since these wind turbines have started their production as of March 2011, the wind power and load data starting from March 2011 are used for this analysis. The wind power from the rest of the wind turbines is aggregated with the load. The simplified diagram of the resulting system is shown in Fig. 3.18.

The majority of grid codes require that wind turbines should have a capability of operating between 0.95 PF lagging and leading at full production [83]. This indicates that, for these wind turbines, the rated power of the converter should be at least five percent higher than the full power output of the wind turbines. Hence S_i^{\max} , for each wind turbine, is taken to be five percent higher than the rated power output.

Fig. 3.19 compares the number of tap changes with and without RPC when the wind turbines are controlled to operate between 0.95 lagging and leading power factor so as to avoid a tap change

3. EFFECT OF WIND POWER ON FREQUENCY OF TAP CHANGES

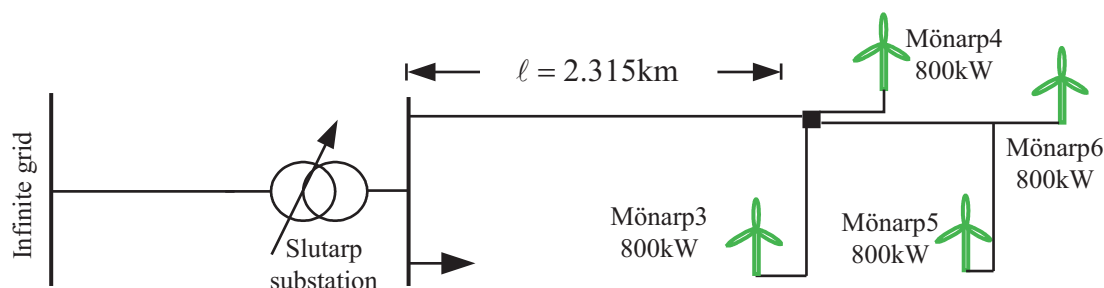


Figure 3.18: Simplified diagram of the 10 kV distribution network.

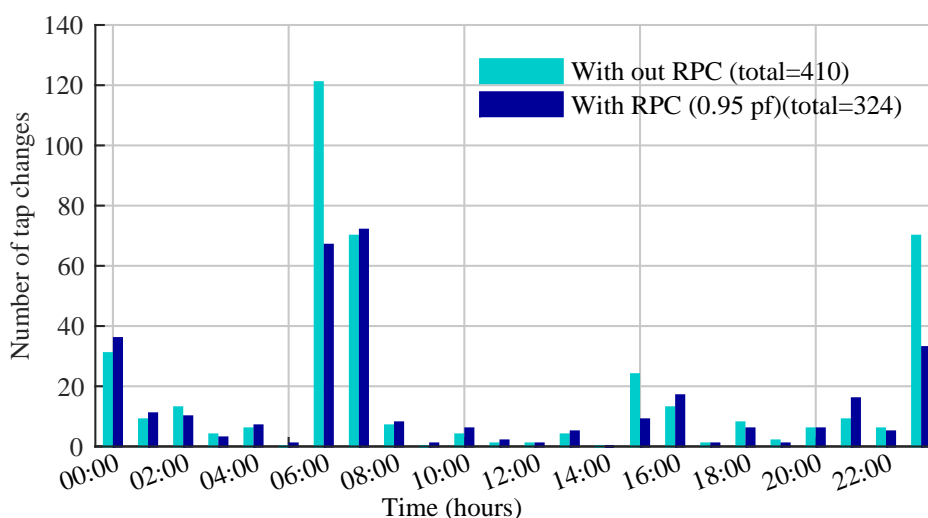


Figure 3.19: Number of tap changes on 24hr basis with and without RPC.

whenever possible. The figure shows a decrease in the FTC by 21%. Reactive power is consumed at light load or at windy conditions when there is a potential tap up-regulation. This brings down the voltage at the substation busbar and avoids an up-regulation of the tap. Reactive power is supplied to boost the voltage during high loading condition to avoid a potential tap down-regulation. In this way, reactive power contributes to the reduction in the number of tap changes. One can also notice that RPC sometimes only delays a tap change to a later time. This is seen in Fig. 3.19 when the number of tap changes decreases at 23:00 while the number of tap changes increases at 00:00. However, this delay of tap changes does not appear to be a significant issue.

Table 3.1 summarizes the main points that can be used in the comparative analysis of using RPC to reduce the FTC. It also includes results from some more scenario analysis. The results in Table 3.1 are for a grid with SCC=171 MVA and X/R=10. Table 3.2 provides the results of the same analysis for a weaker grid having SCC=80 MVA and X/R=1. Moreover in Table 3.1 and 3.2, the wind turbines are located 2.3 km from the substation. On the other hand, Table 3.3 provides the results of the same analysis for wind turbines located 15 km from the substation. The analysis with longer distance is used to see if the magnitude of the impedance between the wind farm and the substation has some effect on the proposed solution. Over all, the results provided in Table 3.1-3.3 shows that RPC can be used for reducing the FTC in most grids.

In terms of achieving a specific level of reduction in the FTC, the distance of wind turbines from

Table 3.1: Effect of using RPC to reduce the FTC in a distribution system connected to a stronger grid (SCC=171 MVA,X/R=10)

Case	Φ^{\min}	Change in the FTC (Δ FTC)		Average power Loss (kW)	Reactive power from the wind turbines	
		Δ FTC	% Δ FTC		Average (kVAr)	Maximum (MVAr)
1	1	0	0	16	0	0
2	0.95	-86	-21	16	15	0.7
3	0.90	-124	-30	16	25	0.9
4	0.80	-166	-40	16	36	1.0
5	0.0	-410	-100	14	176	1.0

Table 3.2: Effect of using RPC to reduce the FTC in a distribution system connected to a weaker grid (SCC=80 MVA and X/R=1)

Case	Φ^{\min}	Change in the FTC (Δ FTC)		Average power Loss (kW)	Reactive power from the wind turbines	
		Δ FTC	% Δ FTC		Average (kVAr)	Maximum (MVAr)
1	1	0	0	86	0	0
2	0.95	-394	-22	85	33	1.0
3	0.90	-502	-28	85	64	1.4
4	0.80	-663	-37	85	121	2.0
5	0.0	-1 738	-97	91	724	3.4

Table 3.3: RPC from wind turbines located 15 km away from the substation (SCC=171 MVA,X/R=10)

Case	Φ^{\min}	Change in the FTC (Δ FTC)		Average power Loss (kW)	Reactive power from the wind turbines	
		Δ FTC	% Δ FTC		Average (kVAr)	Maximum (MVAr)
1	1	0	0	28	0	0
2	0.95	-90	-22	28	16	0.8
3	0.90	-120	-29	28	25	1.0
4	0.80	-166	-40	28	36	1.0
5	0.0	-416	-100	27	176	1.0

the substation has no effect at all. That is, almost the same amount of reactive power is necessary to achieve the same level of reduction in the FTC. Thus, the cable does not make any significant impact on the reactive power requirement from the wind turbines. However, compared to strong grids, in weak grids more reactive power is required from the wind turbines to achieve the same level of reduction in FTC. This is because, in weak grids, higher number of tap changes need to be avoided to achieve the same percentage of reduction in the FTC.

Generally, the change in the network loss relative to the base case (Case 1) is found to be negligible in all cases except in Case 5 of Table 3.2. This is apparent from the fact that, in this case, the network resistance is relatively large and the amount of reactive power consumed or produced by the wind turbines relatively high.

Finally, the analysis presented in this subsection is carried out assuming constant power loads,

3. EFFECT OF WIND POWER ON FREQUENCY OF TAP CHANGES

however similar results are obtained assuming constant impedance load.

3.5.7.1 Reactive power flow in the network

This subsection compares the reactive power consumption in the network with and without RPC in the network to see if RPC would result in unfavorable grid operating conditions. The results of the analysis for Case 5 (worst case in terms of reactive power consumption) from Table 3.1 are presented here in Fig. 3.20 and Fig. 3.21. However similar results are observed for the analysis in Tables 3.2 and 3.3.

Fig. 3.20 shows that reactive power is consumed during light load or windy conditions and produced at heavy load conditions. From the point of the external grid, this is beneficial because during low load conditions the voltage in the power system is generally high due to the Ferranti effect, consuming reactive power will mitigate the voltage rise. During high loading condition the grid may approach its voltage stability and low voltage limit and providing local reactive power is vital to improve the voltage stability and level, respectively, of the system.

Fig. 3.21 compares the reactive power supplied by the external grid in Case 1 (when the wind turbines are not involved in RPC) and in Case 5 (where RPC is used to avoid totally the use of OLTC to regulate the network voltage). The figure shows that the maximum amount of reactive power supplied from the external grid in Case 5 is not higher than Case 1. However the average reactive power supplied from the external grid is generally higher when RPC is used. Thus, based on the observations made in Fig. 3.20 and Fig. 3.21, one can conclude that the use of RPC for decreasing the FTC does not pose any technical challenge to the grid from the reactive power demand point of view.

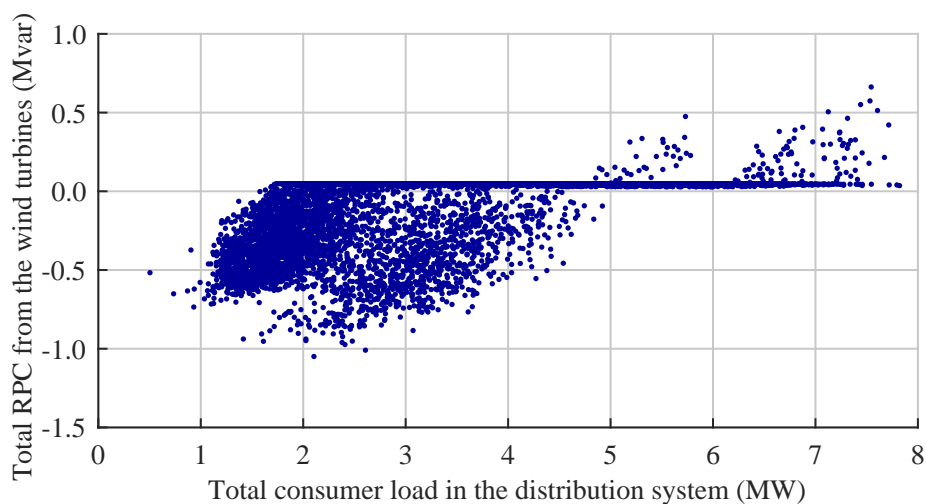


Figure 3.20: Reactive power production from the wind turbines as the function of the load in the system for Case 5.

Moreover, in Case 5, the total amount of reactive power used in achieving such a high level of reduction in FTC depends on the initial tap position of the transformer. If RPC is to be used to eliminate the use of OLTC for voltage regulation, the initial tap position should be chosen such that it is in the middle of the tap positions the tap changer has ever operated at. This can be observed

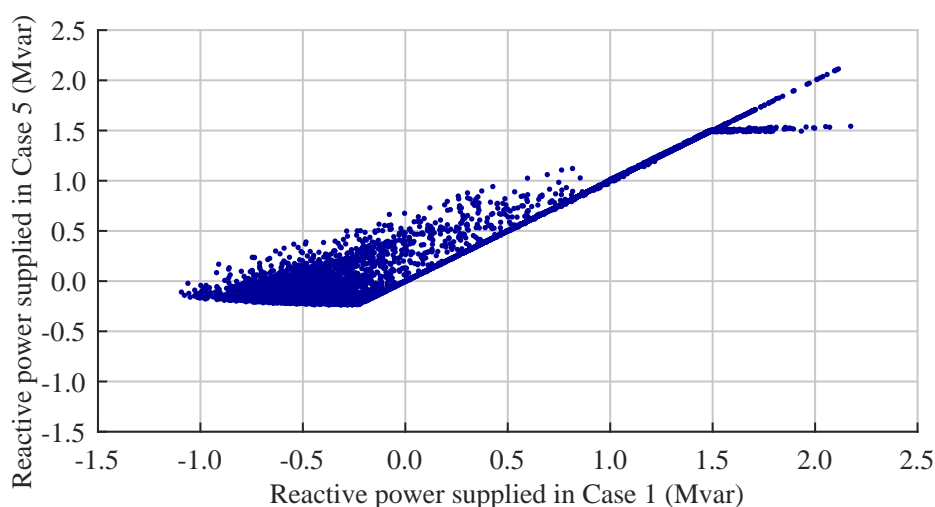


Figure 3.21: Comparison of reactive power supplied from the external grid.

from the historical data. In the present case study the transformer is found to operate between the tap positions zero and two. Hence the reference (initial) tap position is chosen to be one. If the reference tap position is chosen to be zero, the average reactive power used from the wind turbines would have been above 700 kVAR. This is even without achieving 100% reduction in the number of tap changes. Moreover the loss could have been higher than the base case.

3.5.7.2 Voltage in the network

Due to a relatively high amount of reactive power consumed by the wind turbines, one may expect the voltage on wind turbine terminals to be below the acceptable level. Fig. 3.22 compares the voltage at the wind turbine terminals between the base case (Case 1) and Case 5 from Table 3.1. On the contrary, the figure shows that the voltage at the wind turbine terminals remains within $\pm 5\%$ of the nominal (reference) voltage, 10.7kV. Moreover, on average, the voltage at wind turbine terminals are higher in Case 5 than in the base case. When reactive power is consumed to avoid a tap change, the voltage at the secondary side of the transformer is kept at the upper limit of the voltage deadband. This results in a voltage gain at terminals of the wind turbines. Even though there is voltage drop due to reactive power consumption, the overall effect is a general increase in voltage at the wind turbine terminals.

Moreover, by using this voltage regulation strategy, it is possible to minimize the overvoltage that happens in the system due to the slow reaction time of the tap changers. This is especially of great importance if some other wind turbines in the system are tripped due to fault resulting in a sudden voltage drop in the system.

3.5.7.3 Effect of voltage set point on the effectiveness of reactive power compensation to reduce the number of tap changes

Though the voltage set point at the secondary side of the transformer may be chosen to provide customers with the appropriate voltage level, there is some degree of freedom in the choice. This

3. EFFECT OF WIND POWER ON FREQUENCY OF TAP CHANGES

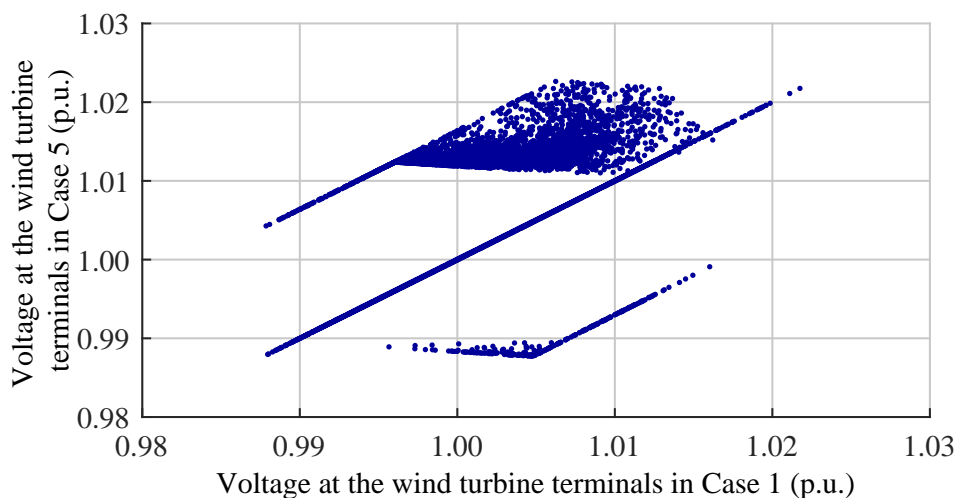


Figure 3.22: Comparison of distribution of voltage on the wind turbine terminals.

subsection investigates how the choice of the voltage set point at the secondary side of the transformer can affect the performance of RPC in reducing the FTC.

The voltage set point affects how the tap positions are distributed. For the case presented in Table 3.1, Fig. 3.23 shows the tap position distribution of the substation transformer for two different voltage set points at the secondary side of the transformer.

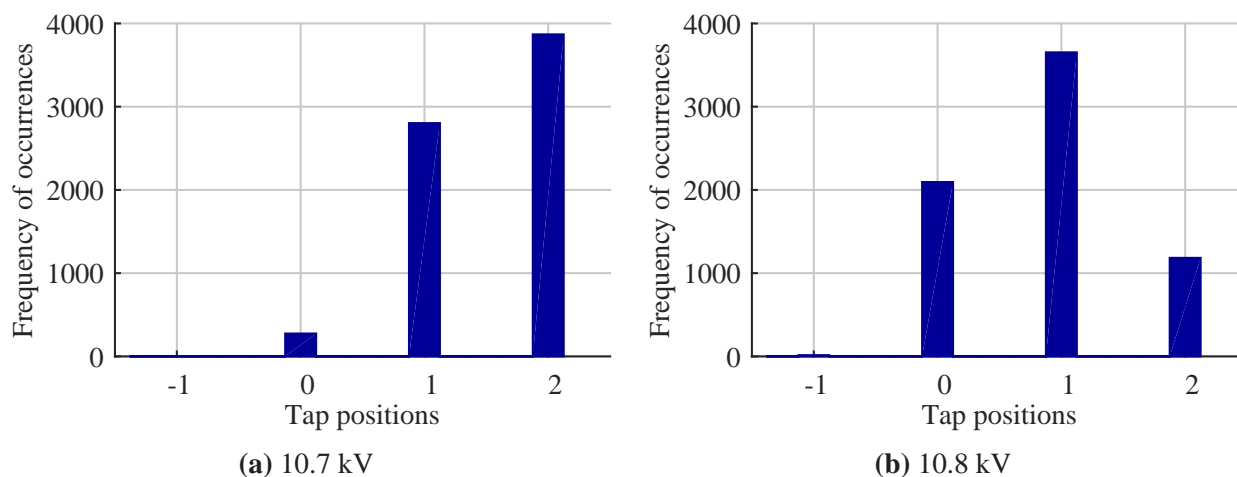


Figure 3.23: Tap position distribution of the substation transformer for two different voltage set points.

To totally eliminate the tap changes using RPC, naturally it is more effective to set the tap position at the median of the tap position distribution. The more evenly distributed the tap positions are around the median tap position, generally, the lower is the average reactive power demand from the wind turbines to avoid a tap change. In Fig. 3.23 the tap positions are more evenly distributed around the median when the reference voltage is 10.8 kV. If we compare the average reactive power requirement to avoid tap changes totally, we see that it is 176 kVAr with a 10.7 kV as a reference voltage and 56 kVAr with 10.8 kV. Therefore, the RPC would be more effective if the reference voltage is set to 10.8 kV, showing that the reference voltage chosen can affect the effectiveness of

the RPC. This also shows that the demand on reactive power from the wind farms depends on the reference voltage setting.

3.6 Summary

In this chapter an analysis of the effect of wind power on the frequency of tap changes (FTC) is carried out. In general, for distribution networks connected to external grids with $X/R \geq 5$, no significant effect on the FTC is seen due to introduction of wind power. However, in a distribution system connected to grids with a lower X/R ratio wind power can affect the FTC significantly as wind power penetration increases.

An analysis is done to decrease the FTC using reactive power compensation (RPC) from the wind turbines. Two types of distribution systems are considered: one connected to a relatively strong (SCC=171 MVA, X/R= 10) external grid and the other to a weak (SCC=80 MVA, X/R= 1) external grid. The results show that RPC can be used to effectively reduce the FTC in both cases. However, the reactive power required to reduce the FTC by a specific percent depends on the SCC and the X/R ratio. The reactive power requirement decreases with a higher SCC and X/R ratio.

A further investigation on RPC is carried out for wind farms located farther from the substation. However, the change in reactive power requirement and network loss is found to be only minor. Hence the RPC method is found to be effective even when wind farms are far away from the substation.

Finally the practical implementation of RPC to reduce the number of tap changes depends on the maintenance cost of the tap changers involved, the cost of reactive power from the wind turbines, and the change in power loss that occurs within the network due to RPC.

3. EFFECT OF WIND POWER ON FREQUENCY OF TAP CHANGES

4

Siting wind turbines in a distribution system

In the previous chapters the effect of wind turbines on power quality and reliability of distribution systems is investigated. This and next chapter provide the methodologies to determine the optimal hosting capacity of distribution systems. Unlike many other works where the optimal siting and hosting capacity problem are treated as a single problem, in this thesis the problem is decomposed into two sub-problems. As the discussion in this chapter shows, as long as the objective is to maximize the hosting capacity of a given distribution system, such approach provides optimal results without facing the dimensionality problem that occurs when the two sub-problems are solved as a single problem.

The aim of this chapter is to investigate the optimal siting of wind turbines or farms in a given distribution system. The chapter starts by presenting background knowledge to the optimal siting problem. Then, the siting problem is discussed with respect to the different integration issues of wind power discussed in Chapter 2. These include overvoltage, overloading, flicker, harmonics, increase in fault level as well as loss considerations. The problem of determining the optimal capacity will be treated in the next chapter.

4.1 Background

The location of a wind turbine or farm is mainly affected by the windiness and the accessibility of a given site. However, it is possible that the distribution system has a couple of sites with nearly the same average wind speed and it may be required to choose one or more sites among them for wind power installation. In this regard, extensive research effort has been devoted to the optimal siting and sizing of distributed generations (DGs) [84–110]. The siting problem has been studied to achieve different objectives, such as loss minimization [84–91, 94–99, 102, 105, 106, 109, 110], hosting capacity maximization [93, 98, 103, 104], and reliability improvement [92, 94, 98]. Also different methodologies have been proposed to solve the problem. These include but not limited to genetic algorithm [84, 85, 89, 90, 93, 94, 98, 103, 106], particle swarm optimization (PSO) [86, 87, 91, 92, 96, 97, 105], analytical methods [88, 95, 101, 102, 110], fuzzy logic [99], ordinal optimization (OO) [104], and artificial bee colony (ABC) [107].

The main objective of the majority of the papers cited above is loss reduction. However, our

4. SITING WIND TURBINES IN A DISTRIBUTION SYSTEM

main objective in this chapter is to identify the optimal connection point of a wind power plant in electrical distribution system, so that the hosting capacity of the network is maximized while keeping the power quality and security concern within the acceptable limits.

4.2 Siting wind power

The connection point of a wind turbine determines the power quality and security concerns it poses to a given distribution system. These power quality and security concerns discussed in Chapter 2 include overvoltage, overloading, flicker and harmonic emission, and increase in fault level. In subsequent subsections, the siting problem is investigated according to each power quality and security concern.

4.2.1 Overvoltage

The effect of wind power in increasing the voltage level in a distribution system has been shown in Section 2.2.4 using (2.14) (rewritten here as (4.1) with a slight rearrangement).

$$|V_2| \approx |V_1| + PR + QX \quad (4.1)$$

From (4.1), since the voltage at the substation $|V_1|$ is regulated around a reference voltage, the voltage $|V_2|$ at the PCC will be higher for higher wind power generation P and cable resistance R . Higher cable resistance R arises from longer cable or overhead line. Fig. 4.1 shows the capacity of wind power that can be installed based on the $\pm 5\%$ voltage limit for different cable types with varying lengths. The data for these two cable types are given in Table 2.1. The wind farm is assumed to operate at unity power factor, which is the current operating practice of most wind turbines.

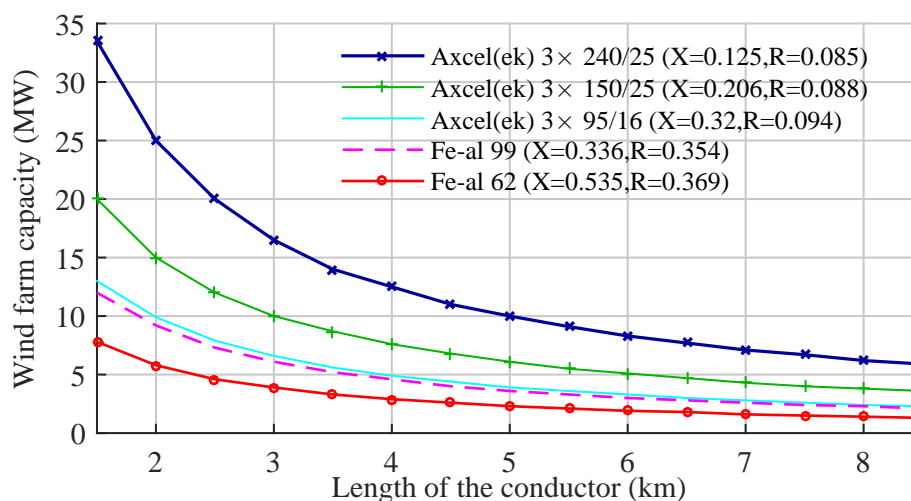


Figure 4.1: The capacity of wind power that can be installed based on $\pm 5\%$ limit.

From Fig. 4.1, one can notice that the capacity of wind power that can be installed based on the $\pm 5\%$ voltage limit is severely limited when the wind farm is further away from the substation.

Hence when the limiting factor to wind power integration is the voltage rise problem, the wind power hosting capacity of the distribution system can be increased by siting the wind turbines as electrically close to the substation as possible.

The above analysis works when one is investigating the siting of a single wind farm along a single feeder. However, in a given distribution system there are usually a number of feeders and laterals and the DSO may need to identify those buses that maximize the hosting capacity of the system. For example, consider the distribution system shown in Fig. 4.2¹, with the indicated candidate wind farm sites (Buses 2 to 4 and 6 to 9) and the network impedances. It is assumed that the minimum loading condition at the buses is 0 MW. The worst case voltage rise occurs in the system when the load is at its minimum and the generation is at its maximum. The analysis done assuming these extreme conditions of load and wind power is usually called the worst case analysis. Thus, an optimal power flow (OPF) analysis implemented in GAMS (a high-level modeling software for mathematical programming and optimization) is carried out based on the worst case consideration with the objective of maximizing the hosting capacity while keeping the voltage within $\pm 5\%$. Table.4.1 shows the hosting capacity that is achieved with different bus combination options.

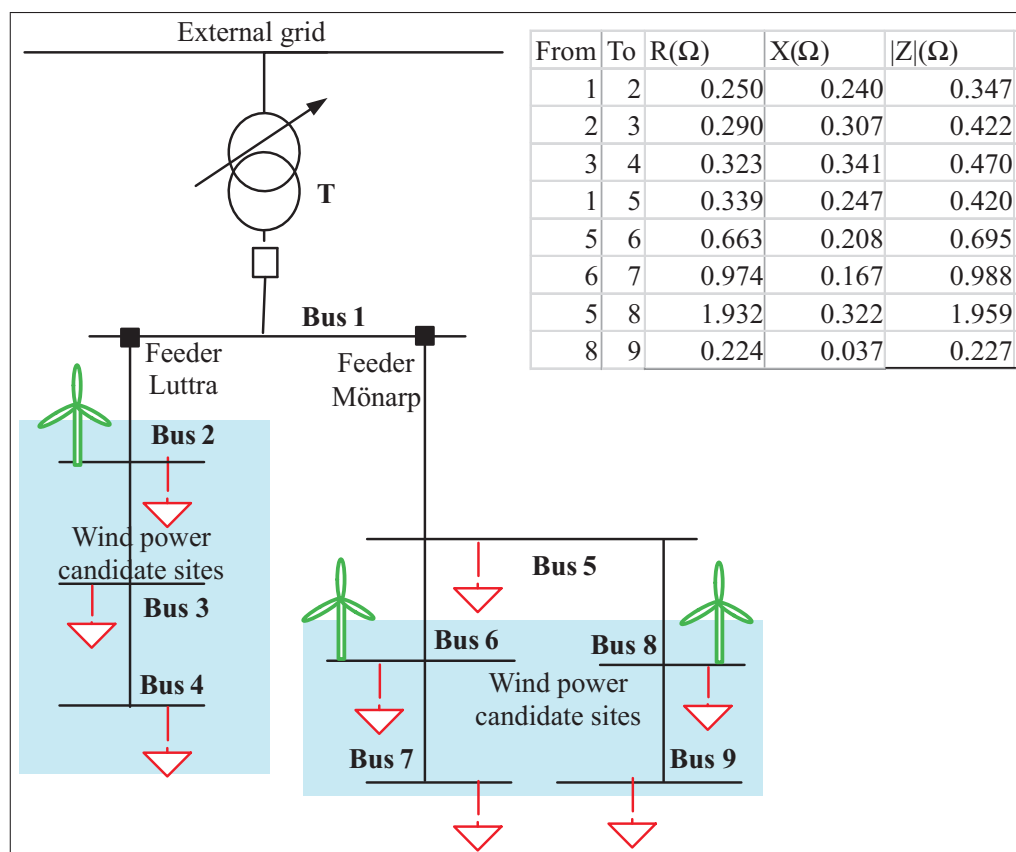


Figure 4.2: Siting wind power in distribution system.

It is clear from Table.4.1 that wind farm site selection containing Buses 2, 6, 8 has the highest hosting capacity among the five options considered. That is, distributing the connection points on different feeders maximizes the hosting capacity. Since the voltage at the substation bus is

¹it is a section of an actual distribution system operated by Falbygden energi, sectioned out for easier analysis

4. SITING WIND TURBINES IN A DISTRIBUTION SYSTEM

Table 4.1: Installed wind power capacity with different bus selection alternatives

Option	1			2			3			4			5		
buses	2	6	8	2	3	4	2	8	9	6	7	8	4	7	9
power (MW)	26.0	5.7	2.0	26.0	0.0	0.0	26.0	2.8	0.0	5.7	0.0	2.0	7.6	2.9	2.2
Total (MW)	33.7			26.0			31.0			7.7			12.6		
Loss (MW)	1.6			1.3			1.6			0.4			0.6		
Net (MW)	32.1			24.8			29.5			7.3			12.0		

regulated, if the wind turbines are located on different feeders, the maximum capacity of each feeder will be installed without any effect from the wind power on the other feeder. The same is true for the lateral branches of a feeder. That is, if the wind farms, for some reason, should be located at the lateral branches of a feeder, the hosting capacity can be maximized if they are situated in different lateral branches and as electrically close to the substation as possible.

Moreover, if the wind turbines are not connected as electrically close to the substation as possible, the hosting capacity will significantly be affected. For example, from Table 4.1 in the case of Option 2, if wind power is installed only on Bus 2, the maximum hosting capacity of Feeder Luttra is 26 MW. Consider now that there is a 2 MW wind turbine installed at Bus 4 on Feeder Luttra. As a result of this pre-installed 2 MW wind power, Bus 2 can now only host 19 MW. Though the hosting capacity is still high, the reduction is significant: -23%. Note that the analysis done here is based on voltage rise consideration only; other consideration, such as overloading, may further limit the hosting capacity of the system as shown in Section 4.2.2.

In conclusion, voltage rise severely limits the capacity of wind power that can be installed in a given distribution system when the connection point is electrically far from the station. Thus, installing wind turbines as close as possible to the substation increases the hosting capacity of a distribution system limited due to voltage rise problem. Moreover when a couple of wind farms are to be connected to a given distribution system, higher hosting capacity can be achieved by locating the wind farms at different feeders or lateral branches of a feeder.

4.2.2 Overloading

With overvoltage as the only limiting factor, Fig. 4.1 shows that a considerable amount of wind power can be installed using any of the cables if the wind turbine or farm is located, e.g. at 1.5 km distance from the substation. Table 4.2 shows the current rating of the conductors, the maximum capacity of wind power that the cable can accommodate, and the maximum distance of the wind farm site above which the voltage rise will further limit the capacity of wind power that can be installed. From the table one can see that when the wind turbines are sited electrically close to the substation, the thermal capacity of the cables further limits the wind power hosting capacity of the distribution system. Similar analysis done on the distribution system in Fig. 4.2 shows that the hosting capacity of the system is well below the capacity indicated in Table 4.1 due to the thermal capacity of the cables involved. It can generally be concluded that for wind turbines installed in relatively strong distribution network at sites close to the substation, the capacity of the wind farm is more likely to be limited due to the thermal capacity of the involved components.

Given a situation where the thermal capacity of the network components is the limiting factor,

Table 4.2: Maximum capacity based on ampacity of different cable types

Cable	Current rating	Pmax (MW)	Maximum cable length (km)
AXCEL(EK) 3X240/25	360	6.7	7.3
AXCEL(EK) 3X150/25	280	5.3	5.7
AXCEL(EK) 3X95/16	215	4.1	4.8
FE-AL 99	435	8.3	2.2
FE-AL 62	305	5.8	2

it may be of interest to decide both the location and the capacity of the wind farm. Consider Feeder Luttra in network of Fig. 4.2, where the thermal rating of the feeder is 280 A with zero MW minimum loading condition. Table 4.3 shows the maximum hosting capacity of the feeder for different choices of the wind turbine connection point.

Table 4.3: Hosting capacity of Feeder Luttra based on thermal limit

Connection point	Capacity (MW)	Voltage at Bus 2 (p.u.)	Voltage at Bus 3 (p.u.)	Voltage at Bus 4 (p.u.)	Feeder loss (MW)	Net (MW)
2	5.39	1.011	1.011	1.011	0.06	5.33
3	5.46	1.011	1.024	1.024	0.13	5.33
4	5.53	1.011	1.023	1.037	0.20	5.33

Table 4.3 shows a slightly higher wind power hosting capacity for connection points electrically further from the station. This is due to a higher voltage rise that occurs for connection points further from the station for the same level of current injection. But, the last column of the table shows that the extra hosting capacity gained, becomes a part of the network power losses. The same analysis is also done assuming a higher minimum loading conditions and the results have yielded a similar conclusion.

Therefore, in general, one can conclude that installing the wind turbines close to the substation is a preferred option in a distribution system where the hosting capacity is limited due to overloading. On one hand, usually the cables electrically close to the substation have higher ampacity than the cables or overhead lines that are located electrically far from the substation. Hence the hosting capacity can be maximized by installing the wind turbines close to the substation. On the other hand, even if the capacity of the cables along the feeder are similar, it is still better to install wind turbines electrically close the substation. Though this does not increase the hosting capacity of the system, it reduces the power losses as shown in Table 4.3.

4.2.3 Loss consideration

In general power losses do no limit the capacity of installed wind power. However, since the increase in power losses leads to loss in revenue to the DSO, there is a need to minimize the power losses in the system. Thus, in loss minimization, the strategy is usually to supply the power demand in a distribution network as locally as possible. This reduces the current flow through the network cables compared to the case where the loads are supplied from the external grid through the transformers. The reduction in current flow leads to reduced power losses in the system.

4. SITING WIND TURBINES IN A DISTRIBUTION SYSTEM

Consider the same example on Feeder Luttra discussed in Subsection 4.2.2. Assume now that there are average loads of 0.2 MW, at Buses 2 and 3, and 1 MW, at Bus 4, with a lagging power factor of 0.95. Table 4.4 shows the power generation and loss before and after connecting a DG. The results show that installing an approximately 1.2 MW of wind power at Bus 4 results in the minimum loss in the feeder. Compared with the capacity that is installed based on hosting capacity maximization, this capacity of wind power is considerably low. When wind turbines are installed based on hosting capacity maximization there is usually a high reverse power flow to the external grid. In such cases installing wind power as electrically close as possible to the substation will result in lower power losses in the system. This is clearly seen on Table 4.3.

Table 4.4: Siting wind power based on loss minimization

Buses	Power production (MW)			
	Without DG	With DG at Bus 2	With DG at Bus 3	With DG at Bus 4
External grid	1.412	-0.007	0.105	0.218
2	0	1.414	0	0
3	0	0	1.299	0
4	0	0	0	1.184
Loss (MW)	0.012	0.007	0.004	0.001

4.2.4 Flicker emission

Though flicker emission is not a concern with advent of variable speed wind turbine, it can clearly be seen from equations used for calculating flicker from wind turbines [111], the flicker emission from the wind turbines is inversely proportional to the short circuit capacity of the distribution system at the point of connection. Therefore, installing wind turbines as close to the substation as possible minimizes the effect of wind power on flicker emission.

4.2.5 Harmonic emission

Equation (4.2) can roughly be used to estimate the voltage harmonic u_h introduced to the voltage of the network by a wind turbine producing a harmonic current of i_h [62]. Here Z_h is the harmonic impedance seen from the wind turbine site and S_{\max} is the maximum apparent power of the wind turbine and U is the nominal voltage of the system.

$$u_h = \frac{i_h Z_h S_{\max}}{U^2} \quad (4.2)$$

Equation (4.2) shows that a wind turbine which is sited electrically far from the substation, thus experiencing a higher harmonic impedance Z_h , introduces higher voltage harmonics. Hence siting wind turbines as close electrically as possible to the substation can maximize the hosting capacity of a network constrained due to harmonic voltage emission.

4.2.6 Increase in short circuit level

The increase in fault level can become a limiting factor to wind power integration depending on:

- the capacity of the wind farm and the technology of the wind turbines in the wind farm,
- the distance of the wind farm from the station,
- the SCC at the station due to the external grid,
- and the rating of the switchgear at the substation i.e. the available fault level margin of safety to handle additional fault current from the wind turbines

Therefore, an increase in fault level can only become a limiting factor in a distribution system connected to a quite strong grid where the available margin of safety to handle additional fault level is very low. Moreover the wind turbines connected to the grid need to be of type other than Type D. In general, it is less likely for the grid to be very strong in rural areas, where favorable windy sites are usually located. As the distribution systems in this area are often far from the main grid, they have comparatively low grid strength. Therefore, increased fault level becomes a limiting factor only in rare cases.

When it is a limiting factor, in most cases, it is the substation bus that is our main concern. This is because fault contribution from the external grid is more likely to be higher than the fault contribution from the wind turbines. With higher impedance between the fault source and the fault point, these fault contribution from the external grid substantially decreases at buses located electrically further from the substation. Therefore, it is less likely for increased short circuit level to be a problem on these buses.

With increased impedance between the wind turbine site and the substation, fault current contribution at the substation decreases as the wind turbines are sited further from the substation. Hence the total fault level at the substation decreases. Thus, in distribution systems where the available fault level margin of safety is relatively low, installing wind farms away from the station could be an option to increase the hosting capacity of the network. This is especially true when the wind turbines in the wind farm are not of Type D.

4.3 Summary

In a distribution system where the hosting capacity is limited due to overvoltage, overloading, voltage flicker, and harmonics, installing wind turbines as electrically close to the substation as possible, maximizes the hosting capacity of a distribution system. Moreover, when more than one PCC is sought, the PCCs should be distributed on different feeders as well as laterals. Even with regard to loss consideration, when large scale integration of wind power is sought, installing wind turbines electrically close to the substation minimizes the loss in the system. It is also mentioned in Chapter 3 that the effect of wind power on the FTC is almost independent of the location of wind farms in a given distribution system. Therefore, based on the integration issues of wind power discussed in this thesis, the increase in fault level is the only reason that one may need to install wind turbines away from the substation when trying to maximize the wind power hosting capacity of distribution systems.

4. SITING WIND TURBINES IN A DISTRIBUTION SYSTEM

5

Wind power hosting capacity of a distribution system

This chapter deals with the determination of the optimal hosting capacity of a distribution system. The chapter starts with a discussion of the traditional worst-case approach of assessing the hosting capacity of a distribution system. Then the role of active management strategies in increasing the hosting capacity of a given distribution system is discussed. Incorporating these active management strategies, an optimization model is developed to assess the optimal hosting capacity of a given distribution system. A discussion on stochastic wind power and load data modeling is also included in this chapter. This will provide a useful tool for load and wind power data generation whenever the available load and wind power data are not of the required size or type. The chapter concludes by presenting and discussing results from two case studies.

5.1 Assessing the hosting capacity of a distribution system

5.1.1 Worst case analysis

Current distribution systems are operated passively. This means these systems are not actively controlled to insure that system components operate only within the allowed range of voltage and thermal loading. Therefore, while permitting a given wind power installation, distribution system operators (DSOs) consider the worst condition under which the system can operate. Under this operating condition, the philosophy is the system should function with every power quality and reliability indices of the system being within the acceptable limit.

In Chapter 4, voltage rise and overloading of system components have been identified as the most common problematic effects of wind power. Voltage rise occurs due to reverse power flow. If the power generation from a wind turbine/farm is locally consumed the reverse power flow decreases. Thus, the worst case reverse power flow, corresponding to the maximum voltage rise, happens when the load is at its minimum and the power generation is at its maximum. The same holds true for the overloading which happens due to wind power production. That is, the higher the reverse power flow, the more likely it is for the network elements to be overloaded. Hence the

5. WIND POWER HOSTING CAPACITY OF A DISTRIBUTION SYSTEM

maximum generation and the minimum loading condition in the system ends up being the worst condition. The maximum loading together with the minimum generation can cause overloading and undervoltage. However, the same condition can arise in the system even without wind power installation. Thus, the analysis of such condition is not necessary to assess the wind power hosting capacity of the system. The analysis based on such assumption of minimum load and maximum wind power generation is called worst case analysis. In the worst case analysis, the objective is for the voltage to remain within, e.g., $\pm 5\%$ of the nominal voltage and the power flow to remain within the thermal ratings of the system elements. Based on the worst case, a number of optimization approaches have been proposed to assess the hosting capacity of a distribution system [89, 90, 98, 103, 112]. Optimal power flow (OPF) based approach is proposed in [112] to determine the available headroom for DG. Genetic algorithm (GA) [89, 98], and combined OPF and GA [90, 103] are used to determine the optimal position and size of DGs.

5.1.2 Active management strategies

The approach based on maximum generation and minimum load ensure the network from potential power quality and security concerns. However, due to high variability of both load and wind power generation with a low level of correlation, maximum generation and minimum load condition in the system rarely, if ever, coincides in practice. Hence this approach unnecessarily hinders the penetration of wind power into the electricity grid. It also deprives DSOs from potential benefit they could gain. Hence the use of active management strategies have been proposed to deal with this rare event and increase the penetration of wind power into the electricity grid [3, 5–9, 113]. The discussion of these active management strategies is presented in the following subsections.

5.1.2.1 Reactive power compensation

The use of reactive power for mitigating the voltage rise effect due to DGs can be found in literature as early as 1998 [113]. Later on, many others have included it in optimization models that assess the DG hosting capacity of distribution systems [3, 5–9]. The use of reactive power has also been further investigated for loss minimization [114–116] and mitigating other integration issues of wind power, such as voltage flickers [113, 117, 118]. In this thesis, RPC is used for increasing the wind power hosting capacity of distribution networks limited due to voltage rise problems. The reactive power required for overvoltage mitigation can be supplied by the wind turbines themselves, which is the case with variable-speed wind turbines, or by some other components such as static VAR compensator (SVC) or static synchronous compensator (STATCOM).

5.1.2.2 Coordinated on-load tap changer voltage control

The traditional or the existing practice of controlling tap changers is based on two main principles, as discussed in Section 2.2.4.1. The first one is based on keeping the voltage within a given dead-band around some reference voltage. In the second approach the controllers are augmented with line-drop compensation to boost voltages more during heavy loading condition [59]. Due to introduction of wind power, however, the voltages at different feeders may differ widely. This makes it difficult to properly regulate the voltages at different feeders with just one substation OLTC. Even if separate regulators are assigned for each feeder, the power factor of the feeder where wind

power is installed can vary considerably depending on the wind condition. This makes voltage regulation very difficult especially for second approach [59]. Even for the first approach, a better voltage regulation, hence, higher hosting capacity can be achieved with the use of coordinated OLTC (C-OLTC) voltage control in a distribution system limited due to voltage rise problem. In C-OLTC voltage control, the OLTC is controlled to keep the voltage on various critical points in the system within the acceptable voltage limits. This idea is found in literature as early as 2002 [3]. Moreover, it has been incorporated into a number of optimization models [5–10] that assess the DG hosting capacity of distribution networks.

5.1.2.3 Wind energy curtailment

The principle behind wind energy curtailment (WEC) is to curtail part of wind power production in case of overvoltage or overloading. This is the only solution in case of overloading unless some expensive solutions, such as energy storage and capacity enhancement, are made. The idea of using curtailment for overvoltage mitigation is not new either [3]. It has further been incorporated into optimization models for overvoltage mitigation [5–10] as well as overload mitigation [7–10].

5.1.3 Comparison of the different active management schemes for voltage regulation

The previous subsection has listed the different voltage rise mitigation solutions without stating the order of preference. Most papers in literature have shown preference to OLTC over RPC and RPC over curtailment [23–26]. However, some have preferred curtailment over RPC [21, 22]. Thus, the aim of this subsection is to investigate the order of preference of these voltage rise mitigation solutions under different grid conditions. For this analysis the simple network shown in Fig. 5.1 is used. This is a simplified version of an 11-kV network operated by Falbygdens Energi located in Falköping area in Sweden. The network is fed by a 40-kV grid through a 10-MVA $45 \pm 8 \times 1.67\% / 11.5\text{-kV}$ transformer with reactance of 8%. The upstream grid is of 170 MVA short circuit capacity with X/R of 4.6. The task is to analyze the change in network losses due to increased introduction of DGs with the different voltage rise mitigation solutions for different X/R ratio and impedance (Z) of the power cable between the wind farm and the substation.

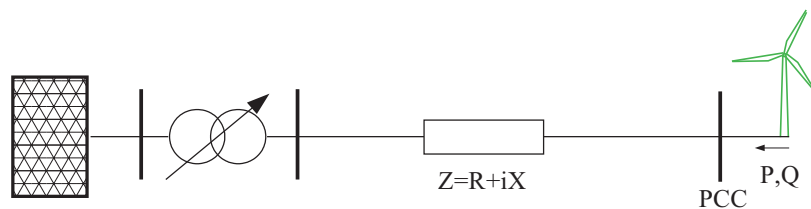


Figure 5.1: A simple network with wind power.

Case 1: $Z = 1.5\Omega$ and $\frac{X}{R} = 1$, in the first case investigated, the impedance of the cable connecting the DG to the substation is assumed to be 1.5Ω with the X/R ratio of 1. The results of the analysis,

5. WIND POWER HOSTING CAPACITY OF A DISTRIBUTION SYSTEM

presented in Fig. 5.2, show that the power losses (which includes both curtailment and resistive losses) due to the different active management schemes are the same as long as the voltage is within the allowed operating limit, assumed to be $\pm 5\%$ in this analysis. This is because the active management schemes are not in use when the voltage is within the allowed operating limit. When the different schemes are used for overvoltage mitigation (when the installed wind power capacity is above ≈ 6.2 MW), Fig. 5.2a shows that curtailment introduces a significant loss of energy compared to RPC or C-OLTC. However, the losses due to C-OLTC and RPC are comparable for significant levels of wind power integration. This is because, as shown in Fig. 5.2b and Fig. 5.2c, though RPC may increase the network losses through the increase in reactive power flow, C-OLTC also increases the network losses by lowering the voltage level at the PCC.

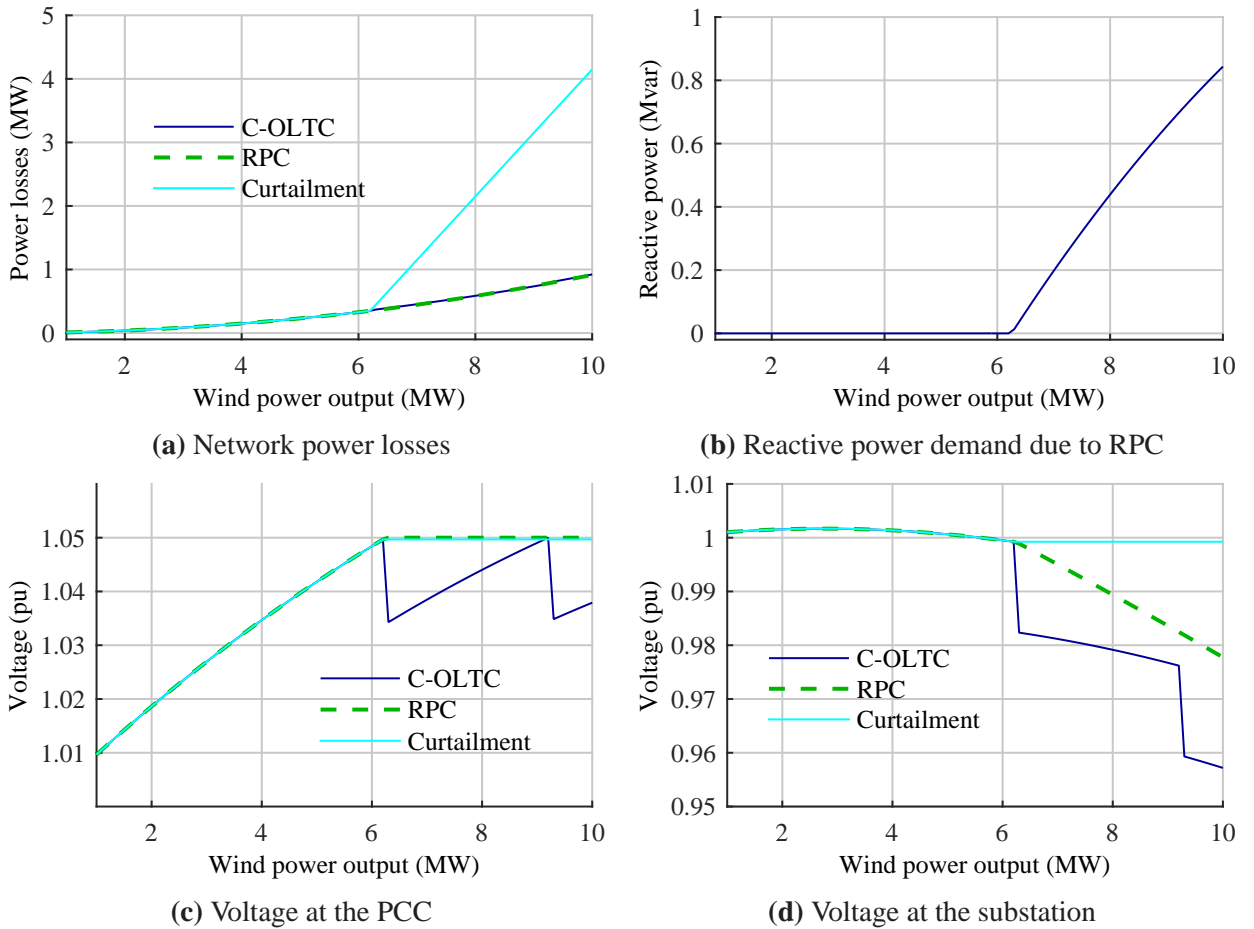


Figure 5.2: Comparison of the different active management schemes for voltage regulation when the impedance of the cable is 1.5Ω and its X/R ratio is 1.0.

Case 2: $Z = 1.5\Omega$ and $\frac{X}{R} = 0.5$, with decreased X/R ratio, Fig. 5.3 shows that curtailment is still not an option to consider for voltage mitigation. However, now, as shown in Fig.5.3e more reactive power will be required to mitigate the voltage rise in case of RPC. This increase in reactive power demand makes RPC more lossy than C-OLTC. Yet, as shown in Fig.5.3b, the difference between the losses due to RPC and C-OLTC is not significant compared to the actual losses in the system.

5.1 Assessing the hosting capacity of a distribution system

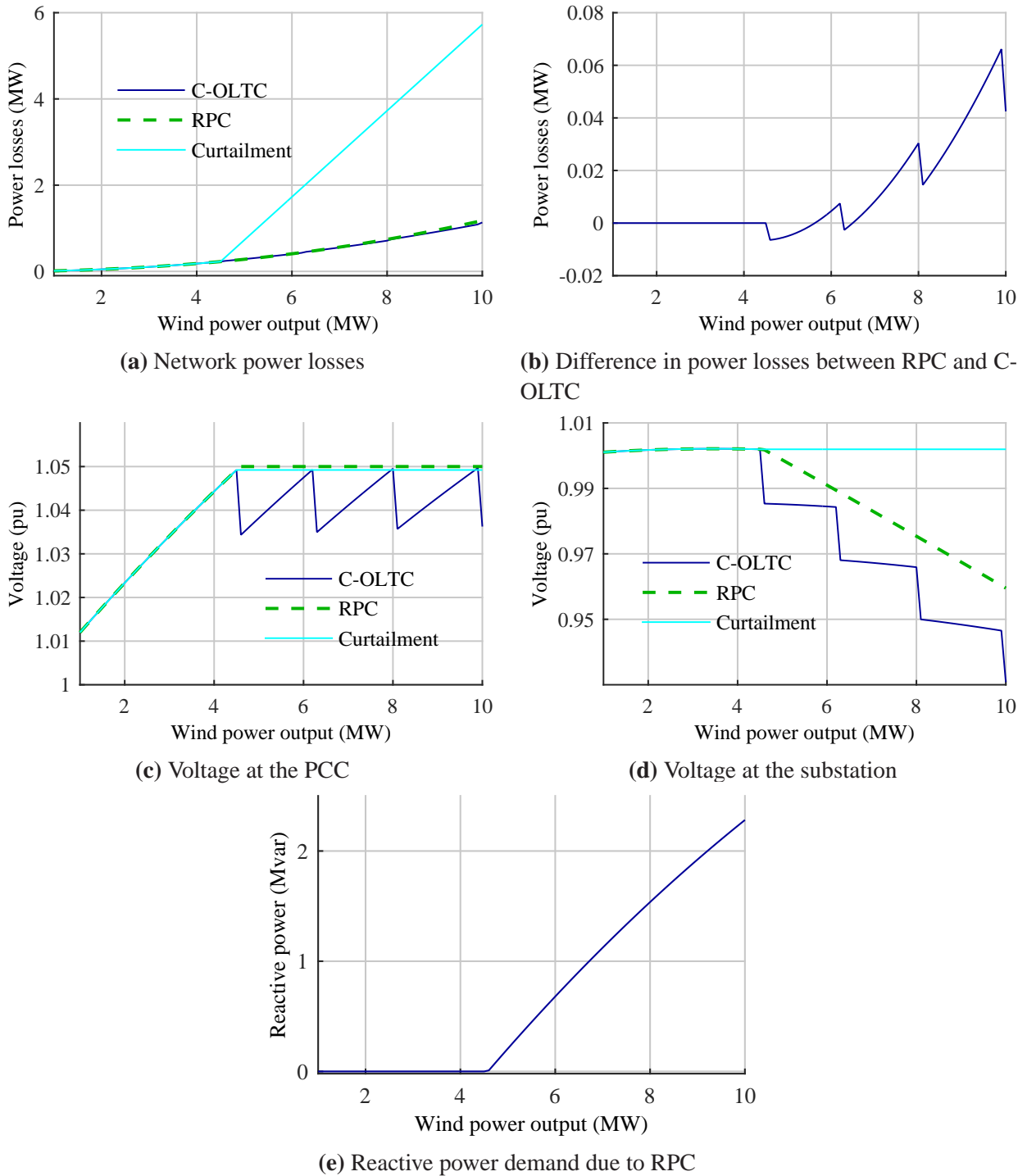


Figure 5.3: Comparison of the different active management schemes for voltage regulation when the impedance of the cable is 1.5Ω and its X/R ratio is 0.5.

The loss analyses in Fig. 5.2 and Fig. 5.3 consider only wind power in the system. From Fig. 5.2d and Fig. 5.3d one can see that C-OLTC generally imposes lower voltage level in the system compared to RPC. Thus, when there are loads in the system, the effect of C-OLTC and RPC on the

5. WIND POWER HOSTING CAPACITY OF A DISTRIBUTION SYSTEM

loss level of the system will depend on the load composition of the system. Constant current loads more or less will introduce the same amount of power losses irrespective of the voltage mitigation schemes used. If the majority of the loads are constant impedance loads RPC will introduce more power losses and C-OLTC will be the preferred option for voltage mitigation. If, on the other hand, the majority of loads are constant power loads, C-OLTC imposes more power losses than those shown Figs. 5.2a and 5.3a. Then RPC may become the preferred option for voltage mitigation depending on the X/R ratio of the cable. The available data from literature shows that the real power of a load is mostly of constant current or constant power type while reactive power part of the load can be considered generally as constant impedance or constant current [119–121]. Since in most cases the active power part of the load is dominant, the fact that C-OLTC affects the entire network voltage level may introduce more power losses than what is shown in Fig. 5.2a. But it is difficult to say if RPC would be the preferred voltage mitigation solution as the overall loss from C-OLTC depends on the load level in the system and in the case of RPC there is an extra loss in converter of the wind power due to the reactive power consumption which is not taken into account in the above analysis. Nevertheless, considering that C-OLTC can lead to an increase in the frequency of tap changes which may result in increased maintenance requirement, RPC can be preferable in such cases. Another advantage of RPC over C-OLTC is that it provides a continuous voltage regulation as there is no need for a delay in the operation of RPC, unlike tap changer operations. Moreover, as shown in Fig. 5.3d, the use of C-OLTC for voltage mitigation may result in undervoltage for other loads in the system. Hence, there is a limitation to how much wind power one can accommodate using the C-OLTC voltage regulation scheme.

Case 3: $Z = 0.5\Omega$ and $\frac{X}{R} = 0.055$, on the other hand, given, the per unit voltage change ΔV due to a given active P and reactive Q power flow along a given power line can be approximated by:

$$\Delta V = PR + QX \quad (3.16 \text{ revisited})$$

one can expect if the the X/R ratio of the cable decreases further with increased impedance more reactive power will be necessary to mitigate a voltage rise leading to a higher loss. Then, curtailment may be an attractive option compared to RPC. To verify this, DG installations in LV networks are considered as the X/R ratio in LV networks is very low compared to the X/R ratio in MV networks. Consider a PV panel installed in an LV network where the Thevenin impedance as seen from the PCC is 0.5Ω with X/R ratio of 0.055. The result of the analysis presented in Fig. 5.4 shows that as long as the loss is below 22% ($= \frac{4.6}{20.6} \times 100$) of the PV output power, RPC is a better solution compared to curtailment for overvoltage mitigation even in LV networks.

In general the above analysis shows that C-OLTC and RPC provide comparable performance in terms of their effect on the power losses in the system with C-OLTC being slightly better when the Thevenin impedance seen from the wind turbine site has lower X/R. However, if the wear and tear of the transformer tap changers is a concern, RPC can be used as the best option for voltage regulation. On the other hand, in almost all practical cases, RPC is a better solution than using curtailment to mitigate voltage rise. However, curtailment is something that the owner of the DG deals with whereas RPC involves an increase in power losses of the system which the distribution network operator (DNO) has to face. Unless there is some regulatory arrangement whereby the DG owner compensates for the loss increase it has introduced due to RPC, the DNO may prefer to use curtailment to mitigate the overvoltage caused by the DG. Thus, our recommendations is that such arrangement should be facilitated for the benefit of both parties.

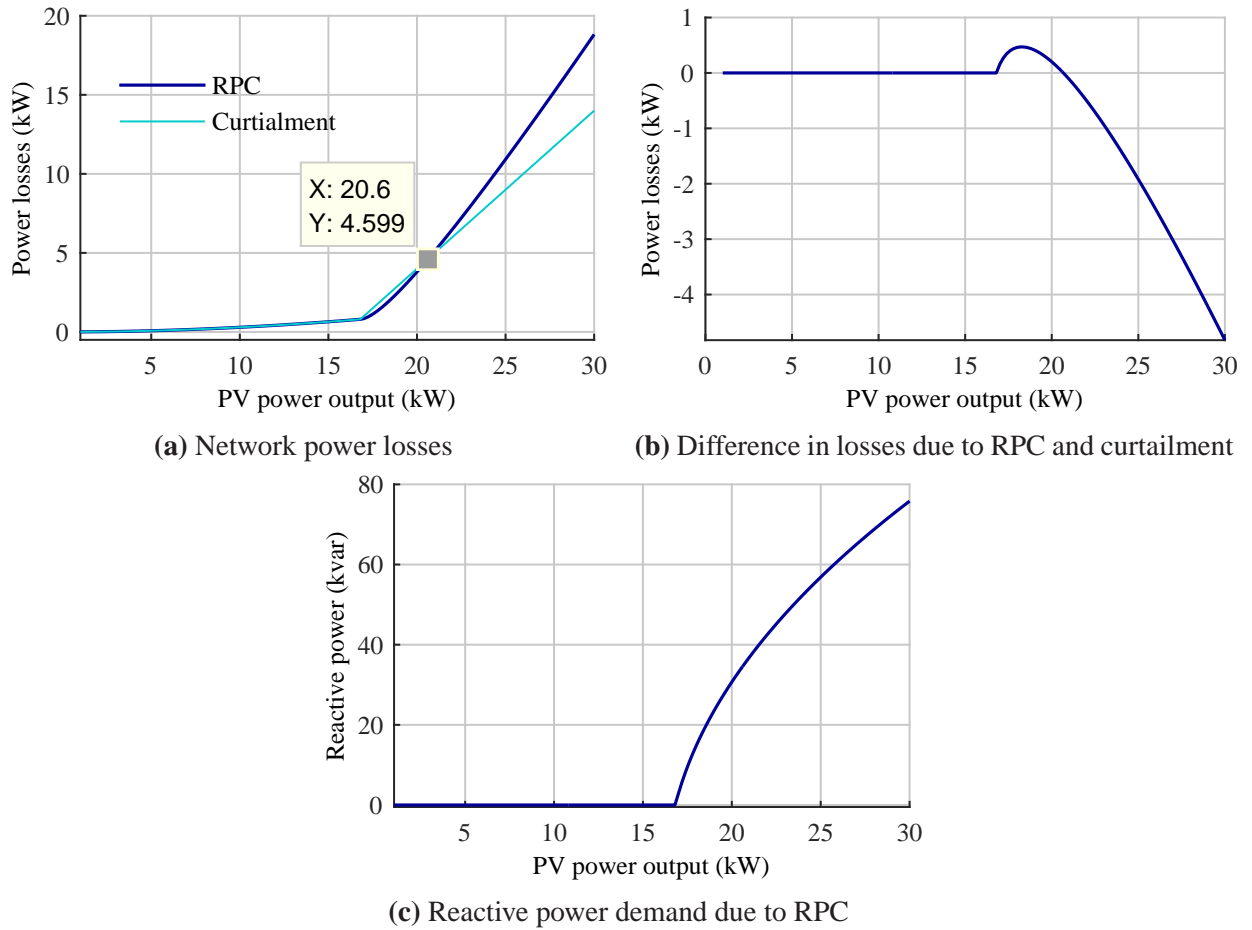


Figure 5.4: Comparing curtailment and RPC for voltage rise mitigation in a LV network with Thevenin impedance of 0.5Ω and X/R ratio of 0.055 at the PCC.

5.2 Costs and benefits of wind power

The active management strategies (AMS) subject the DSO and the wind farm owner (WFO) to costs of their own. For example, WEC causes loss in revenue for the WFO and cannot be used excessively. Similarly, RPC, if used excessively, may lead to unacceptable power losses in the network. Therefore, one needs to identify the capacity of wind power that can be installed using AMS while maximizing the profit gained by the DSO and the WFO. Though the level of detail varies, cost benefit analysis is also discussed in [9, 122] as means of determining the capacity of DG that can be accommodated in a given distribution system. The difference between the model proposed in this chapter to those found in literature lies mainly in the way the amount of curtailed energy is constrained. In [9] the amount of curtailed energy is constrained by indirectly constraining the maximum capacity the DG can have. The problem with this approach is that the maximum capacity is chosen arbitrarily, the result may not be optimal. In [122], the amount of curtailed energy is constrained only when it is not profitable to increase the hosting capacity by using curtailment. However, the analysis done in this thesis shows that, depending on the costs and benefits of the WFO, the capacity obtained in this way can result in a high cost of curtailed energy.

5. WIND POWER HOSTING CAPACITY OF A DISTRIBUTION SYSTEM

That is, for such capacity of wind power, rather than using curtailment the WFO could have been more profitable by using grid reinforcement. Thus, the model proposed in this thesis constrains maximum energy curtailment level by comparing its cost with the cost of grid reinforcement (see (5.16) below).

The next subsections discuss the main costs encountered and benefits gained by WFO and DSO due to integration of wind power. The focus is only on the monetary costs and benefits. Hence, for example, the extra benefit gained by a society due to environmental benefits of wind power is not taken into account. Moreover, the discussion of some financial tools from economics, which are used in our cost-benefit analysis, is included.

5.2.1 Costs & benefits of a distribution system operator

5.2.1.1 Costs of a distribution system operator

The DSO may encounter a significant cost during the connection stage of the wind turbine. The DSO faces these costs only if there is a need to reinforce the network [123]. Otherwise the connection costs up to the point of common coupling are endured by WFO. Since this study focuses on increasing the hosting capacity using the existing system, no connection cost is assumed on the DSO. Other sources of cost for the DSO due to the connection of wind power may include:

- Increase in network losses due to reverse power flow
- Curtailed wind energy, depending on the agreement between the DSO and WFO
- Infrastructure for implementing AMSs

5.2.1.2 Benefits of a distribution system operator

Network investment deferral can be seen as the major benefit of distributed generations in general. However, due to uncontrollability of the energy source (i.e wind speed) at the wind turbines and low correlation between load and wind power data, wind farms can only make minor contribution to network investment deferral. In other words, wind power cannot be relied on to meet the peak power demand in a distribution system as the power output from wind turbines depends on the wind condition in the area.

On the other hand, in countries like Sweden and UK, the WFO pays the DSO network fee for using the network [124]. This network fee usually breaks down into a combination of any of the following ones as determined by different regulatory frameworks [125–127]:

- Fixed charge per month or per year
- A fee based on kW installed or maximum power injected per month or per year
- A fee based on kWh energy transmitted by the network
- A fee based on kVarh reactive power consumed and transmitted

5.2.2 Costs & benefits of a wind farm owner

5.2.2.1 Costs of a wind farm owner

The overall expenses of the WFO are affected by numerous parameters such as the capital and variable costs of the wind turbine, the discount rates, and the economic life time of the wind turbine [128].

Capital costs: The capital cost includes the costs of the wind turbines, foundation, road construction, grid connection and other project development and planning costs. Usually, these costs contribute to 80% of the total cost of the project over its entire life [128]. The actual value of the capital cost differs significantly between countries as well as between projects. According to the report by European Wind Energy Association (EWEA) [2], the capital cost in Europe differs between 1 million €/MW and 1.35 million €/MW and the average turbine installed in Europe costs 1.23 million €/MW. Future forecasts by both European commission and European wind energy association show that the capital cost will be lower than what it is today [2]. Moreover, the lifetime of the wind turbine is around 20 years for onshore wind turbines and 25 years for offshore ones [2].

Variable costs: Variable costs include expenses pertaining to [128]

- operation and maintenance (O&M) cost, which includes regular maintenance, repairs and spare parts
- Land rental
- Insurances and taxes
- Administration, including audits, management activities, forecasting services and remote control measures.

The current estimate of these variable costs obtained from EWEA is between 12 to 15 €/MWh [2].

5.2.2.2 Benefits of a wind farm owner

In most countries, renewable energy, including wind power, is supported through regulating either the price or quantity of electricity from these sources [2]. In price based schemes, the supplier of electricity from renewable sources receive subsidy per kW of capacity installed, or payment per kWh produced and sold. This can be in terms of soft loans during the investment stage or the supplier is able to sell the electricity at a fixed feed-in tariff or at a fixed premium (in addition to the electricity market price).

Tendering and Tradable green certificate (also known as renewable portfolio standard models in US and Japan states) systems are the two commonly used quantity based schemes. In the former case, a tender is launched by a government body to supply a given amount of electricity with a guaranteed tariff for a specified period of time. In the latter case, the supplier of electricity from renewable sources sell two products: electricity, which is sold in electricity markets, and green certificate, which is sold in a market for fulfilling the political obligation to supply renewable energy [2].

In Sweden, green certificates are used to support energy from renewable sources. The average green certificate price in Sweden for 2011 was 27.92 €/MWh [129] and the average electricity

5. WIND POWER HOSTING CAPACITY OF A DISTRIBUTION SYSTEM

price at spot market was 47.85 €/MWh [130]. Hence the average revenue gained in 2011 by producing a MWh of electricity from wind power was 75.77 €.

5.2.3 Tools for cost benefit analysis

When dealing with costs and benefits occurring at different time, there are a number of tools that can be used to facilitate decision making about an investment. Here two of them are presented.

5.2.3.1 Present worth analysis

Present worth analysis is a method by which costs and savings at different time are compared for decision making.

Given f_t^{PW} as a present worth factor, then the amount of net cash flow B_t at a future year n is equal to A amount at present, where B_t and A are related as follows

$$A = B_t f_t^{\text{PW}} \quad (5.1)$$

Using the discount rate, r , the present worth factor, f_t^{PW} , of money at year n is given by [131]

$$f_t^{\text{PW}} = \frac{1}{(1+r)^t} \quad (5.2)$$

The net present value, v^{NP} , of cash flows occurring at a different time is the sum of the present worth of individual cash flows i.e.

$$v^{\text{NP}} = \sum_{n=1}^N B_t f_t^{\text{PW}} \quad (5.3)$$

where N is the total period of the investment in years. If identical net cash flows occur in every year t starting from year one i.e. $B_t = B, \forall n$, then we have

$$v^{\text{NP}} = B \times f^{\text{NPW}} \quad (5.4)$$

where

$$f^{\text{NPW}} = \frac{(1+r)^N - 1}{r(1+r)^N} \quad (5.5)$$

5.2.3.2 Levelized values

Levelized values, v^{L} , is the constant annual cost of the project having the same present worth as the actual cost of the project.

$$v^{\text{L}} = v^{\text{NP}} \frac{r(1+r)^N}{(1+r)^N - 1} \quad (5.6)$$

Levelized costs can give a better platform for comparing different projects with different life times [131].

5.3 Modeling the hosting capacity problem

Based on the discussions in Section 5.1 and 5.2 , this section develops an optimization model that that can be used to determine the optimal hosting capacity of a distribution system and the optimal usage level of active management strategies.

5.3.1 The Objective function

Since the optimal capacity could be different based on who covers the different costs incurred due to the active management strategies involved, separate objective functions are developed for each actor, i.e. DSO and WFO. The aim of the objective functions, in each case, is to maximize the net benefit of the corresponding actor taking into account the different costs and benefits discussed in Section 5.1. Moreover, some costs of wind power integration, such as curtailed energy, may be covered by either the DSO or the WFO.

Both objective functions are subject to the same equality and inequality constraints provided in the subsequent sections.

5.3.1.1 The Objective function of the DSO

The objective function of the DSO is developed assuming that the DSO agrees to pay the WFO for the curtailed energy. Hence, the DSO's objective is to maximize the net benefit it gets while covering the cost of curtailed energy and increase network losses over the economic life time of the wind turbine and is formulated as

$$\max_{n_i, P_{i,t}^{\text{cur}}} O = \sum_i a_i n_i - \sum_i \sum_t b_i P_{i,t}^{\text{cur}} - c \Delta P^{\text{loss}} + d \quad (5.7)$$

where

$a_i, b_i, c,$ and d are coefficients to be calculated based on cost benefit data of the DSO
 n_i is number of wind turbines with 1 MW capacity
 $P_{i,t}^{\text{cur}}$ is curtailed power in MW at each bus i and time t
 ΔP^{loss} is the change in power losses P^{loss} due to wind power introduction, where

$$P^{\text{loss}} = \frac{1}{T} \sum_t \sum_k \sum_{j < k} g_{k,j} \left(\left(\frac{V_{k,t}}{n_{k,j,t}} \right)^2 + V_{j,t}^2 - \frac{2 \cdot V_{k,t} \cdot V_{j,t}}{n_{k,j,t}} \cos(\delta_{j,t} - \delta_{k,t}) \right) \quad (5.8)$$

In (5.7), the first term accounts for revenue from network fee while the second and the third term represents the cost of curtailed and increase in network losses respectively. The last term represents any constant revenue or expense, e.g. subscription fee, investment cost of the infrastructure for implementing AMSs. Moreover, the coefficients of each term should be calculated as the present worth of the associated costs or benefits during the life time of the wind turbine. Moreover, one can calculate b_i (excluding the cost of curtailed energy) to investigate the case where the DSO covers only the cost of increase in network losses.

5. WIND POWER HOSTING CAPACITY OF A DISTRIBUTION SYSTEM

5.3.1.2 The objective function of the WFO

Similarly, the objective function of the WFO is developed assuming the WFO bears the cost of curtailed energy. Hence the objective function which maximizes the net benefit of the WFO is formulated as

$$\max_{n_i, P_{i,t}^{\text{cur}}} O = \sum_i \alpha_i n_i - \sum_i \sum_t \beta_i P_{i,t}^{\text{cur}} - \kappa \quad (5.9)$$

where α_i , β_i and κ are coefficients to be calculated based on cost benefit data of the WFO

In (5.9) the first term accounts for revenues (including electricity and green certificate sell) and costs (investment cost, O&M costs) per kW of installed capacity while losses in revenue due to curtailed energy is accounted for by the second term. The last term represents any constant revenues or expenses. Similar to the case of DSO, the coefficients in (5.9) should also be calculated as the present worth of the associated costs or benefits during the life time of the wind turbine.

5.3.2 The constraints

The objective functions proposed in the previous subsection are subject to different equality and inequality constraints. These constraints are described below.

5.3.2.1 Equality constraints

The equality constraints are the load flow equations [79]

$$\begin{aligned} P_{i,t} - P_{i,t}^D &= \sum_j Y_{i,u} V_{i,t} V_{u,t} \cos(\theta_{i,u} + \delta_{u,t} - \delta_{i,t}) \\ Q_{i,t} - Q_{i,t}^D &= - \sum_j Y_{i,u} V_{i,t} V_{u,t} \sin(\theta_{i,u} + \delta_{u,t} - \delta_{i,t}) \end{aligned} \quad (5.10)$$

where for buses to which wind power is connected, $P_{i,t}$ can be replaced by

$$P_{i,t} = n_i P_{i,t}^W - P_{i,t}^{\text{cur}} \quad (5.11)$$

and $P_{i,t}^W$ is the available wind power at time t and at bus i [p.u.]

However, whenever the hosting capacity is limited due to the voltage rise problem, the limits on the tap ratio may be violated. Under such a condition, there is a need to constrain the tap ratio within its limit. One way of doing this can be to model the elements of the admittance matrix that are affected by the tap ratio as decision variables. Another way could be to use the modified load flow equations proposed in Section 3.2.3. The first approach, besides the variables of the original load flow equations (5.10), will have some elements of the admittance matrix and the tap ratio as additional variables while the second approach will have only the tap ratio as an additional variable. Hence the second approach takes less simulation time. Thus, the modified load flow equations derived in Section 3.2.3 ((3.9 revisited) and (3.10 revisited)) replace (5.10).

For bus in $k \in K$:

$$\begin{aligned} P_{k,t} - P_{k,t}^D &= \sum_j P_{k,j,t}^F \\ Q_{k,t} - Q_{k,t}^D &= \sum_j Q_{k,j,t}^F \end{aligned} \quad (3.9 \text{ revised})$$

where

$$\begin{aligned} P_{k,j,t}^F &= \left(\frac{V_{k,t}}{n_{k,j,t}} \right)^2 g_{k,j} - \frac{V_{k,t}V_{j,t}}{n_{k,j,t}} y_{k,j} \cos(\delta_{j,t} - \delta_{k,t} + \varphi_{k,j}) \\ Q_{k,j,t}^F &= -V_{k,t}^2 \left(\frac{b_{k,j}}{n_{k,j,t}^2} + \frac{b_{k,j}^c}{2} \right) + \frac{V_{k,t}V_{j,t}}{n_{k,j,t}} y_{k,j} \sin(\delta_{j,t} - \delta_{k,t} + \varphi_{k,j}) \end{aligned} \quad (3.7 \text{ revised})$$

For bus $j \in J$:

$$\begin{aligned} P_{j,t} - P_{j,t}^D &= \sum_k P_{j,k,t}^F \\ Q_{j,t} - Q_{j,t}^D &= \sum_k Q_{j,k,t}^F \end{aligned} \quad (3.10 \text{ revised})$$

where

$$\begin{aligned} P_{j,k,t}^F &= V_{j,t}^2 g_{j,k} - \frac{V_{j,t}V_{k,t}}{n_{k,j,t}} y_{j,k} \cos(\delta_{k,t} - \delta_{j,t} + \varphi_{k,j}) \\ Q_{j,k,t}^F &= -V_{j,t}^2 \left(b_{j,k} + \frac{b_{j,k}^c}{2} \right) + \frac{V_{j,t}V_{k,t}}{n_{k,j,t}} y_{j,k} \sin(\delta_{k,t} - \delta_{j,t} + \varphi_{k,j}) \end{aligned} \quad (3.8 \text{ revised})$$

5.3.2.2 Inequality constraints

The inequality constraints include:

- the limit on the thermal capacity (current limit) of network components; this includes the limit on the ampacity of network cables $I_{k,j}^{\text{rat}}$, as given by (5.12)¹, and the power rating of the substation transformer $S_{k,j}^{\text{rat}}$, as given by (5.13),

$$y_{k,j}^2 (V_{k,t}^2 + V_{j,t}^2 - 2V_{k,t}V_{j,t} \cos(\delta_{j,t} - \delta_{k,t})) \leq \left(I_{k,j}^{\text{rat}} \right)^2 \quad \forall k > j \quad (5.12)$$

$$y_{k,j}^2 V_{k,t}^2 \left(\left(\frac{V_{k,t}}{n_{k,j,t}} \right)^2 + V_{j,t}^2 - \frac{2 \cdot V_{k,t} \cdot V_{j,t}}{n_{k,j,t}} \times \cos(\delta_{j,t} - \delta_{k,t}) \right) \leq \left(S_{k,j}^{\text{rat}} \right)^2 \quad \forall k > j \quad (5.13)$$

- the limit on the available range of tap ratio,

$$n_{k,j}^{\min} \leq n_{k,j,t} \leq n_{k,j}^{\max} \quad (5.14)$$

¹In π -model of a line (Fig. 3.2), the current that passes through the resistive element and causes thermal overheating can be calculated using $I_{k,j} = y_{k,j} e^{i\varphi_{k,j}} (V_{k,t} e^{i\delta_k} - V_{j,t} e^{i\delta_j})$ and this gives (5.12). Similar analysis on the π -model of a transformer (Fig.3.3) gives (5.13).

5. WIND POWER HOSTING CAPACITY OF A DISTRIBUTION SYSTEM

- the voltage limits on each bus,

$$V_i^{\min} \leq V_{i,t} \leq V_i^{\max} \quad (5.15)$$

- the limit on cost of curtailed energy, mainly compared to the cost of alternative investment such as reinforcement,

$$\gamma \sum_i \sum_t P_{i,t}^{\text{cur}} + C^{\text{am}} \leq \chi \quad (5.16)$$

where

γ the net present worth of a MWh of electricity from wind power [€/MWh]

C^{am} the net present value of the cost of active management strategy

χ the net present value of the cost of the alternative investment

If the projects (the AMS system and reinforcement) are known to have different life time, it would be more reasonable to compare based on levelized costs rather than the net present value. Moreover, this constraint assumes that the costs both on the left and the right side of the equation are covered by the same stakeholder, i.e. either DSO or WFO. That is, when a case by case analysis is done later, in the respective cases either the DSO or the WFO is assumed to cover both costs.

- whenever necessary, a limit on the curtailed energy as a percentage of the total available wind energy at each bus i can be set as,

$$\sum_t P_{i,t}^{\text{cur}} \leq \lambda_i \sum_t n_i P_{i,t}^{\text{W}} \quad (5.17)$$

where λ_i is the maximum allowed percentage of curtailed energy with respect to the total available wind energy

- and the limit on available active and reactive power at each bus.

$$\begin{aligned} P_{i,t}^{\min} &\leq P_{i,t} \leq P_{i,t}^{\max} \\ Q_{i,t}^{\min} &\leq Q_{i,t} \leq Q_{i,t}^{\max} \end{aligned} \quad (5.18)$$

$P_{i,t}$ and $Q_{i,t}$ do not need to be bounded at the slack bus. Hence $P_{i,t}^{\min}$ and $Q_{i,t}^{\min}$ can be assigned $-\infty$ and $P_{i,t}^{\max}$ and $Q_{i,t}^{\max}$ can be set to $+\infty$. For buses with wind power, where $P_{i,t}$ is replaced as in (5.11), the constraint on $P_{i,t}^{\text{cur}}$ can be given by (5.19),

$$0 \leq P_{i,t}^{\text{cur}} \leq n_i P_{i,t}^{\text{W}} \quad (5.19)$$

and $Q_{i,t}^{\min}$, $Q_{i,t}^{\max}$ are given by (5.20).

$$\begin{aligned} Q_{i,t}^{\min} &= -n_{i,t} P_{i,t}^{\text{W}} \frac{\sqrt{1 - (\Phi^{\min})^2}}{\Phi^{\min}} \\ Q_{i,t}^{\max} &= n_{i,t} P_{i,t}^{\text{W}} \frac{\sqrt{1 - (\Phi^{\min})^2}}{\Phi^{\min}} \end{aligned} \quad (5.20)$$

where Φ^{\min} is the minimum operating power factor level of the wind turbine. For the rest of the buses all limits $-P_{i,t}^{\min}$, $P_{i,t}^{\max}$, $Q_{i,t}^{\min}$, and $Q_{i,t}^{\max}$ —should be zero.

5.3.3 Model implementation

From the formulation above, it can be observed that the model is a nonlinear programming (NLP) problem with multiperiod OPF. In this thesis, the model is implemented in GAMS and solved using an interior-point-based solver (IPOPT) [80].

5.4 Stochastic wind power and load data modeling

Determining the optimal wind power capacity of a given network depends on the load and wind power condition in the system. Some articles in literature [89, 90, 98, 103, 112] have used single loading level of customer loads. However, consumer loads and wind power are variable by nature and can have different magnitude at different time of the day or week or year. Hence this approach does not provide sufficient information about hosting capacity of the distribution networks. Whenever available, time series load and wind power data can be used to represent this stochastic nature [3]. However, time series data are rarely available at every bus in a given distribution system. Moreover, when time series data are available, the length of the series can be large. Depending on the network size and the number of equality and inequality constraints involved, this may result in longer convergence time of the optimization model. This demands for another way of generating load and wind power data. In [7, 10], clustering techniques are used based on load duration curve and cumulative distribution function or measurement data; where full correlation is assumed among loads as well as between power outputs of wind turbines at different buses. Though the approach captures the stochastic nature of wind power and load data to some level, it lacks flexibility to model load data with different correlation levels. Moreover it is known that customer loads are not fully correlated though they could be highly correlated. Hence this section provides a discussion of a mathematical (statistical) model that captures the stochastic nature of load and wind power data as well as the correlation that exists between them. Using this model, data of required size can be generated based on existing measurement data or some established models such as load duration curves (for load data) and Weibull distribution (for wind power data).

A statistical modeling usually means coming up with a simple (or mathematically tractable) model without the knowledge of the physical aspects of the situation. However the model should try to capture the important characteristics of the physical situation such as the appropriate density shape of the univariate margins and the appropriate dependence structure [132]. Though a number of alternatives have been proposed to model multivariate random processes [133], the copula method is found to be more flexible and more suited for modeling the stochastic nature of load and wind power data [134, 135]. Hence, in this thesis, the copula approach is chosen for modeling the stochastic nature of load and wind power data, which is briefly discussed below.

5.4.1 Using copula to model the stochastic nature of load and wind power

Copulas provide an easy way to model and generate random vectors when one believes that the dependence structure between the random variables can be expressed independent of the marginal distributions of the random variables [133]. The univariate marginal distribution functions can be modeled by using parametric or non-parametric models while the dependence structure is captured

5. WIND POWER HOSTING CAPACITY OF A DISTRIBUTION SYSTEM

by using a copula. In this thesis, the Weibull distribution is used for modeling the wind data. However, since the parametric models are not flexible enough, a non-parametric model [136] is used to model the load data. The dependence structure among the data is captured using the Gaussian copula.

The following subsection introduce the concept of copula and the copula types investigated for use in stochastic modeling of load and wind power data.

5.4.1.1 Copula: definition

Given p uniform random variable u_1, u_2, \dots, u_p in the unit interval, where these random variables are not necessarily assumed to be independent, the dependence between them is expressed as follows using copula [137].

$$C(u_1, u_2, \dots, u_p) = \text{prob}(U_1 \leq u_1, U_2 \leq u_2, \dots, U_p \leq u_p) \quad (5.21)$$

where C is the copula and U is a uniform random variable and u is the corresponding realization. Thus given p random variables x_1, x_2, \dots, x_p with the corresponding marginal distribution $F_1(x_1), F_2(x_2), \dots, F_p(x_p)$, their multivariate distribution function can be given by

$$F(x_1, x_2, \dots, x_p) = C[F_1(x_1), F_2(x_2), \dots, F_p(x_p)] \quad (5.22)$$

The marginal functions $F_1(x_1), F_2(x_2), \dots, F_p(x_p)$ can assume any distribution independent of each other and the copula structure. There are both parametric and non-parametric copulas. Copulas are usually grouped into copula families.

5.4.1.2 Families of copula

There are a number of families of copulas which have different capabilities in dependence modeling and have their own pros and cons. The two main families of copula are: the elliptical copula and the Archimedean copula. Elliptical copulas have elliptical contoured distributions. Their key advantage is that one can specify different levels of correlation between the marginals. Their key disadvantages are that elliptical copulas do not have closed form expressions and are restricted to have radial symmetry which means they cannot model asymmetric dependence [138]. Unlike elliptical copulas, Archimedean copulas have a simple closed form and they can model asymmetry available in empirical data. The Archimedean copulas reduce the study of multivariate copula to a single univariate function. However, these copulas use only one parameter which limits their flexibility in modeling the dependence of multivariate vectors. Though there are variants of Archimedean copulas that provide better flexibilities for modeling multivariate random variables [139], they are computationally intensive [140]. Therefore, due to their low computation complexity and high versatility in dependence modeling, elliptical copulas are preferred in this thesis for modeling the dependence among load and wind power data.

5.4.1.3 Elliptical copulas

Elliptical copulas are of two types: Gaussian copula and t-copula. Both copulas have a dispersion matrix, ρ , and t-copula has one more parameter, the degree of freedom, ν . As reported in [140], the

Gaussian copula does not model upper tail dependence unless $\rho = 1$, whereas the t-copula could do that for different values of ρ . However the degree at which it models upper tail dependence gets weaker as the degree of freedom increases. While both copulas can cover the modeling of dependence from perfect negative dependence (countermonotonicity, $\rho = -1$) to perfect positive dependence (comonotonicity, $\rho = 1$), the t-copula does not model independence unless ν tends to infinite [141].

However, on one hand, no tail dependence is seen between load and wind power data, hence there is no need for the ability to model tail dependence. On the other hand, the Gaussian copula has a much lower computational complexity than the t-copula. Hence, the Gaussian copula is used in this thesis for modeling the dependence among load and wind power data. Mathematically the Gaussian copula is represented by [140]:

$$C(u_1, u_2, \dots, u_p; \rho) = \Psi_\rho[\Psi^{-1}(u_1), \Psi^{-1}(u_2), \dots, \Psi^{-1}(u_p)] \quad (5.23)$$

where Ψ_ρ the standardized multivariate normal distribution with correlation matrix ρ and Ψ^{-1} the inverse of the normal distribution.

5.4.2 Estimating parameters of the Gaussian copula from empirical data

In general the maximum likelihood method [142] can be used for estimating the parameters of a copula based on observed data set. In this method, the parameters of both the marginal functions and the dependence structure are jointly estimated which makes the method computationally intensive. An alternative approach is to estimate the parameters of each margin independently before the parameters of the dependence structure. This approach is called the inference functions for margins (IFM) method. Yet another approach is to transform the observed data set (x_1^t, \dots, x_N^t) at time t into the uniform variate (u_1^t, \dots, u_N^t) using an empirical distribution and then to determine the parameter of the copula using the uniform variate. This method is called the canonical maximum likelihood method or CML. The IFM (or CML) estimator for the Gaussian copula is given as [142]¹:

$$\rho_{CML} = \frac{1}{T} \sum_{t=1}^T \zeta_t^\top \zeta_t \quad (5.25)$$

where $\zeta_t = (\Psi^{-1}(u_1^t), \dots, \Psi^{-1}(u_N^t))$.

5.4.3 Sample generation using the Gaussian copula

The reason behind searching for a statistical model to represent the stochastic nature of load and wind power data is to finally generate synthetic data of a required length. This generated data can further be used to make load flow calculations.

¹ this is asymptotically equivalent to calculating the Spearman's correlation and to deduce the correlation parameter using the relation [140]:

$$\rho = 2 \sin \frac{\pi}{6} \rho \quad (5.24)$$

5. WIND POWER HOSTING CAPACITY OF A DISTRIBUTION SYSTEM

For Gaussian copula, random numbers having the required dependence structure is generated from the Gaussian distribution. Then, the Gaussian (normal) cumulative distribution function is applied to get a random uniform variables, (U_1, \dots, U_N) . Finally, $X_i = F_{X_i}^{-1}(U_i)$ gives the synthetic data that possess the dependence structure as well as the margins of the original random variables (in our case load and wind power data).

5.5 Case study

This section provides the results of two independent case studies. The first one is based on a widely studied 69 bus system found in literature [143]. The second one is based on a real case study: a rural 11kV distribution system operated by Falbygdens Energi located in Falköping area in Sweden. Further description of the distribution systems will be given in the respective sections below.

5.5.1 Cost-benefit data

Here the main focus is to discuss the monetary value of the assumed costs and benefits of both the DSO and the WFO. It is based on these costs and benefits that the coefficient of the objective functions of the DSO and the WFO are calculated for each scenario. Moreover, these same cost benefit data are used for both case studies.

5.5.1.1 Cost-benefit data of the distribution system operator

The monetary values of the benefits of the DSO are taken to be the network fees charged by Falbygdens Energi. These fees are shown in Table 5.1¹ [125].

Table 5.1: Network fees for rated power above 1.5 MW connected to 11 kV network

Subscription fee (ρ^{sf}) [€/yr]	Peak power fee (ρ^{pf}) [€/MW/mon]	Distribution fee (ρ^{df}) [€/MWh]	Transmission benefit (ρ^{tb}) [€/MWh]
3975	812	1.30	-2.27

The different fees in Table 5.1 are explained as follows:

- Subscription fee (ρ^{sf}): a yearly fee paid for subscription of service.
- Peak power fee (ρ^{pf}): the monthly fee paid by WFO based on the maximum one hour average wind power injected.
- Distribution fee (ρ^{df}): the amount paid by WFO per MWh of electrical energy injected.
- Transmission benefit (ρ^{tb}): the payment made by the DSO to the WFO to account for the benefits of distributed power production. On the other hand, Falbygdens energi gets the same level of reduction in payments made to the transmission system operator.

¹The data are original given in SEK. It is converted into € using the all time average exchange rate, 9.2319 SEK = 1 €, obtained from European central bank

The costs of the DSO are the expense due to increase in network losses and the refund made to the WFO for curtailed energy. The monetary value of the cost of increase in power losses is taken to be the average spot market price for Sweden in 2011: 47.85 €/MWh. For the curtailed energy the DSO is assumed to pay the WFO the opportunity cost of the curtailed energy. This equals to the average spot market price plus the average cost of a green certificate: 75.77 €/MWh. Besides the DSO will lose some portion of the revenue from network fee due to WEC. On the other hand, the DSO needs to invest on communication and control infrastructure that implements the AMSs. The review of investment costs of AMS from different projects shows that the cost varies between 100 k€ - 850 k€ [144–149]. The costs vary depending on the number of points being monitored and controlled and the type of active management strategies being implemented. However, as pointed out in [150], the DSO may refund this cost by increasing the network fees. Of course, this will put additional cost on the WFO. Since some of these projects include the cost of research and development (R & D), the cost of AMS is expected to decrease in the future. Hence the capital cost of AMS in forth coming analysis is assumed to be 100 k€ per substation with 12 k€ for each additional wind power connection point, as in [144]. That is, its taken to be roughly 200 k€ for Case study I with eight PCCs and 100 k€ in Case study II with one PCC.

Based on these cost-benefit data, the formulas for calculating the coefficients of the objective function of the DSO in (5.7) are given as:

$$\begin{aligned}
 a_i &= f^{\text{mp}} n^{\text{mon}} \rho^{\text{pf}} + f_i^{\text{cf}} \rho^{\text{df}} \\
 b_i &= \frac{f^{\text{mp}} n^{\text{mon}} \rho^{\text{pf}}}{\sum_t P_{i,t}^{\text{W}}} + \frac{h^{\text{yr}}}{T} (\rho^{\text{df}} + C^{\text{e}} + C^{\text{gc}}) \\
 c &= C^{\text{e}} h^{\text{yr}} \\
 d &= \rho^{\text{sf}}
 \end{aligned} \tag{5.26}$$

where

- f^{mp} the average monthly peak power from the wind turbines [p.u.]
- n^{mon} number of months per year
- f_i^{cf} capacity factor in numbers of hours of full power production in a year
- h^{yr} number of hours per year
- T sample length
- C^{e} cost of electricity based on spot market [€/MWh]
- C^{gc} cost of green certificate [€/MWh]

Here, it is assumed that the cash flows of the DSO due to the wind power do not change from year to year. Thus, the expression for coefficients are formulated to maximize the annual net benefit of the DSO. This provides the possibility to assess the net benefit of the DSO with different discount rates.

5.5.1.2 Cost-benefit data of the wind farm owner

As for the WFO, most of the monetary values of costs and benefits are given in Section 5.2, which are summarized in Table 5.2, including the network fees presented in Table 5.1.

Based on the cost and benefits of the WFO presented in Table 5.2, the formulas for calculating the coefficients of the objective function of the WFO in (5.9) are given in (5.27). One should note

5. WIND POWER HOSTING CAPACITY OF A DISTRIBUTION SYSTEM

Table 5.2: An estimate of costs and benefits of a WFO

Benefit	Revenue from electricity sale (C^e) [€/MWh]	47.85	
	Revenue from green certificate sale (C^{gc}) [€/MWh]	27.92	
	Revenue from transmission benefit (ρ^{tb}) [€/MWh]	2.27	
Costs	Investment cost (C^c) [€/MW]	1 225 000	
	O&M costs (C^v) [€/MWh]	14.5	
	AMS implementation cost (C^{am}) [€]	100-200 k	
	Network fee	Distribution fee (ρ^{df}) [€/MWh]	1.3
		Peak power fee (ρ^{pf}) [€/MW/month]	812
Subscription fee (ρ^{sf}) [€/yr]		3975	

that these coefficients correspond to the case where the WFO concedes the cost of curtailed energy but not that of increase in power losses. In the case where the WFO concedes both costs, another coefficient is added to account for the loss increase.

$$\begin{aligned}
 \beta_i &= ((C^e + C^{gc} + \rho^{tb} - C^v - \rho^{df})f_i^{cf} - f^{mp}n^{mon}\rho^{pf}) \times f^{npw} \\
 \alpha_i &= \beta_i - C^c \\
 \kappa &= \rho^{sf} \times f^{npw} + C^{am}
 \end{aligned} \tag{5.27}$$

where

f^{npw} the net present worth factor given in (5.5) and n which is the life time of the wind turbine is taken to be 20 years

C^v variable costs of wind power [€/MWh]

C^c capital cost of wind power [€/MW]

5.5.1.3 Comparing energy curtailment with grid reinforcement

Using constraint (5.16) a comparison is made between WEC and investment on capacity enhancement of the substation transformer to determine if and when investing on substation capacity enhancement could be a better option. Substation capacity enhancement is chosen because it is the constraint that needs major investment to increase the hosting capacity of the system. The cost of curtailed energy is taken as $\gamma = 75.77$ €/MWh. This includes the loss in revenue from both green certificate and energy sell. The cost of new substation construction is roughly estimated to be 93 000€/MVA¹ [151]. Thus (5.16) can be rewritten as:

$$75.77 \sum_i \sum_t P_{i,t}^{cur} + C^{am} \leq 93000 \sum_i n_i \tag{5.28}$$

Besides substation capacity enhancement it is possible to investigate enhancement in the form of reconductoring, new cable installation, etc.

¹Its average value is given in the reference as 112 000\$/MVA, but it is converted into € here using the all time average exchange rate between € and \$ i.e. 1.2103

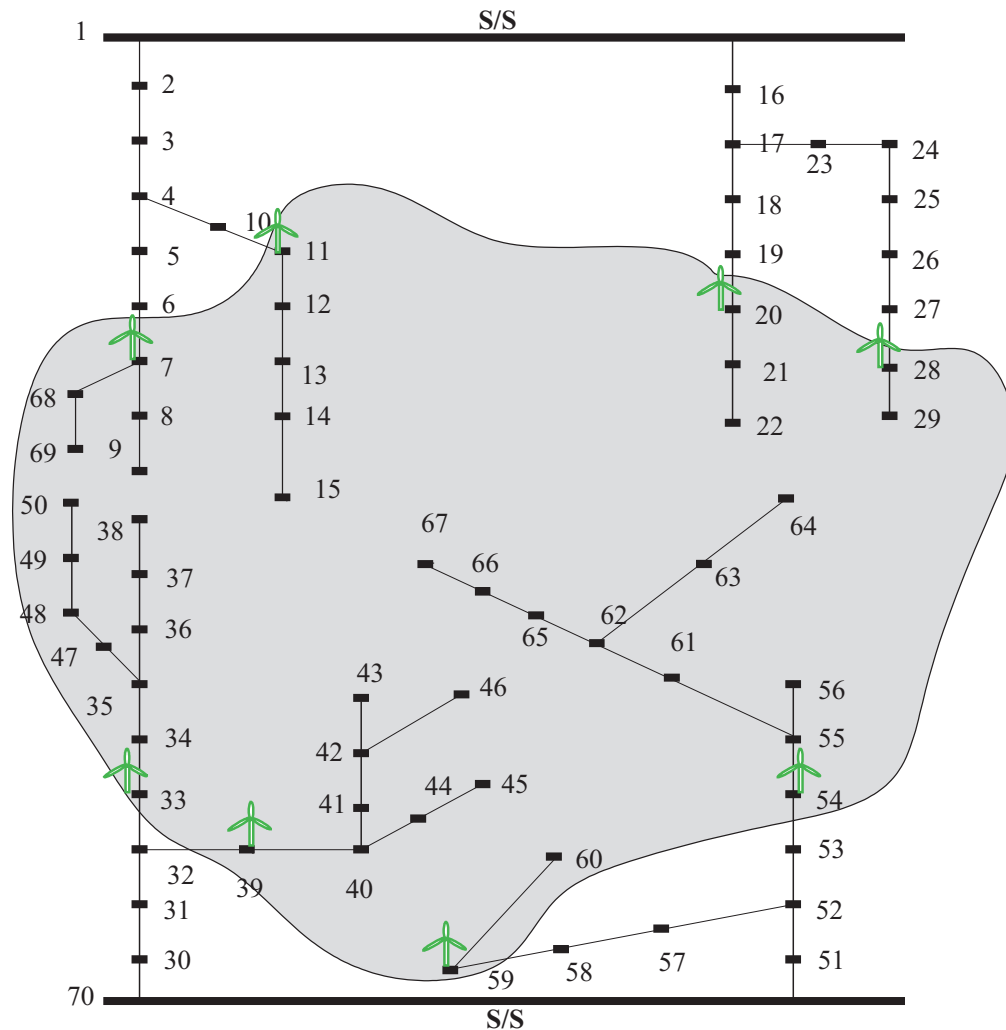


Figure 5.5: The 69 bus system [143].

5.5.2 Case study I: 69 bus system

5.5.2.1 Network and data description

Network description: This is an 11-kV radial distribution system having two substations, four feeders, 69 nodes, and 68 branches as shown in Fig. 5.5. It is also assumed that

- each substation has a 10 MVA transformer with $X(\%) = 8$ and $X/R = 16$
- the external grid has a SCC of 250 MVA with $X/R = 10$
- only those buses within the shaded area are available for connection

Data description: To use the optimization model developed in Section 5.3, load and wind power data are needed as an input. In [143] average load data on each bus are provided. Assuming the load duration curve of Fig 5.6, synthetic data of 1000 samples are generated for the load at each buss. Full correlation is assumed among load data on different buses. The synthetic data generation is done in such a way that the mean value of the synthetic load data is equal to the values given

5. WIND POWER HOSTING CAPACITY OF A DISTRIBUTION SYSTEM

in [143] for the corresponding bus. Inline with the discussion in Section 5.4.3, The synthetic load data are generated in Matlab. For wind power data, the Weibull distribution has been used to

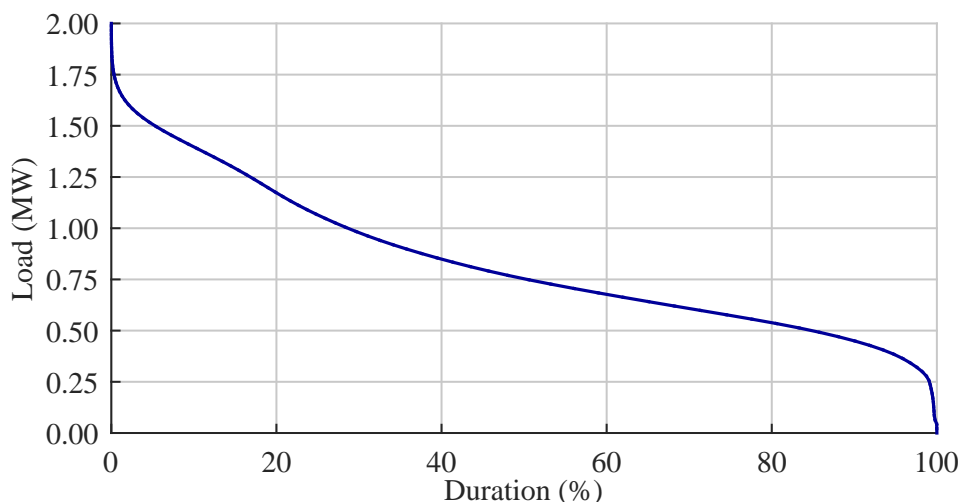


Figure 5.6: Load duration curve.

generate the wind speed data, which are converted into wind power data using the power curve of a typical wind turbine. Moreover, since usually wind power and load data have only a low level of correlation [135], independence is assumed between wind and load data. However, wind power data at different sites are assumed to be fully correlated. This is valid since in a distribution system of this size the correlation between the wind speeds at different area are high. For example, in the network analyzed as Case study II, there are wind turbines from around eleven locations in the network. The correlation between them varies between 0.83 and 0.96.

5.5.2.2 Siting the wind farms for maximizing the hosting capacity of the network

Before any optimization is done on the hosting capacity of the network, the optimal siting of the wind farms should be chosen based on the objective in consideration: maximizing the wind power hosting capacity of the network, in this case. Based on the discussion in Chapter 4, buses 7, 11, 20, 28, 33, 39, 54, 59 can be determined as those combination of buses which result in maximum hosting capacity, thus in the forthcoming analysis the wind turbines are assumed to be connected to these buses.

5.5.2.3 Hosting capacity and the active management strategies

In this section the role of each active management strategy in increasing the hosting capacity of the system is presented. Two cases of average wind speeds are considered:

- Case 1: with average speed of 7.5 m/s with a shape factor of 2 resulting in a capacity factor of 33.4%
- Case 2: with average speed of 6.5 m/s with a shape factor of 2 resulting in a capacity factor of 25.6%

Fig. 5.7 shows the capacity of wind power that can be installed using different AMSs. The hosting capacity is found to be the same for both Case 1 and 2. This is partly because the same load data

are taken for both cases. This means that the amount of wind power that can be installed in both cases is the same for the first three scenarios—no active management strategy (No AMS), C-OLTC voltage control, and RPC—as the hosting capacity depends on the minimum loading condition rather than the wind power condition on the system. In the fourth scenario, which is the case of WEC, wind energy is curtailed so as to achieve the same level of hosting capacity as in the case of RPC. Consequently, 0.8% and 0.5% of the wind energy is respectively curtailed for Case 1 and Case 2. With this amount of curtailed energy, together with RPC and C-OLTC, the final capacity with all AMSs involved is calculated, which is shown as the last bar of Fig. 5.7.

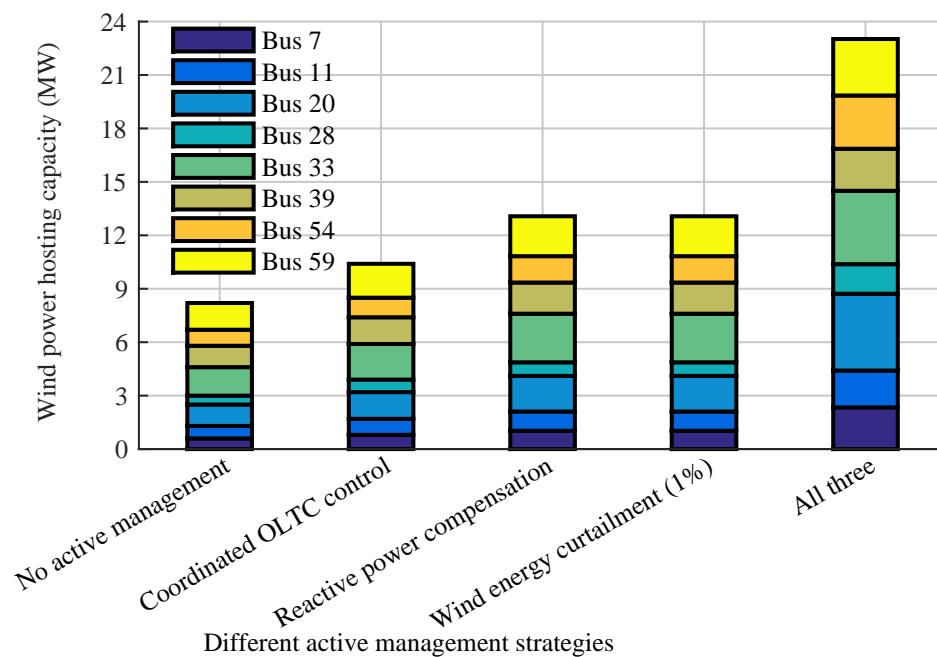


Figure 5.7: The role of AMS in increasing the hosting capacity (for both Case 1 & 2).

Fig. 5.7 shows that the hosting capacity can be increased significantly by using AMSs. The actual increase in hosting capacity in the case of RPC depends on the level of reactive power available from the wind turbines—here operation up to a minimum power factor of 0.95 is assumed. However, even if there is sufficient amount of reactive power, after some level, the thermal capacity of the involved components, such as cables and transformers, limits the amount of wind power that can be installed using RPC. In the case of energy curtailment, the hosting capacity can be increased infinitely in theory. However, the economics of the wind power installation determine the amount of wind energy one is willing to curtail.

On the other hand, if the capacity of wind power installed on per bus basis is investigated, for the first three cases the hosting capacity increases through Buses 28, 7, 11, 54, 39, 20, 59 to Bus 33. This order is mainly determined by impedance of the cable that connects the PCC to the substation. That is, generally, the lower this impedance is the higher the hosting capacity will be. However, this is not always the case. For example, the equivalent impedance between the substation and Bus 39 is lower than the same impedance for Buses 59 and 20. In spite of this, Buses 59 and 20 host higher wind power capacity as the hosting capacity of Bus 39 is limited due to wind power installed in the same feeder at bus 33, which has even lower equivalent impedance compared to Bus 39. In the last case where all AMSs are involved, some redistribution of hosting capacity occurs within

5. WIND POWER HOSTING CAPACITY OF A DISTRIBUTION SYSTEM

buses in the same feeder. However, similar to the cases before, those buses with lower equivalent impedance between the substation and the PCC host more wind power.

Table 5.3 shows the amount of energy lost annually due to introduction of wind power using the various AMSs. It can be seen that for both cases (Case 1 and Case 2) that energy is saved due to loss reduction when wind power is installed using No AMS and C-OLTC. This is mainly due to low level wind power in the system. In case of RPC, due to extra consumption of reactive power there is an increase in power losses. In case of WEC there is a loss in energy due to curtailment and gain in energy due to saving in power losses.

Table 5.3: Lost energy due to active management strategies (AMSs)

AMS type	Increase in Losses (MWh)		Curtailed energy (MWh)		Total energy lost (MWh)	
	Case 1	Case 2	Case 1	Case 2	Case 1	Case 2
No AMS	-524	-495	0	0	-524	-495
C-OLTC	-341	-410	0	0	-341	-410
RPC	-21	-267	0	0	-21	-267
WEC	-68	-289	305	144	236	-145
RPC & WEC & C-OLTC	3267	1639	572	266	3838	1905

Moreover, given the same capacity of wind power, wind farms with higher capacity factors result in higher losses in the system, as shown in Table 5.3. This is because on one hand the current flow through the network will be higher which results in higher losses. On the other hand, with a higher capacity factor, the curtailed energy increases due to the increase in coincidence of high wind power and low load condition in the system.

5.5.2.4 Optimal hosting capacity of the distribution system

The analysis in this section is done by limiting RPC in such way that the minimum operating power factor is equal to or greater than 0.95 while the optimal level of curtailed energy is determined. Moreover any present worth calculation in this section is done with a discount rate of 5%.

Case DSO^{CE&Loss} : In this case the DSO is assumed to pay the cost of curtailed energy and power losses in the network.

Table 5.4 also shows the optimal capacity, the optimal curtailed energy, increase in network power losses, and the net benefit (NB) generated by each actor during the life time of the wind farm. The cases refer to the two cases of wind speed considered in Section 5.5.2.3. When calculating the net benefit of the WFO using (5.7) the formula for coefficient β_i in (5.27) is modified as the WFO does not pay for curtailed energy. Similar modification is done to the coefficient b_i in Case WFO^{CE&Loss} below.

For Case 2, compared to the No AMS case considered in Section 5.5.2.3, the hosting capacity of the network is increased by as much as 136 % ($= \frac{19.8-8.4}{8.4} \times 100$), with a corresponding increase in NB generated by the DSO and WFO. Such an increase is achieved mainly by using RPC with very little support from WEC.

Table 5.4: The optimal hosting capacity of the system for Case DSO^{CE&Loss}

Cases	Case 1	Case 2
Hosting capacity (MW)	16.7	19.8
Curtailed energy (%)	0.01	0.02
Increase in average power losses (kW)	33	41
NB of the DSO(€)	2 550 000	2 810 000
NB of the WFO(€)	15 200 000	7 700 000

Inline with the observation made in Section 5.5.2.3, RPC is favored instead of WEC as it results in lower energy loss. Moreover, the cost of WEC includes not only the cost of electricity curtailed but also the cost of green certificate not sold. However, RPC causes power losses for which the DSO covers the cost of electricity only.

With respect to the DSO, lower capacity factor wind farms are preferred in this system as can be seen in Table 5.4. This is because, for a given wind farm size, wind farms with higher capacity factor introduce higher power flows and cause more loss than lower capacity factors. However, the network fee arrangement does not favor that much wind farms with higher capacity factor. To explain the situation, in this analysis, there are two main components of the network fee: the peak power fee and the distribution fee. The peak power fee is assumed to be invariant with respect to the capacity factor of the wind farm. This is based on the observation of one year measurement data available from wind turbines of various capacity factor i.e. the average monthly peak power is not seen to increase with capacity factor. Hence, in this analysis, the average monthly peak power is taken to be 0.94 pu for both cases, i.e. Case 1 and Case 2. The other is the distribution fee which depends on the capacity factor of the wind farm. But compared to the cost of power loss due to a MWh of electricity from the wind farm, the income generated from distribution fee is not significant.

Clearly, for the WFO, the net benefit increases with the capacity of the wind farm. As can be seen in Table 5.4, though the capacity of the wind farm is greater in Case 2, due to higher capacity factor the WFO have generated more NB in Case 1.

Over all, as can be seen in Fig. 5.8, the main source of income for the DSO is the network fee while the main cost of the DSO is the increase in power losses in the system. Though the cost of the increase in power losses are considerably low compared to the revenue gained from network fee, it is the main limiting factor that hinders further increase in hosting capacity. Moreover, the figure also shows that the cost of curtailed energy is negligible.

Case WFO^{CE&Loss} : In this case the WFO is assumed to pay the cost of curtailed energy and power losses in the network.

Table 5.5 shows that the optimal capacity of the network is increased compared to the DSO^{CE&Loss} case by 33 % ($= \frac{26.3-19.8}{19.8} \times 100$). This is a staggering increase of 213 % ($= \frac{26.3-8.4}{8.4} \times 100$) compared to the No AMS case. The optimal level of energy curtailment has also increased to 3% compared to the DSO^{CE&Loss} case. This is because RPC alone cannot assist a further increase in hosting capacity when the thermal rating is also a limiting factor. The power losses in the system have also increased considerably. Now, since no cost is assumed on the DSO, the NB of the DSO has increased significantly. The NB of the WFO has also increased.

5. WIND POWER HOSTING CAPACITY OF A DISTRIBUTION SYSTEM

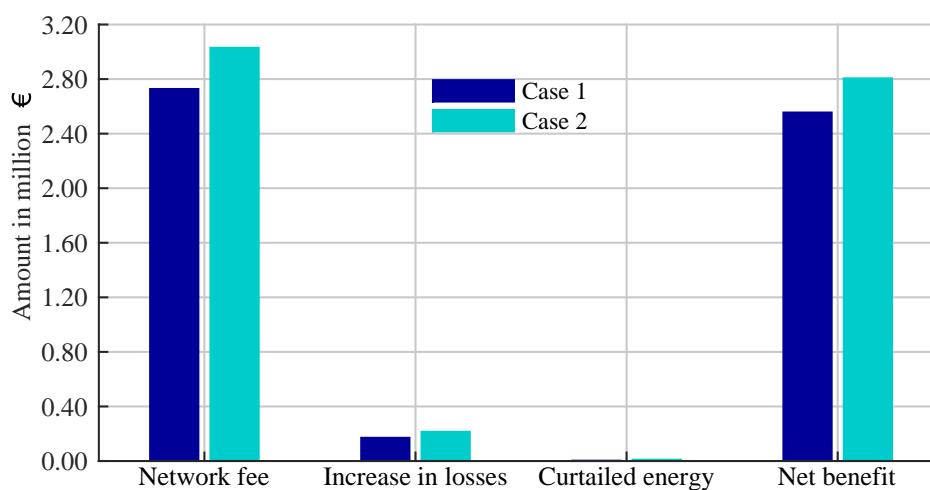


Figure 5.8: The cash flows of the DSO.

Table 5.5: The optimal hosting capacity of the system for Case WFO^{CE&Loss}

Cases	Case 1	Case 2
Hosting capacity (MW)	26.3	26.2
Curtailed energy (%)	3.0	1.6
Increase in average power losses (kW)	472	236
NB of the DSO(€)	4 200 000	3 940 000
NB of the WFO(€)	20 100 000	8 300 000

When it comes to the determination of the limiting factor to the increase in hosting capacity, the two cases of wind farm capacity factor can be seen separately. In Case 1, the hosting capacity is limited as a further increase in hosting capacity using energy curtailment is found to be less profitable than investing on a new substation. In other words, a further increase in hosting capacity is limited by the constraint in (5.28). In Case 2 the hosting capacity is limited as further curtailment is less profitable due to costs of power losses and curtailed energy.

Moreover, different cash flows of the WFO are shown in Fig. 5.9. Though there is a substantial income from electricity and green certificate sell, this income covers a number of costs. However, the AMS costs (which includes the cost curtailed energy and the implementation cost of AMSs) is very low compared to costs like investment cost and operation and maintenance costs (O&M costs).

One can also further investigate the case where the DSO covers for the cost of power losses in the network and the WFO bears the cost of curtailed energy. However, as seen in Fig. 5.8, since there is only a negligible cost associated with curtailed energy in the DSO^{CE&Loss} case, waiving the cost of curtailed energy from the DSO will not increase the hosting capacity of the network with respect to the DSO. Hence unless the WFO covers part of or all of the increase in loss due to the wind farm, the hosting capacity of the network will be limited to 16.7 MW in Case 1 and 19.8 MW in Case 2.

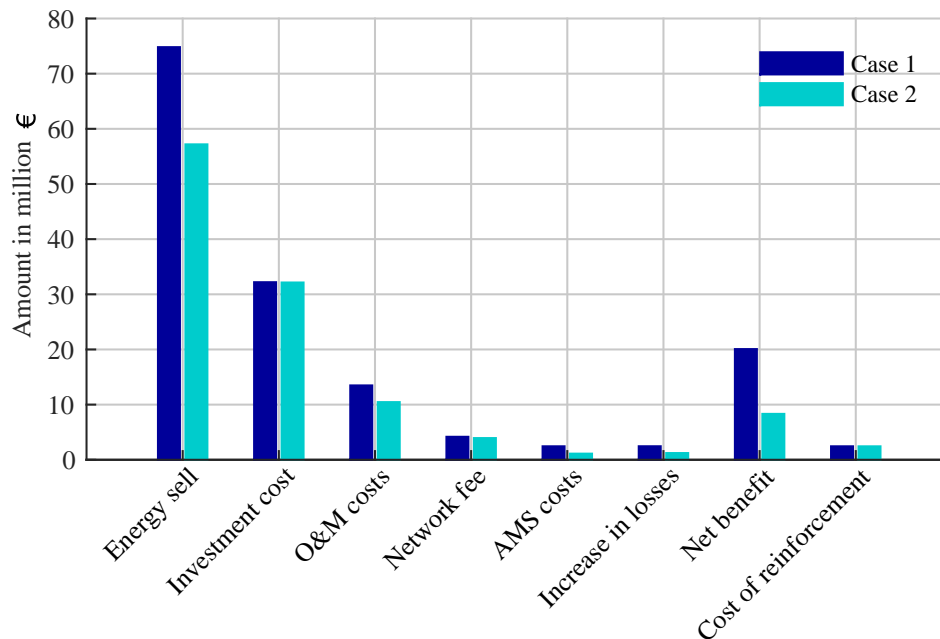


Figure 5.9: The different cash flows of the WFO.

5.5.3 Case study II: Falbygdens Energi's network

5.5.3.1 Network and data description

Network description: Case study II is based on a rural 11 kV distribution system operated by Falbygdens Energi located in Falköping area in Sweden. The network is fed by a 40 kV grid through a $45 \pm 8 \times 1.67\%/11.5$ kV, 10 MVA transformer. The tap changer of the transformer regulates the low voltage side of the transformer at 0.97 ± 0.012 pu¹. The voltage in the distribution system should be within $\pm 5\%$ of the nominal value, i.e. 0.97 pu. There are 13 wind turbines, with an overall installed capacity of 12.225 MW, already connected to the distribution system. A new wind farm is to be connected directly to the substation with an independent cable (see Fig 5.10). The distance of the wind farm from the substation is 5 km.

Data description: The existing 13 wind turbines in the distribution system have a varying capacity factor (CF) between 20% and 28% based on the available one year measurement data. From each of these wind turbines there is one year hourly measured active power data. Hourly measured active and reactive power data at the substation are also available for the same period. Adding the wind power data and the active power data from the substation, the load along with active power losses in the network is extracted. This calculation shows the minimum loading condition in the system to be 0.5 MW. The reactive power is assumed to come from the load. These time series load and wind power data are directly used in the optimization model.

Fig 5.11 shows the existing condition of load and wind power and the power flow through the substation transformer. Though the substation transformer is 10 MVA with minimum loading condition of 0.5 MW and installed wind power capacity of 12.225 MW, the maximum reverse

¹11 kV is taken as the base voltage

5. WIND POWER HOSTING CAPACITY OF A DISTRIBUTION SYSTEM

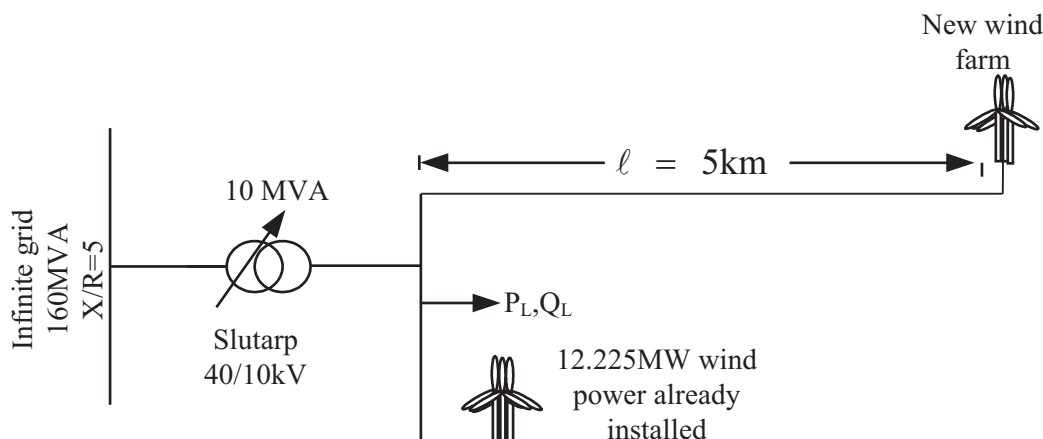


Figure 5.10: Simplified network of Fabygdens Energi.

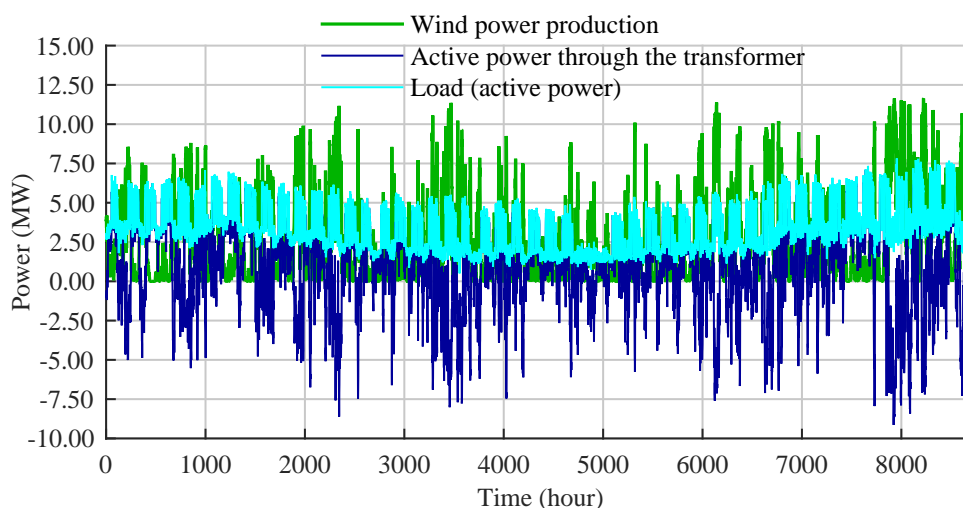


Figure 5.11: The load, wind and reverse power flow condition in the existing system.

power flow through transformer based on the one year measurement data shown in Fig 5.11 is 9.14 MW.

5.5.3.2 Optimal hosting capacity of the distribution system

It should be noted that, with the given transformer size and the observed minimum loading condition, even without additional wind power, there is a probability of overloading the substation transformer. Hence the optimal hosting capacity of the system is calculated using energy curtailment and C-OLTC voltage control as an AMS. RPC is not used here since C-OLTC voltage control is enough to deal with the voltage rise during high wind power output. Thus, the wind turbines are assumed to operate at unity power factor.

Case DSO^{CE&Loss} : Similar to the same case considered in Section 5.5.2.4, here the DSO is assumed to cover the cost of curtailed energy and power losses in the system. Then, the optimal hosting capacity is determined for three cases of wind power capacity factor: 28%, 24%, and 20%.

The results of the analysis, presented in Table 5.6, show that with a small percentage of curtailed energy a significant increase in hosting capacity can be achieved. With the existing transformer size and the minimum loading condition, it is only possible to install 10.5 MW of wind power without overloading the transformer. But by allowing 1% WEC, the hosting capacity can be increased up to 16.825 MW (= 12.225 MW + 4.6 MW). This amounts to an increase of 60% in hosting capacity of the distribution system. Moreover the table shows that, depending on the cost and benefit structure of the DSO, the wind power hosting capacity of a distribution network may not necessarily increase with the capacity factor of the wind turbine. In this analysis, the main source of revenue for the DSO is the peak power fee which increases with the installed capacity and does not depend on the capacity factor of the wind turbine. On the other hand, with the increase in capacity factor, the DSO gets more revenue from energy fee but there is also an increase in cost due to the increase in power losses. Therefore the increase in the capacity factor does not necessarily result in the increase in hosting capacity with respect to the DSO.

Table 5.6: Optimal level of additional wind power in the system with respect to the DSO

Capacity factor	28%	24%	20%
Additional capacity (MW)	4.6	4.0	4.4
Curtailed Energy (%)	0.9	1.3	1.6
Increase in average power losses (kW)	27	18	17
Cost of curtailed energy (€)	100 000	110 000	120 000
Cost of increased network losses (€)	140 000	90 000	90 000
Revenue due to network fee (€)	760 000	630 000	660 000
DSO's net benefit (€)	520 000	430 000	450 000
WFO's net benefit (€)	2 634 000	1 086 000	31 000
Cost of grid reinforcement (€)	430 000	370 000	410 000

The increase in hosting capacity gained here is not as much as the $DSO^{CE\&Loss}$ case in Section 5.5.2.4. This is due to the fact that here it is mainly energy curtailment and coordinated voltage control that are used to increase the hosting capacity unlike in the aforementioned case, where RPC is used. And, as mentioned previously, the loss increase due to RPC costs less than the energy loss due to curtailment.

Table 5.6 shows also different cash flows of the DSO during the life time of the project due to this additional wind power. These cash flows are calculated assuming a discount rate of 5%. Compared to the cost of grid reinforcement needed, the cost of curtailed energy is less than one third. This clearly shows the advantage of using AMSs, such as WEC, to increase the hosting capacity of a distribution system.

Moreover, the limiting factors with respect to the DSO in this case study are costs of both curtailed energy and increase in network power losses; in the same scenario considered in Case study I, the limiting factor was the loss increase. It is interesting to see that, even though the cables between the wind farm and the substation are not as lossy as in the network in Case study I, the increase in network losses still plays a significant role in determining the hosting capacity of the network.

Unlike the case studied in Section 5.5.2.4, Table 5.6 does not show the hosting capacity to follow a specific trend with the CF of the wind turbine. This is because the effect of increase in loss with

5. WIND POWER HOSTING CAPACITY OF A DISTRIBUTION SYSTEM

capacity factor is not as severe as in the Case study I.

In summary, the analysis shows that, in networks of different types, DSO can use AMSs to increase the hosting capacity of the network thereby increasing the benefit obtained from wind power as well as promoting the cost effective way of integrating wind power to the power system.

Case WFO^{CE}: In Case study I, though it seems unlikely, in one of the cases the WFO is assumed to cover the cost of curtailed energy and the increase in network power losses. Otherwise, the hosting capacity will be limited to a lower value as determined in the Case DSO^{CE&Loss}. In contrast, here the WFO is assumed to cover only the cost of curtailed energy. The increase in power losses will be covered by the DSO.

Table 5.7 presents the optimal hosting capacity, WEC level, and the net benefit of the WFO for three cases, which differ based on the CF of the wind power and the discount rate (DR) of the investment. The cases are:

- Case 1: CF = 28% and DR = 5%.
- Case 2: CF = 28% and DR = 7.5%.
- Case 3: CF = 24% and DR = 5%.

Table 5.7: Optimal wind power capacity with respect to WFO for different capacity factors and discount rates

Case	1	2	3
Additional capacity (MW)	7.0	7.5	6.0
Curtailed Energy (%)	3.3	4.1	3.8
Increase in average power losses (kW)	53	59	34
WFO's net benefit (€/life time)	3 420 000	1 250 000	1 190 000
DSO's net benefit(€/lifetime)	810 000	847 000	731 000

The different cash flows of the WFO are provided in Fig 5.12. These include revenues from energy sales (which includes the revenue from both electricity and green certificate sell), the cost due to network fee, O&M costs, the expected investment cost, the cost of AMSs (which includes the cost of curtailed energy and the implementation cost of AMSs), and the net benefit.

Compared to the the same case in Table 5.6 where the wind turbine has a capacity factor of 28%, the additional curtailment in wind power, e.g. $\frac{3.3\% - 0.9\%}{0.9\%} = 2.7$, does not result in a comparable boost in hosting capacity of the network, e.g. $\frac{7.0 - 4.6}{4.6} = 0.5$. But still a significant increase in hosting capacity, 83% ($= \frac{12.225 + 7.0 - 10.5}{10.5}$), is achieved with a relatively small curtailed energy, 3.3%. Moreover the AMS costs, as shown in Fig 5.12, is very low compared to other costs of the WFO.

Table 5.7 shows also that the hosting capacity decrease with the decrease in CF of the wind turbine in case of the WFO. This is reasonable as less CF implies less revenue for the WFO. Hence the WFO has less motivation to install more wind power when parts of the energy production is to be curtailed. However, in contrast to our expectation, the table shows that when the DR is increased i.e. from Case 1 to Case 2, more wind power is installed. This is because the hosting capacity in the analysis is limited due to the constraint in (5.28) i.e. a further increase in hosting capacity using

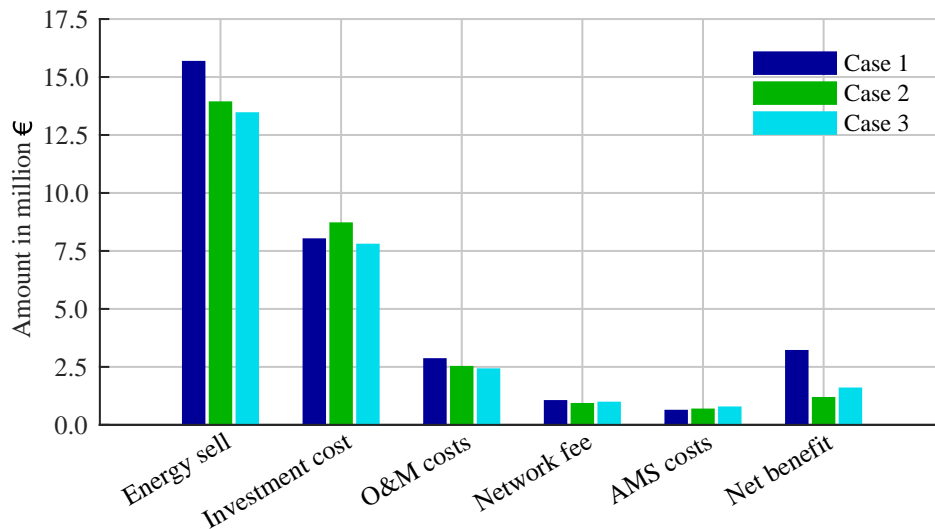


Figure 5.12: Expected cash flows of the WFO for each scenario shown in Table 5.7.

WEC is found to be less profitable than investing in new substation. Since grid reinforcement is assumed to be composed of upfront costs only, it does not depend on DR. However, higher DR decreases the net present value of the cost of curtailed energy. This means with higher DR, larger wind power capacity can be installed by curtailing more wind energy.

Fig. 5.13 presents more clearly the idea discussed in the above paragraph. The analysis is done for wind power having a CF of 28%. The figure shows that the hosting capacity of the distribution

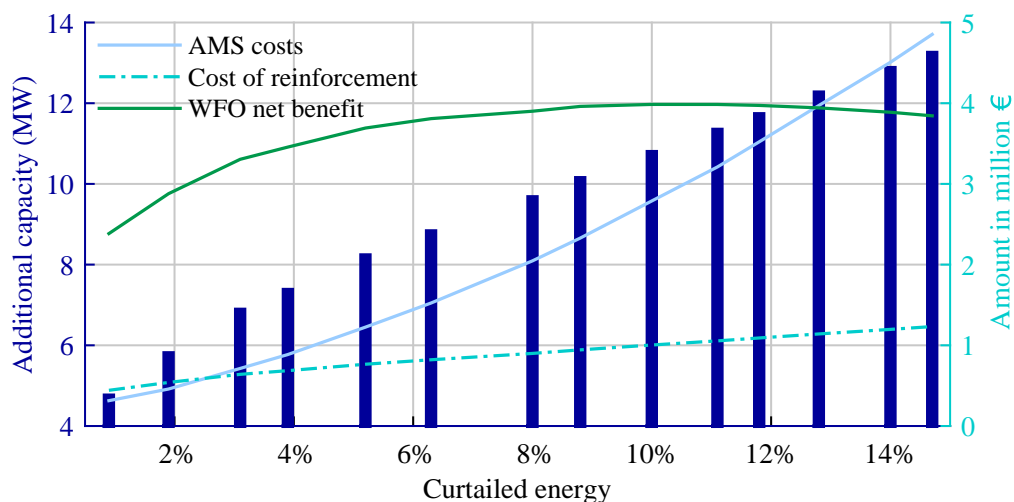


Figure 5.13: Comparing the investment options of the WFO.

system can be increased indefinitely using curtailment. But the net benefit of the WFO increases only until the curtailed energy reaches 10%. Even curtailing this level of energy is unreasonable as grid reinforcement can generate more profit. In fact, as can be seen from Fig. 5.13, WEC is attractive only up to 3.3%.

On the other hand, Fig. 5.14 shows the costs and benefits of the DSO when the WFO bears the

5. WIND POWER HOSTING CAPACITY OF A DISTRIBUTION SYSTEM

cost of curtailed energy. Despite significant loss in revenue due to increased power losses, the DSO continues to generate more revenue as the capacity of wind power in the system is increased. However, this observation holds true only for this case study. In Case study I, we have noticed that the increase in loss alone determines the optimal hosting capacity of the network with respect to the DSO. For example, in case of a wind farm with capacity factor 33.4%, almost immediately after 16.7 MW capacity of wind power the net benefit of the DSO would have declined if a similar analysis is done.

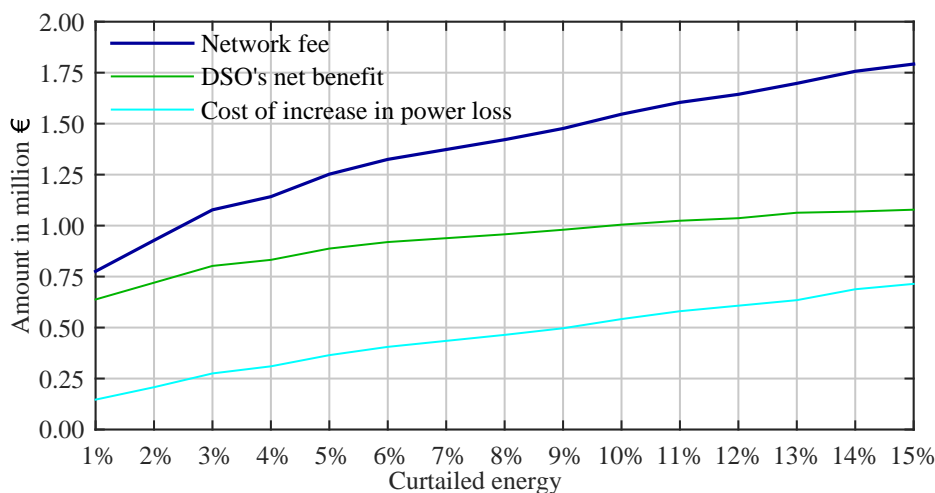


Figure 5.14: Costs and benefits of the DSO.

5.6 Summary

The analyses in this chapter have identified voltage rise and thermal overloading as the two most likely limiting factors of wind power integration to a distribution system. Consequently, three active management strategies (AMSs) have been investigated to increase the hosting capacity of a distribution network constrained due to these limiting factors. The AMSs include coordinated on-load tap changer voltage control (C-OLTC), reactive power compensation (RPC), and wind energy curtailment (WEC). C-OLTC is a preferred option to deal with voltage rise problems followed by RPC. If both solutions fail to achieve their objective, they can be assisted by WEC. To deal with the overloading of system components due to wind power the only solution considered in this thesis is WEC.

To further facilitate the investigation, a mathematical model based on a cost-benefit analysis is developed. The model also assesses the profitability of using AMSs with respect to grid reinforcement. The result of the investigation shows that the wind power hosting capacity of a distribution system can be increased up to twice the capacity that could be installed based on worst case analysis.

The optimal level of hosting capacity and curtailed energy depends on the capacity factor of the wind power plant and the discount rate. With respect to the WFO, higher capacity factor implies higher hosting capacity. But it is also affected by the discount rate, the cost of curtailed energy,

and the cost of grid reinforcement. On the other hand, the optimal level of curtailed energy in our analysis is found to be of low magnitude. After some level, e.g. a maximum of 3.8% in Case study II, it is not attractive to curtail more wind energy in order to increase the hosting capacity of the network.

5. WIND POWER HOSTING CAPACITY OF A DISTRIBUTION SYSTEM

6

State Estimation Algorithms for Distribution System Application

In Chapter 5 it is shown that active management strategies help distribution system operators to increase the available headroom for connecting distributed generations (DGs) and operate the network more efficiently. But the implementation of active management strategies requires the knowledge of the state of the network. To acquire such knowledge about the network, one can install measuring equipments at each and every node of the network but it would be extremely expensive. That is, the benefit obtained from such investment would most likely not justify the cost. Hence an alternative approach which still enables the implementation of active management strategies with reasonable cost is the use of state estimation (SE). Thus the aim of this chapter is to investigate state estimation algorithms for a distribution system application.

6.1 Introduction

In distribution system SE, one uses the less accurate historical data of power consumption (pseudo-measurement data) at every customer node together with a few real-time measurement data to determine bus voltages and branch currents. Even in the presence of smart meters which can provide load and voltage data from every customer node (as in Malta, Finland, Italy, Sweden [152]), these data are not available in the frequency that is required, for example, for voltage control. The highest data refresh rate currently available is 10 minutes in Italy [152], while for voltage control one need to have a data refresh rate in seconds. On the other hand, when energy data from smart meters are available, it can effectively be used to set up more accurate pseudo-measurement data.

A substantial amount of research work has been done with regards to SE algorithms for distribution systems. In [153] the various state estimators used in the transmission system (i.e. weighted least square, weighted least absolute value, Schweppe Huber generalized M estimator) are assessed for distribution system SE. It is found that the weighted least square method better fits SE in distribution systems. Reference [11] has also used the weighted least square formulation for SE in distribution systems where the state vectors are node voltages. The result of the SE is used to

6. STATE ESTIMATION ALGORITHMS FOR DISTRIBUTION SYSTEM APPLICATION

control the target voltage of automatic voltage control relays of the substation transformer. Similar SE approach is provided in [154]. The difference is that the model in [154] uses three-phase representation of the state variables. On the other hand, in [155] a branch-current-based SE algorithm is proposed where the state vectors considered to be branch currents. This algorithm is later improved in [156] and is found to be computationally efficient compared to the node-voltage-based SE algorithm. Reference [157] has proposed a SE algorithm where branch current magnitudes and angles are used as state variables. But the benefits obtained in using branch current as state variable are lost in this approach as the real and imaginary part of the state vector can not be decoupled and there is a need to update the Jacobian matrix at each iteration of the algorithm. Another computationally efficient method compared to the node-voltage-based method is proposed in [158]. Here the node voltages are still the state vectors, but rather than using actual power flow and power injection, it is proposed to use the equivalent current of these measurements. By so doing, the need to update the Jacobian matrix at each iteration of the algorithm is eliminated. Further studies related to SE in a distribution system include the effect of measurement placement on SE accuracy [157, 159, 160], and comparison of state vectors for SE [161].

In this chapter, two of the SE algorithms proposed in literature are compared in terms of the accuracy of the estimates and the computational intensiveness of the SE algorithm. One of these algorithms is the branch-current-based SE algorithm proposed in [155] which is later improved in [156]. As stated above, the reason for choosing this SE algorithm is its high computational efficiency. The other is the node-voltage-based SE algorithm used widely in transmission system SE and applied to distribution system in [11, 154]. The effects of measurement location and the type of measurement on the accuracy of these SE algorithms are also investigated through simulation.

6.2 Voltage profile in distribution system with DG: The need for state estimation

Before the introduction of DGs to distribution systems, it was fairly easy to identify the critical points along any uncompensated feeder. During high loading, the end of the feeders would be the most likely place to encounter under-voltage. During light loading or no loading, the voltage profile in the system would depend on the cable type in the system, whether it is overhead line or underground cable. If it is an overhead line, the voltage profile along the feeder would be close to the voltage set point at the substation whereas if underground cables are used in the system, the highest voltage in the network most likely occur at the end of the feeder. Hence, if the voltage magnitude at the beginning and the end of the feeder are known, any voltage regulation decisions could be made based on this information alone. In fact, utilities have learned to effectively regulate the network voltage based on the voltage at the substation alone, sometimes with additional current magnitude measurements at the substation. There are also cases where the voltage regulation at the substation would not be enough. Even in those cases, utilities have a good knowledge of the voltage profile in the network to carry out the required control actions, with the help of additional regulators or capacitors, and maintain the voltage within the allowed range.

However, the introduction of DGs, especially of renewable sources, have made estimation of the voltage profile in a given distribution system more complex. This is because renewable sources

6.2 Voltage profile in distribution system with DG: The need for state estimation

are much less predictable than customer loads with respect to their output. Thus, depending on the power output of the DG and the load, the voltage profile varies a lot along the feeder. Over-voltage most likely occurs at DG sites when the load in the distribution system is low whereas under-voltage occurs when the distribution system is highly loaded but the location of the under voltage depends on the magnitude of the DG output relative to the load. Consider the radial network in Fig. 6.1 with 14 buses, which is one of the feeders of an actual distribution system. The load demand from the rest of the feeders in the network is aggregated and is connected to the substation bus-bar. Fig. 6.2a presents three different cases of load profile along the feeder and power output from the wind power plant at bus 14. In Case 1 the load is uniformly distributed along the feeder while the power output from the wind turbine is relatively low. In Case 2 the load profile along the feeder is the same as in Case 1 but there is an increase in the power output of the wind turbine at bus 14. In Case 3 the load is somehow redistributed while the wind power output is kept constant as in Case 2. The resulting voltage profile along the feeder for the different cases is provided in Fig. 6.2b. In this analysis the voltage at the substation bus (Bus 1) is not regulated while the voltage at the infinity bus is assumed to be 1 p.u.. Thus, since there is voltage drop on the upstream grid and the substation transformer, the voltage at the substation busbar is not seen to be equal to 1 p.u..

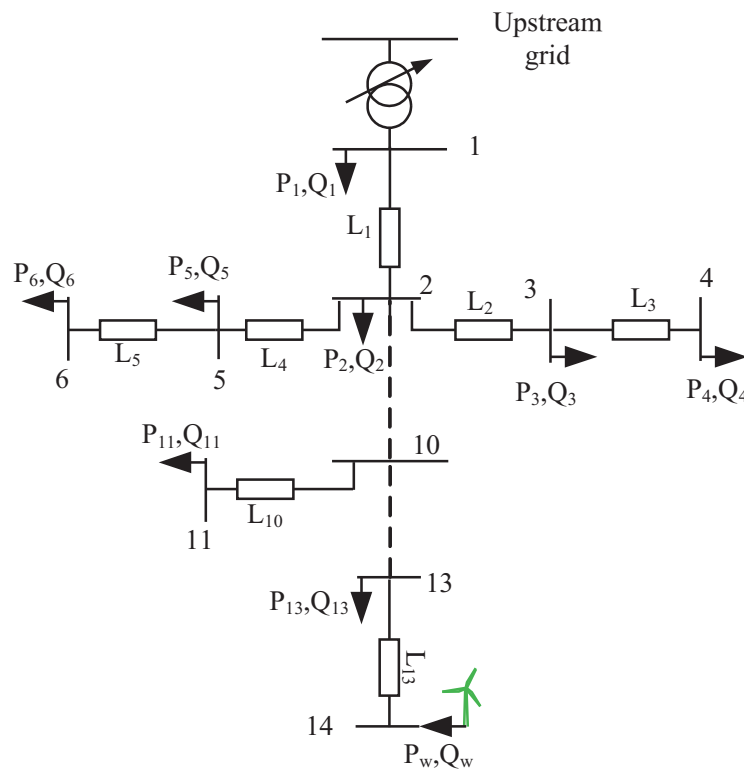


Figure 6.1: 14-bus feeder.

From Fig. 6.2b it is clear to see the bus at which the lowest voltage occurs depends on the load profile along the feeder and the output of the wind power plant. In Case 1, where the power from the wind turbine is low, the lowest voltage occurs at Bus 6 and 13. In Case 2, where the load profile along the feeder shows the same trend as in Case 1 except for the wind power output, the

6. STATE ESTIMATION ALGORITHMS FOR DISTRIBUTION SYSTEM APPLICATION

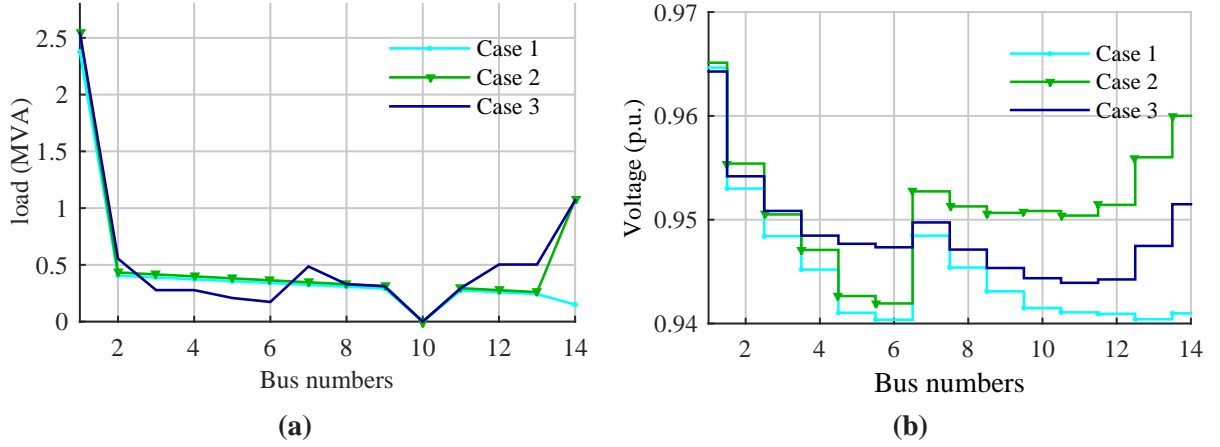


Figure 6.2: (a) Load profile of the feeder and (b) voltage profile along the feeder for the different cases.

lowest voltage occurs at Bus 6. In Case 3 the power output of the wind turbine is the same as Case 2 but the load profile along the feeder is changed resulting in the lowest voltage to occur at Bus 11. Thus, Figs. 6.2a and 6.2b show that the introduction of the DGs in distribution system makes it difficult to know the voltage profile along the feeder and initiate the right voltage regulation measures. Consequently, with increased introduction of DGs into the distribution system DNOs require more tools that can make them monitor the voltage magnitude throughout their network. As mentioned in the introduction of the chapter, SE is one such appropriate tool for this purpose.

6.3 State Estimation Algorithms

In this section, the mathematical background of the two SE algorithms chosen for comparison are presented. The basic principle of SE in both algorithms under investigation is similar: minimize the weighted error between measured values and estimated ones. The weighting is done based on the expected error of the measurement data. That is,

$$\min_{\mathbf{x}} J(\mathbf{x}) = \sum_{l=1}^n \frac{[z_l - f_l(\mathbf{x})]^2}{\sigma_l^2} \quad (6.1)$$

Where

l a measurement point in the network

z_l measurement at point l

\mathbf{x} the state vector

$f_l(\mathbf{x})$ the measurement function that relate the state vector with measurement at point l

σ_l standard deviation of the l^{th} measurement

and the state vectors are iteratively calculated using:

$$\mathbf{x}^{h+1} = \mathbf{x}^h + \left(H^\top(\mathbf{x}^h) \mathbf{W}_z^{-1} H(\mathbf{x}^h) \right)^{-1} H^\top(\mathbf{x}^h) \mathbf{W}_z^{-1} [\mathbf{z} - f(\mathbf{x}^h)] \quad (6.2)$$

where h is the iteration number and H is the Jacobian of $f(x)$, i.e.

$$H(\mathbf{x}^h) = \left[\frac{\partial f(\mathbf{x})}{\partial \mathbf{x}} \right]_{\mathbf{x}=\mathbf{x}^h} \quad (6.3)$$

and \mathbf{W}_z is the diagonal matrix of measurement covariance:

$$\mathbf{W}_z = \begin{bmatrix} \sigma_1^2 & & \\ & \sigma_2^2 & \\ & & \ddots \end{bmatrix} \quad (6.4)$$

The difference between the two SE algorithms lies in the choice of the state vector and, hence, on how the measurement function is set up and the Jacobian is calculated. In node-voltage-based algorithm, bus voltage magnitude and angle are used as state vector while in the branch-current-based algorithm the rectangular form of the branch currents are used as state vector. Below is provided a brief discussion of these two SE algorithms.

6.3.1 Node-voltage-based state estimation algorithm

Node voltage is widely used as state vector in transmission system SE long before the SE is considered for distribution system. Hence it quiet natural to adapt it to a distribution system SE.

In this SE algorithm one proceeds by developing measurement functions that relate the state vectors, i.e. voltage angle and magnitude, (6.5) with measurement data available at each point.

$$\mathbf{x} = \begin{bmatrix} V_1 \\ V_2 \\ \vdots \\ V_n \\ \delta_1 \\ \delta_2 \\ \vdots \\ \delta_n \end{bmatrix} \quad (6.5)$$

Thus, if the measurements available are active and reactive power injection at buses, the measurement function can be given as

$$\begin{aligned} f_l(\mathbf{x}^h) &= P_i^h = \sum_j Y_{i,j} V_i^h V_j^h \cos(\theta_{i,j} + \delta_j^h - \delta_i^h) \\ f_l(\mathbf{x}^h) &= Q_i^h = -\sum_j Y_{i,j} V_i^h V_j^h \sin(\theta_{i,j} + \delta_j^h - \delta_i^h) \end{aligned} \quad (3.5 \text{ revisited})$$

and if the available measurements are branch power flow, i.e. active power flow ($P_{i,j}$) and reactive power flow ($Q_{i,j}$), then the measurement function is

6. STATE ESTIMATION ALGORITHMS FOR DISTRIBUTION SYSTEM APPLICATION

$$\begin{aligned} f_l(\mathbf{x}^h) &= P_{i,j}^h = (V_i^h)^2 g_{i,j} - V_i^h V_j^h y_{i,j} \cos(\delta_j^h - \delta_i^h + \varphi_{i,j}) \\ f_l(\mathbf{x}^h) &= Q_{i,j}^h = - (V_i^h)^2 \left(b_{i,j} + \frac{b_{i,j}^c}{2} \right) + V_i^h V_j^h y_{i,j} \sin(\delta_j^h - \delta_i^h + \varphi_{i,j}) \end{aligned} \quad (3.8 \text{ revisited})$$

and for branch currents $I_{i,j}$ the measurement function is given by

$$f_l(\mathbf{x}^h) = (I_{i,j})^2 = y_{i,j}^2 \left((V_i^h)^2 + (V_j^h)^2 - 2V_i^h V_j^h \cos(\delta_j^h - \delta_i^h) \right) \quad (5.12 \text{ revisited})$$

The next step is to develop the Jacobian of the measurement function using (6.3) and the measurement covariance as given in (6.4). The iterative steps of the algorithm are as follows

1. starts by setting all bus voltage magnitudes equal to 1 p.u. and bus voltage angles to zero, except in places where voltage measurements are available.
2. calculate the estimate of the Jacobian matrix $H(\mathbf{x}^h)$ and the measurement function $f(\mathbf{x}^h)$.
3. use (6.2) to calculate the next estimate of the state vector \mathbf{x}^{h+1} .
4. check if $|\Delta \mathbf{x}^{h+1}|_\infty < \varepsilon$ if yes go to step (v) other wise go to step (ii). Here ε is some small positive value.
5. use (6.6) to calculate covariance matrix of the state vectors C_x where the diagonal of the matrix represents the variances of the state variables [154].

$$C_x = (H^\top \mathbf{W}_z^{-1} H)^{-1} \quad (6.6)$$

6.3.2 Branch-current-based state estimation algorithm

The SE algorithm discussed in the previous subsection works for any type of network radial or meshed but it is computationally intensive due to the need for recalculating the Jacobian matrix at every iteration of the algorithm and the coupling between the voltage magnitude and voltage angle state vectors. With these problems in mind and making use of the radial nature of distribution systems Baran [155] has proposed an innovative branch-current-based SE algorithm. This algorithm is latter improved by Lin [156]. The state vector in this approach can be represented as in (6.7).

$$\mathbf{x} = \begin{bmatrix} I_{1,2} \\ \vdots \\ I_{N-1,N} \end{bmatrix} \quad (6.7)$$

Two state vectors can be developed, one for real part and one for the imaginary part of the branch currents and each can be estimated independently as long as they are insured to be decoupled. This greatly reduces the computational burden of the algorithm. Once each part is calculated, they can

be combined to calculate the bus voltages in the network using forward sweep¹. For the sake of clarity of the presentation, in the forth coming discussion it is assumed that the buses are numbered from substation bus to the end of the feeder in increasing order.

Similar to the previous case, in this approach one tries to develop measurement functions that relate branch current with every measurement available. What follows is the discussion of such measurement functions for different measurement types.

6.3.2.1 Bus power injection

For bus power injections the equivalent current measurement (ECM) and the related measurement function can be set up as shown in (6.8)

$$\begin{aligned} z_l^h &= I_i^{\text{ECM},h} = \left[\frac{P_i + iQ_i}{V_i^h} \right]^* \\ f_l(\mathbf{x}^h) &= \sum_{j=1, j \neq i}^{j=N} I_{i,j}^h \end{aligned} \quad (6.8)$$

and the Jacobian terms can easily be calculated as

$$\begin{aligned} \frac{\partial f_l(\mathbf{x}^h)}{\partial I_{j,i}^h} &= -1 \quad \forall \quad j < i \quad \& \quad I_{j,i} \neq 0 \\ \frac{\partial f_l(\mathbf{x}^h)}{\partial I_{i,j}^h} &= 1 \quad \forall \quad i < j \quad \& \quad I_{i,j} \neq 0 \end{aligned} \quad (6.9)$$

Here the Jacobian terms are the same for both real and imaginary parts of the state vectors.

6.3.2.2 Branch current magnitude

Usually branch current measurements are given in absolute values hence originally Baran [155] proposed to use the measurement data directly and the measurement function as provide in (6.10).

$$\begin{aligned} z_l &= |I_{i,j}| \\ f_l(\mathbf{x}^h) &= \sqrt{(I_{i,j}^{r,h})^2 + (I_{i,j}^{i,h})^2} \end{aligned} \quad (6.10)$$

However, as pointed out by Lin [156], the application of this equation results in the coupling of the real and imaginary part of the calculation. Moreover, the Jacobian matrix needs to be updated at each iteration of the calculation. Hence a better alternative is proposed by Lin [156] where the ECM and the measurement function are modified as in (6.11).

$$\begin{aligned} z_l^h &= \left| I_{i,j}^{\text{ECM},h} \right| = \frac{I_{i,j}^h}{|I_{i,j}^h|} |I_{i,j}| \\ f_l(\mathbf{x}^h) &= I_{i,j}^h \end{aligned} \quad (6.11)$$

¹Forward sweep is a method by which the voltage at different buses are calculated progressively from the substation using voltage drop at preceding branches, and the voltage in the substation busbar is assumed to be given.

6. STATE ESTIMATION ALGORITHMS FOR DISTRIBUTION SYSTEM APPLICATION

Using (6.11) one can calculate the Jacobian terms as in (6.12).

$$\frac{\partial f_i(\mathbf{x}^h)}{\partial I_{i,j}^h} = \frac{\partial I_{i,j}^h}{\partial I_{i,j}^h} = 1 \quad (6.12)$$

6.3.2.3 Branch power flow

The power flow measurement, if there are any, would usually be in terms of both active and reactive power. Thus, the ECM and its measurement function is given by

$$\begin{aligned} z_i^h &= I_{i,j}^{\text{ECM},h} = \left[\frac{P_{i,j} + iQ_{i,j}}{V_i^h} \right]^* \\ f(\mathbf{x}^h) &= I_{i,j}^h \end{aligned} \quad (6.13)$$

assuming the measurement is made at the sending end of the line (point i). The Jacobian terms can be expressed in the same way as in (6.12).

6.3.2.4 Bus voltage

Sometimes there can be voltage magnitude measurement available from some buses in the network. If the voltage is represented using the same approach proposed by [157], the decoupling that exists between the real and imaginary part of the calculation will be lost. Hence voltage measurements are not directly included in the SE algorithm. However, in this estimation algorithm, unlike the node-voltage-based estimation algorithm, voltage is not an immediate result of the SE process. That is, an additional forward sweep stage is used at each iteration to calculate the bus voltages from the estimated branch currents. This voltage calculation stage is necessary to get a better estimate of the various ECMs. Now let there be a voltage magnitude measurement $|V_i^{\text{meas}}|$ at bus i and with forward sweep process let the calculated voltage be V_i^{cal} . We propose to replace the voltage at bus i with

$$V_i = \frac{V_i^{\text{cal}}}{|V_i^{\text{cal}}|} |V_i^{\text{meas}}| \quad (6.14)$$

and the forward sweep will continue with this updated voltage to calculate bus voltages downstream point i .

6.3.2.5 The algorithm

The steps of the algorithm are as follows:

1. set $|V_i| = 1$ for buses without voltage magnitude measurement and $\delta_i = 0$ for all buses
2. set up the state vector and the ECM for each measurement type using (6.8), (6.11) and (6.13), assume current magnitude measurements to be equal to the real part of the current (where the imaginary is assumed to be zero). Develop Jacobian and covariance matrix.

3. set the initial estimate of the state vectors, i.e. branch currents, to some low value, even zero.
4. forward sweep to calculate the bus voltages
5. recalculate the ECM \mathbf{z}^h using (6.8), (6.11) and (6.13) and calculate the estimate of the measurement functions $f(\mathbf{x}^h)$ from branch currents, this usually reduces to calculating $f(\mathbf{x}^h) = H\mathbf{x}^h$
6. calculate \mathbf{x}^{h+1} using (6.2)
7. if $|\Delta\mathbf{x}^{h+1}|_\infty = |\mathbf{x}^{h+1} - \mathbf{x}^h|_\infty \leq \varepsilon$ go to step (viii) otherwise go to step (iv)
8. forward sweep to calculate the final estimate of the bus voltages

Though the application of the branch-current-based approach is described here for purely radial system, it can also be effectively applied to weakly meshed systems as discussed in [156].

6.4 Case study system

6.4.1 Network and data description

The case study is based on a rural 11 kV distribution system operated by Falbygdens Energi located in Falköping area in Sweden. The network is fed by a 40 kV grid through a $45 \pm 8 \times 1.67\% / 11.5$ kV, 10 MVA transformer as shown in Fig. 6.1. The feeder is of 14 buses including the substation busbar. The available measured data include one-year hourly measured active and reactive power (at the substation) and wind power generation at bus 14. However, this measurement is only available from the main substation and consists of the power flow from all the feeders. Thus, some portion of these power data which are assumed to come from other feeders is directly connected to the substation busbar (see Fig. 6.1). The remaining amount is distributed to the different MV/LV substations of the feeder under investigation. The wind power data are similarly scaled and used to model a 2.5 MW wind turbine. Fig. 6.3a shows the total load of the feeder under investigation, the total load from the rest of feeders, and the wind power output. Fig. 6.3b shows the voltage variation at the different buses in the feeder for a given day. The calculation is based on uniformly distributed load along the feeder.

6.4.2 The simulation set up

In the forth coming discussion, the analysis of the SE results is done according to the block diagram shown in Fig. 6.4. Time-series data of load and wind power with 30 sec resolution are generated by interpolating the load and wind power data obtained from Falbygdens Energi. A 24 hour length of these data are used for load flow calculations. Then, in the SE, for buses where measurements are assumed to be available, data of the required kind are directly taken from the load flow results. On the other hand, for buses where no measurement is assumed to be available, Gaussian noise of the required magnitude is added to the load flow simulation results to emulate

6. STATE ESTIMATION ALGORITHMS FOR DISTRIBUTION SYSTEM APPLICATION

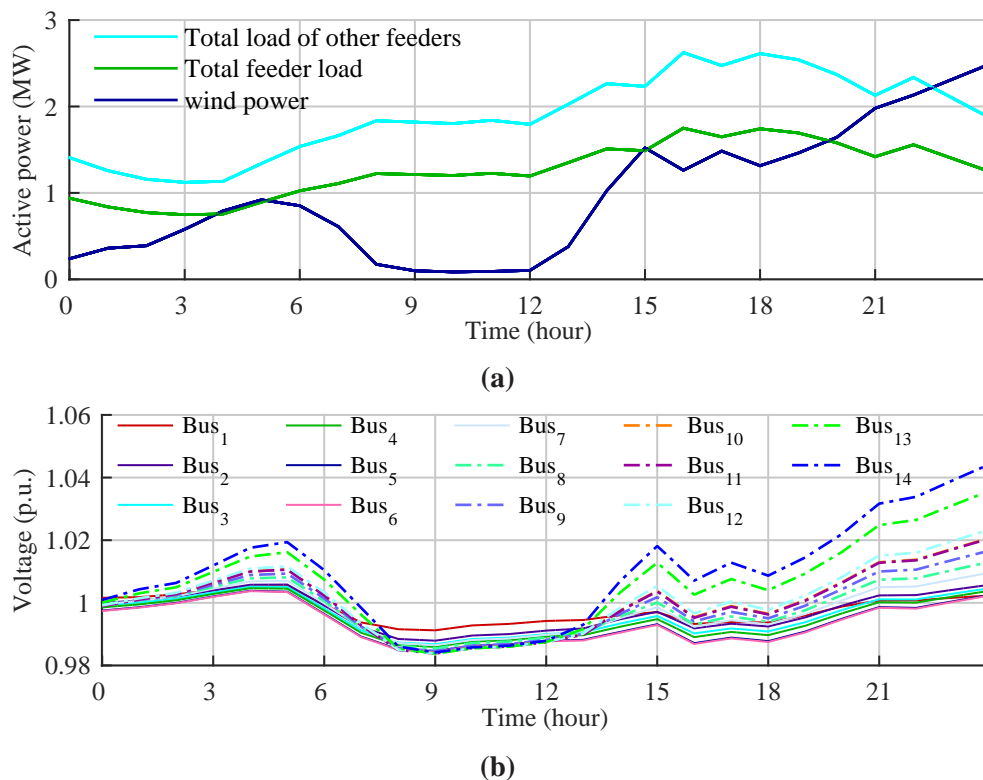


Figure 6.3: (a) Load profile and (b) voltage profile of the different buses on the feeder over 24 hour.

pseudo-measurement. These pseudo-measurements, in practice, can be synthesized based on customer load curves, weather and time of the day data and billing information [162]. If no such data are available, the measured power flow at each feeder at the substation bus can be distributed to each bus in proportion to the size of MV/LV substation transformer or recoded maximum power flow at the transformer.

Once the required data are obtained, the SE is carried out to determine the voltage at the different buses of the feeder for each time instant. One such example is shown in Fig. 6.5 for the case the

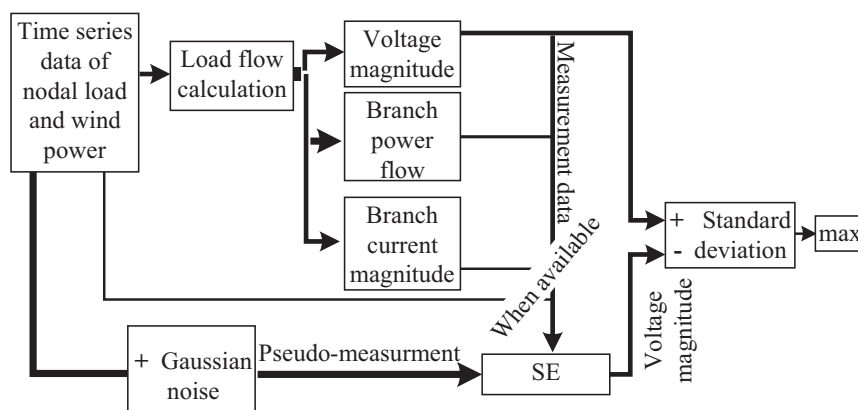


Figure 6.4: The outline of the simulation process.

wind turbine is located at Bus 14 and voltage and bus injection measurements are also available from Bus 14. Figs. 6.5a and 6.5b show the actual and the estimated voltage profile over 24-hour

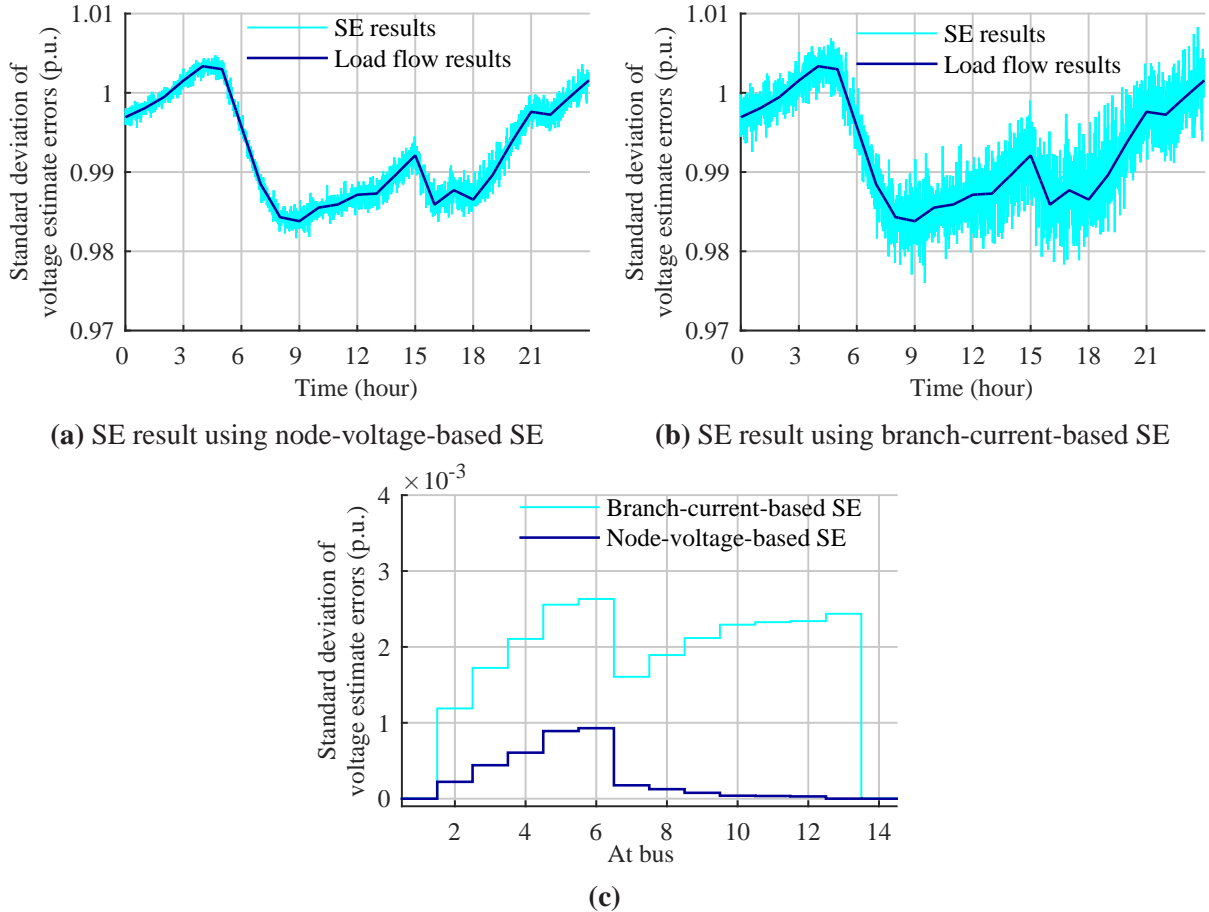


Figure 6.5: ((a), (b)) The actual and estimated voltage profile on Bus 6 over 24-hour, and (c) the standard deviation of the voltage estimate error at various buses for the case wind turbine is located at Bus 14 and power injection and voltage measurements are also available from Bus 14.

period at Bus 6. Similar plots can be obtained for different buses for the same case. Then, the error between voltages from load flow analysis and SE is calculated and the standard deviation of the error over the whole period is taken at each bus. In the case of Fig. 6.5 the results of such calculation are presented in Fig. 6.5c. Then the maximum of these standard deviations is used below to evaluate the accuracy of the estimation for each measurement location. In the case of Fig. 6.5, the maximum standard deviation of the voltage estimate error occurs at Bus 6, for which the voltage profile over 24-hour period is shown in Figs. 6.5a and 6.5b. This maximum standard deviation is found to be 0.001 for the case of node-voltage-based SE algorithm and 0.0027 for the case of branch-current-based SE algorithm. These values are shown in Fig. 6.6d at Bus 14. This means that when the power injection and voltage measurements are available from Bus 14, the actual voltage at Bus 6 lies within $\pm 3 \times 0.001 = \pm 0.003$ (for the case of node-voltage-based SE) or within $\pm 3 \times 0.0027 = \pm 0.0081$ (for the case of branch-current-based SE) around the estimated value with 99.7% confidence. Of course, since the standard deviation of the voltage estimate error is lower on the other buses, the estimated voltage there will be more accurate.

6. STATE ESTIMATION ALGORITHMS FOR DISTRIBUTION SYSTEM APPLICATION

The overall analysis is implemented in the Matlab-GAMS interface. Much of the data analysis and SE is carried out in Matlab while the load flow calculation is carried out in GAMS.

6.4.3 Analysis of the accuracy of the state estimation algorithms for different measurement types and their placement

This section investigates the different measurements types and their placement on the feeder to see their effect on the accuracy of the SE from the two algorithms. As usually is the case, the voltage measurement at the substation is assumed to be always available. The additional measurements available can be either bus power injection, branch power flow, or branch current magnitude. It is assumed that voltage magnitude measurement is also available from the buses where these measurements are taken. Moreover, the pseudo-measurement error is normally distributed with 99.7% of the time being within $\pm 100\%$ of the actual value, henceforth, simply stated as a pseudo-measurement accuracy within $\pm 100\%$. The aim of the analysis in this subsection is to find out:

- if any of these measurement types provide better voltage estimate with any of the two algorithms and to compare the two algorithms in terms of overall performance
- the measurement points which provide the best estimates for the different measurement types

Moreover, the results provided below are based on uniform load distribution in the network. However, similar analysis is done with uniformly increasing and decreasing load profile along the feeder, the results obtained are almost similar to what is presented below.

6.4.3.1 Bus voltage and power injection measurement

Fig. 6.6 shows the resulting estimation errors from placing voltage magnitude and power injection measurements at the corresponding buses in the network. The sub-figures present the result when the wind turbine is located at different buses in the feeder. In each sub-figure measurement at Bus 1 implies that the only measurement available is voltage magnitude at the substation (Bus 1). It is used to compare and assess the role of additional measurements in improving the SE results.

From Fig. 6.6, one can see that, for both branch-current-based and node-voltage-based SE algorithms, measuring at the wind turbines site reduces the observed voltage estimation error of the feeder. This is due to higher assumed variance in the estimate of the wind power output. This is valid since, on one hand, the wind power output is higher in magnitude and, on the other hand, wind power output is less predictable than load consumption. In general, however, for both SE algorithms setting the measurement points on lateral branches is not preferable, unless the wind turbine is located there.

Moreover, one can observe that the node-voltage-based SE algorithm generally provides a better result than the branch-current-based SE algorithm. The reason for these is that in case of node-voltage-based SE algorithm z_l is an actual or pseudo-measurement data whereas in branch-current-based SE case z_l is an ECM whose proximity to the actual current is dependent on the SE process. Thus, it is noticed, when the branch-current-based SE converges, even though the error between the ECM and the calculated current is zero, the error between the actual current and the calculated one is not.

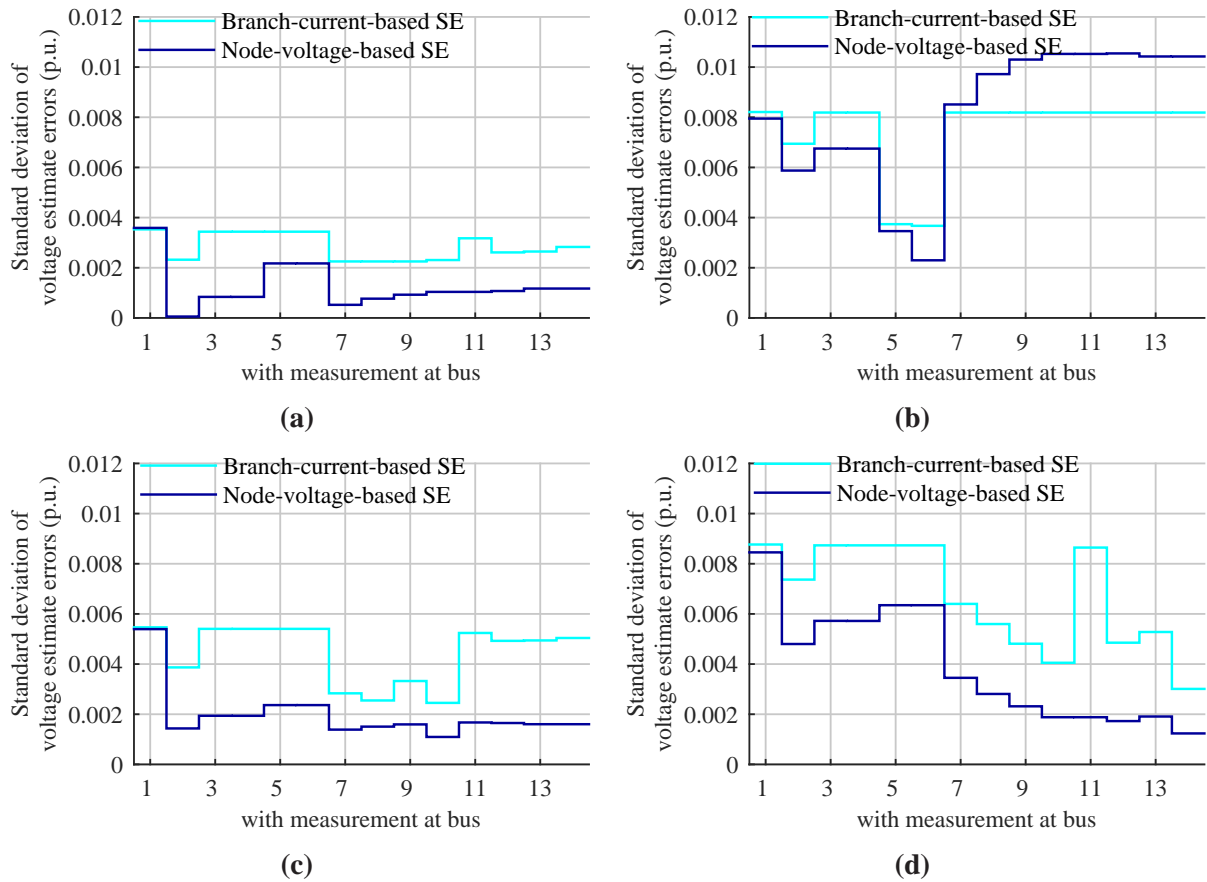


Figure 6.6: The observed maximum standard deviation of the voltage estimation error for voltage and bus power injection measurements at different buses when (a) there is no wind power in the feeder (b) there is wind power at Bus 6 (c) there is wind power at Bus 10 (d) there is wind power at Bus 14.

In Fig. 6.6b one can see that, in case of node-voltage-based SE, when measurements are done at Buses 7 to 14, the voltage estimates gets worse even compared to the case where the only real-time measurement available is voltage magnitude at Bus 1. This is because when no voltage measurement is available in the network, all pseudo-measurements are used almost without any modification for estimating the nodal voltages, as in load flow calculation. However, whenever there is voltage measurement, it is mainly the estimate of the wind power output, owing to the high variance of the wind power pseudo-measurement, that is manipulated in the estimation process to match the measured nodal voltage. When voltage measurement is available from one of the buses between 7 to 14, and if the loads on those buses are underestimated or overestimated above a certain level, this process results in bad estimate of the wind power output. Though this results in better voltage estimate at Buses 7 to 14, it adversely affects the voltage estimates at Buses 5 and 6. This problem is not observed when voltage measurements are done at, for example, Buses 3 and 4 because the load capacity connected to this lateral branch is smaller which means there is a lower load estimation error. Thus, the required correction in the estimate of the wind power output to correct the voltage at Buses 3 and 4 is not significant.

6. STATE ESTIMATION ALGORITHMS FOR DISTRIBUTION SYSTEM APPLICATION

6.4.3.2 Bus voltage and branch power flow measurement

Fig. 6.7 shows the results of the analysis when branch power flow together with bus voltage magnitude is measured. Both measurements are done at the beginning of the respective branch as seen from the main substation. Branch L_0 should be interpreted as absence of any additional measurement besides substation bus voltage. The rest of the branch numbers are as indicated in Fig. 6.1. From Fig. 6.7 it is difficult to determine where the best position is for branch power flow measurement to get better voltage estimates. However, in general, as seen from Figs. 6.7b, 6.7c and 6.7d, measuring close to the wind turbine and before it provides better results for both type of SE algorithms. In the absence of wind power in the network, as seen from Fig. 6.7a, measuring close to the beginning of the feeder provides better voltage estimate for the whole network. Similar to the previous case measuring at lateral branches, unless the wind turbine is located there, is seen to provide relatively less accurate voltage estimates.

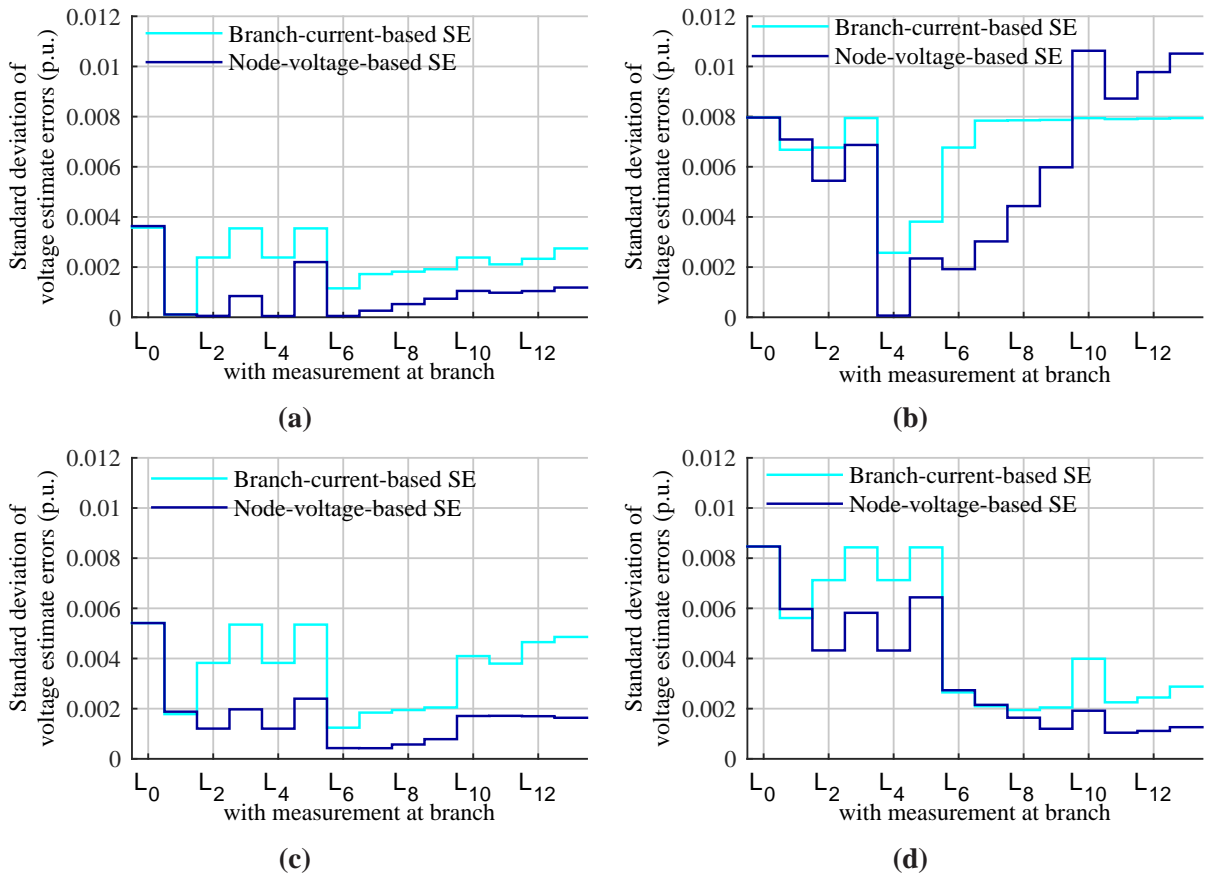


Figure 6.7: The observed maximum standard deviation of the voltage estimation error for voltage and branch power flow measurements at different branches when (a) there is no wind power in the feeder (b) there is wind power at Bus 6 (c) there is wind power at Bus 10 (d) there is wind power at Bus 14.

One can observe that, once again, the node-voltage-based SE generally provides a better voltage estimate compared to the branch-current-based SE. The same explanation described in previous subsection can be applied to what is observed in Fig. 6.7b when voltage measurements are done at branches between L_{10} and L_{14} . However, the SE algorithm, here, does not simply adjust the the estimate of the wind power output as in the previous case. The algorithm tries also to match

the estimates of the power injections of buses located downstream with branch power flow measurement upstream. That is why, unlike the previous case, the error in voltage estimate increases progressively as the measurement point moves towards the end of the feeder. The high voltage estimate error seen when the measurement is done at branch L_{10} arises due to the fact that branch L_{10} is another lateral branch with one injection node connected to it. Hence its result ends up being similar to the case in the previous subsection.

6.4.3.3 Bus voltage and branch current magnitude measurements

From Fig. 6.8 it can be observed that, the estimates provided by current magnitude measurement are almost as good as those obtained with the branch power flow measurement or bus power injection for both SE algorithms. This is even when the current magnitude measurement lacks di-

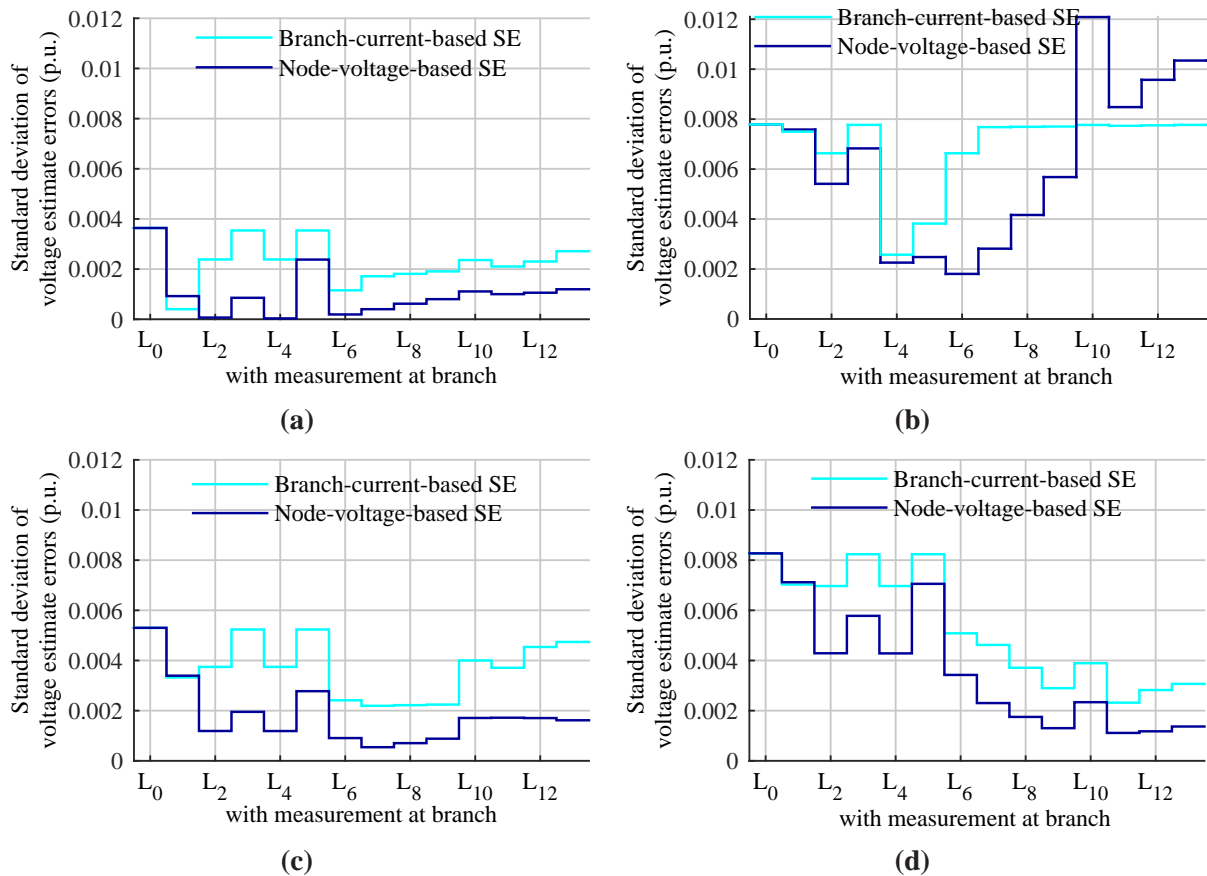


Figure 6.8: The observed maximum standard deviation of the voltage estimation error for voltage and current magnitude measurements at different branches when (a) there is no wind power in the feeder (b) there is wind power at Bus 6 (c) there is wind power at Bus 10 (d) there is wind power at Bus 14.

rectional information compared to the power flow measurement. However, there are two issues associated with the use of branch current magnitude measurement in SE process as observed in our analysis. On one hand, it faces convergence problems. On the other hand, an adjustment has to be done in the Jacobian matrix of the node-voltage-based algorithm to obtain the results presented in Fig. 6.8. Without this adjustment, for example, in case the wind power is located at Bus

6. STATE ESTIMATION ALGORITHMS FOR DISTRIBUTION SYSTEM APPLICATION

10, the result of the SE would have looked as shown in Fig. 6.9. In this figure, it is noticed that when the node-voltage-based algorithm converges, the objective function does not converge to its appropriate local minimum.

To explain why this happens, consider the case where current magnitude measurement is taken at Branch 7 $|I_{7,8}|$. During the first iteration all bus angles are initialized to zero and all bus voltages, except the measured voltages V_1 and V_7 , are assumed to be 1 pu. The state variables that constitute the current magnitude measurement function $f_{7,8}(x)$ are only V_7, δ_7, V_8 and δ_8 . Hence, in the first iteration the Jacobian row for $\partial f_{7,8}(x)/\partial x$ are all zero except $\partial f_{7,8}(x)/\partial V_8$. Hence the initial estimation of V_8 will be highly dependent on the difference between $|I_{7,8}|$ and $f_{7,8}(x)$. Generally, this is found to negatively affect the succeeding steps of the algorithm, hence, the final estimate the bus voltages in the network. Hence to get rid of these effect, the corresponding Jacobian term is set to zero at the first iteration. As shown in Fig. 6.8 this approach has effectively dealt with the specified problem.

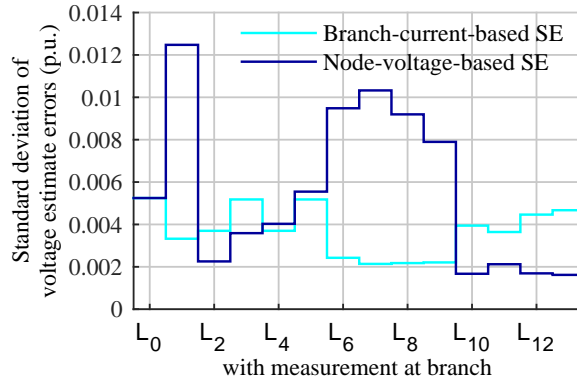


Figure 6.9: The observed maximum standard deviation of the voltage estimation error for voltage and current magnitude measurements at different branches when the wind turbine is located at Bus 10.

As for the sitting of these measurement types for better SE results, the same conclusion as drawn for sitting of branch power flow measurements can be made.

6.4.4 Two measurement points with two wind turbine sites and the accuracy of the state estimation algorithms

In the previous subsections, it is seen that in a feeder where the pseudo-measurement accuracy is within $\pm 100\%$ of the nominal value, a well placed single measurement is just enough to get the required level of SE accuracy. Now in this section the aim is to investigate the case where more than one measurement point may be necessary. These can arise if the error in pseudo-measurement is increased or wind turbines are located at more than one bus. Here, similar to the previous case, it is assumed that the wind power output is significantly higher than the load at each MV/LV bus.

The results presented in Fig. 6.10 and Fig. 6.11 deal with the case where the measurement errors in pseudo-measurement is increased to 200% of the nominal value and wind turbines are sited at two different buses. In Case 1, wind turbines are located at Bus 5 and 6 and in Case 2 the wind turbines are located at bus 5 and 9. The SE is carried out with real time measurement of either

bus power injection (in case of Fig. 6.10) or branch power flow (in case of Fig. 6.11) and voltage at points indicated by the respective x-axis entries of the sub-figures. These measurements are in addition to those measurements specified by the caption of each sub-figure.

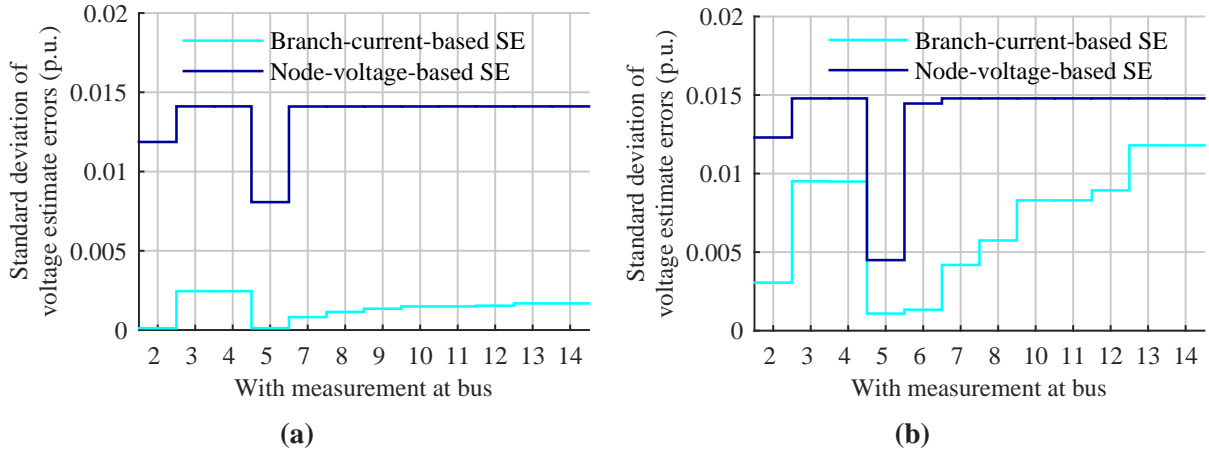


Figure 6.10: The observed maximum standard deviation of the SE error for power injection and voltage measurement when (a) Case 1: there is wind power at Bus 5 and 6 and there is an additional measurements at Bus 6 (b) Case 2: there is wind power at Bus 5 and 9 and there is an additional measurements at Bus 9.

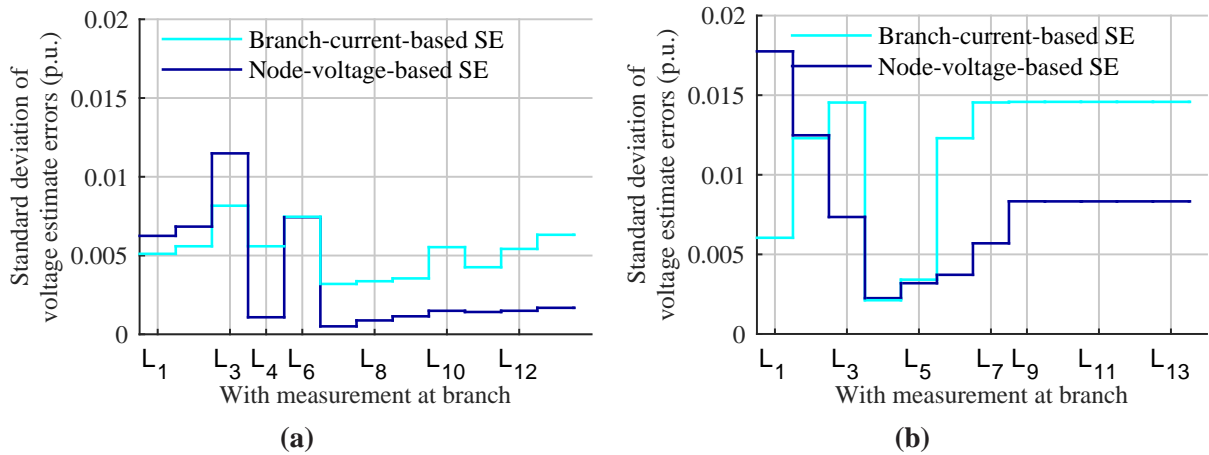


Figure 6.11: The observed maximum standard deviation of the SE error for branch power flow and voltage measurement when (a) Case 1: there is wind power at Bus 5 and 6 there is an additional measurements at Branch 5 (b) Case 2: there is wind power at Bus 5 and 9 there is an additional measurements at Branch 8.

From Fig. 6.10, in the case of node-voltage-based SE, one can observe that, whether the wind turbines are located close to each other or distributed in space, a better SE is obtained by placing the measuring equipment at the wind turbine sites. Moreover, one can see that the node-voltage-based SE performs even better in this case compared to branch-current-based SE estimations. However, in case of branch power flow measurement, as shown in Fig. 6.11, the accuracy of the branch-current-based SE gets closer to that of the node-voltage-based one. But still the node-voltage-based SE generally provides better estimations. The siting of power flow measurements, with respect to

6. STATE ESTIMATION ALGORITHMS FOR DISTRIBUTION SYSTEM APPLICATION

branch-current-based SE, is similar to what is discussed in the previous section: Better, if not best, SE accuracy can be obtained by placing the measurements at branches just before (towards the substation) the wind turbines.

Moreover, comparing the results in Figs. 6.6, 6.7, 6.10, and 6.11, one can observe that the branch-current-based SE algorithm performs better with branch power measurement while the node-voltage-based one provides similar level of accuracy with both measurement types.

6.4.5 Variance calculation of the voltage estimates

In the above analysis the standard deviation of the voltage estimate error is calculated by taking standard deviation of the difference between actual voltages obtained from power flow analysis and estimated voltage obtained from the SE process. In reality the actual voltage is not known and it is the estimated voltage we have at each bus. For the node-voltage-based SE, the variance of the voltage estimates can be determined using (6.6). The analysis in this thesis shows that (6.6) can sometimes overestimate or even underestimate the variance. However, it can provide satisfactory information in the absence of other information sources. Nonetheless, for the branch-current-based SE such an equation for calculating the variance of the voltage estimates is not available. Since the branch currents are the state vector, one can use (6.6) to calculate the variance of the branch current estimates. However the determination of the voltage estimate variance from branch current estimate variance is not straight forward. Since it is important to know the variance of the estimates to make any decision based on them, this can be considered another downside of the branch-current-based SE algorithm.

6.5 Summary

This chapter has compared two SE algorithms and their SE accuracy when applied to different measurement types, distribution of load, and location of wind power. The situation analyzed is the case where the capacity of the wind turbine is assumed to be considerably bigger than the loads on MV/LV nodes. The results of the analysis show that the node-voltage-based SE algorithm gives better accuracies compared to the branch-current-based SE algorithm. However, the branch-current-based SE algorithm is found to be a lot faster than the node-voltage-based SE algorithm. On average, for the case analyzed, it is 35 times faster when bus power injection measurements are used and 15 times faster when branch power flow measurements are used. In the case of current magnitude measurement, however, both SE algorithms are found sometimes to face convergence problems. Otherwise, the branch-current-based SE algorithm is still faster.

On the other hand, considering the power output from wind turbines are considerably larger and less predictable than the loads in the system, power injection measurements at wind turbine sites have been found to be the most attractive option in terms of obtaining better accuracy from the SE algorithms. Besides, since bus voltage and power injection measurements can be done at the low voltage side of the MV/LV transformer, its installation cost can be considerably cheaper than the branch power flow measurement.

7

Control algorithms for the different active management strategies

In Chapter 5, it is shown that the use of active management strategies increases significantly the wind power hosting capacity of distribution systems. The materials presented in the chapter help the DSO in determining the optimal level of wind power that can be effectively accommodated in the system using active management strategies. But once the planning is done, the DSO needs the control system that carryout the active management strategies to deal with overvoltage and overloading that may happen in the system. Thus, the aim of this chapter is to provide control algorithms that can be used to effectively carryout the active management strategies with minimum cost as well as loss of energy. The chapter starts by revising the available literature in the area. Then it will discuss the proposed control algorithms and try to point out the strength of the proposed solutions compared to those available in literature. Later on, the applicability of the proposed control algorithms are demonstrated using a case study system.

7.1 Introduction

The active management strategies proposed in literature include coordinated OLTC voltage control and reactive power compensation for voltage regulation and curtailment for both overvoltage and overload mitigation [3, 113].

Considerable research effort has been devoted to the investigation of the control of OLTC [11–16], reactive power compensation (RPC) [17–20], and curtailment [21, 22] for voltage regulation in a distribution system with DG. The control algorithms for voltage regulation through the combined control of RPC and curtailment from wind turbines [23, 24], or of OLTC and RPC [28], or through the combination of all three active management strategies [25–27, 29] have also been discussed. Though the ultimate aim of either RPC, OLTC, or curtailment is to maintain the voltage within a given deadband, e.g. $\pm 5\%$, various research works have proposed different control algorithms to achieve the same.

When it comes to using the OLTC for voltage regulation a number of papers [13–16] have proposed a solution in which a number of measurements are obtained from critical locations throughout the

7. CONTROL ALGORITHMS FOR THE DIFFERENT ACTIVE MANAGEMENT STRATEGIES

network and the voltage set point is changed according to this information. However as shown in Section 6.2 the identification of the critical points is not an easy task. Others have assumed the availability of voltage measurements from every node [25, 27]. But this is rarely the case in existing rural distribution systems. State estimation (SE) based on real-time measurement along with pseudo-measurement is also proposed to determine the voltage level of the network and this information is used to control the target voltage of automatic voltage control (AVC) relays of the substation transformer [11, 28]. In [26], load estimation based on customer class curves together with measurement data at the substation and from remote DG are used to determine the maximum and minimum voltage in the network. Then the appropriate control decision is taken to limit the voltage in the system within the allowed operating range. Reference [12] proposes to make separate local measurements on feeders with load only and on feeders that contains generation. Based on these measurement data and previous knowledge of load sharing between the different feeders, the power output from the DG is estimated and used to determine the voltage setting required at the substation to mitigate voltage rise at DG terminal. On the other hand, knowing the load in the feeder, the traditional line drop compensation approach is used to determine the voltage setting required to mitigate undervoltage in the system. By combining these two strategies the voltage setting that mitigates undervoltage and overvoltage in the system is determined.

In the case of RPC, Reference [25, 28] has proposed the use of PI controller where the difference between the voltage set point and the actual voltage level is passed through a deadband to make sure the PI controller works only when the voltage is above the maximum voltage level. Similarly, the active power control for voltage rise mitigation is carried out through PI controllers in [25]. The PI controller is augmented with reactive power deadband to ensure that curtailment is only carried out when there is a shortage of reactive power. In [17], the PI controller is used as well, however, the authors have used a method based on power factor tracking rather than deadband to make sure the PI controller works only when the voltage is above the maximum voltage level. An alternative control approach based on fuzzy logic is also proposed in the same reference. These control approaches ensure that RPC does not unnecessarily increase the power losses in the network. In [18], the aim is to eliminate the voltage rise introduced due to active power injection from the wind turbine. Though this approach keeps the voltage at various points of the system at the same level as before wind power introduction, it increases the power losses in the system. In [19], fuzzy logic based location adaptive droop method is proposed to coordinate RPC from multiple DG for voltage rise mitigation. In [20], RPC using droop control function is proposed to mitigate voltage rise in multiple PV installations in distribution systems. The change in the power losses of the system is also given due consideration. The droop function works based on the amount of active power generation to ensure that the PVs are not penalized based on their location, which would happen if the droop function works based on the voltage level at the PV terminal. Moreover, local voltage measurements are used to ensure the proper operation of the droop based compensator. In [23, 24] the required change in reactive or active power to mitigate the voltage rise problem is calculated using sensitivity analysis while an optimization approach is preferred in [26]. In [27] state estimation is used for the same purpose. In [29] the OLTC and the DG in a given feeder are given voltage regulation zones. The OLTC is operated with line drop compensation (LDC) within its allotted working zone while the amount of active and reactive power required for voltage regulation is determined using proportional controller which works in a similar fashion as a tap changer with a time delay.

Some articles, especially dealing with voltage rise in LV system, have even considered curtailment as a primary means of voltage rise mitigation. Among these [21] has investigated the equal sharing of curtailed energy between PVs installed on a given feeder operating in droop based active power curtailment to mitigate the voltage rise problem. In [22], the Thevenin equivalent of the grid at the PCC is used to determine the droop to be used in curtailing the power output from PVs. The aim in using the Thevenin equivalent for determining the slope of the droop is to avoid power curtailments that are conservative.

Curtailed for overload mitigation is discussed in [24, 30] where the sensitivity of the line loading with respect to the nodal power injection is used to determine the amount of active power output that needs to be curtailed. In [163] power flow management algorithms based on constraint satisfaction problem and optimal power flow are discussed for real-time application.

In this chapter, a new control strategy for voltage regulation by using RPC and curtailment from wind turbines and OLTC of the substation transformer is provided. The control of wind power curtailment for overload mitigation is also discussed. Overall the proposed control algorithms in this chapter differ from those found in the literature in the following aspects: 1) in the case of OLTC based voltage control, a strategy that changes the voltage deadband instead of the voltage set point of the AVC relay of the tap changing transformer is proposed, 2) coordination of reactive power from multiple wind turbines for voltage regulation is also discussed, 3) the coordination of voltage regulation from OLTC and RPC is achieved by using a higher voltage deadband in the case of OLTC than of RPC, 4) to coordinate voltage control through RPC and curtailment the use of slightly different reference voltage levels are proposed, 5) and, finally, overload mitigation through curtailment is achieved by using PI-controllers.

7.2 Voltage regulation using coordinated OLTC control

As shown in 6.2, with the introduction of wind power into the distribution system, the buses in the network where the lowest or the highest voltage occur depend on the level of load and wind power in the system i.e. it can not be known with certainty beforehand. Thus, the traditional control principles of OLTC can not provide satisfactory voltage regulation in such a network. The other alternative where one can obtain voltage measurements from every node possible renders itself to be expensive. Hence SE estimation which makes use of the historical data of power consumption at every customer node together with a few real-time measurement data is proposed in Chapter 6 as the most attractive solution for implementing active management strategies in a distribution system. In this section, the node-voltage-based SE algorithm is used to obtain the voltage estimate at different nodes of the network. Then this information is used to carry out OLTC based voltage regulation as discussed below. Unlike the case of SE in a transmission system, SE in a distribution system, as presented in this paper, lacks measurement redundancy which makes bad data detection impractical. Therefore, to validate the results of the state estimation, the DSO can use an online voltage measurement data at one or more buses (as required) with lower sampling time (or smart meter data whenever available).

Fig. 7.1 shows the overall set up of the coordinated OLTC voltage control algorithm. The distribution system state estimation (DSSE) block estimates the voltage level at various buses of

7. CONTROL ALGORITHMS FOR THE DIFFERENT ACTIVE MANAGEMENT STRATEGIES

the distribution network. Then, based on the voltage estimate from the DSSE block, the voltage level analyzer determines the voltage input to the AVC relay. The output signal of the voltage level analyzer block is determined based on the following logic:

- ↔ If $\max|\hat{\mathbf{V}}^t \pm 3\boldsymbol{\sigma}_v^t - V_{\text{set}}| \leq \Lambda_v$ pu, $\hat{V}_{\text{min/max}}^t = V_{\text{set}}$
- ↔ Else if $\max(\hat{\mathbf{V}}^t + 3\boldsymbol{\sigma}_v^t - V_{\text{set}}) \geq \Lambda_v$ AND $\min(\hat{\mathbf{V}}^t - 3\boldsymbol{\sigma}_v^t - V_{\text{set}}) \leq -\Lambda_v$, $\hat{V}_{\text{min/max}}^t = \hat{V}_{\text{min/max}}^{t-1}$ and Set INFEASIBLE STATE alarm on.
- ↔ Else if $\max(\hat{\mathbf{V}}^t + 3\boldsymbol{\sigma}_v^t - V_{\text{set}}) \geq \Lambda_v$, $\hat{V}_{\text{min/max}}^t = \max(\hat{\mathbf{V}}^t + 3\boldsymbol{\sigma}_v^t)$
- ↔ Else if $\min(\hat{\mathbf{V}}^t - 3\boldsymbol{\sigma}_v^t - V_{\text{set}}) \leq -\Lambda_v$, $\hat{V}_{\text{min/max}}^t = \min(\hat{\mathbf{V}}^t - 3\boldsymbol{\sigma}_v^t)$

where

- Λ_v The allowed voltage variation in the network around the nominal voltage level, e.g. 0.05, [p.u.]
- $\hat{\mathbf{V}}^t$ the voltage magnitude estimate vector of the network at time t [pu]
- V_{set} the voltage set point of the AVC relay [pu]
- $\hat{V}_{\text{min/max}}^t$ the voltage signal estimate sent to the AVC relay by the voltage level analyzer[pu]
- $\boldsymbol{\sigma}_v^t$ vector of the standard deviation of voltage estimates at time t [pu]

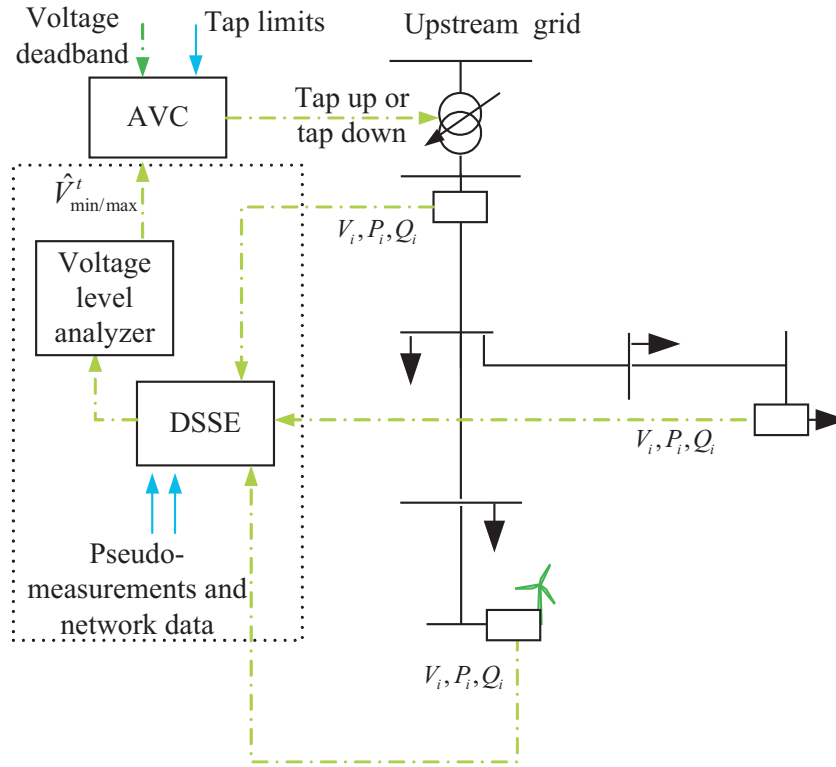


Figure 7.1: Block diagram of the proposed OLTC voltage regulation.

The idea behind the logic above is that if the voltage is estimated to be within the allowed operational voltage range with 99.7% confidence, the signal sent to the AVC relay as measured voltage is V_{set} and no tap changer action is expected. Otherwise, if the estimate cannot ensure that the voltage is within the allowed voltage deadband with 99.7% confidence, the appropriate voltage

7.3 Voltage regulation with reactive power compensation

magnitude is sent to the AVC relay which will trigger a tap up or a tap down action if the voltage persists outside the deadband over the duration of the time delay of the tap changer.

The AVC relay would operate as usual except that the voltage input to the AVC is fed from the voltage level analyzer block.

As shown in the block diagram, in this thesis the voltage deadband is changed instead of voltage set point of the AVC relay for the tap changing transformer. One can keep the voltage set point at the nominal value. Under normal operation, the voltage deadband is changed to $\pm 5\%$ and the AVC relay sends the Tap-up or Tap-down signal to the OLTC when the voltage obtained from the voltage level analyzer block is outside the given deadband for a given time delay. The AVC relay would also check for the tap limits as it would conventionally do [29].

Due to the lack of measurement redundancy, as mentioned above, if there are measurement errors or a communication failure, the SE may face convergence problems or provide poor confidence on the voltage estimates. If this situation persists for the time delay of the AVC relay, the deadband can be changed to the default value. The voltage set point can be changed to the voltage level at the secondary side of the transformer at the moment of communication failure or convergence problem. The voltage input to the AVC relay would be the voltage level at the secondary side of the transformer. Then, the tap changer would operate as it would traditionally until the problem is resolved.

The OLTC control approach, as presented above, is simpler compared to changing the voltage set point proposed in [11, 13, 15, 25] as the calculation of the voltage set point is not straight forward. In [15] fuzzy logic is used to calculate the reference voltage while References [13] and [11] have proposed to increase or decrease the voltage set point by a magnitude equal to the voltage deadband. In [25] PI controller is used for the calculation of the voltage set point. However in the proposed approach the AVC relay automatically detects an out of range voltage and sends a tap up or tap down signal to the tap changer.

7.3 Voltage regulation with reactive power compensation

7.3.1 The control algorithm

The basic idea of RPC from wind turbines is to consume reactive power when the voltage at the wind turbine terminal is above the allowed level and to inject reactive power whenever the voltage is below the acceptable minimum level. Furthermore, the amount of reactive power consumed or produced should be such that it is just enough to get the voltage back within the allowed deadband.

As discussed in Chapter 2, not all wind turbine types have this capability of reactive power regulation. Therefore, voltage regulation through RPC mainly deals with Type C, i.e. double fed induction generator (DFIG), and Type D, i.e. full power converter, wind turbines [31]. In the case of Type C wind turbines, although reactive power injection can also be obtained from the grid-side converter, the rotor-side converter is the preferred option for reactive power regulation. The main reason for this is a reactive injection through the rotor circuit is effectively amplified by a factor of $1/slip$ [46]. In the case of Type D wind turbines, it is the grid-side converter that is used for reactive power regulation [46].

7. CONTROL ALGORITHMS FOR THE DIFFERENT ACTIVE MANAGEMENT STRATEGIES

Assuming the cross-coupling and the feed forward terms are properly implemented, the reactive power control loop of the wind turbine can be reduced to the one shown in Fig. 7.2 in both Type C [164, 165] and Type D wind turbines [166, 167], i.e. a cascade of current control and reactive power control loops.

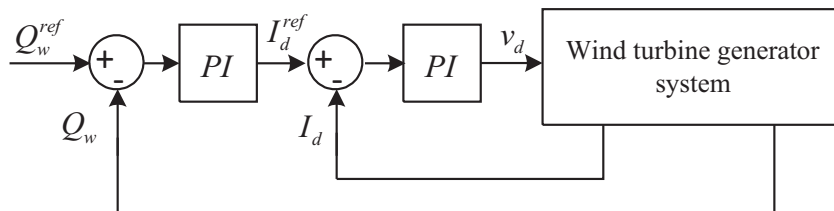


Figure 7.2: Reactive power control in a wind turbine.

where in the figure

- I_d the d-axis component of the current vector [pu]
- I_d^{ref} the reference for the d-axis component of the current vector [pu]
- Q_w The reactive power output of the wind turbine [pu]
- Q_w^{ref} The reactive power reference to the wind turbine controller [pu]
- v_d the d-axis component of the voltage vector [pu]

Then, the task of the RPC based voltage controller is to determine the Q_w^{ref} which is sent to this cascade controller to regulate the voltage. Based on this, some researchers [23, 24, 30] have proposed the use of sensitivity analysis to determine the amount of reactive power and curtailment to mitigate overvoltage. But sensitivity analysis requires the use of more measurement data or some approximation assumptions on the voltage level or loads at different buses. Moreover it is computationally more intensive than the use of PI controllers and it is also difficult to ensure the actual value follows the reference exactly. Hence in this thesis the PI-based control algorithm provided in the block diagram of Fig. 7.3 is used. It is more effective, requires less measurement data and the computational overload is minimal.

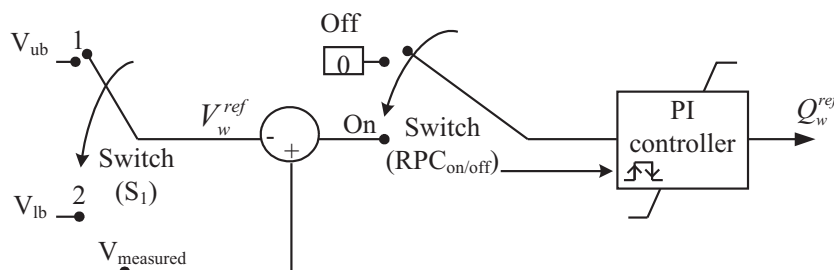


Figure 7.3: Block diagram of the proposed reactive power compensation control algorithm.

where in the figure

- V_{ub} the magnitude of the upper bound voltage [pu]
- V_{lb} the magnitude of the lower bound voltage [pu]

7.3 Voltage regulation with reactive power compensation

In the block diagram of Fig. 7.3 there are two switches which are controlled using two separate switching logic. Switch S_1 is set to V_{ub} if the measured voltage is above 1 pu otherwise it is set to V_{lb} . In the case of Switch $RPC_{on/off}$ the switching logic is provided in the block diagram of Fig. 7.4. Whenever $V_{measured}$ is greater than or less than 1 pu by an amount Λ_v , the switch $RPC_{on/off}$ is turned on and the RPC is engaged. Then, it will be turned off only when—for example, in the case of an overvoltage—the control algorithm senses that reactive power is being generated rather than being consumed to keep the voltage at V_{ub} , i.e. $Q_{measured}$ is greater than ϵ_Q . Here one should note that reactive power is consumed to mitigate an overvoltage. Based on the sign convention adopted here, $Q_{measured}$ is negative for consumption. Thus, $Q_{measured} \geq \epsilon_Q$ implies that reactive power is being generated by the wind turbine to keep the voltage at V_{ub} . Turning of the PI controller at this point avoids the unnecessary use of reactive power to keep the voltage at high values which, on the other hand, may increase the power losses in the system. Here one needs to notice that Switch $RPC_{on/off}$ is also used to reset the PI controller at both rising and falling edge of the switching.

Note that in Fig. 7.3, it is also possible to provide a direct I_d^{ref} from the voltage controller to the d-axis current controller in Fig. 7.2 without the need for reactive power controller [46]. But, the focus of this thesis is the idea presented in Fig. 7.3.

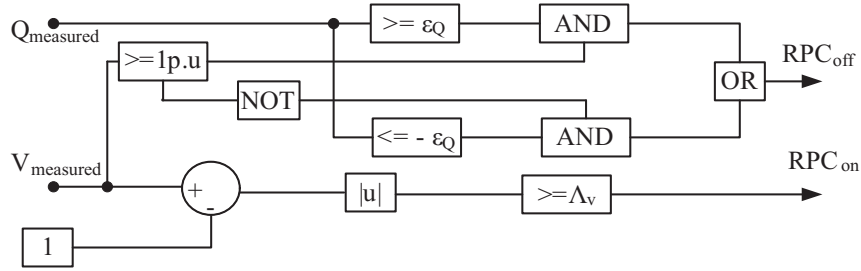


Figure 7.4: Block diagram of the switching logic for Switch $RPC_{on/off}$ in Fig. 7.3.

where in the figure

ϵ_Q	A small positive value, e.g. 0.025, [p.u.]
$Q_{measured}$	Measured reactive power output of the wind turbine [p.u.]
$V_{measured}$	Measured voltage at the terminal of the wind turbine [p.u.]

The control logic so far enables a wind turbine to regulate the voltage level at its terminal by using RPC with minimum increase in the power losses of the distribution system. One can further use the reactive power capability of a local wind turbine at a given site to mitigate voltage rises at the terminal of a remote wind turbine in the same feeder. This can be valuable if the wind turbine at the remote site has limited or no RPC capability. To carry out the task, the local wind turbine requires the measured voltage at the terminal of the remote wind turbine. To efficiently coordinate RPC from local as well as remote wind turbines, the RPC controller of a wind turbine has two reference voltages: one for the local bus and another for remote buses. In the case of overvoltage these values can be, for example, 1.05 pu for the local bus and 1.051 pu for the remote bus. Thus, if the local wind turbine could not limit the overvoltage at 1.05 pu, the voltage increases. When the voltage becomes above 1.051 pu, the remote wind turbines will sense this and activate RPC to limit the voltage at 1.051 pu. This approach demands that two inputs to the PI controller should be changed, i.e. the measured voltage and the reference voltage. To make these changes a switching

7. CONTROL ALGORITHMS FOR THE DIFFERENT ACTIVE MANAGEMENT STRATEGIES

signal V_r^{status} is generated locally using the measured voltage from the terminal of the remote wind turbine. The proposed switching logic is presented in Fig. 7.5. That is, the RPC controller of the local wind turbine is engaged when the voltage of the remote wind turbine is above the nominal voltage by Λ_v plus $\epsilon_{v,r}$. Here $\epsilon_{v,r}$ is a small positive number considerably smaller than Λ_v .

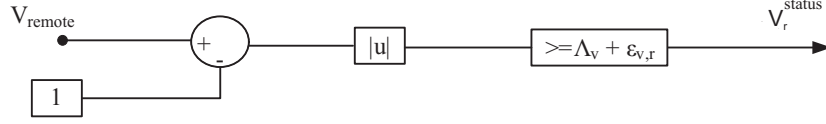


Figure 7.5: The status of the voltage at the remote wind turbine terminal.

Using the signal V_r^{status} , the measured voltage input to the PI controller is changed as in Fig. 7.6. That is, when the V_r^{status} signal is 0 the measured voltage fed to the PI controller in Fig. 7.3 will be the local voltage since the remote voltage will be assigned a value of 1 pu. But if the V_r^{status} signal is 1, the maximum or the minimum of the two voltage inputs are fed to the PI controller depending on which one is further from 1 pu. For example, assume that the local voltage is 0.98 pu and the remote voltage is 1.052 pu. If $\Lambda_v = 0.05$ pu and $\epsilon_{v,r} = 0.001$ pu, then $V_r^{\text{status}} = 1$. Now, since $V_{\text{max}} (= 1.052 \text{ pu})$ is further away from 1 pu compared to $V_{\text{min}} (= 0.98 \text{ pu})$, $V_{\text{measured}} (= 1.052 \text{ pu})$ will be the voltage at the terminal of the remote wind turbine.

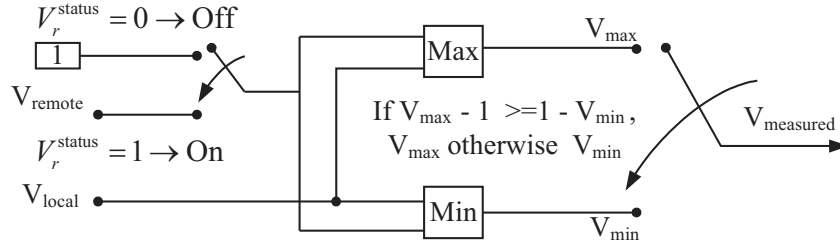


Figure 7.6: The modification of the measured voltage input of Figs. 7.3 and 7.4 to incorporate the voltage control of a remote wind turbine.

Moreover, the changes in reference voltage is done according to the logic presented in Fig. 7.7. For example, in the case of overvoltage, if $V_r^{\text{status}} = 1$ and $|V_{\text{measured}} - V_{\text{local}}| > 0$, $\epsilon_{v,r}$ is added to V_{ub} to obtain a new reference voltage. This way the voltage at the remote wind turbine terminal is controlled at a higher reference compared to the local bus reference voltage. The $|V_{\text{measured}} - V_{\text{local}}| > 0$ term is included to make sure that the voltage at the terminal of the local wind turbine is controlled at V_{ub} if $V_{\text{local}} > V_{\text{remote}}$ while $V_r^{\text{status}} = 1$. Otherwise if there is an overvoltage at the local wind turbine and $V_{\text{local}} < V_{\text{remote}}$ while $V_r^{\text{status}} = 1$, then the reactive power consumed to mitigate the overvoltage at the remote bus will have more impact on the voltage level on the local bus. Hence the overvoltage at the local bus will effectively be mitigated.

In the case the remote wind turbines are controlling the voltage of a local wind turbine, when the overvoltage recedes, the RPC controllers on the remote wind turbines are disengaged first before the local wind turbine. This is valid since the remote wind turbines control the voltage at a higher reference voltage. This approach minimizes the amount of reactive power used to mitigate an overvoltage as it ensures that the remote wind turbine reactive power is only used when the local reactive power is fully utilized. One should note here that a local RPC is more effective compared to a remote RPC to mitigate an overvoltage.

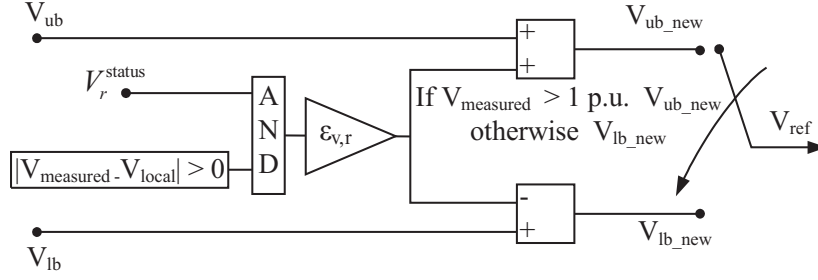


Figure 7.7: Generating the reference voltage.

In general rapid voltage control performances (with response time less than 100 ms) can be obtained by using RPC from wind turbines [166]. But some practical implementation issues related with stability may impose a higher response time (as much as 10 s) [168].

7.3.2 Design of the PI controller

To design the PI controller parameters, the bandwidth of the voltage controller can be made sufficiently low so that the dynamics of the inner loop current and reactive power controllers can be neglected. Fig. 7.8 shows the equivalent circuit representation of a wind turbine connected to a distribution system. In a steady state, the voltage V_w at the terminal of the wind turbine can be calculated using (7.1)

$$V_w = E_{th} + \frac{R_{th}P_w + X_{th}Q_w}{V_w} + j \frac{X_{th}P_w - R_{th}Q_w}{V_w} \quad (7.1)$$

Since $V_w = |V_w| \angle 0^\circ$, taking the real part gives

$$V_w = E_{th,r} + \frac{R_{th}P_w + X_{th}Q_w}{V_w} \quad (7.2)$$

where

- V_w voltage magnitude at the wind turbine terminal [pu]
- E_{th} the Thevenin voltage seen from the wind turbine terminal [pu]
- $E_{th,r}$ the real part of the Thevenin voltage seen from the wind turbine terminal [pu]
- R_{th} the calculated Thevenin resistance seen from the wind turbine terminal [pu]
- X_{th} the calculated Thevenin reactance seen from the wind turbine terminal [pu]
- P_w the active power output of the wind turbine [pu]
- Q_w the reactive power output of the wind turbine [pu]

Fig. 7.9 shows the block diagram of the closed loop system where $d = E_{th,r} + \frac{R_{th}P_w}{V_w}$ is considered as a disturbance.

If the bandwidth of the closed loop system is chosen to be α_r with

$$\frac{F(s)G(s)}{1 + F(s)G(s)} = \frac{\alpha_r}{\alpha_r + s} \quad (7.3)$$

7. CONTROL ALGORITHMS FOR THE DIFFERENT ACTIVE MANAGEMENT STRATEGIES

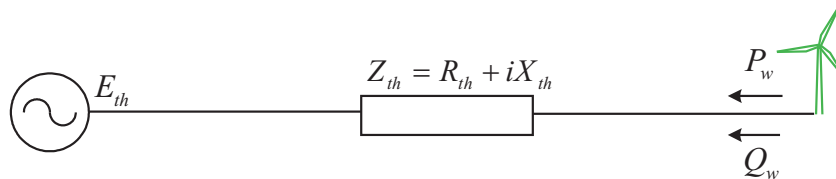


Figure 7.8: Equivalent circuit model of a wind turbine connected to a distribution system.

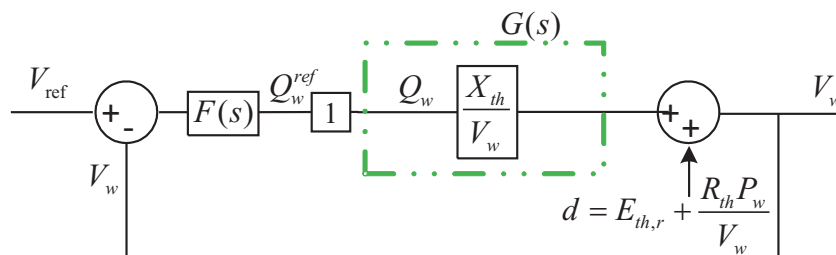


Figure 7.9: The block diagram model of the closed loop system.

and the PI-controller parameters can be set as

$$F(s) = G(s)^{-1} \frac{\alpha_r}{s} \Rightarrow K_I = \frac{\alpha_r V_w^0}{X_{th}} \quad \text{and} \quad K_P = 0 \quad (7.4)$$

where V_w^0 is the assumed voltage magnitude at the wind turbine terminal in pu.

One can use the same PI controller for voltage control at the terminal of a remote wind turbine, as changes in V_w or X_{th} will only change the bandwidth of the voltage control system to a new bandwidth α_{new}

$$\alpha_{new} = \frac{\alpha_r V_w^0 X_{th}^{ac}}{V_w^{ac} X_{th}} \quad (7.5)$$

where

V_w^{ac} actual voltage magnitude at the wind turbine terminal [pu]

X_{th}^{ac} the actual value of the Thevenin reactance seen from the wind turbine terminal [pu]

7.4 Curtailment of wind power

Under normal condition, when the wind turbine is operating below rated speed, the pitch angle β of the pitch angle of the wind turbine blade is kept at pitch angle β_0 . The rotational speed of the wind turbine is controlled for maximum power capture. This operation is termed as maximum power-point tracking (MPPT). The MPPT control can be achieved by using current-mode control or speed-mode control [164].

The idea behind curtailment, as the name implies, is to curtail part of the wind power output of the wind farm when an overvoltage or overloading is detected. The curtailed power should be an amount just enough to keep the voltage or the loading within the allowed voltage or loading limit.

A number of control principles have been proposed for automatic power control of wind turbines [169–171]. The general active power control principle as proposed in [169] can be simplified as in Fig. 7.10. The reference torque generator blocks takes in the reference power P_w^{ref} and generates the appropriate torque reference depending on the speed of rotation of the wind turbine ω [169]. The constant K is the gain term that converts the torque reference τ_e^{ref} to the q-component current reference I_q^{ref} [46]. In DFIG wind turbines this torque control is achieved through rotor side converter [46, 164] where in case full power converter wind turbines it can be achieved either from the grid side [166] or generator side converter [46]. The available wind power P_w^{avail} in the wind can be calculated using the characteristic of the wind turbine operating at MPPT and the estimated wind speed [172].

With these torque controller in place, the required amount of power P_{cur}^{ref} can be curtailed from the power output of the wind turbine

- by either increasing the speed of rotation of the wind turbine and, hence, running at sub-optimal tip-speed ratio
- or by pitching of the wind turbine blades.

Curtailing by increasing the speed of rotation is possible only when the wind turbine is not running at rated speed. Otherwise, when the wind turbine operates at rated speed, curtailment is achieved by pitching the wind turbine blades. This pitching sheds the extra aerodynamic power available in the wind. The control of the pitching system is accomplished by using gain-scheduled PI controller on the speed error between the actual and the rated speed of the generator [173]. One should note here that no modification is done in the pitch controller to accomplish curtailment, rather the pitching controller acts to maintain the rotational speed of the wind turbine at rated speed when the electrical torque is decreased.

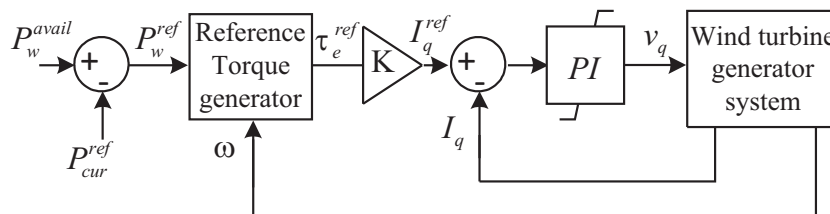


Figure 7.10: Active power control in a wind turbine.

The dynamics of the pitching system determine how fast the controller can be in carrying out the curtailment. Moreover, due to the characteristic of the power vs rotor speed curve of the wind turbine, the speed at which curtailment can be achieved varies depending on the power output of the wind turbine. But in general, a ramp rate of 10%/sec in response to step changes in curtailment is fairly attainable with most modern wind turbines [174].

7. CONTROL ALGORITHMS FOR THE DIFFERENT ACTIVE MANAGEMENT STRATEGIES

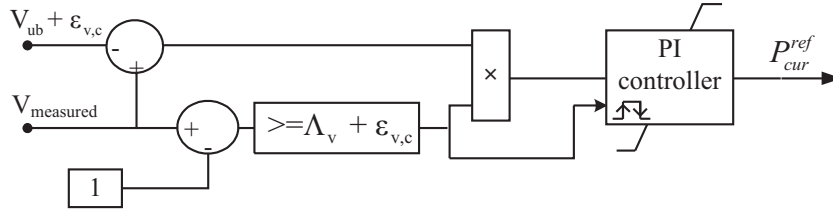


Figure 7.11: The proposed PI based wind power curtailment controller for overvoltage mitigation.

7.4.1 Controlling curtailment for overvoltage mitigation

Wind power curtailment cannot be used for undervoltage mitigation hence it is only usable for overvoltage mitigation. Similar to the case of RPC, we opt to use PI controllers. Fig. 7.11 shows the outline of the PI based wind power curtailment controller proposed for overvoltage mitigation. The switching logic of the curtailment controller is similar to the one used in RPC when controlling the voltage of a remote wind turbine. The wind power curtailment controller sends curtailment reference to the wind turbine controller only when the voltage at the local bus is greater than $\Lambda_v + \epsilon_{v,c}$ i.e. when the wind turbine is not able to mitigate the overvoltage using RPC. Here $\epsilon_{v,c}$ is a small positive number. Furthermore, the integrator is reset whenever the controller starts or stops to output curtailment reference. In case RPC from remote wind turbine is employed, $\epsilon_{v,c}$ should be greater than $\epsilon_{v,r}$ to ensure curtailment is only used when reactive power is exhausted. The Matlab model of the detailed control logic used at different parts is provided in the Appendix.

When it comes to the design of the PI controller, Eq. (7.2) can be used again to develop the block diagram of the closed loop control system as shown in Fig. 7.12. In the block diagram the available input power from the wind P_w^{avail} is considered as input noise and $d = E_{th,r} + \frac{R_{th}P_w}{V_w}$ is an output disturbance.

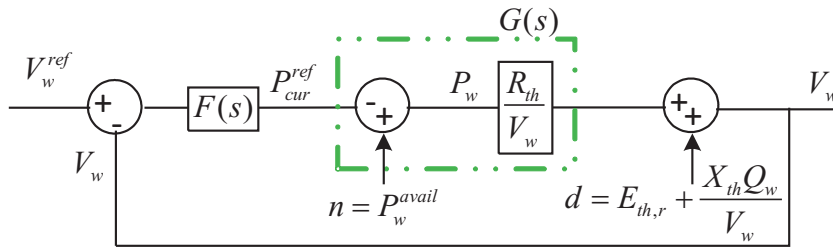


Figure 7.12: The block diagram model of the closed loop system for curtailment.

Choosing the bandwidth of the system as α_{cur} will result in the closed transfer function as

$$\frac{F(s)G(s)}{1 + F(s)G(s)} = \frac{\alpha_{cur}}{\alpha_{cur} + s} \quad (7.6)$$

and similar to the case of RPC controller, the PI parameters of the controller here can be chosen as

$$F(s) = G(s)^{-1} \frac{\alpha_{cur}}{s} \Rightarrow K_I = \frac{\alpha_{cur} V_w^0}{R_{th}} \quad \text{and} \quad K_P = 0 \quad (7.7)$$

Here the bandwidth α_{cur} should be chosen such that it is within the bandwidth of the curtailment system of the wind turbine. More information on the value of α_{cur} is provided in Section 7.6.3.4.

7.4.2 Curtailment for overload mitigation

Unlike the case of overvoltage mitigation, curtailment is the only option which can be used for overload mitigation unless costly energy storage solutions are utilized. Such energy storage solutions are not considered in thesis. As for the control system, here as well, the use of PI controller is found to be easier to implement and highly effective in overload mitigation. Fig. 7.13 shows the block diagram of the proposed controller. The PI controller parameters can be selected using the closed loop system given in Fig. 7.14. In the figure the input noise n comes from the variation in the input wind energy and the output disturbance d comes from system load variations.

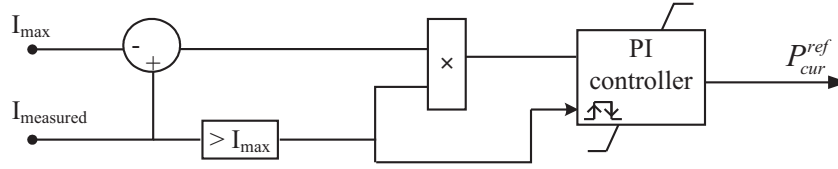


Figure 7.13: Wind power curtailment controller for overload mitigation.

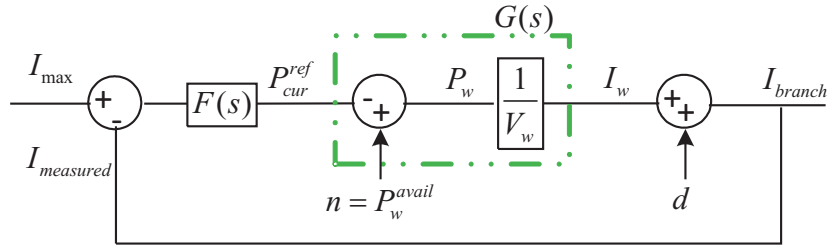


Figure 7.14: The close loop system of the curtailment system for overload mitigation.

Using the same parameter selection procedure presented above, the parameters of the PI controller can be chosen as

$$F(s) = G(s)^{-1} \frac{\alpha_{cur}}{s} \Rightarrow K_I = \alpha_{cur} V_w^0 \quad \text{and} \quad K_P = 0 \quad (7.8)$$

7.5 Coordination of the different active management strategies

So far, the control algorithm algorithms of individual active management strategies have been discussed. For example, we have seen the control algorithms of OLTC, RPC, and curtailment to mitigate an overvoltage. The problem remains which active management strategy takes precedence when an overvoltage is detected in the network and how to achieve that. In the case of curtailment, which can be used for both overvoltage and overload mitigation, one needs to know how to carry out the curtailment in case both overloading and overvoltage occur on the system. Fig. 7.15 shows the overall control and coordination method proposed in this thesis.

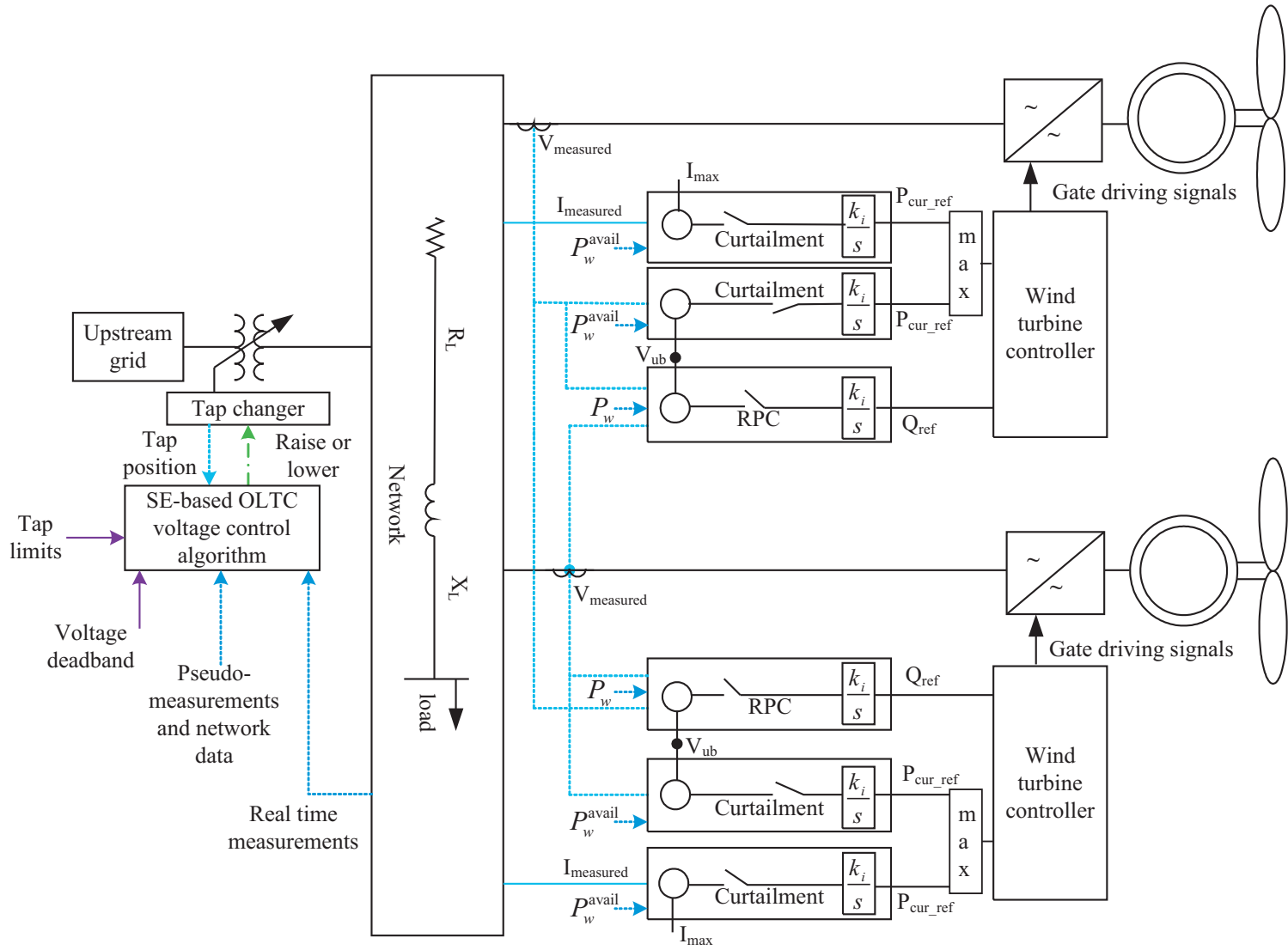


Figure 7.15: The general outline of the control and coordination algorithm proposed in this chapter.

7.5.1 Coordinating the active management strategies for overvoltage mitigation

It is discussed above that the coordination of overvoltage mitigation from local and remote RPC as well as curtailment can be achieved by choosing different reference voltage, one greater than the other, for the respective active management strategy. That is, the reference voltage for local RPC will be $1 + \Lambda_v$, and it will be higher at $1 + \Lambda_v + \epsilon_{v,r}$ for voltage control through RPC from remote wind turbine, and it will be even higher at $1 + \Lambda_v + \epsilon_{v,c}$ (with $\epsilon_{v,c} > \epsilon_{v,r}$) for voltage control from curtailment of the power output of the local wind turbine.

When coordinating voltage control from OLTC and RPC, overvoltage mitigation through RPC is given precedence over OLTC for voltage control at the wind turbine terminals. This is more effective from various angles. To begin with, the voltage at the wind turbine terminals are highly variable; and due to the mechanical nature of the OLTC, the control of this highly variable voltage may expose the OLTC to a rapid wear and tear. RPC, which does not involve any mechanical component, provides a more flexible and fast enough alternative for regulation of such a rapidly changing voltage. Moreover, the control of the voltage at the wind turbine terminal through the OLTC requires the use of communication infrastructure, which is vulnerable to failure; while voltage control through RPC can be carried in most cases using local measurements. On the other hand, it is also shown in Section 5.1.3 that RPC does not increase the losses too much.

Based on this preference of precedence, the coordination of voltage control from OLTC and RPC can be dealt depending on whether or not voltage measurement from the wind turbine terminals is available in the SE algorithm.

7.5.1.1 When voltage measurements from the terminals of the wind turbines are available in the SE process

In this case the coordination between OLTC and RPC can be easily achieved. That is, the OLTC control algorithm knows exactly the voltage at the wind turbines. Then, due to the inherent time delay present in the OLTC based voltage control, the RPC from the wind turbine mitigates an overvoltage before the OLTC takes any action. On the other hand, if the wind turbine encounters a shortage in reactive power, the overvoltage will persist even after the delay, then the OLTC will take action.

Here the deadband of the AVC relay should be $> 2 \times (\Lambda_v + \epsilon_{v,r})$. Based on our assumed values above, this would mean that the deadband should be $> 2 \times (0.05 + 0.001) = 0.102$. Otherwise, for example, in the case of overvoltage, if RPC from remote wind turbines is also used, the voltage would be limited at $1 + \Lambda_v + \epsilon_{v,r} (= 1.051)$. If the deadband is $\leq 2 \times (\Lambda_v + \epsilon_{v,r}) = 0.102$, e.g. 0.10, since the AVC relay considers the voltage $\geq 1 + 0.1/2 = 1.05$ as an overvoltage, a tap change would occur rendering the effort of the RPC useless.

If curtailment is also to be used for overvoltage mitigation, OLTC should take precedence over curtailment as the use of curtailment is, in general, more expensive than changing a tap position as shown in Section 5.1.3. That is, if the overvoltage can not be mitigated even by using OLTC, then curtailment is used. This is achieved by using the curtailment controller in Fig. 7.16. The controller here controls the voltage at two reference values. The first reference voltage, given in

7. CONTROL ALGORITHMS FOR THE DIFFERENT ACTIVE MANAGEMENT STRATEGIES

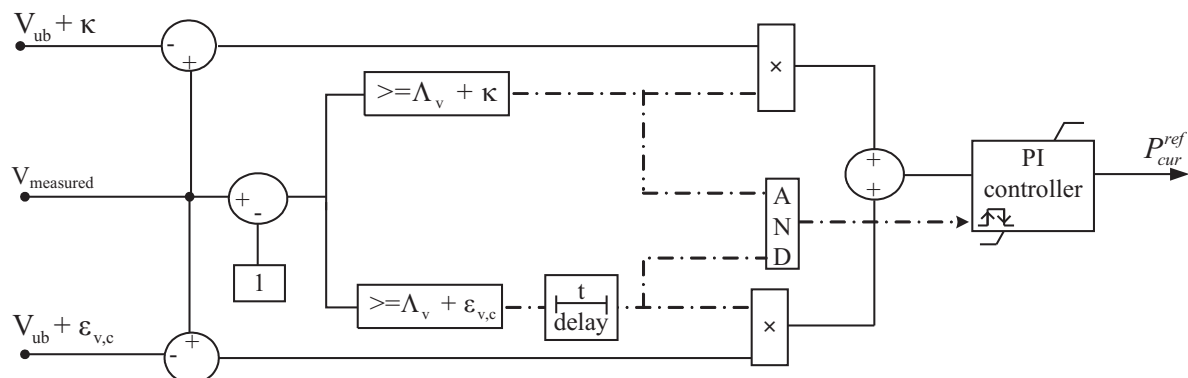


Figure 7.16: Coordinating OLTC and curtailment with real time voltage measurement available in the SE process.

the figure as $V_{ub} + \kappa$, is the highest of the two and the current controller will immediately (without a delay) starts curtailing if the overvoltage happens to be above this value. Then the curtailment controller is engaged, after a time delay, to limit the voltage at the second reference voltage, given in the figure as $V_{ub} + \epsilon_{v,c}$. The time delay here should be greater than the time delay of the OLTC as voltage regulation through OLTC is preferred over curtailment. The logic blocks $\geq V_{ub} + \kappa$ and $\geq V_{ub} + \epsilon_{v,c}$ are used to engage the PI controller to the respective reference voltages. Moreover, the deadband of the OLTC should be $< 2(\Lambda_v + \epsilon_{v,c})$ to avoid curtailment when the OLTC could mitigate the overvoltage.

Consider the case where the tap changer regulates the voltage in the network within $\pm 5\%$ of the nominal voltage. If the voltage increases beyond 1.06 pu, curtailment can be used to limit the voltage at 1.06 pu until the tap changer takes action to set it back below 1.05 pu. If the tap changer is not able to deal with the overvoltage for some reason, the power output of the wind turbine can be curtailed further to limit the voltage at the wind turbine terminal at 1.051 pu.

7.5.1.2 When real-time voltage measurement at the wind turbine terminals is not communicated to the SE process

In this case the voltage at the wind turbine terminal would be, for example in the case of an overvoltage, overestimated even if the RPC has limited the voltage within the allowed operating deadband. Thus, to coordinate the different voltage controllers under this situation, either

- the RPC from the wind turbines should be able to control the voltage at their terminals even at the worst system condition i.e. minimum load and maximum generation.
- or curtailment should be used without a delay (as given in Fig. 7.11) to mitigate the overvoltage whenever the RPC is incapable of doing that; the coordination between curtailment and RPC can be achieved by using higher reference voltage for curtailment controller as discussed above

Provided that this holds true, when the SE results show that the voltage at the terminals of the wind turbines is outside the allowed operating range, the SE is rerun with the voltage at the wind turbines' terminals assumed to be at the margin of the allowed operating range. This is because if voltage is limited by using the RPC or curtailment, it would be limited at the margin of the

operating range. Thus, under this coordination approach the role of the OLTC is to control the voltage of only non-wind-turbine buses (i.e. where wind turbine is not installed), and the voltage at the terminals of the wind turbine is assumed to be always kept within the limit by using RPC or curtailment.

7.5.2 Coordinating curtailment for overvoltage and overload mitigation

Coordination of curtailment for overvoltage mitigation and overload mitigation, if both happen at the same time, can be easily carried out by taking the maximum of the two PI controller outputs as shown in Fig. 7.15.

7.6 Case study system

7.6.1 Network and data description

The case study is based on a rural 11kV distribution system operated by Falbygdens Energi located in Falköping area in Sweden. The network is fed by a 40 kV grid through a $45 \pm 8 \times 1.67\% / 11.5$ kV, 10 MVA transformer. The aim of the case study is to investigate the performance of the different control algorithms discussed above by using one feeder of this distribution system. The circuit diagram of the feeder in consideration is presented in Fig. 6.1. The feeder consists of 14 buses including the substation busbar. A 50-Hz-sampled load data available from EPFL campus [175] is used to model the load variation in the given distribution system. A one day long 1-Hz-sampled wind power data is also available from a 2-MW wind turbine which is scaled and used to model the wind power variation in the system.

7.6.2 Simulation set up

The software used for simulation is Matlab/Simulink. The electrical network is modeled using the SymPowerSystems toolbox in Matlab. The transformer with the AVC relay and tap changer is modeled using the three-phase OLTC regulating transformer available in SymPowerSystems toolbox. The wind turbine is represented as a simple P-Q load where the available wind power data are used to model the active variation of the wind turbine and the reactive power reference is supplied from the voltage controller. Similarly, the load data obtained from the EPFL campus is used to model the load variation at each bus of the feeder. Moreover, since we are only interested in controlling the rms value of the network voltage, phasor simulation is used for the analysis. The state estimation is done assuming a balanced three phase system. This is mostly the case in the Nordic distribution system [27]. The refresh rate of the SE depends on the delay time of the tap changer. In our case study, where the delay time of the tap changer is 1 min, the refresh rate is taken to be 1 sec but a lower refresh rate such as 5 sec is found to work well.

7.6.3 Simulation results from the proposed active voltage regulation schemes

7.6.3.1 Voltage regulation using OLTC of the substation transformer

In this section we investigate the results from the proposed SE-based OLTC voltage control. Fig. 7.17 shows the load (Fig. 7.17a) and wind power (Fig. 7.17b) profile of the network. For the brevity of the presentation, the actual and estimated active load at different buses is not shown here. Moreover, the relatively low magnitude reactive power is omitted from Fig. 7.17. Load assigned to Bus 1 includes loads directly connected to the substation as well as those coming from other feeders than the one being investigated. It is assumed that real time measurement of the voltage magnitude at the substation as well as wind power output and voltage magnitude from Bus 6 are available. However, no measurement is assumed to be communicated to the SE process from wind turbine at Bus 14.

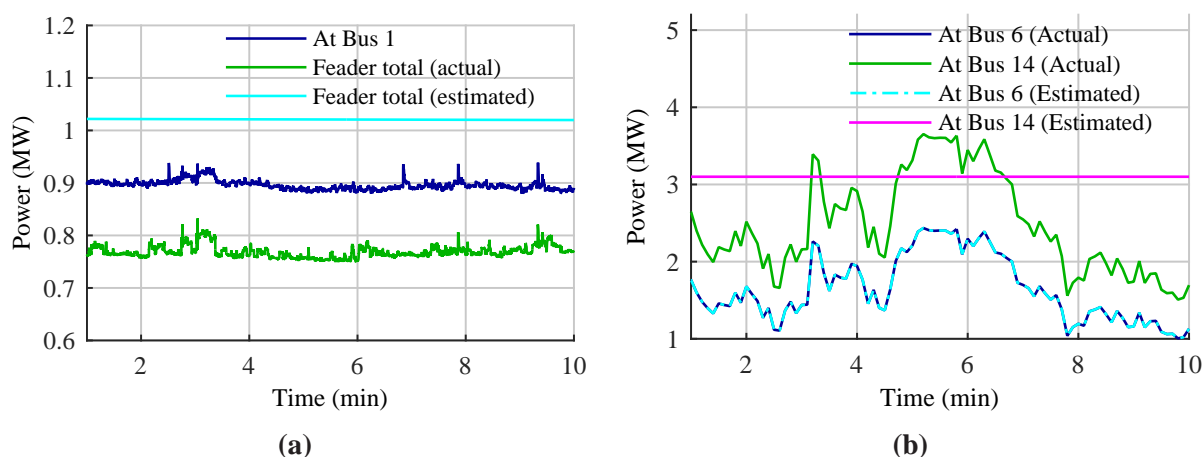


Figure 7.17: (a) Load profile and (b) wind power output at different buses in the network.

As can be inferred from Fig. 7.17, the load pseudo-measurement data have a constant error of around 35% compared to the actual value while the wind power pseudo-measurement data have a statistical error of around 100% (i.e. for 99.7% of the time the error between the actual and the estimated values is within $\pm 100\%$). The pseudo-measurement data are generated by taking the 10-minute moving average of the actual data and adding a bias to it. The pseudo-measurement data for the load directly connected to the substation bus is not provided in Fig. 7.17 as this load does not affect the SE process and, hence, is not used in the process.

In practice, load pseudo-measurements can be synthesized based on customer load curves, weather and time of the day data and billing information [162]. Moreover, if there are smart meters in the system, the data available from smart meters would be valuable in setting up more accurate pseudo-measurement data hence better voltage estimate. If no such data are available, the measured power flow at each feeder at the substation bus can be distributed to each bus in proportion to the size of MV/LV substation transformer or recoded maximum power flow at the transformer. The wind power pseudo-measurement data can be constructed from weather forecast data.

With the real-time and pseudo-measurement load and wind power data, the SE algorithm (DSSE block in Fig. 7.1) provides the voltage estimate at different buses in the network.

Figs. 7.18a and 7.18b shows the actual, maximum, and minimum voltage level in the network and the estimated minimum-maximum voltage level by the SE algorithm. The minimum voltage estimation appears to be more accurate than the maximum voltage. But this is due to the fact that the minimum voltage occurs at the substation where the voltage is measured while the maximum voltage occurs at Bus 14 which is not measured. Fig. 7.18c shows the input signal fed to the AVC relay by the voltage level analyzer block of Fig. 7.1. Then the AVC relay initiates a tap changer operation and the resulting tap positions are shown in Fig. 7.18d.

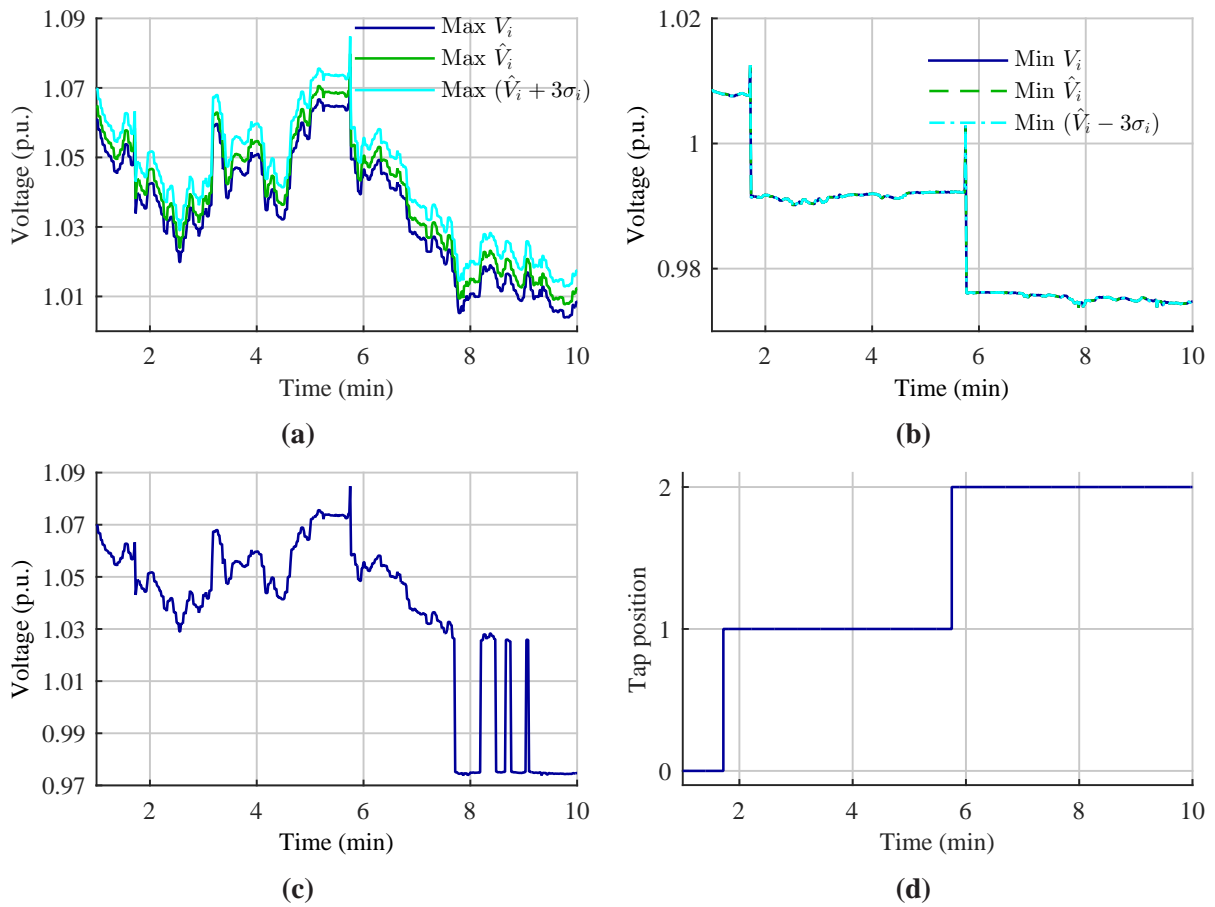


Figure 7.18: The actual (V_i) and estimated (\hat{V}_i) a) maximum, b) minimum voltage of the network, c) the $V_{\min/\max}$ signal fed to the AVC relay by the voltage level analyzer, and (d) the position of the tap changer.

From Figs. 7.18a, 7.18b and 7.18d one can see that whenever the estimate $\text{Max}(\hat{V}_i + 3\sigma_i)$ goes outside the $\pm 5\%$ deadband for over one minute (the delay time of the tap changer), the tap changer acts to bring the voltage within the deadband. Overall Figs. 7.18a, 7.18b and 7.18d show that the proposed SE-based OLTC voltage control regulates the voltage in the network effectively with limited measurement data from the network. That is, it does not fail to act whenever the voltage is outside the deadband. It can, however, unnecessarily operate the tap changer even when the actual voltage in the network is within the deadband due to the overestimation of the voltages at

7. CONTROL ALGORITHMS FOR THE DIFFERENT ACTIVE MANAGEMENT STRATEGIES

different buses. For example, in Fig. 7.18a, the actual voltage is not above 1.05 pu for the whole duration between Minute 1 and Minute 2 but the estimate is. This means the tap changer operates unnecessarily at around Minute 2. In this case, however, even with voltage measurement available from Bus 14, the tap change can only be delayed to minute 4 but not avoided. In general the more measurements are available the less will be the number of unnecessary tap changes.

7.6.3.2 Voltage Regulation using reactive power compensation from the wind turbines

In this section our main focus is to show the results when RPC is utilized to mitigate an overvoltage at the terminal of a local or remote wind turbine. Thus the operation of the tap changer is disabled. The same load and wind power data shown in Fig. 7.17 are used for the analysis. The wind power outputs of the wind turbines at Bus 6 and 14 are shown again in Fig. 7.19a for the clarity of the presentation. In Fig. 7.19b the voltages at the terminals of the wind turbines are shown. Fig. 7.19c shows the reactive power consumed by the wind turbines.

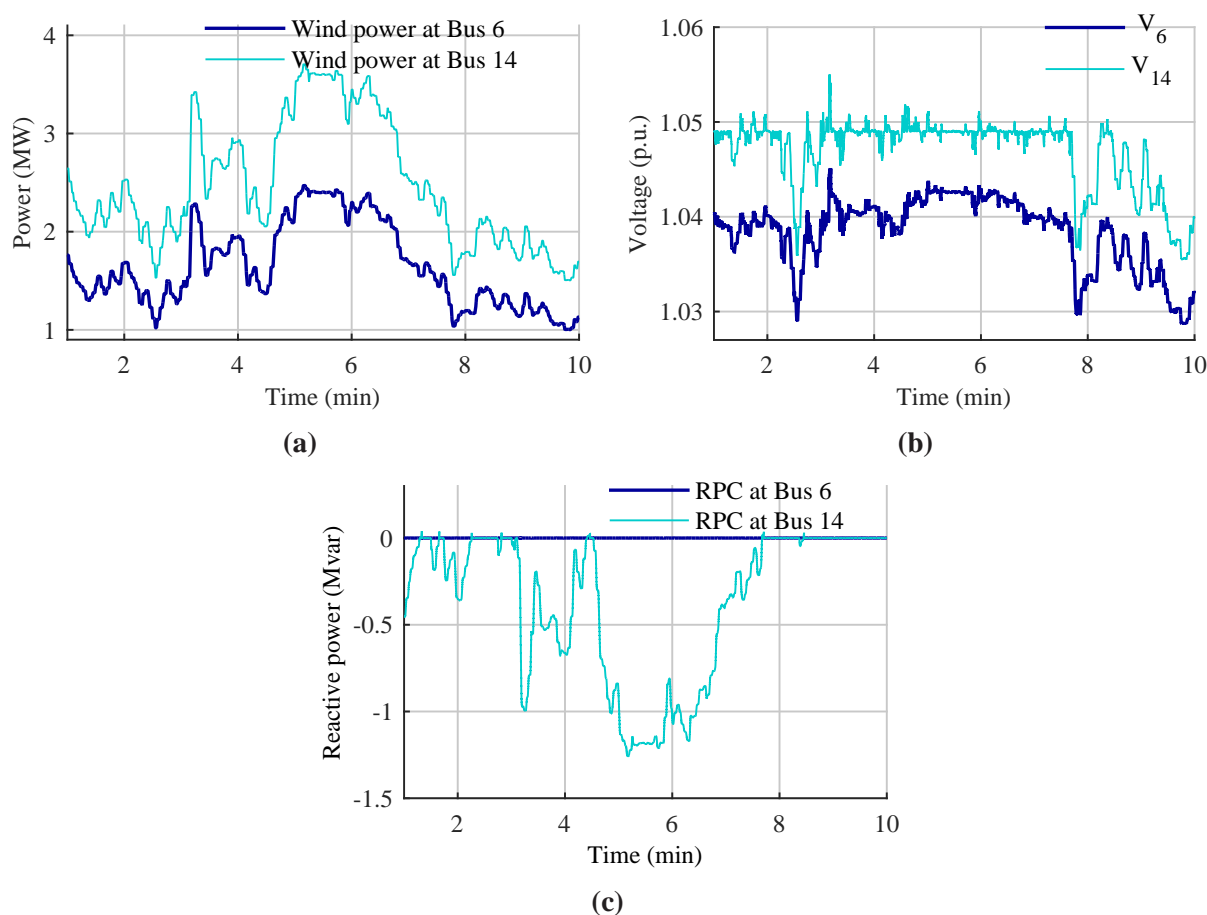


Figure 7.19: (a) Wind power profile, (b) voltage profile, and (c) reactive power profile of the wind turbines at Bus 6 and 14.

One can observe from Fig. 7.19 that with the help of RPC, the voltage at the terminal of the wind turbines is kept within $\pm 5\%$ except for short time voltage overshoots. Moreover, Fig. 7.19c shows that reactive power is consumed only when the voltage is about to be outside the $\pm 5\%$ deadband,

as desired. The same figure shows also that it is only the wind turbine at Bus 14 that is engaged with RPC. This is because the overvoltage occurs only at the terminal of this wind turbine. Note here that without the RPC by the wind turbine, the voltage at Bus 14 could have risen to as much as 1.08 pu between Minute 5 and 6.

Assume now that wind turbine at Bus 14 has a limited reactive power capability of 1 Mvar while it needs a maximum value of 1.2 Mvar reactive power. As a result, as shown in Fig. 7.20, the voltage at Bus 14 is outside the $\pm 5\%$ deadband between minute 5 and 6 due to the limited reactive power capability of the wind turbine at Bus 14. Nonetheless, with the right communication signals between wind turbines at Bus 6 and 14 this voltage rise can be avoided with the help of RPC from the wind turbine at Bus 6. This is presented in Fig. 7.21.

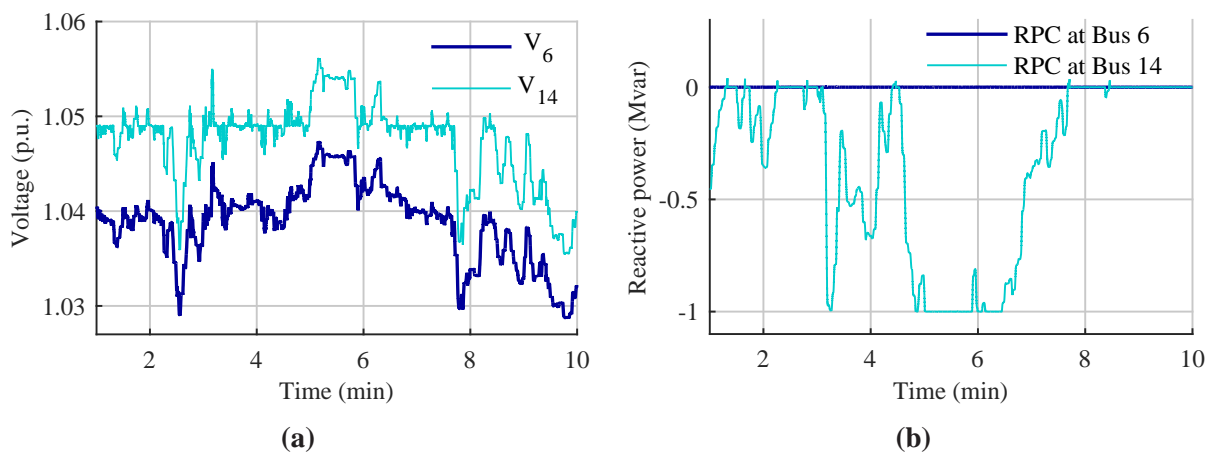


Figure 7.20: a) Voltage profile, b) reactive power profile of the wind turbines at Bus 6 and 14 when there is a limited reactive power at Bus 6.

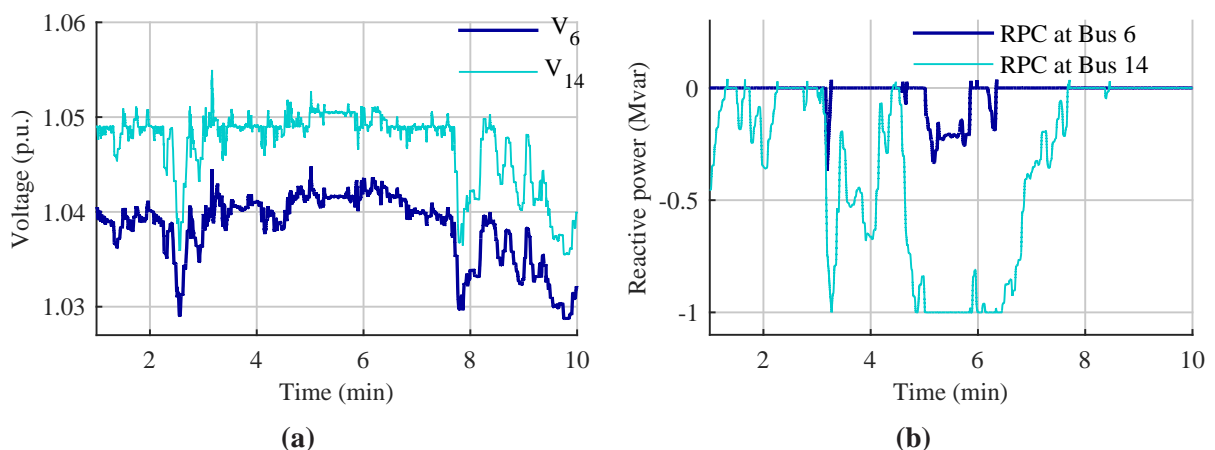


Figure 7.21: a) Voltage profile and b) reactive power profile of the wind turbines at Bus 6 and 14 when the RPC is coordinated.

From Fig. 7.21 one can see that whenever the wind turbine at Bus 14 hits its reactive power limit, the voltage keeps increasing until it reaches 1.051 pu at which point the wind turbine at Bus 6 engages in RPC (see Fig. 7.21b) to limit the voltage at 1.051 pu (see Fig. 7.21a).

7. CONTROL ALGORITHMS FOR THE DIFFERENT ACTIVE MANAGEMENT STRATEGIES

7.6.3.3 Voltage regulation with both OLTC and reactive power compensation

This section combines the SE-based OLTC voltage control and the RPC, and investigates the overall performance of the two control strategies. As mentioned in Subsection 7.6.3.1, no measurement is assumed to be communicated from the wind turbine at Bus 14 to the SE process. So the corresponding method discussed in Section 7.5.1 is used to coordinate the voltage regulation based on OLTC and RPC. The results of the simulation are shown in Fig. 7.22. Since the SE adjusts its voltage estimate assuming that the RPC will take care of the voltage at the wind turbine terminal, there is no tap change. If such adjustments were not made, the SE would have overestimated the voltage at Bus 14 and there would have been tap changes similar to the ones in Fig. 7.18d. Moreover, between Minute 5 and 6 the voltage at Bus 14 is above 1.05, i.e. it is 1.051, due to voltage control coordination principle adopted between the two wind turbines. If real-time measurements from Bus 14 were used in the SE, this would have induced a tap change. To avoid a tap change happening in such cases one may relax the deadband by 0.002pu or reduce the value of Λ_v in voltage control algorithm of the wind turbines by 0.001.

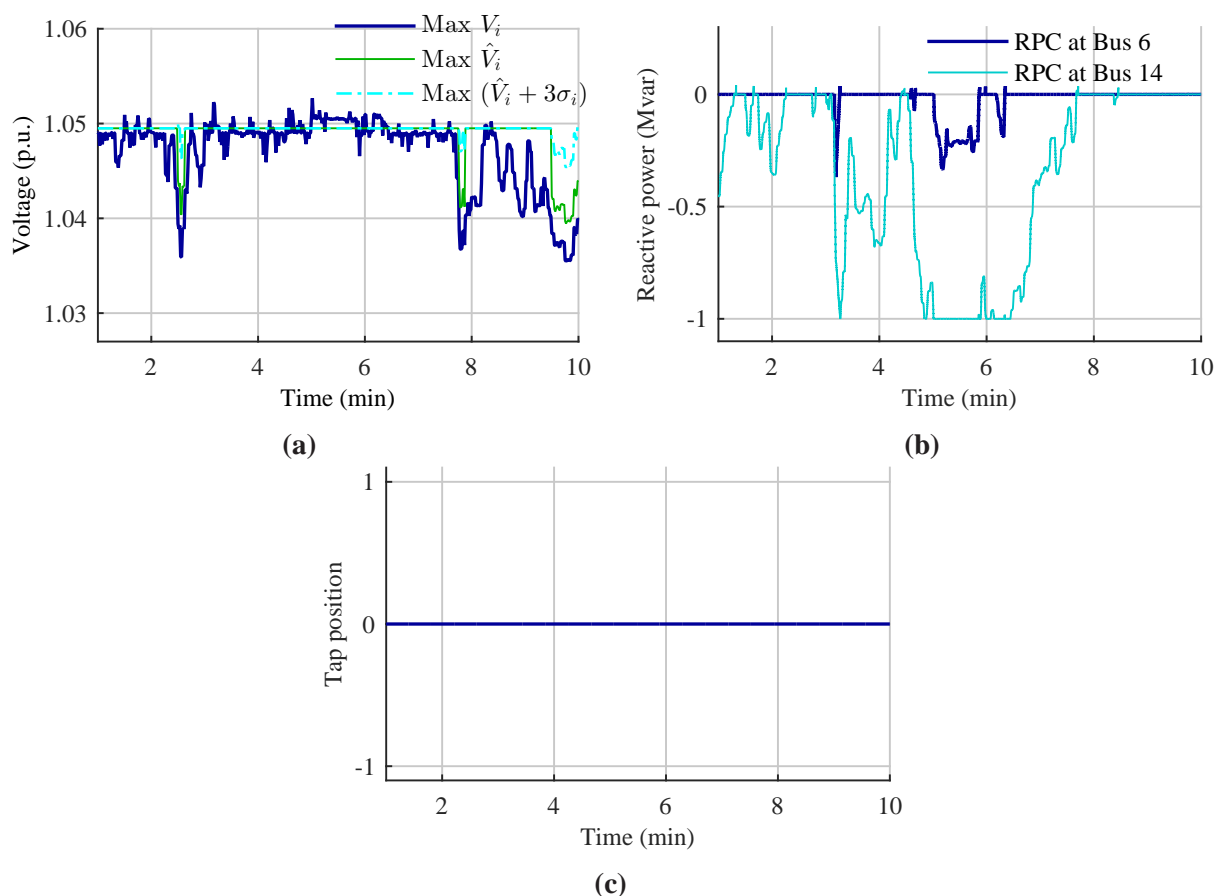


Figure 7.22: a) The actual and estimated minimum and maximum voltage of the network, b) the reactive power compensation by the wind turbines, and c) the position of the tap changer.

In the analysis so far no measurement is assumed to be available from the wind turbine at Bus 14 in the SE algorithm. This is done to test more clearly the SE algorithm, hence the effectiveness of the OLTC based voltage control algorithm, and the coordination between the RPC and the SE-based

OLTC voltage control algorithm. Generally, it is always better to have measurements from the wind turbine buses as:

- wind turbine buses are the most likely places where an overvoltage can happen and it is thus better to measure it than to estimate it,
- wind power outputs are less certain and can be of higher magnitude than load buses and with measurement at the wind turbine buses a better voltage estimate of the network would be achieved,
- and finally one can achieve a better coordination between the RPC and the SE-based OLTC voltage control system.

7.6.3.4 Voltage regulation using RPC and curtailment

In Fig. 7.21 the overvoltage at the terminal of a wind turbine is mitigated using reactive power compensation from a remote wind turbine. This is found to be effective for mitigating voltage rise in case the local wind turbine does not have sufficient reactive power to mitigate its voltage rise. However, the approach requires to have a another wind turbine in the network with excess reactive power. Moreover, it requires to have a communication channel between the wind turbines. When either of these two requirements are not fulfilled, the local wind turbine needs to resort to curtailment of its power output. Fig. 7.23c shows the results of the analysis when curtailment, together with RPC, is used based on the control strategy outlined in Section 7.4.1. From the figure one can see that when the reactive power of the local wind turbine is exhausted, its active power output is curtailed to mitigate the overvoltage at its terminal. Moreover, as per the discussion in Section 7.4.1, the overvoltage limit is relaxed by 0.0025 pu. As one can see from Fig. 7.23b, the reactive power limit in this case is 1 Mvar at all wind power output level. But if we assumed that the wind turbine can consume 1 Mvar at full power output and then it should be able to consume more at partial power output. Then, by varying the reactive power capability of the wind turbine with respect to the active power output of the wind turbine, assuming 1 Mvar at maximum power output, we get the results as presented in Fig. 7.24. The comparison of results in Fig.7.23c and Fig.7.24c shows that, by allowing the reactive capability of the wind turbine to vary according to the power output of the wind turbine, 95% of the curtailed energy in former is saved in the latter.

Note here that the bandwidth of the curtailment system is selected such that the wind turbine curtails 10% of the total curtailment amount in 1 sec and this is within the capability of most modern wind turbines [174]. From this, the settling time of the curtailment system is taken as $T_s = 10 \text{ sec}$. Assuming the system to have a first order system response, then the bandwidth of the system will be $\alpha_{\text{sys}} = 4/T_s = 0.4 \text{ rad/sec}$. Even though this value is low compared to the bandwidth of the reactive power compensation controller ($\alpha_r = 2 \text{ rad/sec}$), the difference in the performance of the voltage regulation as seen in Fig. 7.21a and Fig. 7.23a is insignificant. This is due to the fact that the wind power output and consumer loads do not vary that much within the given bandwidths. Besides the quality of the voltage regulation, the use of RPC is superior in terms of minimizing the energy loss in the system (see Sections 5.1.3 and 5.5.2.3).

7. CONTROL ALGORITHMS FOR THE DIFFERENT ACTIVE MANAGEMENT STRATEGIES

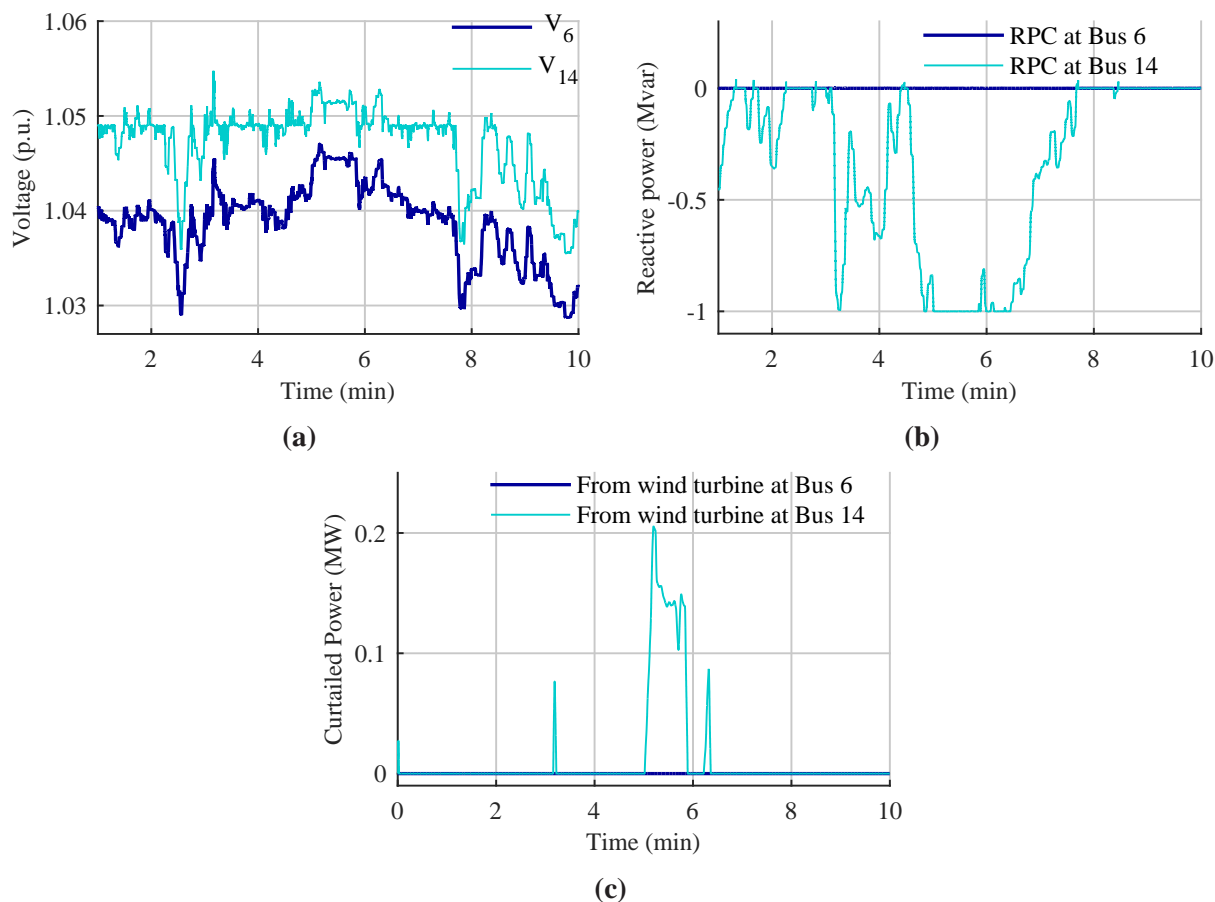


Figure 7.23: a) Voltage at the wind turbine terminals, b) the reactive power compensation by the wind turbines, and c) wind power curtailment.

7.6.3.5 Coordination of overvoltage mitigation with RPC, OLTC and wind power curtailment

In Subsection 7.6.3.3, the coordination of RPC and OLTC is investigated where it is assumed that real time measurement from wind turbine 14 is not available in the SE process. Moreover, the wind turbine at Bus 14 is supported with RPC from wind turbine at Bus 6 to mitigate the overvoltage whenever the wind turbine at Bus 14 faces a reactive power shortage. Almost similar results are observed if the local RPC at Bus 14 is supported by local curtailment rather than RPC from remote wind turbine.

Now this section presents the results of the simulation when real time measurement from wind turbine at Bus 14 is assumed to be available in SE process. Thus, the coordination of voltage regulation through OLTC and curtailment is carried out using the method provided in Fig. 7.16. On the other hand, to experience an overvoltage level for an extended time that will trigger the OLTC and the curtailment system, it is assumed that the maximum available reactive power from the wind turbine at Bus 14 is 0.6 Mvar. To illustrate the effect of using OLTC or curtailment, Fig. 7.25 shows the result when neither OLTC nor curtailment is engaged and RPC is used only locally. Note that there is an overvoltage at Bus 14 between roughly Minute 4.5 and 7 and its magnitude is above 1.06 pu between roughly Minute 5 and 6.5.

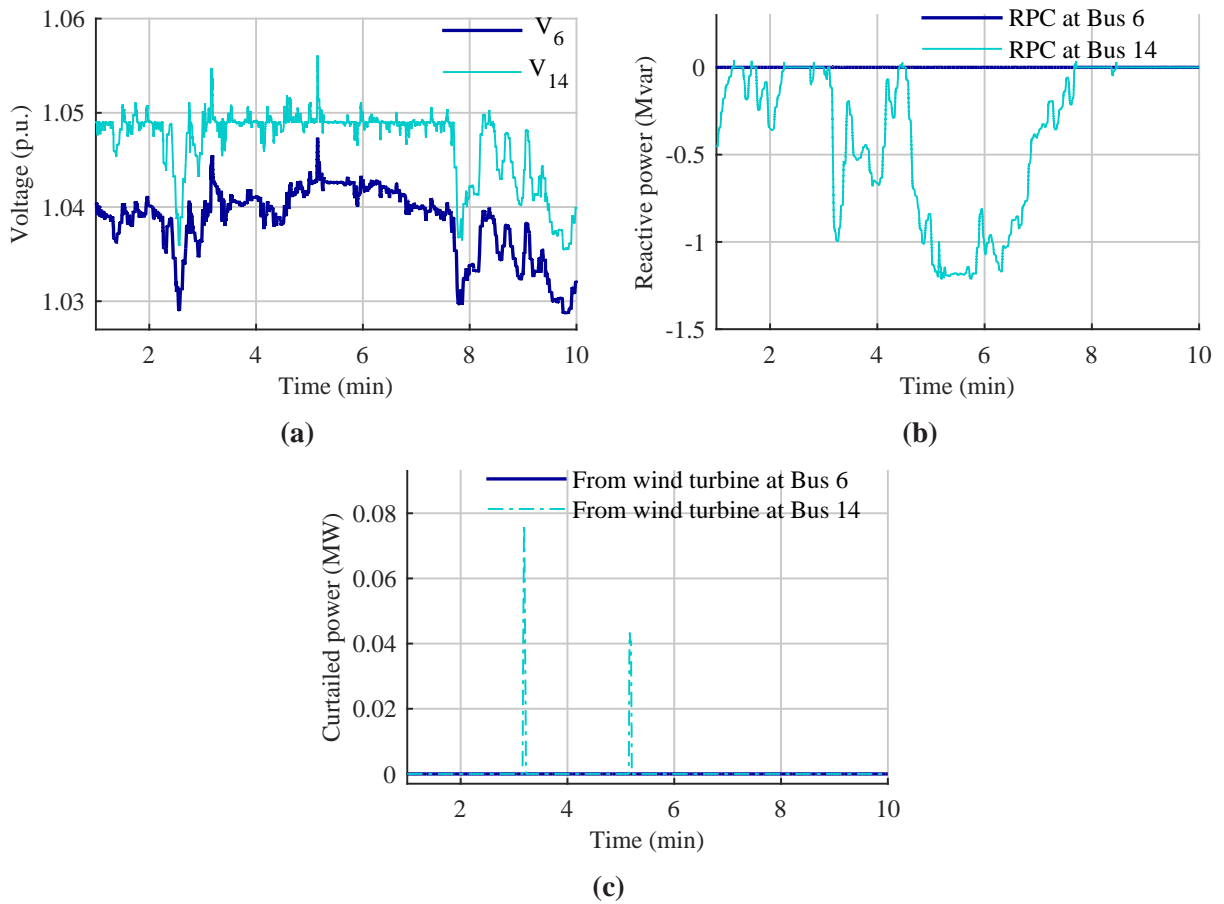


Figure 7.24: a) Voltage at the wind turbine terminals, b) the reactive power compensation by the wind turbines, and c) wind power curtailment.

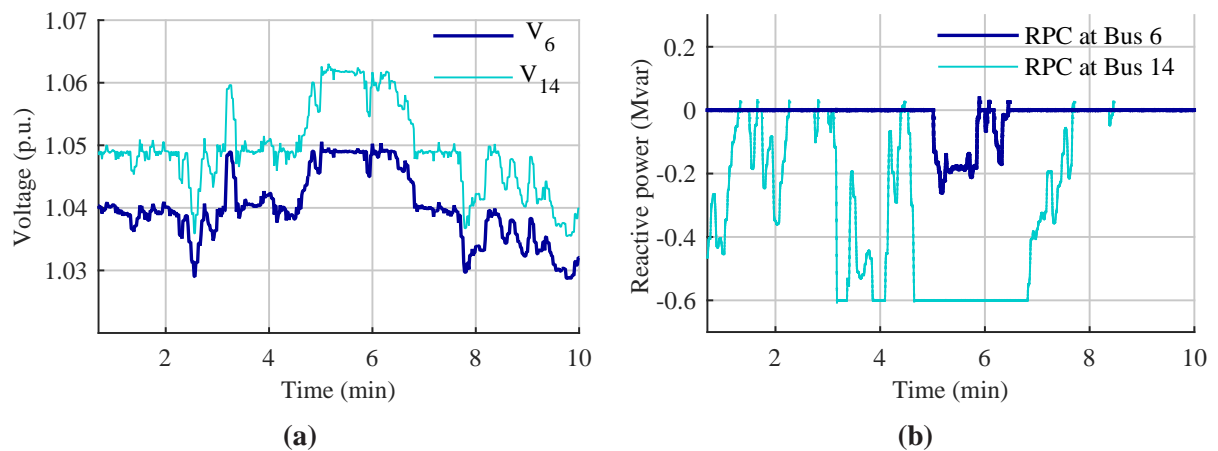


Figure 7.25: a) Voltage at the wind turbine terminals and b) the reactive power compensation by the wind turbines, When both curtailment and OLTC does not operate to mitigate the overvoltage.

7. CONTROL ALGORITHMS FOR THE DIFFERENT ACTIVE MANAGEMENT STRATEGIES

Based on our setting, the OLTC should operate after a delay of 1 min and curtailment should be engaged after 1.3 min delay. Fig. 7.26 shows the results of the simulation when all the three active management strategies are involved. At around Minute 3.3 there occurs an overvoltage for which neither the OLTC nor the curtailment responds as it occurs for a short duration (see in Fig.7.26a). Though, in the meantime, RPC is activated, it could not mitigate the overvoltage(see in Fig.7.26b). Between roughly 4.6 min and 5.7 min, an overvoltage occurs again. During this period, curtailment carried out (see in Fig.7.26d) to limit the overvoltage at 1.06 pu as discussed in Section 7.5.1. Then at Minute 5.7 the tap changer operates (see in Fig.7.26c), as the result the voltage is set back below 1.05 pu. At this point RPC is still being used to keep the overvoltage at 1.05 while curtailment is no more necessary. Thus, Fig.7.26 shows that when the OLTC is able to mitigate the overvoltage the coordination of voltage regulation among the three active management strategies works well.

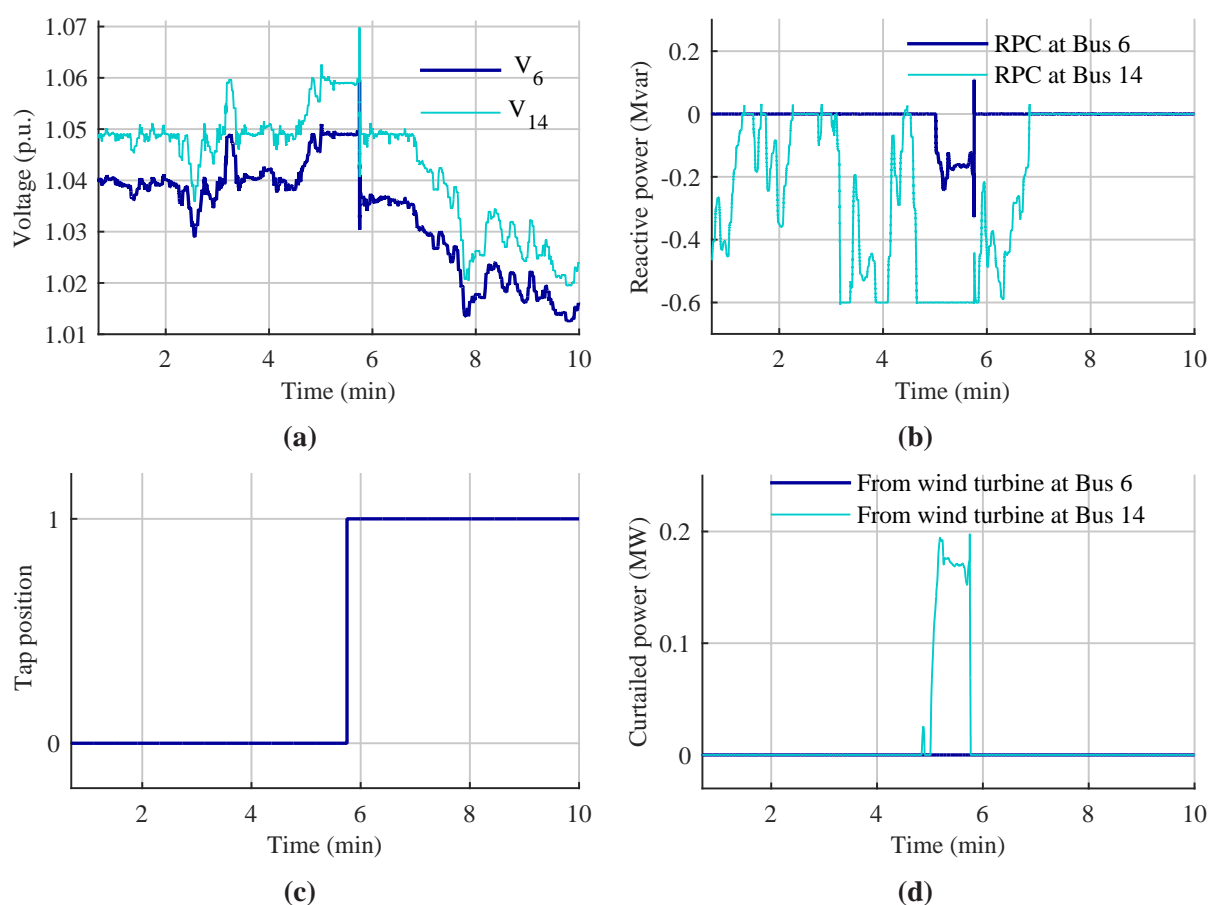


Figure 7.26: a) Voltage at the wind turbine terminals, b) the reactive power compensation by the wind turbines, c) tap position of the tap changer, and d) wind power curtailment when all the three active management schemes are operational.

Now we want to see how well the coordination principle proposed in Section 7.5.1 works if the OLTC does not operate to mitigate the overvoltage, for some reason. The results of the simulation are presented in Fig.7.27. One can see that until Minute 6, which is roughly a time delay of 1.3 after the voltage has passed the 1.052 pu mark, the curtailment is only used to keep the voltage around 1.06. After that curtailment is engaged to limit the voltage at 1.052 pu. But, as can be seen

in the Fig. 7.27a, the voltage stays at 1.052 pu for only a short duration as the wind power output of the wind turbine decreases. In fact, this decrease, after a short while, results in disengaging even the RPC system.

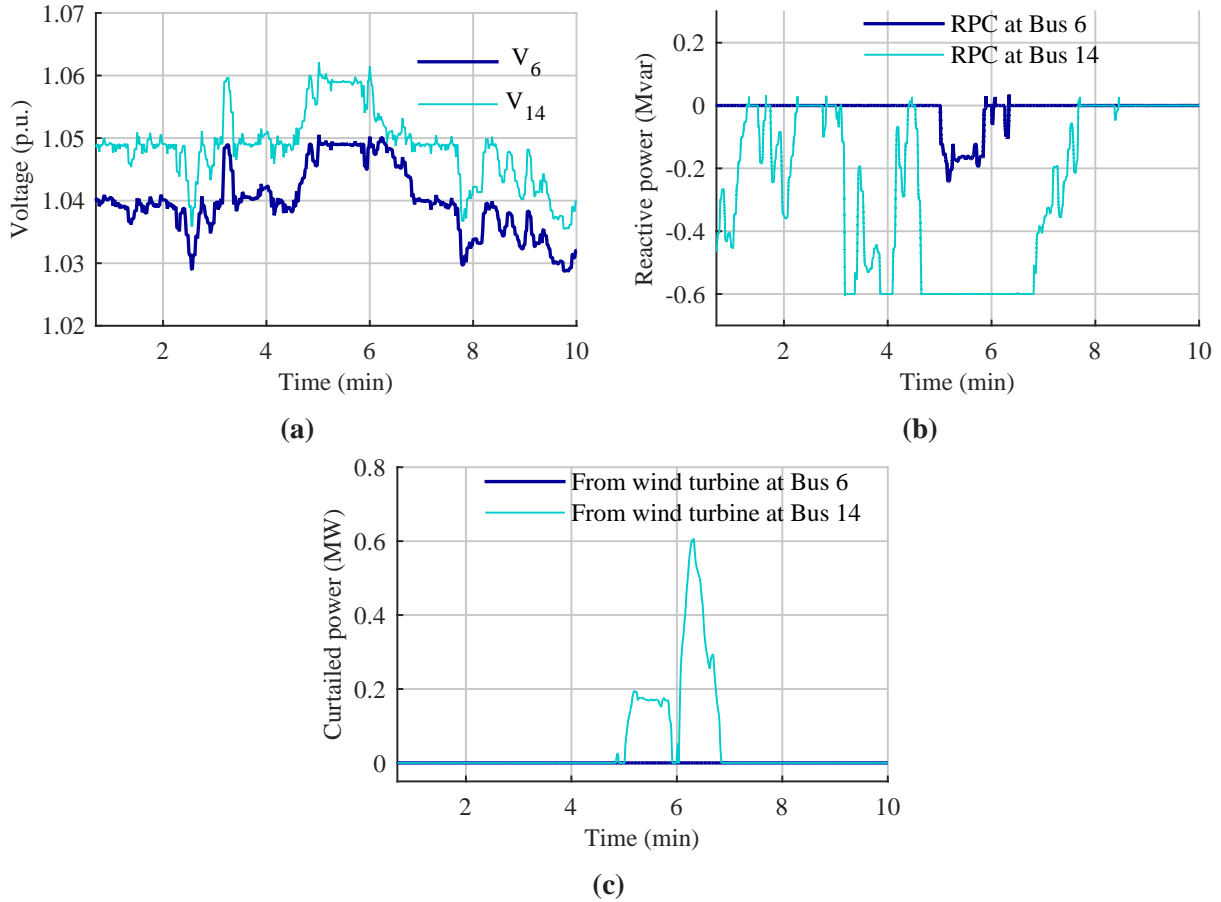


Figure 7.27: a) Voltage at the wind turbine terminals, b) the reactive power compensation by the wind turbines, and c) wind power curtailment, when the OLTC does not operate to mitigate the overvoltage.

Overall, from analysis given based on Figs. 7.25, 7.26, and 7.27 one can observe that the proposed voltage control and coordination algorithm works as intended.

7.6.4 Simulation results from overload mitigation using curtailment

So far the discussion is concentrated on the voltage regulation of the network. This section presents the performance of the curtailment controller when mitigating an overloaded components in the network. The component selected for monitoring is the power line between Bus 1 and Bus 2 (see Fig. 6.1). Unlike the case of voltage regulation where state estimation based on pseudo-measurement and a few real time measurement are used to determine the voltage magnitude, it is recommended to utilize real time measurement for this purpose. This is because, on one hand, in properly designed network, it would not be difficult to determine as to which component of the network can be overloaded due to the introduction of the wind turbine. On the other hand, overloading entails energy curtailment and, since energy curtailment is expensive, it should be as low

7. CONTROL ALGORITHMS FOR THE DIFFERENT ACTIVE MANAGEMENT STRATEGIES

as possible. Thus, it should not be based on estimation which can provide incorrect loading levels and unnecessary energy curtailment. Therefore, Fig. 7.28 shows the performance of the curtailment controller using current magnitude measurement from the specified branch. In Fig. 7.28 it is

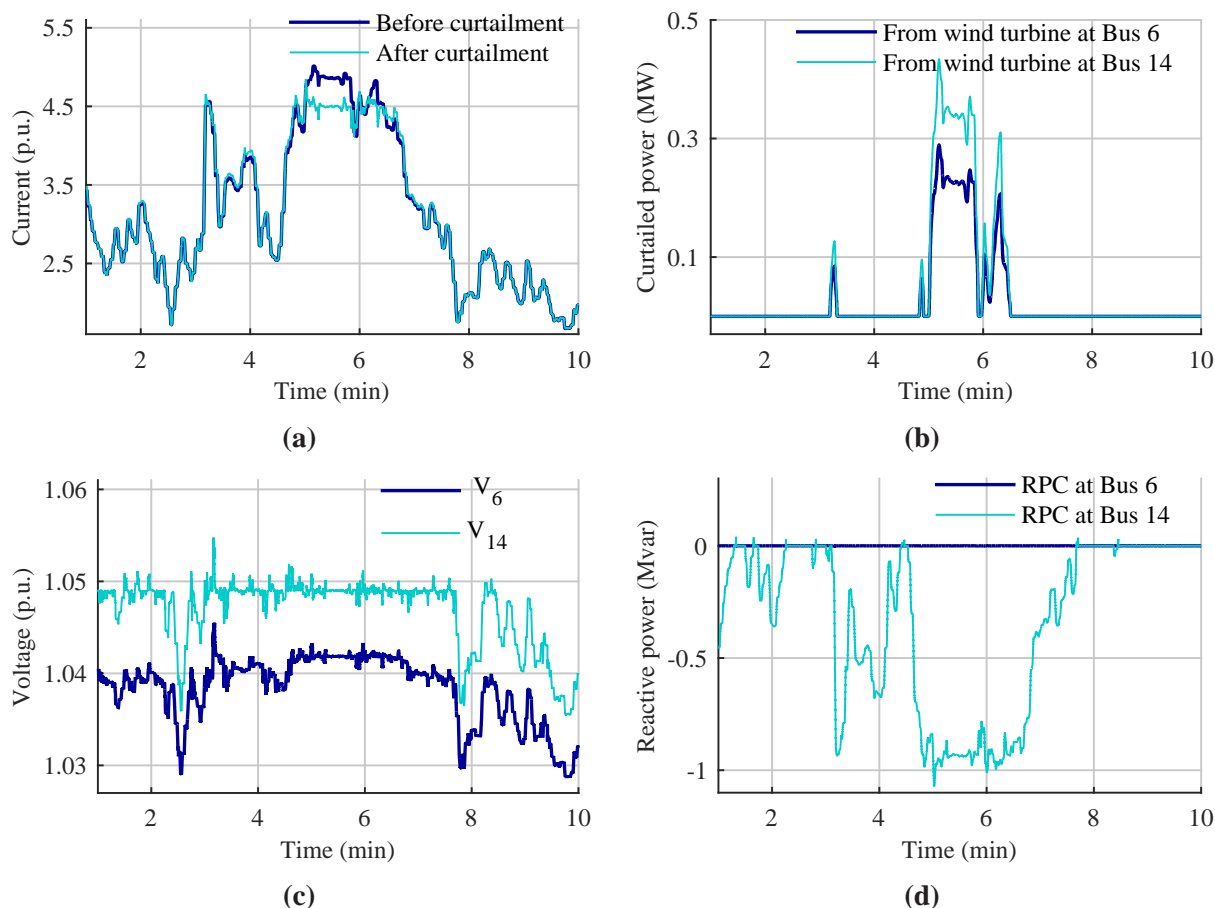


Figure 7.28: a) Current flow in the branch, b) curtailed wind power, c) Voltage at the wind turbine terminals, and d) the reactive power compensation by the wind turbines.

assumed that the overload capability of the branch is 4.5 pu whereas the consumer loads and the power output of the wind turbines are unchanged from the previous cases. Fig. 7.28 shows that wind power is only curtailed when the branch is overloaded. Moreover the power output of each wind turbine is curtailed proportional to its capacity. This is achieved by tuning the gains of the integral controller given in (7.9) as follows.

$$K_{I_6} = \frac{P_6^{\max}}{P_{14}^{\max}} \alpha_{cur} V_w^0 \quad (7.9)$$

$$K_{I_{14}} = \alpha_{cur} V_w^0$$

where K_{I_6} and $K_{I_{14}}$ are the integral gains of the controllers of the wind turbine at bus 6 and 14, respectively; P_6^{\max} and P_{14}^{\max} are the maximum power outputs of the wind turbines at Bus 6 and Bus 14, respectively. Here it is assumed that $P_{14}^{\max} \geq P_6^{\max}$ so that the bandwidth of the controller is within the capability of the wind turbine curtailment system.

One may notice that, due to the limited bandwidth of the overload controller, whenever the branch is overloaded it takes a while before the loading is regulated within the limit. Overall, however, the controller is effective in relieving the overloading with minimum wind energy curtailment.

Furthermore, due to the curtailment to mitigate the overloading, reactive power compensation from the wind turbine in Bus 14 is sufficient to mitigate overvoltage as shown in Figs. 7.28c and 7.28d. If the wind turbine did have a shortage in reactive power to mitigate overvoltage and if it cannot get support through OLTC or RPC from the other wind turbine to mitigate the overvoltage, the wind turbine needs to use curtailment for both overvoltage and overload mitigation. The coordination of the two curtailment controllers, i.e. overvoltage mitigation and overload mitigation curtailment controllers, can simply be carried out by taking the maximum of the output of the two controllers as discussed in Section 7.5.2.

Finally, the presentation so far has used the same load and wind power data to test the effectiveness of the voltage regulation algorithms proposed in this paper. However, though not presented here, the algorithms are tested with different load data and wind power data and are found to successfully carry out the task of voltage regulation as well as overload mitigation in the given radial distribution system.

7.7 Summary

This chapter discusses the control and coordination of the different active management schemes that can be used to maximize the integration of wind power in distribution systems. The aim of these active management schemes is to deal with the voltage regulation and overloading problems that arise with the introduction of wind power.

For voltage regulation, coordinated control of transformer OLTC, reactive power compensation (RPC), and energy curtailment can be used. The control of the OLTC is achieved by using SE to obtain the voltage estimate at different buses. Moreover the deadband of the OLTC is relaxed to cover the allowable voltage range of the network. This approach shows a good voltage regulating capability and its implementation is much simpler than adjusting the set point of the OLTC which is done if the deadband is left at its conventional setting. For RPC and energy curtailment, simple integral controllers with some on-off logic is used to carry out the voltage regulation with minimum RPC and energy curtailment. The on-off logic is mainly used to determine when the RPC and curtailment need to be engaged and disengaged.

The OLTC of the substation transformer can be used to regulate the voltage on the load buses of the network whereas RPC can be used to regulate the voltage at the wind turbine terminals. Moreover, reactive power from a wind turbine can be used to mitigate an overvoltage that occurs locally as well as at the terminal of any remote wind turbine on the same feeder. This is valuable when the remote wind turbine has limited or no reactive power capability to mitigate an overvoltage at its terminal. In this way, unnecessary tap regulation is avoided. Curtailment can be used to mitigate an overvoltage when all wind turbines in the network have used up their reactive power capability and when sufficient measurements are not available to use the SE-based OLTC voltage control to mitigate the voltage at the wind turbine terminal. It can also be used if the operation of the OLTC introduces an undervoltage on some buses on the other feeders or the tap limits are reached.

7. CONTROL ALGORITHMS FOR THE DIFFERENT ACTIVE MANAGEMENT STRATEGIES

For the proper coordination of voltage regulation through the SE based OLTC voltage control, RPC, and curtailment, the voltage magnitude measurements from the wind turbine terminals need to be available as input to the state estimation algorithm. Then, the SE based OLTC voltage control takes action only when the wind turbines are not able to regulate the voltage at their terminal using RPC. In addition, curtailment can be used after a delay if the OLTC does not mitigate the overvoltage.

Even if real time voltage measurements from the wind turbine terminals are not available in the SE process, it is still possible to avoid unnecessary tap changes if the results of the SE algorithm is adjusted to reflect the effect of voltage control through RPC. But in this case one needs to ensure that the available reactive power from the wind turbines is sufficient to mitigate an overvoltage that occurs at the worst system condition, i.e. minimum load and maximum generation. Otherwise, the wind turbine needs to resort to curtailment under such situation for proper coordination.

As for the coordination of voltage regulation using RPC from different wind turbines, the controller at each wind turbine needs to know the voltage level at the other wind turbines on the same feeder. Then, the wind turbines in the network shall have two voltage set points. During an over voltage, the local wind turbine tries to set the voltage at its terminal to the lower voltage set point. If the local wind turbine does not have enough reactive power, the voltage keeps on increasing. Then, when the voltage level becomes above the higher voltage set point, the remote wind turbines engage in RPC to limit the voltage at the higher voltage set point. As the loads and the power output of the wind turbines change the voltage starts to decrease, the reactive power output of the remote wind turbines is decreased before the reactive power of the local wind turbine starts to decrease. This ensures that the minimum amount of reactive power is used to mitigate the overvoltage. Similarly, if the reactive power from all wind turbines cannot mitigate the overvoltage, and OLTC cannot be used for reasons mentioned before, the overvoltage keeps on increasing until it reaches another voltage set point. At this point the local curtailment controller is engaged to limit the overvoltage.

For overload mitigation, curtailment is the only option discussed in the thesis. The controller is similar to the one used for overvoltage mitigation. On the other hand, the required sharing of wind power curtailment to mitigate an overloading between the different wind turbines involved can be achieved by properly tuning the integral gains of the curtailment controllers of the different wind turbines. Finally, curtailment of wind power output of a single wind turbine for overload and overvoltage mitigation can be coordinated by taking the maximum output from the two curtailment controllers.

8

Conclusions and future work

This thesis provides an analysis of wind power in distribution systems aimed at maximizing the wind power hosting capacity of such systems. The problem is approached from two angles. The first part of the thesis discusses the issues related with the planning perspective of maximizing wind power in a distribution system. Various power quality and reliability effects of wind power are analyzed. In particular, the effect of wind power on the frequency of tap changes is investigated using a model developed in this thesis. A mitigation solution based on reactive power compensation from the wind turbines is proposed to decrease the frequency of tap changes. The thesis also identifies the limiting factors of wind power integration based on which the siting of wind turbines in a given distribution system is proposed. Finally an optimization model is developed that can be used to assess the optimal hosting capacity of distribution systems. The second part of the thesis investigates the operation of a large amount of wind power in a distribution system. Thus, the control and coordination of the active management strategies proposed in the first part are discussed. Different investigations in the thesis are supported by case studies based on a real-life network, and measured load and wind power data obtained from Falbygdens Energi.

8.1 Main conclusions

In addition to the common integration issues of wind power (such as overvoltage, overloading, etc) some DSOs are concerned about the effect of wind power on increasing the frequency of tap changes (FTC).

- Based on our analysis, for distribution systems where the X/R ratio of the grid is high ($X/R \geq 5$) at the point of voltage regulation, no significant effect on the FTC is seen due to the introduction of wind power. However, in a distribution system where the X/R ratio is low at the point of voltage regulation, the FTC can be affected significantly due to the introduction of wind power.
- A further investigation is carried out to decrease the FTC using the reactive power available from variable speed wind turbines. The result shows that the methodology is very effective. However, the reactive power required to reduce the FTC by a specific percent depends on the SCC and the X/R ratio. The reactive power requirement decreases with higher SCC and X/R ratio.

8. CONCLUSIONS AND FUTURE WORK

Our analysis identifies the following conditions at which each of the different integration issues could become a limiting factor.

- Overvoltage has been identified as one of the main limiting factors in radial distribution networks. It usually occurs when wind turbines are connected to a PCC away from the station where the grid is weak and has low X/R ratio.
- Overloading of network components such as cables and transformers becomes a limiting factor when the wind turbines are installed close to the substation in such a way that overvoltage is not a problem.
- Harmonics and flicker can become a limiting factor in a distribution system connected to a relatively weak external grid and the wind farm is close to the substation. However, with the advent of variable speed wind turbines, flicker is less likely to be a limiting factor.
- Increased fault level can become a limiting factor in rare cases where the distribution system is connected to a relatively strong grid, and the wind turbines, which are of Type A, B, or C, connected close to the station. Moreover the substation has higher overload capacity, so overloading is not a problem. However, it depends on the rating of the switchgear which will determine the short-circuit capacity margin left to handle additional fault current from the wind turbines. In case of Type D wind turbines the fault current contribution is minimal due to the limitation in the output current of the converter. Thus, such wind turbines pose little concern with respect to increasing the fault level.
- In general, however, the usual and main limiting factors of wind power integration are voltage rise and overloading.

Moreover, with the different limiting factors in place corresponding to the different characteristic of the distribution system and the wind turbines, the optimal siting problem has been investigated in this thesis. The main conclusions are:

- In a distribution system where there are a couple of equally favorable sites/buses to wind power connection, then the ones electrically closest to the substation—located on different feeders or laterals—would maximize the hosting capacity of the distribution system.
- Installing the wind turbines away from the substation would effectively limit the hosting capacity of the feeder, especially if the limiting factor is the voltage rise problem.
- The only case when one may want to connect the wind turbines away from the substation is if the wind power hosting capacity of the distribution system is limited due to increased fault level.

For a distribution system whose hosting capacity is limited due to voltage or overloading, different active management strategies are proposed in literature to increase the hosting capacity of the network. To assess the optimal use of these active management strategies thereby determine the optimal hosting capacity of the network, an optimization model based on cost benefit analysis is developed in this thesis. This model is applied to two separate case studies and the following conclusions are made:

- Coordinated OLTC voltage control and reactive power compensation can be effectively used to increase the wind power hosting capacity of a distribution system limited due to the voltage rise problem. A case study based on such systems has shown an increase in hosting capacity up to double the capacity that would be installed based on worst case analysis. Such an increase is achieved with very little help from energy curtailment.

- Energy curtailment is the only option investigated in this thesis to increase the hosting capacity of a network constrained due to thermal overloading of network components. A case study carried out shows that the optimal hosting capacity of such a network depends on who covers the cost of curtailed energy: the DSO or the WFO. In either case the hosting capacity is increased considerably. In the case when the DSO covers the cost, the hosting capacity of the network is increased by as much as 60% by allowing a mere 1% WEC. When WFO covers the cost, the increase in hosting capacity depends on the capacity factor of the wind turbines and the discount rate. In our analysis, the hosting capacity is increased by as much as 83% with the curtailed energy being only 3.3%. Unlike the case when the DSO covers the cost of curtailment, here the hosting capacity is limited as the alternative option, i.e. grid reinforcement, becomes more attractive than curtailment if the WFO wants to install more. Hence when determining the optimal level of wind power curtailment, one should not only focus on the profitability of the WEC but also a comparison should be made with an alternative option, such as grid reinforcement.

In the second part of the thesis where the operation of a distribution system with a large amount of wind power is investigated, the control and coordination of SE-assisted OLTC, RPC, and WEC are presented. To begin with, among the different distribution system SE algorithms proposed in the literature, two of them are chosen for comparison. The first one is the widely used node-voltage-based weighted least square SE algorithm and the other is the computational efficient branch-current-based SE algorithm. The effects of measurement location and type of measurement on the accuracy of these SE algorithms are also investigated through simulation. From the results of this analysis the following conclusions are made:

- Though the branch-current-based SE provides superior computational efficiency, the node-voltage-based SE algorithm is chosen for the use in the SE-assisted OLTC voltage control. This is because the node-voltage-based SE algorithm is superior in terms of SE accuracy. Since there are only few real time measurements in the system being investigated, the accuracy of the SE is given more preference.
- The SE provides more accurate results when realtime measurements are done at the wind turbine sites rather than load buses. This is because, on one hand, as per the objective of the study, the wind power output on each site is considerably larger than the load on each bus, and, on the other hand, wind power output is less predictable than load in a distribution system. Thus, the constructed pseudo-measurement data of wind power affects the SE results more negatively than the pseudo-measurement load data would do. Hence measuring the wind power improves the SE results more.
- Power injection measurement is preferred over branch power flow measurement as the former can be done on the low voltage side of the transformer and hence reduces the cost of installation. Moreover the sitting of the power injection measurement is more apparent than branch power measurements. However, when accurately situated, both measurement types are seen to provide around the same level of SE accuracy.

The following points are concluded concerning the control of the different active management strategies.

- The control of the OLTC is achieved by using SE to obtain the voltage estimate at different buses. Moreover the deadband of the OLTC is relaxed to cover the allowable voltage range of

8. CONCLUSIONS AND FUTURE WORK

the network, e.g. $\pm 5\%$ of the nominal voltage around the voltage set point. Then, the OLTC operates when the maximum or minimum value of the voltages estimates is outside the deadband. This approach shows a good voltage regulating capability and its implementation is simpler than adjusting the set point of the OLTC which is done if the deadband is left at its conventional setting.

- The control of voltage through RPC and energy curtailment can be carried out by using simple integral controllers with some on-off logic. The on-off logic is mainly used to determine when the RPC and curtailment need to be engaged and disengaged. This approach is found to do the job with minimum RPC and energy curtailment. Similar controller is used for overload mitigation using curtailment. Moreover, reactive power from a wind turbine is also used to mitigate an overvoltage that occurs at the terminal of any remote wind turbine on the same feeder as long as voltage measurement is available from the remote bus.

When it comes to the coordination of the different active management strategies for voltage regulation, the following methods are employed and are found to work effectively:

- For coordinating voltage regulation through RPC from different wind turbines, or curtailment and RPC at a given wind turbine, different reference voltages are used for each controller. For example, in the case of coordinating RPC and curtailment for overvoltage mitigation, the reference voltage for the voltage control through RPC can be 1.05 pu whereas the reference voltage for voltage control through curtailment can be set to 1.051 pu. In this way curtailment will only be used when RPC lacks enough reactive power to mitigate the overvoltage.
- For the coordination between RPC, OLTC and curtailment, when voltage measurements are available from the wind turbine buses in the SE process, the OLTC works only after a delay which means if the RPC can regulate the voltage it would do so before the OLTC reacts. Similarly, curtailment is implemented with a larger time delay than the delay of the OLTC which means the OLTC is preferred for overvoltage mitigation over curtailment. However, the OLTC will not be operated if it is found that its operation results in an undervoltage on some buses.
- When the real time measurement of the wind turbine terminal voltage is not available in the SE process, the results of the SE are adjusted so that the wind turbine takes control of the voltage regulation at its terminal by using RPC and curtailment while the OLTC regulates the voltage on the rest of the buses in the network.

8.2 Future work

This thesis investigates the planning and operation of large amount of wind power in a radially operated distribution system. Though, the maximum effort has been made to cover the most important issues related to the subject area, it does not cover all the technical issues related to the integration of wind power into a distribution system. Thus, during the planning stage of a wind power project the following issues need further investigation:

- Though voltage flickers are less likely to be limiting factor in a typical distribution system, its assessment would be more complete if it is supported by measuring the actual flicker level in the system.

- Given that the requirement of low order harmonics is more stringent to fulfill by wind turbines and could become a limiting factor to further integration of wind power to the system, it would be valuable if such investigation is supported by the measurement of the harmonic emissions in the system. If there is such a problem, mitigating solutions need to be investigated.
- In the case the switchgear at the substation has a lower margin of safety to handle additional fault current, the effect of the new wind turbine/farm on the fault level can more accurately be calculated using simulations.

Moreover in addition to the active management strategies investigated in this thesis, others such as demand side management and energy storage, which may include electric vehicles, can be analyzed to increase the wind power hosting capacity of distribution systems.

On the other hand, with respect to operational aspect of distribution system with a large amount of wind power, Chapter 7 investigates the control and coordination of the different active management strategies used in Chapter 5 to increase the wind power hosting capacity of the distribution system. These control and coordination principles are, however, analyzed based on simulations only. They are not analyzed in laboratory set up where some of the challenges of practical system—such as noise in measurement signals, delay in signal communication, and imperfect knowledge of the various network parameter—can be experienced. Future works can include such analysis based on which appropriate solutions can be investigated. Moreover, in the case of the state estimation, a balanced three phase system is assumed, which is mostly the case in Nordic distribution systems, but it may not always be the case. Thus, the state estimation can be extended to include unbalanced three phase systems. Moreover, testing the proposed control strategies in a actual distribution network would further verify the algorithms.

8. CONCLUSIONS AND FUTURE WORK

References

- [1] W. R. J.L. Sawin, Freyr Sverrisson, Others, and REN21, “Renewables 2015 global status report,” REN21, Paris, France, Tech. Rep., Jun. 2012.
- [2] S. Krohn, P. E. Morthorst, S. Awerbuch, M. I. Blanco, S. Krohn, P. E. Morthorst, S. Awerbuch, and B. M.I, “The economics of wind energy,” *Eur. Wind Energy Assoc.*, vol. 13, no. 6-7, p. 28–29, Aug. 2009.
- [3] S. N. Liew and G. Strbac, “Maximising penetration of wind generation in existing distribution networks,” *Gener. Transm. Distrib. IEE Proceedings-*, vol. 149, no. 3, p. 256 –262, May 2002.
- [4] C. Schwaegerl, M. Bollen, K. Karoui, and A. Yagmur, “Voltage control in distribution systems as a limitation of the hosting capacity for distributed energy resources,” in *Electricity Distribution, 2005. CIRED 2005. 18th International Conference and Exhibition on*, June 2005, pp. 1–5.
- [5] A. Shafiu, T. Bopp, I. Chilvers, and G. Strbac, “Active management and protection of distribution networks with distributed generation,” in *IEEE Power Eng. Soc. Gen. Meet. 2004*, Jun. 2004, pp. 1098 —1103 Vol.1.
- [6] J. Mutale, “Benefits of active management of distribution networks with distributed generation,” in *Power Syst. Conf. Expo. 2006. PSCE '06. 2006 IEEE PES*, Nov. 2006, p. 601–606.
- [7] P. Siano, P. Chen, Z. Chen, and A. Piccolo, “Evaluating maximum wind energy exploitation in active distribution networks,” *Gener. Transm. Distrib. IET*, vol. 4, no. 5, p. 598 –608, May 2010.
- [8] L. F. Ochoa, C. J. Dent, and G. P. Harrison, “Distribution network capacity assessment: variable DG and active networks,” *IEEE Trans. Power Syst.*, vol. 25, no. 1, p. 87–95, 2010.
- [9] J. Zhang, H. Fan, W. Tang, M. Wang, H. Cheng, and L. Yao, “Planning for distributed wind generation under active management mode,” *Int. J. Electr. Power Energy Syst.*, vol. 47, p. 140–146, May 2013.
- [10] L. Ochoa, C. Dent, and G. Harrison, “Maximisation of intermittent distributed generation in active networks,” in *SmartGrids for Distrib. 2008. IET-CIRED. CIRED Semin.*, Jun. 2008, p. 1–4.

REFERENCES

- [11] C. M. Hird, H. Leite, N. Jenkins, and H. Li, "Network voltage controller for distributed generation," *Gener. Transm. Distrib. IEE Proceedings-*, vol. 151, no. 2, p. 150–156, 2004.
- [12] M. Fila, D. Reid, G. Taylor, P. Lang, and M. Irving, "Coordinated voltage control for active network management of distributed generation," in *Power Energy Society General Meeting, 2009. PES '09. IEEE*, 2009, p. 1–8.
- [13] H. Y. Li and H. Leite, "Increasing distributed generation using automatic voltage reference setting technique," in *2008 IEEE Power Energy Soc. Gen. Meet. - Convers. Deliv. Electr. Energy 21st Century*, 2008, p. 1–7.
- [14] P. Esslinger and R. Witzmann, "Regulated distribution transformers in low-voltage networks with a high degree of distributed generation," in *2012 3rd IEEE PES Int. Conf. Exhib. Innov. Smart Grid Technol. ISGT Eur.*, 2012, p. 1–7.
- [15] M. A. Azzouz, H. E. Farag, and E. F. El-Saadany, "Fuzzy-based control of on-load tap changers under high penetration of distributed generators," in *2013 3rd Int. Conf. Electr. Power Energy Convers. Syst.*, 2013, p. 1–6.
- [16] M. S. El Moursi, H. H. Zeineldin, J. L. Kirtley, and K. Alobeidli, "A Dynamic Master/Slave Reactive Power-Management Scheme for Smart Grids With Distributed Generation," *IEEE Trans. Power Deliv.*, vol. 29, no. 3, pp. 1157–1167, jun 2014.
- [17] A. E. Kiprakis and A. R. Wallace, "Maximising energy capture from distributed generators in weak networks," *Gener. Transm. Distrib. IEE Proceedings-*, vol. 151, no. 5, p. 611 – 618, Sep. 2004.
- [18] P. Carvalho, P. Correia, and L. Ferreira, "Distributed reactive power generation control for voltage rise mitigation in distribution networks," *IEEE Trans. Power Syst.*, vol. 23, no. 2, p. 766 –772, May 2008.
- [19] E. Demirok, D. Sera, P. Rodriguez, and R. Teodorescu, "Enhanced local grid voltage support method for high penetration of distributed generators," in *IECON 2011 - 37th Annu. Conf. IEEE Ind. Electron. Soc.*, 2011, p. 2481–2485.
- [20] K. Turitsyn, P. Šulc, S. Backhaus, and M. Chertkov, "Options for control of reactive power by distributed photovoltaic generators," in *Proc. IEEE*, vol. 99, 2011, p. 1063–1073.
- [21] R. Tonkoski, "Coordinated active power curtailment of grid connected PV inverters for over-voltage prevention," *IEEE Trans. Sustain. Energy*, vol. 2, no. 2, p. 139–147, 2011.
- [22] Y. Wang, P. Zhang, W. Li, W. Xiao, and A. Abdollahi, "Online overvoltage prevention control of photovoltaic generators in microgrids," *IEEE Trans. Smart Grid*, vol. 3, no. 4, p. 2071–2078, 2012.
- [23] V. Calderaro, G. Conio, V. Galdi, G. Massa, and A. Piccolo, "Optimal decentralized voltage control for distribution systems with inverter-based distributed generators," *IEEE Trans. Power Syst.*, vol. 29, no. 1, p. 230–241, 2014.

- [24] T. Sansawatt, L. F. Ochoa, and G. P. Harrison, "Smart decentralized control of DG for voltage and thermal constraint management," *IEEE Trans. Power Syst.*, vol. 27, no. 3, p. 1637–1645, 2012.
- [25] I. Leisse, O. Samuelsson, and J. Svensson, "Coordinated voltage control in medium and low voltage distribution networks with wind power and photovoltaics," *2013 IEEE Grenoble Conf.*, p. 1–6, Jun. 2013.
- [26] H. E. Z. Farag and E. F. El-Saadany, "A novel cooperative protocol for distributed voltage control in active distribution systems," *IEEE Trans. Power Syst.*, vol. 28, no. 2, p. 1645–1656, 2013.
- [27] A. Kulmala, S. Repo, and P. Jarventausta, "Coordinated Voltage Control in Distribution Networks Including Several Distributed Energy Resources," *IEEE Trans. Smart Grid*, vol. 5, no. 4, pp. 2010–2020, Jul. 2014.
- [28] F. Bignucolo, R. Caldon, and V. Prandoni, "Radial MV networks voltage regulation with distribution management system coordinated controller," *Electr. Power Syst. Res.*, vol. 78, no. 4, pp. 634–645, Apr. 2008.
- [29] K. M. Muttaqi, A. D. T. Le, M. Negnevitsky, and G. Ledwich, "A Coordinated Voltage Control Approach for Coordination of OLTC, Voltage Regulator, and DG to Regulate Voltage in a Distribution Feeder," *IEEE Trans. Ind. Appl.*, vol. 51, no. 2, pp. 1239–1248, Mar. 2015.
- [30] S. C. E. Jupe, P. C. Taylor, and A. Michiorri, "Coordinated output control of multiple distributed generation schemes," *Renew. Power Gener. IET*, vol. 4, no. 3, p. 283–297, 2010.
- [31] T. Ackermann, *Wind Power in Power Systems*. John Wiley & Sons, Apr. 2005.
- [32] R. Gasch and J. Twele, *Wind Power Plants: Fundamentals, Design, Construction and Operation*. Springer, Dec. 2011.
- [33] A. Dai and C. Deser, "Diurnal and semidiurnal variations in global surface wind and divergence fields," *J. Geophys. Res. Atmos.*, vol. 104, no. D24, p. 31109–31125, 1999.
- [34] D. Heide, L. von Bremen, M. Greiner, C. Hoffmann, M. Speckmann, and S. Bofinger, "Seasonal optimal mix of wind and solar power in a future, highly renewable europe," *Renew. Energy*, vol. 35, no. 11, p. 2483–2489, Nov. 2010.
- [35] C. Achberger, D. Chen, and H. Alexandersson, "The surface winds of sweden during 1999–2000," *Int. J. Climatol.*, vol. 26, no. 2, p. 159–178, Feb. 2006.
- [36] B. Fox, *Wind power integration: connection and system operational aspects*, ser. IET power and energy series. Institution of Engineering and Technology, Jan. 2007, vol. 50.
- [37] Andrew, "Capacity factors at danish offshore wind farms." [Online]. Available: <http://energynumbers.info/capacity-factors-at-danish-offshore-wind-farms>
- [38] A. D. Hansen, F. Iov, F. Blaabjerg, and L. H. Hansen, "Review of contemporary wind turbine concepts and their market penetration," *Wind Eng.*, vol. 28, no. 3, p. 247–263, 2004.

REFERENCES

- [39] N. Jenkins, *Embedded Generation*, ser. Energy Engineering. Institution of Engineering and Technology, 2000.
- [40] L. Holdsworth, X. G. Wu, J. B. Ekanayake, and N. Jenkins, "Comparison of fixed speed and doubly-fed induction wind turbines during power system disturbances," *Gener. Transm. Distrib. IEE Proceedings-*, vol. 150, no. 3, p. 343–352, 2003.
- [41] M. Bongiorno and T. Thiringer, "A generic DFIG model for voltage dip ride-through analysis," *IEEE Trans. Energy Convers.*, vol. 28, no. 1, p. 76–85, 2013.
- [42] M. Stiebler, *Wind Energy Systems for Electric Power Generation*. Springer, Oct. 2008.
- [43] T. Thiringer, J. Paixao, and M. Bongiorno, "Monitoring of ride-through ability of a 2MW wind turbine in tvååker, halland," Elforsk, Tech. Rep., Feb. 2009.
- [44] T. Lund, P. Sørensen, and J. Eek, "Reactive power capability of a wind turbine with doubly fed induction generator," *Wind Energy*, vol. 10, no. 4, p. 379–394, 2007.
- [45] S. Engelhardt, I. Erlich, C. Feltes, J. Kretschmann, and F. Shewarega, "Reactive power capability of wind turbines based on doubly fed induction generators," *IEEE Trans. Energy Convers.*, vol. 26, no. 1, p. 364–372, 2011.
- [46] O. Anaya-Lara, *Wind energy generation: modelling and control*. John Wiley & Sons, Jan. 2009.
- [47] N. Ullah, K. Bhattacharya, and T. Thiringer, "Wind farms as reactive power ancillary service providers –Technical and economic issues," *IEEE Trans. Energy Convers.*, vol. 24, no. 3, p. 661–672, 2009.
- [48] A. Larsson, "Flicker emission of wind turbines during continuous operation," *IEEE Trans. Energy Convers.*, vol. 17, no. 1, p. 114 –118, Mar. 2002.
- [49] S. N. Salih, "Maximizing the integration of wind power in distribution system," Licentiate thesis, Chalmers University of technology, 2013.
- [50] IEC standard 61000-3-6, "Electromagnetic compatibility (EMC) - part 3-6: Limits - assessment of emission limits for the connection of distorting installations to MV, HV and EHV power systems," 2008.
- [51] T. Sulawa, Z. Zabar, D. Czarkowski, Y. TenAmi, L. Birenbaum, S. Lee, and S. Member, "Evaluation of a 3- ϕ bolted short-circuit on distribution networks having induction generators at customer sites," *IEEE Trans. Power Deliv.*, vol. 22, no. 3, p. 1965 –1971, Jul. 2007.
- [52] P. Bousseau, E. Gautier, I. Garzulino, P. Juston, and R. Belhomme, "Grid impact of different technologies of wind turbine generator systems (WTGS)," in *European Wind Energy Conference (EWEC)*, Jun. 2003.
- [53] T. N. Boutsika and S. a. Papathanassiou, "Short-circuit calculations in networks with distributed generation," *Electr. Power Syst. Res.*, vol. 78, no. 7, p. 1181–1191, Jul. 2008.

- [54] J. Morren and S. W. H. De Haan, "Short-circuit current of wind turbines with doubly fed induction generator," *IEEE Trans. Energy Convers.*, vol. 22, no. 1, p. 174–180, Mar. 2007.
- [55] P. Karaliolios, A. Ishchenko, E. Coster, J. Myrzik, and W. Kling, "Overview of short-circuit contribution of various distributed generators on the distribution network," in *Univ. Power Eng. Conf. 2008. UPEC 2008. 43rd Int.*, 2008, p. 1–6.
- [56] E. Muljadi, N. Samaan, V. Gevorgian, J. Li, and S. Pasupulati, "Short circuit current contribution for different wind turbine generator types," in *2010 IEEE Power Energy Soc. Gen. Meet.*, Jul. 2010, p. 1–8.
- [57] EPRI, "Effects of temporary overvoltage on residential Products: System compatibility research project," EPRI, Palo Alto, CA, Tech. Rep., 2005.
- [58] ABB, "Transformer protection RET670 2.0 ANSI: application manual," Tech. Rep., 2014.
- [59] T. A. Short, "Voltage regulation," in *Electr. Power Distrib. Handb.* CRC Press, Sep. 2003.
- [60] "Medium Voltage - nkt cables." [Online]. Available: <http://www.nktcables.com/products/europe/se/medium-voltage/>
- [61] "ELNORD KRAFT." [Online]. Available: <http://www.elnord.se/friledningar.html>
- [62] Svensk Energi, "AMP - anslutning av mindre produktion till elnätet," 2010.
- [63] United States Department of the Interior Bureau of Reclamation, "Permissible loading of oil-immersed transformers and regulators," Tech. Rep., 1991.
- [64] M. Wang, A. J. Vandermaar, and K. D. Srivastava, "Review of condition assessment of power transformers in service," *IEEE Electr. Insul. Mag.*, vol. 18, no. 6, p. 12–25, Dec. 2002.
- [65] J. N. Jagers, J. Khosa, P. J. D. Klerk, C. T. Gaunt, J. Khosa, P. J. De Klerk, and C. T. Gaunt, "Transformer reliability and condition assessment in a south african utility," in *XVth International Symposium on High Voltage Engineering*, 2007.
- [66] S. Tenbohlen, T. Stirl, G. Bastos, J. Baldauf, P. Mayer, M. Stach, B. Breitenbauch, and R. Huber, "Experienced-based evaluation of economic benefits of on-line monitoring systems for power transformers," *CIGRE Sess. 2002*, p. 12–110, 2002.
- [67] M. S. A. Minhas, J. P. Reynders, and P. J. de Klerk, "Failures in power system transformers and appropriate monitoring techniques," in *High Volt. Eng. 1999. Elev. Int. Symp. (Conf. Publ. No. 467)*, vol. 1, 1999, pp. 94 —97 vol.1.
- [68] CIGRÉ Working Group 05, "An international survey on failures in large power transformers in service," *Electra*, no. 88, p. 21–47, 1983.
- [69] R. Jongen, P. Morshuis, J. Smit, A. Janssen, and E. Gulski, "A statistical approach to processing power transformer failure data," in *Cired 19th Int. Conf. Electr. Distrib.*, 2007.

REFERENCES

- [70] H.-U. Schellhase, R. G. Pollock, A. S. Rao, E. C. Korolenko, and B. Ward, "Load tap changers: investigations of contacts, contact wear and contact coking," in *Proc. Forty-Eighth IEEE Holm Conf. Electr. Contacts, 2002*, 2002, p. 259 – 272.
- [71] P. Kang and D. Birtwhistle, "On-line condition monitoring of tap changers-field experience," in *Electr. Distrib. 2001. Part 1 Contrib. CIRED. 16th Int. Conf. Exhib. (IEE Conf. Publ No. 482)*, vol. 1, 2001, p. 5 pp. vol.1.
- [72] M. Foata, C. Rajotte, A. Jolicoeur, M. Foata, C. Rajotte, and A. Jolicoeur, "On-load tap changer reliability and maintenance strategy," in *Cigre 2006*, Paris, 2006.
- [73] M. A. Redfern and W. R. C. Handley, "Duty based maintenance for on-load transformer tap changers," in *Power Eng. Soc. Summer Meet. 2001*, vol. 3, 2001, p. 1824 –1829 vol.3.
- [74] P. Kang and D. Birtwhistle, "Condition assessment of power transformer onload tap changers using wavelet analysis and self-organizing map: field evaluation," *IEEE Trans. Power Deliv.*, vol. 18, no. 1, p. 78 – 84, Jan. 2003.
- [75] B. Handley, M. Redfern, and S. White, "On load tap-changer conditioned based maintenance," *Gener. Transm. Distrib. IEE Proceedings-*, vol. 148, no. 4, p. 296 –300, Jul. 2001.
- [76] E. G. Romero, "Voltage control in a medium voltage system with distributed wind power generation," Master thesis, Lund University, Lund, 2007.
- [77] D. S. Romero, "Voltage regulation in distribution systems - tap changer and wind power," Master thesis, Lund University, Lund, 2010.
- [78] S. S. Bagsorkhi and I. A. Hiskens, "Impact of wind power variability on sub-transmission networks," in *Proc. IEEE Power Energy Soc. Gen. Meet.*, Jul. 2012.
- [79] H. Saadat, *Power System Analysis*. PSA Publishing, 2010.
- [80] A. Wächter and L. T. Biegler, "On the implementation of an interior-point filter line-search algorithm for large-scale nonlinear programming," *Math. Program.*, vol. 106, p. 25–57, 2006.
- [81] P. Chen, "Stochastic modeling and analysis of power system with renewable generation," PhD thesis, Aalborg university, Aalborg, Jan. 2010.
- [82] P. Chen, T. Pedersen, B. Bak-Jensen, and Z. Chen, "ARIMA-Based time series model of stochastic wind power generation," *Power Syst. IEEE Trans.*, vol. 25, no. 2, p. 667 –676, May 2010.
- [83] B. Singh and S. N. Singh, "Wind power interconnection into the power system: A review of grid code requirements," *Electr. J.*, vol. 22, no. 5, p. 54 – 63, 2009.
- [84] S. Chandrashekhar Reddy and P. Prasad, "Power quality improvement of distribution system by optimal placement of distributed generators using ga and nn," in *Proceedings of the International Conference on Soft Computing for Problem Solving (SocProS 2011) December 20-22, 2011*, ser. Advances in Intelligent and Soft Computing. Springer India, 2012, vol. 130, pp. 257–267.

- [85] M. H. Aliabadi, M. Mardaneh, and B. Behbahan, "Siting and sizing of distributed generation units using GA and OPF," in *Proc. 2nd WSEAS Int. Conf. Circuits, Syst. Signal Telecommun.*, 2008, p. 202–206.
- [86] Y. Alinejad-Beromi, M. Sedighzadeh, and M. Sadighi, "A particle swarm optimization for sitting and sizing of distributed generation in distribution network to improve voltage profile and reduce THD and losses," in *Univ. Power Eng. Conf. 2008. UPEC 2008. 43rd Int.*, Sep. 2008, p. 1–5.
- [87] N. Jain, S. N. Singh, and S. C. Srivastava, "Particle swarm optimization based method for optimal siting and sizing of multiple distributed generators," in *Proc. 16th Natl. Power Syst. Conf.*, 2010, p. 669–674.
- [88] A. Kazemi and M. Sadeghi, "Sitting and sizing of distributed generation for loss reduction," in *Power Energy Eng. Conf. 2009. APPEEC 2009. Asia-Pacific*, Mar. 2009, p. 1–4.
- [89] B. Kuri, M. A. Redfem, and F. Li, "Optimisation of rating and positioning of dispersed generation with minimum network disruption," in *IEEE Power Eng. Soc. Gen. Meet. 2004*, Jun. 2004, pp. 2074 —2078 Vol.2.
- [90] M. Mardaneh and G. Gharehpetian, "Siting and sizing of DG units using GA and OPF based technique," in *TENCON 2004. 2004 IEEE Reg. 10 Conf.*, vol. C, Nov. 2004, p. 331 – 334 Vol. 3.
- [91] R. H. Mohammed Mansoor O., "Optimal siting and sizing of distributed generation by adaptive particle swarm optimization for power distribution system," in *ICTT Electr. Eng. Pap.*, 2010.
- [92] S. Reddy, P. Prasad, and A. Laxmi, "Reliability improvement of distribution system by optimal placement of DGs using PSO and neural network," in *Computing, Electronics and Electrical Technologies (ICCEET), 2012 International Conference on*, Mar. 2012, p. 156–162.
- [93] P. Siano, G. P. Harrison, A. Piccolo, and A. Wallace, "Strategic placement of distributed generation capacity," in *Cired 19th International Conference on Electricity Distribution*, May 2007.
- [94] C. Tautiva, A. Cadena, and F. Rodriguez, "Optimal placement of distributed generation on distribution networks," in *Univ. Power Eng. Conf. (UPEC), 2009 Proc. 44th Int.*, Sep. 2009.
- [95] N. Acharya, P. Mahat, and N. Mithulananthan, "An analytical approach for DG allocation in primary distribution network," *Int. J. Electr. Power Energy Syst.*, vol. 28, p. 669–678, Dec. 2006.
- [96] A. Afraz, F. Malekinezhad, S. J. seyed Shenava, and A. Jlili, "Optimal sizing and sitting in radial standard system using PSO," *Am. J. Sci. Res.*, no. 67, p. 50–58, 2012.
- [97] A. J. Ardakani, A. K. Kavyani, S. A. Pourmousavi, S. H. Hosseinian, and M. Abedi, "Siting and sizing of distributed generation for loss reduction," *Int. Carnivorous Plant Soc.*, 2007.

REFERENCES

- [98] G. Celli, E. Ghiani, S. Mocci, and F. Pilo, "A multiobjective evolutionary algorithm for the sizing and siting of distributed generation," *Power Syst. IEEE Trans.*, vol. 20, no. 2, p. 750–757, May 2005.
- [99] A. L. Devi and B. Subramanyam, "Optimal DG unit placement for loss reduction in radial distribution system-a case study," *ARNP J. Eng. Appl. Sci.*, vol. 2, no. 6, p. 57–61, Dec. 2007.
- [100] L. Devi and B. Subramanyam, "Sizing of DG unit operated at optimal power factor to reduce losses in radial distribution; a case study," *J. Theor. Appl. Inf. Technol.*, p. 973–980, 2008.
- [101] S. S. Ghosh, S. P. Ghoshal, and S. S. Ghosh, "Optimal sizing and placement of distributed generation in a network system," *Int. J. Electr. Power Energy Syst.*, vol. 32, no. 8, p. 849–856, Oct. 2010.
- [102] T. Gözel and M. H. Hocaoglu, "An analytical method for the sizing and siting of distributed generators in radial systems," *Electr. Power Syst. Res.*, vol. 79, no. 6, p. 912–918, Jun. 2009.
- [103] G. P. Harrison, A. Piccolo, P. Siano, and A. Wallace, "Distributed generation capacity evaluation using combined genetic algorithm and OPF," *Int. J. Emerg. Electr. Power Syst.*, vol. 8, no. 2, p. 750 – 757, 2007.
- [104] R. A. Jabr and B. C. Pal, "Ordinal optimisation approach for locating and sizing of distributed generation," *Gener. Transm. Distrib. IET*, vol. 3, no. 8, p. 713–723, 2009.
- [105] S. Kansal, B. B. R. Sai, B. Tyagi, and V. Kumar, "Optimal placement of distributed generation in distribution networks," *Int. J. Eng. Sci. Technol.*, vol. 3, no. 3, 2011.
- [106] M. P. Lalitha, V. C. V. Reddy, N. S. Reddy, and V. U. Redddy, "A two stage methodology for siting and sizing of DG for minimum loss in radial distribution system using RCGA," *Int. J. Comput. Appl.*, vol. 25, no. 2, p. 10–16, 2011.
- [107] M. P. Lalitha, N. S. Reddy, and V. C. V. Reddy, "Optimal DG placement for maximum loss reduction in radial distribution system using ABC algorithm," *Int. J. Rev. Comput.*, 2009.
- [108] M. H. Moradi and M. Abedini, "A combination of genetic algorithm and particle swarm optimization for optimal DG location and sizing in distribution systems," *Int. J. Electr. Power Energy Syst.*, 2011.
- [109] V. Rashtchi and M. Darabian, "A new BFA-Based approach for optimal sitting and sizing of distributed generation in distribution system," *Int. J. Autom. Control Engineering(IJACE)*, *Int. J. Autom. Control Engineering(IJACE)*, vol. 1, no. 1, Nov. 2012.
- [110] C. Wang and M. H. Nehrir, "Analytical approaches for optimal placement of distributed generation sources in power systems," *IEEE Trans. Power Syst.*, vol. 19, no. 4, p. 2068 – 2076, Nov. 2004.
- [111] IEC standard 61400-21, "Wind turbines-part 21: Measurement and assessment of power quality characteristics of grid connected wind turbines," Aug. 2008.

-
- [112] G. P. Harrison and A. R. Wallace, "Optimal power flow evaluation of distribution network capacity for the connection of distributed generation," *Gener. Transm. Distrib. IEE Proceedings-*, vol. 152, no. 1, p. 115–122, Jan. 2005.
- [113] Z. Saad-Saoud, M. Lisboa, J. Ekanayake, N. Jenkins, and G. Strbac, "Application of statcoms to wind farms," *Generation, Transmission and Distribution, IEE Proceedings-*, vol. 145, no. 5, pp. 511–516, Sep 1998.
- [114] V. Quezada, J. Abbad, and T. Roman, "Assessment of energy distribution losses for increasing penetration of distributed generation," *Power Systems, IEEE Transactions on*, vol. 21, no. 2, pp. 533–540, May 2006.
- [115] J. Zhao, X. Li, J. Hao, C. Zhang, and J. Lu, "Wind farm reactive power output optimization for loss reduction and voltage profile improvements," *2009 IEEE 6th Int. Power Electron. Motion Control Conf.*, vol. 3, p. 1099–1103, May 2009.
- [116] X. Wei, X. Qiu, J. Xu, X. Li, W. Xiwen, Q. Xiaoyan, X. Jian, and L. Xingyuan, "Reactive power optimization in smart grid with wind power generator," in *2010 Asia-Pacific Power Energy Eng. Conf.* IEEE, Mar. 2010, p. 1–4.
- [117] T. Sun, Z. Chen, and F. Blaabjerg, "Flicker mitigation of grid connected wind turbines using STATCOM," in *Power Electron. Mach. Drives, 2004. (PEMD 2004). Second Int. Conf. (Conf. Publ. No. 498)*, vol. 1, Apr. 2004, p. 175 – 180 Vol.1.
- [118] S. Tao, C. Zhe, and F. Blaabjerg, "Flicker study on variable speed wind turbines with doubly fed induction generators," *Energy Conversion, IEEE Transactions on*, vol. 20, no. 4, pp. 896–905, Dec 2005.
- [119] A. A. Collin, J. J. Acosta, B. B. Hayes, and S. S. Djokic, "Component-based aggregate load models for combined power flow and harmonic analysis," in *7th Mediterr. Conf. Exhib. Power Gener. Transm. Distrib. Energy Convers. (MedPower 2010)*. IET, 2010, p. 171–171.
- [120] M. Coker, H. Kgasoane, P. Bag, and S. Africa, "Load modeling," in *1999 IEEE Africon. 5th Africon Conf. Africa (Cat. No.99CH36342)*, vol. 2. IEEE, 1999, p. 663–668.
- [121] IEEE task force, "Bibliography on load models for power flow and dynamic performance simulation," *IEEE Trans. Power Syst.*, vol. 10, no. 3, p. 1302–1313, 1995.
- [122] W. Sun and G. Harrison, "Influence of generator curtailment priority on network hosting capacity," in *Electricity Distribution (CIRED 2013), 22nd International Conference and Exhibition on*, June 2013, pp. 1–4.
- [123] R. Barth and C. Weber, "Distribution of the integration costs of wind power," IER-Stuttgart University, Deliverable D7.1, 2005.
- [124] G. P. Harrison, A. Piccolo, P. Siano, and A. Wallace, "Exploring the tradeoffs between incentives for distributed generation developers and DNOs," *IEEE Trans. Power Syst.*, vol. 22, no. 2, p. 21–24, May 2007.

REFERENCES

- [125] F. energi, “Inmatningstariffer,” 2011. [Online]. Available: <http://feab.nu/Inmatningstariffer-2011-2012.htm>
- [126] Fortum Oyj, “Nätpriser - inmatning till lokalnät,” 2013. [Online]. Available: https://www.fortum.com/countries/se/SiteCollectionDocuments/Inm_Da-No_140401.pdf
- [127] Northern Powergrid, *Statement of Use of System Charging*. Northern Powergrid plc, 2012.
- [128] M. I. Blanco, “The economics of wind energy,” *Renewable and Sustainable Energy Reviews*, vol. 13, no. 6–7, pp. 1372–1382, Aug. 2009.
- [129] Energimyndigheten, “Average elcertificate prices,” 2015. [Online]. Available: <https://cesar.energimyndigheten.se/WebPartPages/AveragePricePage.aspx>
- [130] Nord Pool Spot, “Nordpool spot market price,” 2012. [Online]. Available: <http://www.nordpoolspot.com>
- [131] H. L. Willis and W. G. Scott, *Distributed Power Generation: Planning and Evaluation*. CRC Press, 2000.
- [132] J. Harry, *Multivariate models and dependence concepts*. Chapman & Hall, 1997.
- [133] B. Biller and S. Ghosh, “Multivariate input processes,” in *Simulation*, ser. Handbooks in Operations Research and Management Science. Elsevier, 2006, vol. 13, no. 06, p. 123–153.
- [134] H. V. Haghi, M. T. Bina, M. A. Golkar, and S. M. Moghaddas-Tafreshi, “Using copulas for analysis of large datasets in renewable distributed generation: PV and wind power integration in iran,” *Renew. Energy*, vol. 35, no. 9, p. 1991–2000, 2010.
- [135] G. Papaefthymiou and D. Kurowicka, “Using copulas for modeling stochastic dependence in power system uncertainty analysis,” *Power Syst. IEEE Trans.*, vol. 24, no. 1, p. 40–49, Feb. 2009.
- [136] A. Bowman and A. Azzalini, *Applied Smoothing Techniques for Data Analysis : The Kernel Approach with S-Plus Illustrations*. OUP Oxford, 1997.
- [137] E. W. Frees and E. A. Valdez, “Understanding relationships using copulas,” *North Am. Actuar. J.*, vol. 2, p. 1–25, 1998.
- [138] Vose Software BVBA, *Help File for ModelRisk*, Belgium, 2007.
- [139] K. Aas and D. Berg, “Models for construction of multivariate dependence - a comparison study,” *Eur. J. Financ.*, vol. 15, no. 7-8, p. 639–659, 2009.
- [140] B. Eric, V. Durrleman, A. Nikeghbali, G. Riboulet, and T. Roncalli, “Copulas for finance a reading guide and some applications,” *Recherche*, 2000.
- [141] P. Fischbach, “Copula-models in the electric power industry,” Master thesis, University of St.Gallen, St. Gallen, Switzerland, Aug. 2010.

-
- [142] V. Durrleman, A. Nikeghbali, and T. Roncalli, "Which copula is the right one," *Exch. Organ. Behav. Teach. J.*, p. 19, 2000.
- [143] D. Das, "A fuzzy multiobjective approach for network reconfiguration of distribution systems," *IEEE Trans. Power Deliv.*, vol. 21, no. 1, p. 202–209, Jan. 2006.
- [144] D. Pudjianto, D. M. Cao, S. Grenard, and G. Strbac, "Method for monetarisation of cost and benefits of DG options," *Bericht im Rahmen des Eur. Proj. DG Grid, Manchester/London*, 2006.
- [145] EDF Energy Networks Ltd, "IFI/RPZ report for EPN/LPN/SPN," Tech. Rep., 2010.
- [146] SP Energy Networks, "Innovation funding incentive annual report," Tech. Rep., 2012.
- [147] S. GRENARD, A. QUERIC, and O. CARRE, "Technical and economic assessment of centralised voltage control functions in presence of DG in the french MV network," in *Proc. 21st Int. Conf. Electr. Distrib.*, 2011.
- [148] KEMA, "Smart grid strategic review: The orkney islands active network management scheme," Tech. Rep., Mar. 2012.
- [149] Z. Hu and F. Li, "Cost-benefit analyses of active distribution network management, part II: investment reduction analysis," *IEEE Trans. Smart Grid*, vol. 3, no. 3, p. 1075–1081, 2012.
- [150] J. Gordijn and H. Akkermans, "Business models for distributed generation in a liberalized market environment," *Electr. Power Syst. Res.*, vol. 77, no. 9, p. 1178–1188, Jul. 2007.
- [151] P. J. Balducci, L. A. Schienbein, T. B. Nguyen, D. R. Brown, and E. M. Fatherlrahman, "An examination of the costs and critical characteristics of electric utility distribution system capacity enhancement projects," in *Transm. Distrib. Conf. Exhib. 2005/2006 IEEE PES*, May 2006, p. 78–86.
- [152] European Commission, "Cost-benefit analyses & state of play of smart metering deployment in the EU-27," European Commission, Tech. Rep., 2014.
- [153] R. Singh, B. C. Pal, and R. A. Jabr, "Choice of estimator for distribution system state estimation," *Gener. Transm. Distrib. IET*, vol. 3, no. 7, p. 666–678, Jul. 2009.
- [154] K. Li, "State estimation for power distribution system and measurement impacts," *IEEE Trans. Power Syst.*, vol. 11, no. 2, p. 911–916, 1996.
- [155] M. Baran and A. Kelley, "A branch-current-based state estimation method for distribution systems," *IEEE Trans. Power Syst.*, vol. 10, p. 483–491, 1995.
- [156] W. M. Lin, J. H. Teng, and S. J. Chen, "A highly efficient algorithm in treating current measurements for the branch-current-based distribution state estimation," *IEEE Trans. Power Deliv.*, vol. 16, p. 433–439, 2001.
- [157] H. Wang and N. N. Schulz, "A revised branch current-based distribution system state estimation algorithm and meter placement impact," *IEEE Trans. Power Syst.*, vol. 19, p. 207–213, 2004.

REFERENCES

- [158] C. Lu, J. Teng, and W.-H. Liu, "Distribution system state estimation," *Power Systems, IEEE Transactions on*, vol. 10, no. 1, pp. 229–240, Feb 1995.
- [159] A. Shafiu, N. Jenkins, and G. Strbac, "Measurement location for state estimation of distribution networks with generation," *IEE Proc. - Gener. Transm. Distrib.*, vol. 152, no. 2, p. 240, 2005.
- [160] R. Singh, B. Pal, and R. Vinter, "Measurement placement in distribution system state estimation," in *IEEE Power Energy Soc. Gen. Meet. 2009. PES '09*, 2009, p. 1.
- [161] Y. Besanger, R. Caire, O. Chilard, and P. Deschamps, "Distribution state estimation performances with different state vectors," in *PowerTech (POWERTECH), 2013 IEEE Grenoble*, 2013, p. 1–6.
- [162] A. K. Ghosh, D. L. Lubkeman, and R. H. Jones, "Load modeling for distribution circuit state estimation," *Power Deliv. IEEE Trans.*, vol. 12, no. 2, p. 999–1005, Apr. 1997.
- [163] M. Dolan, E. Davidson, I. Kockar, G. Ault, and S. McArthur, "Reducing distributed generator curtailment through active power flow management," *IEEE Transactions on Smart Grid*, vol. 5, no. 1, pp. 149–157, Jan. 2014.
- [164] R. Pena, J. Clare, and G. Asher, "Doubly fed induction generator using back-to-back PWM converters and its application to variable-speed wind-energy generation," *IEE Proc. - Electr. Power Appl.*, vol. 143, no. 3, p. 231, 1996.
- [165] H. J.-b. H. Jia-bing, H. Y.-k. H. Yi-kang, and Z. J. G. Z. J. Guo, "The Internal Model Current Control for Wind Turbine Driven Doubly-Fed Induction Generator," *Conf. Rec. 2006 IEEE Ind. Appl. Conf. Forty-First IAS Annu. Meet.*, vol. 1, no. c, pp. 209–215, 2006.
- [166] A. D. Hansen and G. Michalke, "Modelling and control of variable-speed multi-pole permanent magnet synchronous generator wind turbine," *Wind Energy*, vol. 11, no. 5, pp. 537–554, Sep. 2008.
- [167] M. Bongiorno, "On Control of Grid-connected Voltage Source Converters," PhD, Chalmers University of Technology, 2007.
- [168] K. Clark, N. W. Miller, and J. J. Sanchez-Gasca, "Modeling of GE wind turbine-generators for grid studies," Tech. Rep., 2010.
- [169] J. Aho, A. Buckspan, L. Pao, and P. Fleming, "An Active Power Control System for Wind Turbines Capable of Primary and Secondary Frequency Control for Supporting Grid Reliability," *AIAA/ASME Wind Symp.*, pp. 1–13, 2013.
- [170] H. Ma and B. Chowdhury, "Working towards frequency regulation with wind plants: combined control approaches," *IET Renew. Power Gener.*, vol. 4, no. 4, p. 308, 2010.
- [171] N. W. Miller and K. Clark, "Advanced controls enable wind plants to provide ancillary services," in *IEEE PES Gen. Meet.* IEEE, Jul. 2010, pp. 1–6.

- [172] K. Z. Østergaard, P. Brath, and J. Stoustrup, “Estimation of effective wind speed,” *Journal of Physics: Conference Series*, vol. 75, no. 1, p. 012082, 2007.
- [173] J. Jonkman, S. Butterfield, W. Musial, and G. Scott, “Definition of a 5-MW reference wind turbine for offshore system development,” NREL, Tech. Rep. February, 2009.
- [174] R. Zavadil, J. Zack, N. Miller, R. Piwko, G. V. Knowe, and G. Jordan, “Technical requirements for wind generation interconnection and integration,” Tech. Rep., 2009.
- [175] “EPFL smart grid.” [Online]. Available: <http://smartgrid.epfl.ch/>

REFERENCES

Appendices

Appendix A

Simulink Implementation

A.1 Reactive power compensation control blocks

Fig. A.1 shows the equivalent Simulink model of Fig. 7.3. Fig. A.1 shows that the on and off switch of the PI controller is achieved by multiplying the input signal to the PI controller with the RPC_{OnOff} signal. When the value of the RPC_{OnOff} signal is set to 1, it turns on the PI controller and when its value is set to 0 it turns off the PI controller. The value of the RPC_{OnOff} signal is set using the Simulink model in Fig. A.2 which is the equivalent Simulink block of the logic in Fig. 7.4. The idea presented in Fig. 7.4 dwells on when to turn on or turn off the PI controller, thus it results in two signals which are set 'high' to indicate when the PI needs to be turned on or off, respectively. But when it comes to the Simulink implementation these two decisions need to be combined into one signal. Thus in Fig. A.2, the two signals, i.e. RPC_{on} and RPC_{off} , which are set to 1, respectively, to turn on and off the PI controller are combined into one signal RPC_{OnOff} .

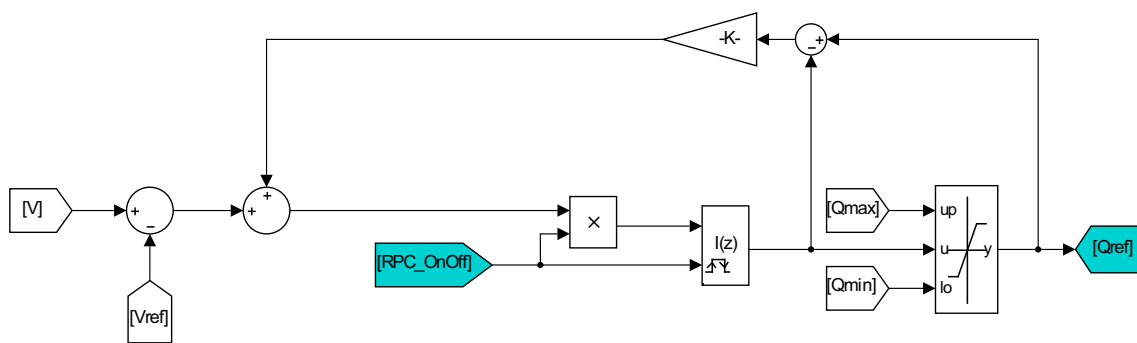


Figure A.1: Simulink model of the proposed reactive power compensation control algorithm.

Fig. 7.5 presents the logic used in deciding when to start controlling the voltage at the terminal of a remote bus. Fig. A.3 shows the equivalent Simulink implementation. The idea presented in Fig. 7.5 is good enough in deciding when to start controlling the voltage at the terminal of a remote bus. However, when voltage decreases for a short while due to decrease in wind power output or load increase in the system, the voltage decreases and suddenly V_r^{status} becomes zero. This may result in a sudden voltage increase at the terminal of the remote bus if the local wind turbine was

A. SIMULINK IMPLEMENTATION

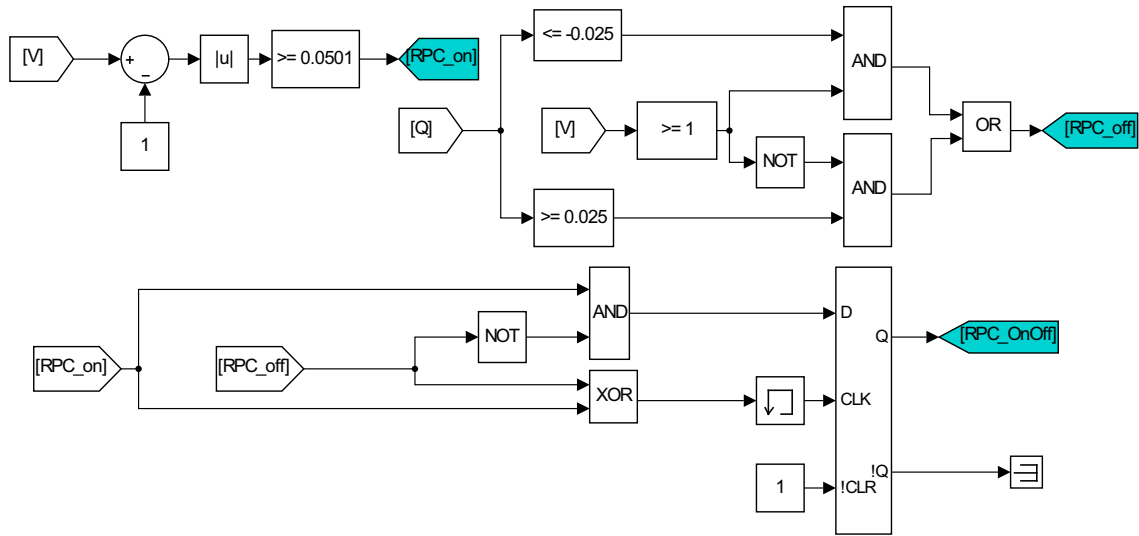


Figure A.2: Block diagram of the switching logic for Switch $RPC_{on/off}$ in Fig. A.1.

where in the figure

- Q Measured reactive power output of the wind turbine [p.u.]
- V Measured voltage at the terminal of the wind turbine [p.u.]

using a significant reactive power output to control the voltage at the remote wind turbine. That is why, in Fig. A.3, it is made sure that the local wind turbine, for example in case of overvoltage mitigation, starts to produce reactive power rather than consume reactive power before voltage regulation of the remote bus is disengaged.

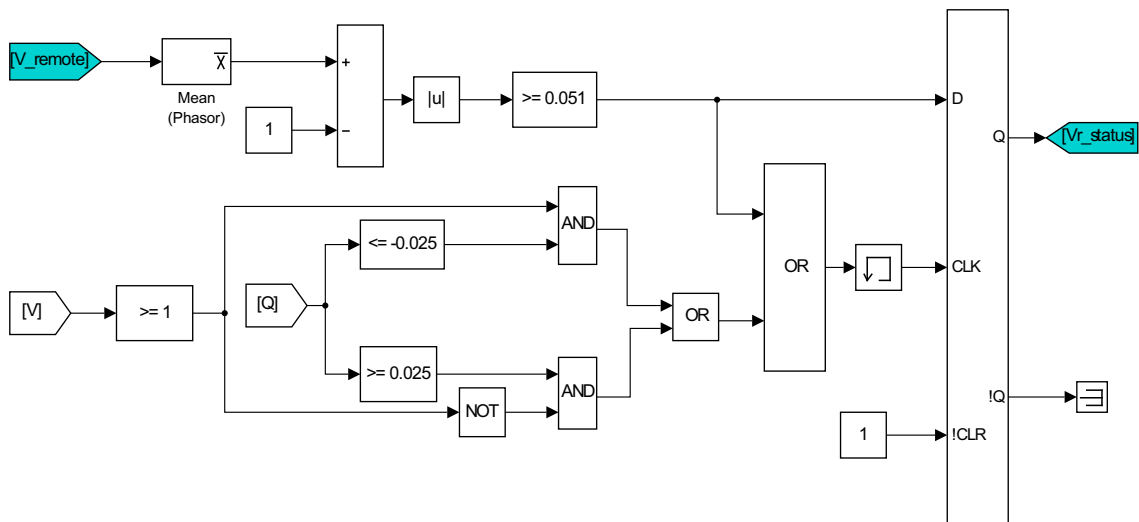


Figure A.3: The status of the voltage at the remote wind turbine terminal.

Fig. A.4 shows the equivalent Simulink model of the logic presented in Fig. 7.6. In terms of logic, the two figures present the same level of information. But in Fig. A.4, an 'enable subsystem' block which is controlled by V_{r_status} is used to engage and disengage the voltage control at the terminal

of the remote wind turbine. That is, the 'enable subsystem' block outputs a value of 1 when it is disabled with V_{r_status} set to 0 and the voltage at the terminal of the remote wind turbine when it is enabled with V_{r_status} set to 1.

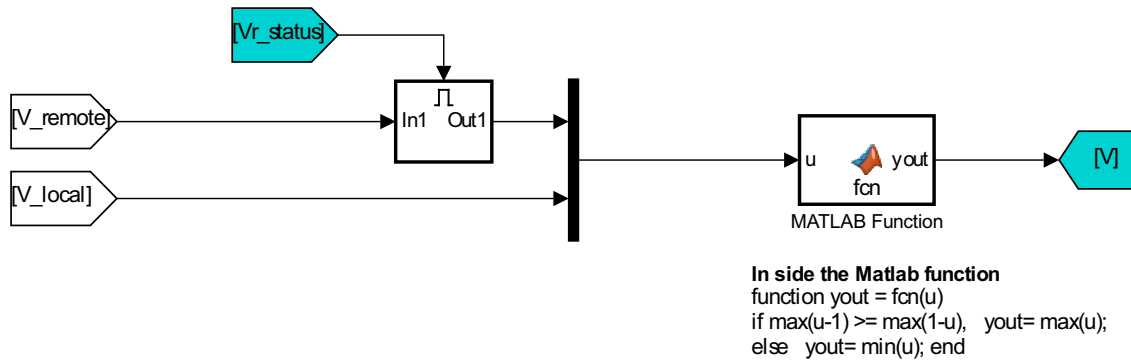


Figure A.4: The modification of the measured voltage V input of Figs. A.1, A.2, and A.3 to incorporate the voltage control of a remote wind turbine.

Similarly, Fig. A.5 shows the equivalent Simulink model of the logic presented in Fig. 7.7 with no additional information in terms of logic. The switching between the upper bound voltage reference and lower bound reference is accomplished by using the 'switch' block in Simulink. The chosen 'Threshold' value and the condition for passing the first input are shown in the figure.

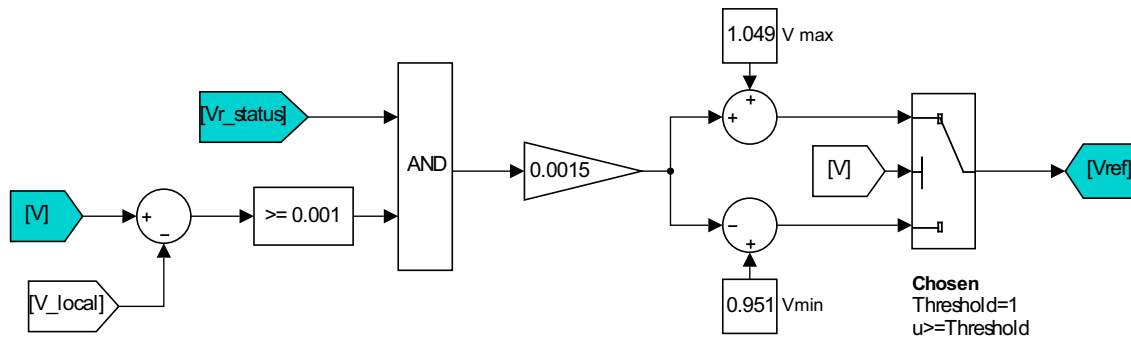


Figure A.5: Generating the reference voltage.

A.2 Curtailment control blocks

The simplified version of the Simulink model shown in Fig. A.6 is provided in Fig. 7.11. In Fig. 7.11, the PI controller is assumed to be turned on and off depending on whether the voltage is above or below a given threshold value. As mentioned above, in connection with the voltage regulation of the remote bus, such approach will result in a sudden increase in voltage when PI controller is abruptly turned off due to changes in load or wind power output. To avoid such scenario in Fig. A.6, the controller is kept on as long as the value of P_{cur_unlim} is greater than zero once it is turned on due to the voltage being above a given threshold value.

A. SIMULINK IMPLEMENTATION

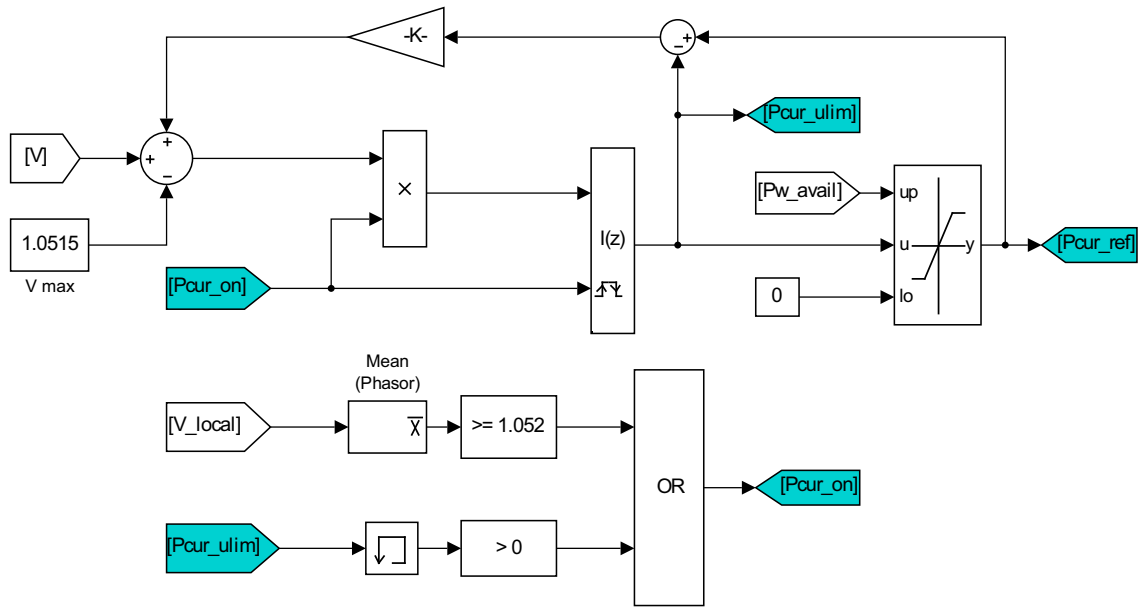


Figure A.6: The proposed PI based wind power curtailment controller for overvoltage mitigation.

Fig. A.7 shows the equivalent Simulink model of the overload mitigation controller proposed in Fig. 7.13. The control of curtailment for overload mitigation is similar to that for overvoltage mitigation. The differences lie only in measured values and the references as well as in the value of the integral gains.

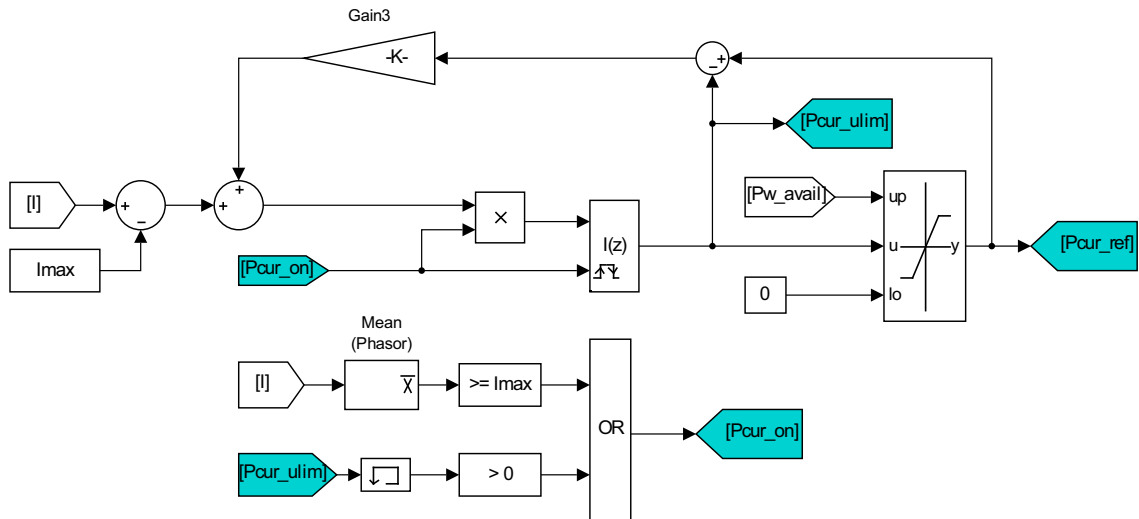


Figure A.7: Wind power curtailment controller for overload mitigation.

Fig. 7.16 proposes a curtailment controller which can be used in coordinating OLTC with curtailment. Its equivalent Simulink model is provided in Fig. A.8. The difference between the model provided in Fig. 7.16 and its equivalent Simulink model provided in Fig. A.8 is similar to that between Fig. 7.11 and Fig. A.6.

